Mechanism of Astrocytoma Progression: Role of RAP2B and HIF2A in Hypoxia

A thesis submitted to the University of Hyderabad

for the award for the degree of

Doctor of Philosophy

in

Biotechnology and Bioinformatics

by

Neera Yadav

(Reg. No: 16LTPH10)

Department of Biotechnology and Bioinformatics

School of Life Sciences, University of Hyderabad

Prof. C.R. Rao Road, Gachibowli

Hyderabad- 500 046, Telangana, India

March, 2024

University of Hyderabad

(A Central University by an Act of Parliament)

Department of Biotechnology and Bioinformatics

School of Life Sciences

P.O. Central University, Gachibowli, Hyderabad-500046

Date: 14/03/2024

CERTIFICATE

This is to certify that the thesis entitled *"Mechanism of astrocytoma progression: Role of RAP2B and HIF2A in hypoxia"* submitted to the University of Hyderabad by **Miss Neera Yadav** bearing registration number **16LTPH10** for the degree of Doctor of Philosophy in the Department of Biotechnology and Bioinformatics is based on the studies carried out by her under my supervision. To the best of my knowledge, this has never submitted for an award or certificate from any other university or institution, including this university.

26/3/2024

Prof. P. Prakash Babu

Supervisor

Prof. P. Prakash Babu
Department of Biotechnology & Bioinformatics
School of Life Sciences
University of Hyderabad
Hyderabad-500 046. (T.S.)

Head

Department of Biotechnology and Bioinformatics

HEAD
Dept. of Biotechnology & Bioinformatics
University of Hyderabad
Hyderabad.

Dean

School of Life Sciences

26/3

संकाय अधिष्ठाता / Dean
जीव विज्ञान संकाय / School of Life Sciences
हैदराबाद विश्वविद्यालय / University of Hyderabad
हैदराबाद / Hyderabad-500 046.

University of Hyderabad

(A Central University by an Act of Parliament)

Department of Biotechnology and Bioinformatics

School of Life Sciences

P.O. Central University, Gachibowli, Hyderabad-50004

DECLARATION

The research work presented in the thesis entitled ***"Mechanism of astrocytoma progression: Role of RAP2B and HIF2A in hypoxia"*** has been carried out by me in the Department of Biotechnology and Bioinformatics, School of Life Sciences, University of Hyderabad, Hyderabad, under the guidance of Prof. P. Prakash Babu. I also declare that this work is original and it has not been submitted previously in part or in full to this University or any other University or Institution for the award of any other degree or diploma.

Date: 26/03/2024

Place: UOH, Hyderabad

Prof. P. Prakash Babu

(Supervisor)

26/3/2024

Prof. P. Prakash Babu
Department of Biotechnology & Bioinformatics
School of Life Sciences
University of Hyderabad
Hyderabad-500 046. (T.S.)

Signature

Neera Yadav

Reg. No.: 16LTPH10

University of Hyderabad

(A Central University by an Act of Parliament)

Department of Biotechnology and Bioinformatics

School of Life Sciences

P.O. Central University, Gachibowli, Hyderabad-500046

Date: 14/03/2024

CERTIFICATE

This is to certify that the thesis entitled ***"Mechanism of astrocytoma progression: Role of RAP2B and HIF2A in hypoxia"*** submitted by **Miss Neera Yadav** bearing registration number **16LTPH10** in partial fulfillment of the requirements for the award of Doctor of Philosophy in the Department of Biotechnology and Bioinformatics, School of Life Sciences is a bonafide work carried out by her under my supervision and guidance.

This thesis is free from plagiarism and has not been submitted previously in part or in full to this or any other University or Institution for the award of any degree or diploma.

A. Published in the following journals:

1. **Neera Yadav**, Deepak Babu, Sailaja Madigubba, Manas Panigrahi, Phanithi Prakash Babu, Tyrphostin A9 attenuates glioblastoma growth by suppressing PYK2/ EGFR-ERK signaling pathway, *Journal of Neurooncol.* **2023** Jul 6. doi: 10.1007/s11060-023-04383-7. (Parts of this thesis have been:)

2. Deepak Babu, Anwita Mudiraj, **Neera Yadav**, Chandrashekhar Y. B. V. K., Manas Panigrahi, Phanithi Prakash Babu, Rabeprazole has efficacy per se and reduces resistance to temozolomide in glioma *via* EMT inhibition. *Cellular Oncology* **2021** Aug;44(4):889-905.

Manuscript under preparation:

- **Neera Yadav,** Phanithi Prakash Babu, Prognostic relevance of EGFR/RAP2B/HIF2A co-overexpression in glioblastoma malignancy (In preparation).

- **Neera Yadav,** Phanithi Prakash Babu, Knockdown of RAP2B enhanced anticancer effect of TYR A9 prevents glioblastoma progression by inhibiting $CoCl_2$ induced pFAK/pPYK2-EMT signaling pathway (In preparation)

- **Neera Yadav,** Phanithi Prakash Babu, $CoCl_2$ induced RAP2C/HIF2A promotes glioblastoma growth through AKT/GSK3β-EMT signaling pathway prevented by Tyrphostin A9 (In preparation).

B. Presented in the following conferences:

1. Participated in AS-UOH Joint workshop on Frontiers in Life Science held at School of Life Sciences, University of Hyderabad on 16-17th Sept. 2016.

2. Participated in The International Congress of Cell Biology Joint meeting of ISCB, APOCB and IFCB Centre for Cellular and Molecular Biology, Hyderabad 27nd-31st JAN 2018

3. Presented poster entitled in Clinical significance of Cortactin (CTTN) in human astrocytoma in 31st annual meeting of Society for Neurochemistry India national level conference in BHU September 20-22, 2017.

4. Presented poster entitled 'The clinical and functional importance of RAP2B gene in astrocytoma growth and malignancy' in 33rd annual meeting of Society for Neurochemistry India national level conference in BHU 10th-12th October 2019.

5. Participation Certificate on the topic of brain diseases, Injuries and Infections: Emerging Challenges and Treatment Strategies in 34th annual meeting of Society for Neurochemistry India national level conference in University of Hyderabad 11-13th December 2020.

6. Presented Oral presentation entitled in Downregulation of RAP2B promotes human astrocytoma inhibited by the involvement of oncogenic mi-RNA in Neuro-Oncology and Brain Tumor (Neuro Oncology 2020) 20-June-2021.

7. Presented poster entitled in Downregulation of RAP2B promotes human astrocytoma inhibited by the involvement of oncogenic mi-RNA in ISNOCON 2021 12th Annual Conference of Indian Society of Neuro-Oncology.

8. Participation Certificate on the topic of Neurodegeneration and Cognition Recent Advances in Neurological Diseases in 35th annual meeting of Society for Neurochemistry India national level conference in University of Hyderabad 2-4th December 2021.

Furthermore, the student has completed the following courses to fulfill the coursework requirement for the Ph.D.

Course Code	Name	Credits	Pass/Fail
BT -801	Analytical Techniques	4	Pass
BT -802	Research ethics, Data Analysis, and Biostatistics	3	Pass
BT -803	Lab Seminar and Record	5	Pass

23-03-2024

Prof. P. Prakash Babu

Supervisor

Dept. of Biotechnology and Bioinformatics

Prof. P. Prakash Babu
Department of Biotechnology & Bioinformatics
School of Life Sciences
University of Hyderabad
Hyderabad-500 046. (T.S.)

23/3/24

Head

Dept. of Biotechnology and Bioinformatics

HEAD
Dept. of Biotechnology & Bioinformatics
University of Hyderabad
Hyderabad.

23/3/24

Dean

School of Life Sciences

संकाय सचिव / Dean
जीव विज्ञान संकाय / School of Life Sciences
हैदराबाद विश्वविद्यालय / University of Hyderabad
हैदराबाद / Hyderabad-500 046.

This work is dedicated to my beloved parents whose patience and sacrifices will remain my inspiration throughout my life.

Acknowledgements

First and foremost, I would like to thank my supervisor, ***Prof. P. Prakash Babu****, for allowing me to work on an exciting aspect of cancer biology. His constant support, stimulating guidance, and encouragement enabled me to complete research work successfully. I am thankful to him for being open to new ideas and for the freedom he provided me to carry out my research work.*

I am grateful to the doctoral committee members ***Prof. KPMSV Padmasree*** *and* ***Dr. Insaf Quresi*** *for their constant support and valuable suggestions during the entire thesis work.*

Dr. Manas Panigrahi, Dr. Chandrasekhar Y.B.V.K (Department of Neurosurgery), Dr. Satish Rao*, and* ***Dr. Sailaja*** *(Department of Pathology) are highly acknowledged for providing clinical samples from Krishna Institute of Medical Sciences for the research work.*

I want to thank the present and former Heads of the Department of Biotechnology and Bioinformatics and current and former Deans of the School of Life Sciences for providing the Departmental/School facilities.

I am thankful to all the non-teaching staff of the department and school, especially Mr. Rajshekhar, Mr. Shekhar, and our lab assistant, Mr. Muthyam, for their help in doing all the official work.

Dr. Anwita Mudiraj, Dr. Deepak Babu, and Dr. Ranjana Singh must be specially acknowledged for their constant support and guidance during my PhD.

All the present and former members of the Neuroscience laboratory are highly appreciated for creating an excellent environment in the lab and outside, which has helped me be stress-free throughout my stay in Hyderabad. The senior lab members, Dr. Prabhaker, Dr. Noble, Dr. Apoorv, and Mr. Kartik, have been so great from the very first day that I never felt new to the group and have trained me in different ways, which helped me to carry out my research in the lab. I want to thank the Postdoctoral fellows of the lab, Dr. Vimal Pandey and Dr. Parimala, for their help and guidance during this work. I express my heartfelt gratitude to Dr. Sireesh, Dr. Ravindra, Dr. Deepak Babu, Dr. Praveen, Dr. Naidu, Dr. Nikhil, Dr. Kishore, Ms. Shubhangi, Mr. Rahul Ms. Shailja, Ms. Mansi, Ms. Sheetal, Ms. Jhansi, Mr. Nishant, Ms., Gulshan and Ms. Pooja for helping me one way or the other during this work.

Dr. Anita, Dr. Anju, Dr. Ranjana, Ms. Priya, and Ms. Rashmi need a special mention for their help in my work as well as being part of all our fun time. I express heartfelt thanks to them.

Acknowledgments

I must thank my friends, Mr. Yogesh Patidar, Miss Shubhangi, Miss Lekha, Miss Mahati, Mr. Salam, Mr. Santosh, and Miss Arpita Sagar, for their constant help and support. I express gratitude to them for always being there for me.

I am indebted to my friend Miss Anita for all the fond memories and for always standing by my side and sharing a great relationship as a compassionate friend. I will always cherish the warmth she showed me.

I am extremely blessed to have a lovely family and would like to thank all, especially my parents, for their infallible love, care, and faith in me, which has always boosted me and helped me carry out my work on a positive note.

A special gratitude to my sisters, Miss. Manisha, Miss. Dolly, and brothers, Mr. Brijesh, Mr. Umesh, Mr. Akhilesh, Manish and my nephew Myansh for their love and affection.

I sincerely thank my life partner, Dr. Sanjay Yadav, for his support and encouragement.

I want to thank everyone for the slightest help they would have given during the entire work. I want to thank Department of Science & Technology (DST-India), Department of Biotechnology (DBT-India), Indian Council of Medical Sciences (ICMR-India) and University with potential for excellence (UPE-India) for funding support to the lab. UGC-CSIR is highly acknowledged for its financial support as a Junior and Senior research fellowship.

Last but the most important one, all that I cherish today is the grace of God. I thank the Almighty for granting me strength, wisdom, and knowledge, and showering his blessings.

Neera Yadav

Chapter 4

Tyrphostin A9 attenuate glioblastoma growth by suppressing PYK2/ EGFR-ERK signaling pathway

Chapter 5

To study the anticancer efficacy and protective role of TYR A9 in the cognitive assessment by targeting RAP2B/HIF2A/pPYK2-EMT signaling in glioma rat hypoxia vs normoxia.

List of Tables

Abbreviation

AO	Acridine Orange
ASR	Age-standardized incidence or mortality Rate
BBB	Blood-Brain Barrier
Bcl-2	B-cell lymphoma protein-2
Bax	Bcl-2 associated X protein
BSA	Bovine Serum Albumin
cDNA	complementary DNA
CNS	Central Nervous System
CTNNB1	Catenin beta 1
$CoCl_2$	Cobalt Chloride
CST	$CoCl_2$+siRAP2B+TYR A9
CON	Control
VCON	Vehicle Control
DAPI	4',6-diamidino-2-phenylindole
DCFDA	2',7'–Dichlorofluorescein diacetate
DMSO	Dimethyl Sulfoxide
ECL	Enhanced chemiluminescence
ECM	Extracellular matrix
EDTA	Ethylene diamine tetra acetate
ERK	Extracellular signal-regulated kinase
EGF	Epidermal growth factor
EGFR	Epidermal growth factor receptor
EMT	Epithelial to mesenchymal transition
EtBr	Ethidium Bromide
FACS	Fluorescence-activated cell sorting
FAK	Focal Adhesion Kinase
FITC	Fluorescein isothiocyanate
GAPDH	Glyceraldehyde-3-phosphate dehydrogenase
GBM	Glioblastoma multiforme

GFP	Green fluorescent Protein
GFAP	Glial fibrillary acidic protein
GIC	Glioblastoma-initiating cells
GSK3β	Glycogen synthase kinase 3β
G2	Grade 2
G3	Grade 3
G4	Grade 4
HIF	Hypoxia-inducible factor
HIF2A	Endothelial PAS domain protein 1
H&E	Haemotoxylin and Eosin
HGG	High-grade glioma
IDH1	Isocitrate dehydrogenase 1 (NADP+), soluble
IP	Intra-peritonial
IF	Immunofluorescence
IHC	Immunohistochemistry
ING4	Inhibitor of growth protein 4
JC-1	Tetramethyl rhodamine methyl ester
LGG	Low-grade glioma
MAPK	mitogen-activated protein kinase
MMP-9	Matrix Metalloproteinase-9
MTT	(3-[4,5-dimethylthiazol-2-yl]-2,5 diphenyl tetrazolium bromide
NaCl	Sodium Chloride
NC	Nitrocellulose Membrane
NOX2	NADPH oxidase 2
OD	Optical Density
PARP	Poly (ADP-ribosyl) polymerase
PAGE	Polyacrylamide gel electrophoresis
PBS	Phosphate Buffered Saline
PCNA	Proliferating cell nuclear antigen
PI	Propidium iodide
PI	Protease inhibitor
PFA	Paraformaldehyde

PH	Pulmonary hypertension
PMSF	Phenylmethylsulphonyl fluoride
PYK2	Proline-rich tyrosine kinase 2
RAP2B	Member of RAS oncogene family
RNase	A Ribonuclease A
RIPA	Radioimmunoprecipitation assay
ROS	Reactive oxygen species
RPM	Revolutions Per Minute
RT-qPCR	Reversed transcribed-quantitative PCR
Snail	Snail family transcriptional repressor 1
SDS	Sodium Dodecyl Sulfate
siRNA	small interference RNA
TAM	Tumor-associated microenvironment
TBST	Tris-buffered saline Tween® 20
TCGA	The Cancer Genome Atlas Program
TFs	Transcription factors
TICs	Tumor initiating Cells
TMZ	Temozolomide
TKI	Tyrosine Kinase Inhibitor
TYR A9	Tyrphostin A9
VIM	Vimentin
VEGF	Vascular endothelial growth factor
WHO	World Health Organization
Wt	Wild type

CHAPTER 1

Introduction

1.1 General Introduction

Cells are abruptly involved in uncontrolled cell growth and division. It acquires persistent proliferation through autocrine and paracrine signals in various alternative pathways [1, 2, 3]. Uncontrolled cell growth and division lead to the formation of a solid lump or tumor known as a cancer cell (The Hallmarks of Cancer). Cancer cells can be of two types: Benign and Malignant tumors. Benign tumors spread gradually with distinct borders and do not invade neighboring tissues or other body parts, whereas malignant tumors spread quickly and develop into local or distant metastasis **(Figure 1)**.

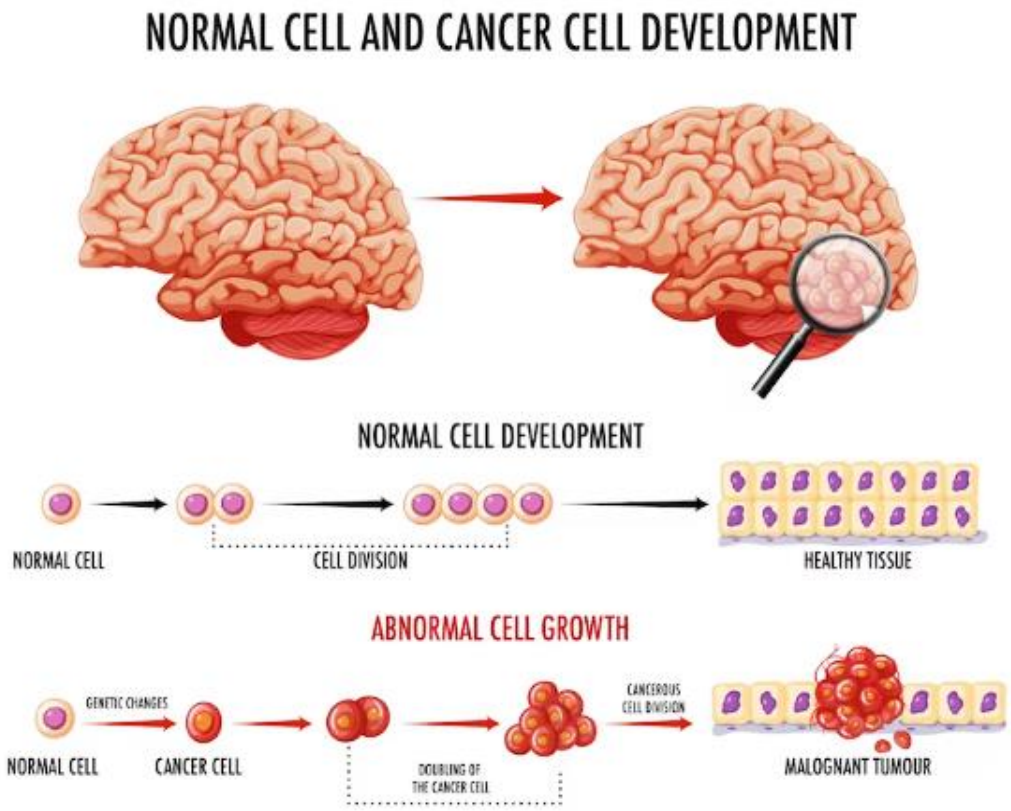

Figure 1: Schematic diagram represents benign and malignant tumors that proliferate, show irregular boundaries, invade surrounding tissue and spread to other body parts that develop metastasis [1].

The primary factor of mortality in cancer is metastasis, which is a hallmark of the tumor. The characteristics of cancer cells are colonizing, invading, and helping in communication with the tumor microenvironment. The molecular mechanisms underlying the metastasis process must established to find a therapeutic approach for effective interventions. Cancer cells disseminate into the bloodstream and reach another site of the body through circulation, where they adapt new biological conditions and

tolerate blood vessel pressure to develop metastasis [2], [3]. The term "metastasis" refers to the growth of secondary tumors away from the primary tumor site of the body [4]. **Figure 2** depicts metastasis and highlights key ideas that help to shape this characteristic feature of cancer [5].

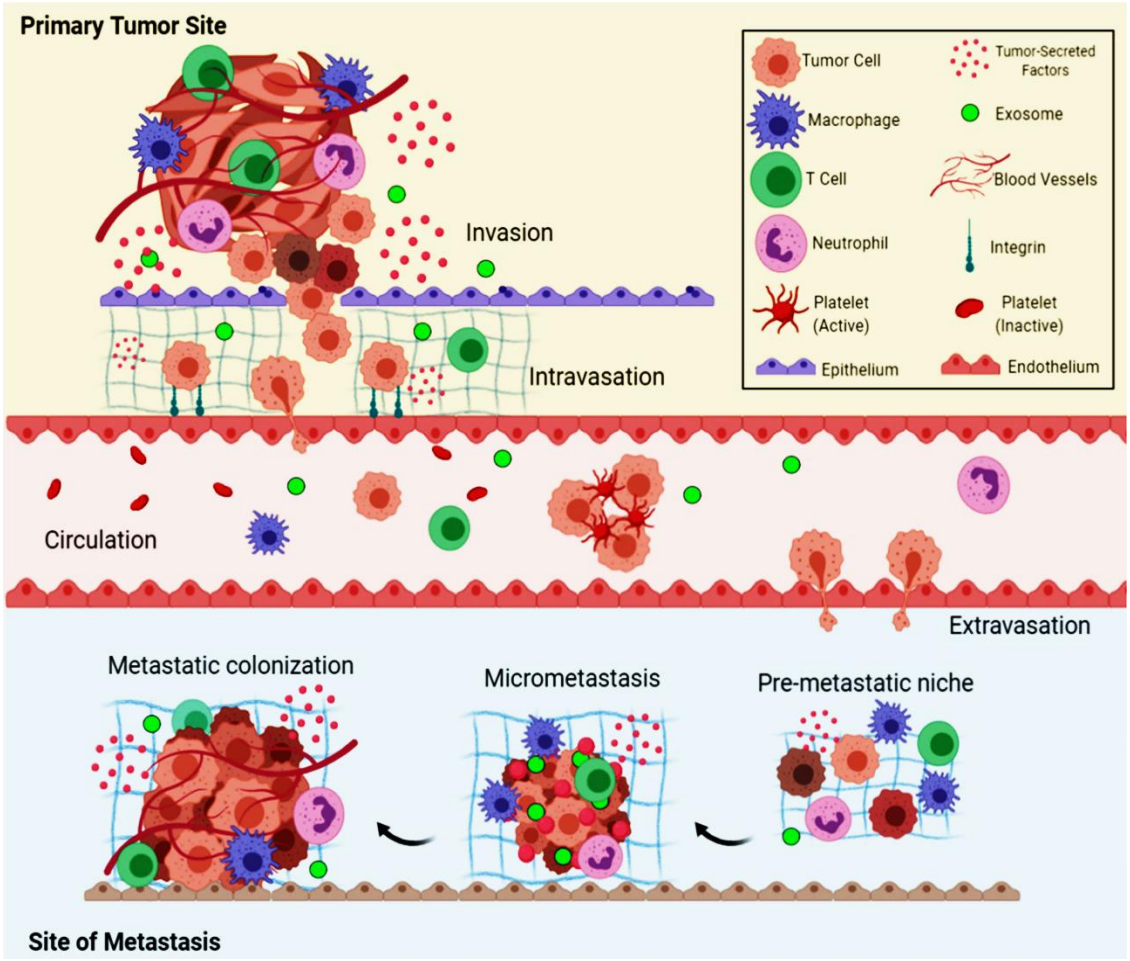

Figure 2: Overview of the metastatic cascade: The five essential stages of metastasis consist of invasion, intravasation, circulation, extravasation, and colonization [5].

1.2. Brain tumors

The primary component of the brain is the central nervous system, which is responsible for the overseeing and processing of the body function. Brain tumors occur when abnormal cells develop solid tumor mass [6]. Depending on the size of the tumor and the area of the brain affected, it causes a variety of symptoms such as chronic headaches, lightheadedness, dizziness, fainting, exhaustion, appetite loss, irritability, behavioral changes, difficulty of focus, changes in eyesight, seizures, vomiting, and mental abnormalities

and other symptoms are among them [7]. Depending on the type of cells **(Figure 3)**, tumors are broadly categorized based on the type of cells from where they originated.

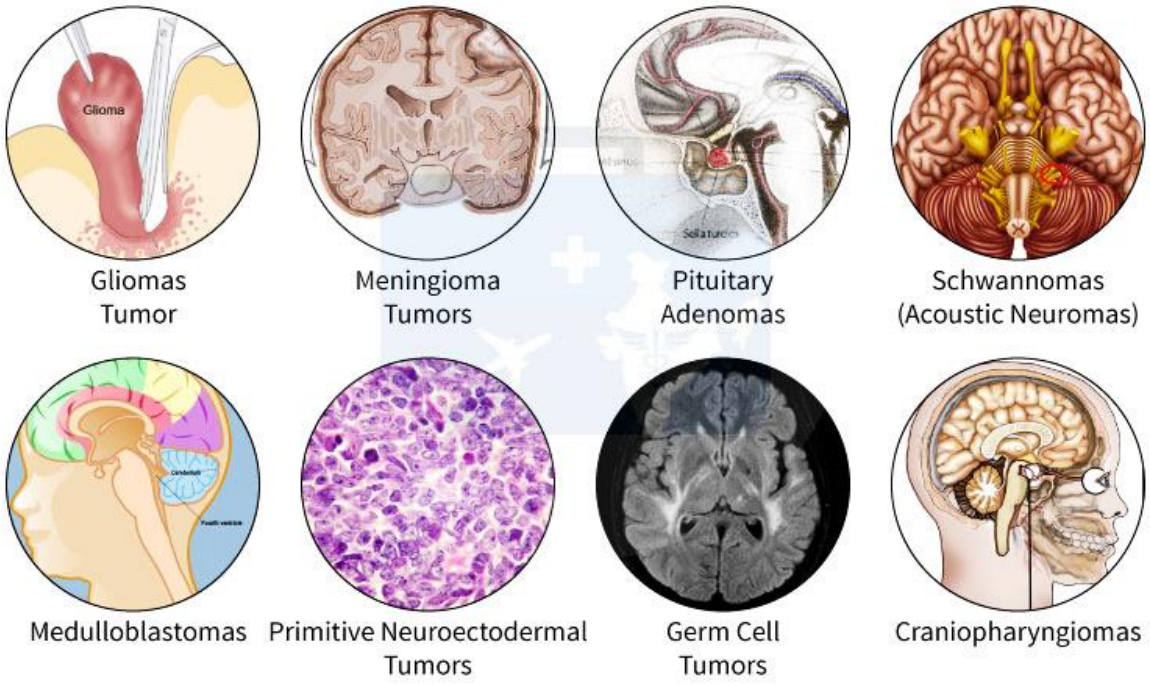

Figure 3: Different types of tumors in the adult brain and spinal cord: Brain tumors are also frequently graded to compare and categorize the severity of tumors within cell type to determine the best possible treatments (source: American Association of Neurological Surgeons).

1.2.1. Glioma

Gliomas represent the most common brain tumor of the central nervous system produced by the brain's glia or supporting cells. They account for about 78 percent of malignant brain tumors predominantly affecting adults. Glioma affects about 40% more in men than women. Analysis of incidence rate temporal patterns of high-grade versus low-grade gliomas in adults aged 15 to 44 revealed a close convergence of their occurrence rates [8]. Previously described the clinical characteristics, imaging results, and molecular profiles of adult-type diffuse gliomas [9]. Gliomas are estimated to have an annual incidence of 6 cases per 100,000 people worldwide, with non-Caucasian populations having a much lower prevalence, particularly for glioblastoma [10], [11]. These tumors have traditionally been grouped according to their histological characteristics like other tumors. However there has been a paradigm shift due to the enormous progress made in cancer genomics, and molecular profiles are now starting to be included in diagnosing gliomas [12], [13].

1.2.2. Classification of gliomas based on World Health Organization (WHO)

The majority of primary brain tumor fatalities are caused by gliomas, which comprise about 30% of all primary brain tumors and 80% of all malignant ones **(Figure 5)**. According to histological classification, gliomas are divided into astrocytoma, oligodendrogliomas, mixed oligoastrocytic gliomas, or ependymoma based on morphological resemblances to the neuroglial cell types present in the brain [14], [15], [16], [17]. The most extensively used approach for classifying CNS tumors is the WHO classification, which is present in its 5th version. The 5th edition (2021) improves upon the previous one by giving more weight to molecular markers when it comes to classification and grading, with the majority of improvements made in the cIMPACT-NOW publications [18].

The 2021 WHO classification identified IDH-mutant astrocytoma as one form and falls into one of three WHO grading categories: 2, 3, or 4 and replaces terminology like "anaplastic astrocytoma" with the grading of tumors inside tumor types. The 5th version of the WHO classification glioma mainly occurs as astrocytoma, which is further classified into four grades based on histopathology and molecular markers **(Figure 4A, B)** such as:

1. **Pilocytic astrocytoma Grade 1 (WHO grade 1):** It exhibits proliferative potential with the possibility of a cure after resection with a proper diagnosis known as a benign tumor, which shows the best prognosis and survival.
2. **Diffuse astrocytoma Grade 2 (WHO grade 2):** It is infiltrative with low proliferative potential, possibility of recurrence associated with hypercellularity, and progresses to higher malignant grades, and survival period of 5 to 8 years.
3. **Anaplastic astrocytoma Grade 3 (WHO grade 3):** Histological data reveals a high rate of hypercellularity, malignant, nuclear atypia, and increased mitotic activity, and a survival time of 3 years.
4. **Glioblastoma Grade 4 (WHO grade 4):** It is the most malignant brain tumor with histological evidence of malignancy, very high rate of hypercellularity, high mitotic activity, vascular proliferation, prone to necrosis, and survival time of 12 to 15 months.

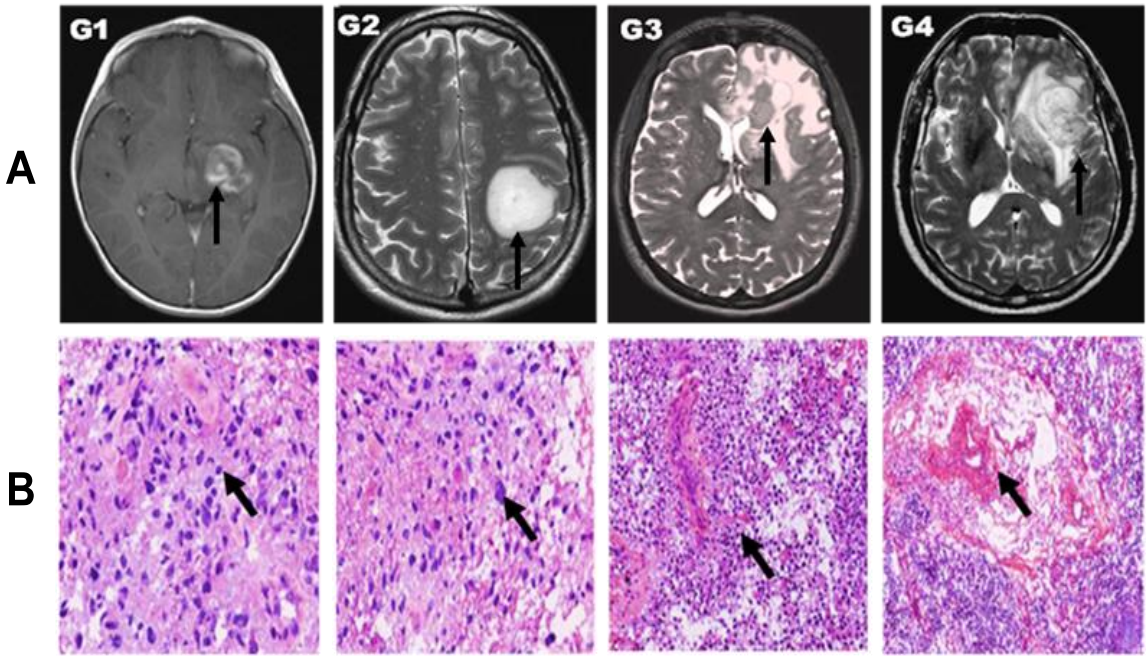

Figure 4: Typical histological features of astrocytoma grades represented by **(A)** MRI images and **(B)** histopathological images showed by H&E staining [19].

In India, the occurrence of CNS tumors ranges from 5 to 10 cases per 100,000 people, showing upward trajectory, and constitutes 2% of all malignancies [20]. Prospective scrutiny is conducted on hospital-based databases that documented CNS malignancies. The data are collected from registrations in the neuro-oncology clinic of a tertiary care center over a span of one year [21]. Astrocytomas, containing 38.7% of cases, stand out as the most widespread primary brain tumors with high-grade gliomas detected 59.5% in the majority of cases. According to reports, subependymal giant cell astrocytoma and pilocytic astrocytoma are the two most common low-grade astrocytic tumors. Similar findings were appeared from a South Indian tertiary care facility with 15 years of experience and 1043 patients [22]. 47.3% of astrocytoma, 11.4% medulloblastoma, 9.7% craniopharyngioma, 4.8% ependymal tumors, and 4.1% nerve sheath tumors are the five most prevalent tumors shown in **(Figure 5)**.

International Association of Cancer Registries (IARC), India records more than 28,000 cases of brain tumors each year, with greater than 24,000 fatal cases. IDH mutation is the most recent classification of astrocytic tumors comes under single diagnosis **(Figure 5)**. These IDH mutant astrocytomas are now categorized into grades 2, 3, and 4 based on histopathological and molecular analysis [23], [24].

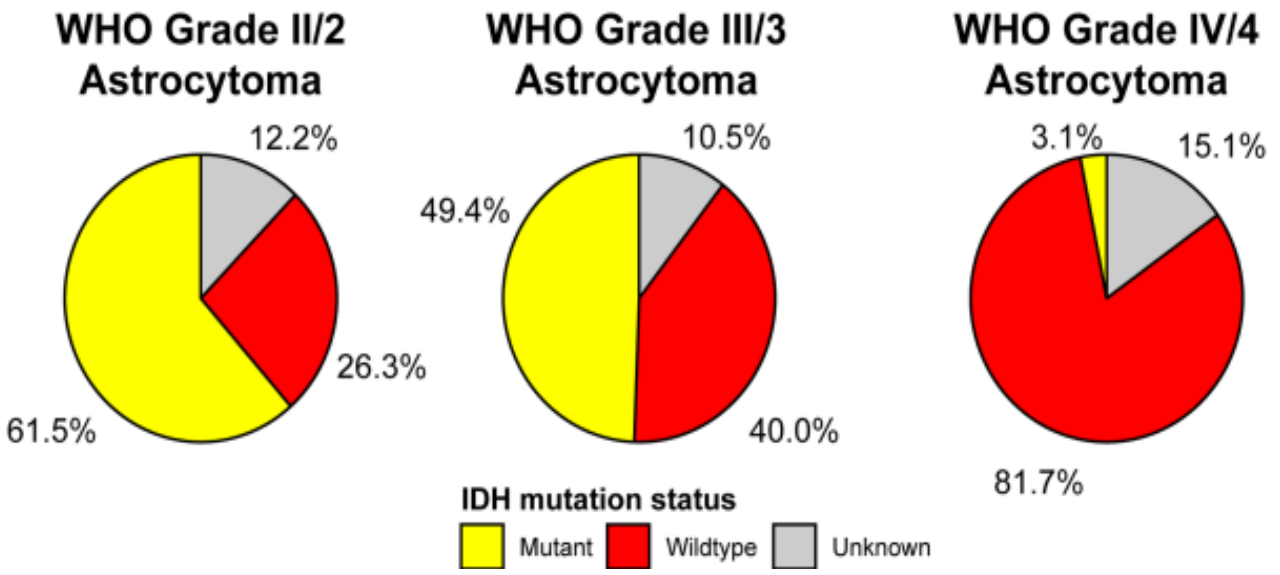

Figure 5: Frequency of IDH mutation by WHO grade for selected astrocytoma histopathologies, CBTRUS Statistical Report: US Cancer Statistics – NPCR and SEER, 2018-2019.

IDH-mutant astrocytomas **(Figure 6)** are graded using both histological characteristics and molecular markers **(**WHO classification of CNS tumors, 5th version 2021) [13]. Grade 2: Well-differentiated cells with minimal necrosis or microvascular proliferation, modest mitotic activity, and no CDKN2A/B homozygous deletion. Grade 3: It is characterized by lack of CDKN2A/B homozygous deletion, anaplasia, considerable mitotic activity, and no necrosis or microvascular proliferation; Grade 4: Necrosis, microvascular proliferation, or homozygous CDKN2A/B loss [18]. At the same time, diffuse astrocytoma with IDH wild-type (IDH wt) shown in **(Figure 6)**, is an uncommon group of tumors with heterogeneous molecular characteristics, clinical features, and dismal prognosis. The cIMPACT-NOW Consortium for the taxonomy of primary brain tumors indicates that IDH wt is present in a particular group of patients who display genetic mutation such as EGFR amplification, 7q gain/10p loss, and pTERT mutation associated with GBM. Diffuse lower-grade gliomas and diffuse astrocytic gliomas are WHO grades 2 and 3, IDH wt with molecular features of GBM, [25].

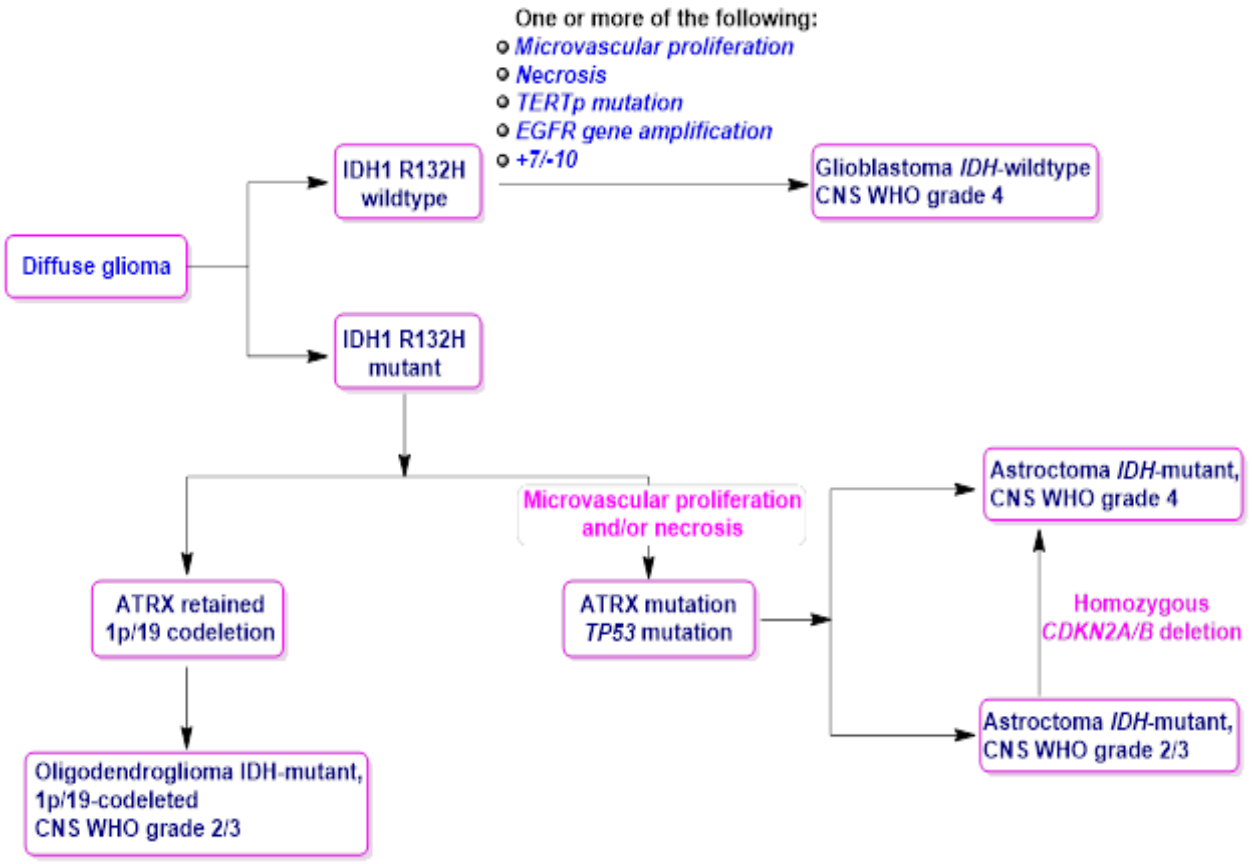

Figure 6: Astrocytoma grades WHO classification based on molecular genetic characteristics [18].

1.2.3. Global incidences of brain tumors

The statistics from the Central Brain Tumor Registry of the United States reveals that the overall incidence of malignant brain tumors in individuals of all ages has experienced a yearly decline of nearly 0.8% from 2008 to 2017 [26]. Whereas it has increased in nonmalignant tumors [27], the incidence of brain tumors between 2014 and 2018 is 24.25 per 100,000, including 7.06 per 100,000 malignant brain tumors and 17.18 per 100,000 nonmalignant ones [28]. The global occurrence of brain tumors has increased by approximately two times in the last 15 years (14.4/100,000) [29]. There will be 88,190 recent cases of brain and other CNS tumors detected in Americans by 2021, including 25,690 aggressive and 62,500 benign tumors of the brain [28]. Only around one-third of brain tumors are malignant, but they account for the majority of disease-related deaths. The average number of deaths from primary malignant brain tumors and other CNS tumors each year is 16,606. Among these death rate, gliomas contribute to 78.3% with GBM representing more than 50% of the glioma-related deaths. Males were more likely to be diagnosed with malignant brain tumors than females (8.28/100,000 *vs*. 5.98/100,000),

but the reverse for nonmalignant tumors (13.07/100,000 *vs*. 20.97/100,000) [28]. Gender disparities in malignant brain tumors progressively emerged above 40 years of age. Glioblastoma multiforme, diffuse astrocytoma, and other gliomas exhibit a higher incidence rate among males compared to females. Among different racial groups, black demonstrates the highest morbidity for benign brain tumors at a rate of 20.14 per 100,000, whereas white exhibits the highest morbidity for malignant brain tumors with a rate of 7.55 per 100,000 [28].

1.2.4. The current standard of care for glioma

Glioblastoma (GBM) is the primary brain tumor that most frequently affects people. However, optimal multidisciplinary treatment consists of maximal surgical resection, followed by radiation therapy plus concurrent and maintenance temozolomide (TMZ) [30]. Subtotal gross total resection, concurrent radio-chemotherapy at a dose of temozolomide (TMZ), localized radiation therapy to the tumor site, and tumor treating areas should be typical therapies for HGG, such as GBM [31], [32]. Even though MGMT promoter methylation predicts TMZ response, it only influences the first line of treatment in GBM patients, but no standard of care exists in the recurrent setting. Without standard therapeutic involvement, all cases of GBM will certainly progress or relapse into recurrent GBM (rGBM).

Additionally, the progression-free survival (PFS) in GBM from bevacizumab, a VEGF (vascular endothelial growth factor) antagonist approved by the US Food and Drug Administration's (FDA) bevacizumab for rGBM [33], [34]. As soon as possible, surgically removed tumors further prevent the development of malignant tumors. Regular treatment associated with supportive care for GBM patients are the prevailing standard of care for GBMs [35]. Despite various treatment approaches, effective therapies for GBM pathogenesis are still lacking because of the small sample size and heterogeneity. Therefore, there is a need to focus on maintaining and improving the patient’s quality of life and increasing survival [36].

1.2.5. Glioma risk factors

Although current research on risk factors due to environment and genes for brain and other CNS malignancies are still lacking significant findings, but some gene regions and uncommon genetic variants may increase the risk of numerous brain tumors [40]**.** Endogenous variables such as allergies, head injuries, virus infections, and others were also examined [41, 42]. The only identified environmental risk factor for brain cancers are ionizing radiation. Numerous reports have demonstrated that low-dose treatment radiation increases the incidence of multiple types of brain tumors, such as gliomas,

meningiomas, and nerve sheath tumors. The risk of ionizing radiation was higher for young individuals with gliomas [43]. However, it remained unclear how exposure of diagnostic radiation may affect brain tumors [44]. Appropriate nutrition practices could prevent 30–50% of cancers, however their impact on brain malignancies has yet to be completely elucidated. Brain tumors were frequently thought to be strongly associated with foods high in precursors of N-nitroso compounds (like nitrite) and antioxidants (such as vitamins) [45, 46]. The most recent meta-analysis examined 12 different dietary classes and discovered the vegetables and tea protected against glioma. However, consuming too many grains and processed meat considerably raised the risk [46]. When viewed as a whole, the mediterranean diet plan demonstrated a greater influence in brain tumors, according to the large prospective cohort study, which did not find a relationship between any particular food group and these malignancies [47].

1.3. Glioblastoma

Glioblastoma is a highly invasive and aggressive type of brain tumor because of the complexity and difficulty of removing all tumor cells and ensuring recurrence. It rarely develops in the cerebellum, brainstem, or spinal cord; instead, it is mainly found in the cerebral hemispheres of the brain, especially in the frontal and temporal lobes [48]. GBM cells can infiltrate normal brain tissue by degrading the extracellular matrix (ECM), penetrating the parenchyma and the perivascular space of the brain [49, 50]. For instance, hypoxia impairs antitumor immune responses and promotes resistance to traditional cancer therapy, which is the most dangerous factor in a GBM patient's life. Targeting hypoxia is thus a desirable approach for GBM treatment [51]; only less than 3 to 5% survive longer than five years after diagnosis, which provides a significant therapeutic challenge [31].

1.3.1. Hypoxia in GBM

The primary cause of mortality and morbidity worldwide is cancer. Based on the latest available data, it revealed that approximately 14.1 million new cases of cancer and 8.2 million related to death [52]. Cancer cells characteristics like uncontrolled cell proliferation, and changes in the tumor microenvironment play an active role in vascular abnormalities and cell invasiveness [53]. It can facilitate angiogenesis, metastasis, and survival in response to various components in the tumor milieu, including pH, growth hormones, O_2 levels, and immune cells [54]. To sustain their survival and development does not appear to be modifying the subjects; tumor cells adapt to their surroundings. Cells that are growing in the absence of O_2 and nutrients create new blood vessels, known as de novo angiogenesis; to fulfill its requirement for survival because of discontinuous endothelium newly generated blood arteries are leaky [55]. Hypoxia is a crucial component for the existence of big tumor masses; the complexity and

variability of the tumor milieu that favor cancer recurrence and growth. Therefore, hypoxia could be an essential target for developing targeted therapy. Tumor-associated microenvironment (TAM) infiltration and tumor core region are significant characteristics in hypoxia to develop resistance to conventional chemotherapeutics. Hence, there is a crucial need to develop innovative therapeutic approaches to target both brain tumor and its surrounding microenvironment.

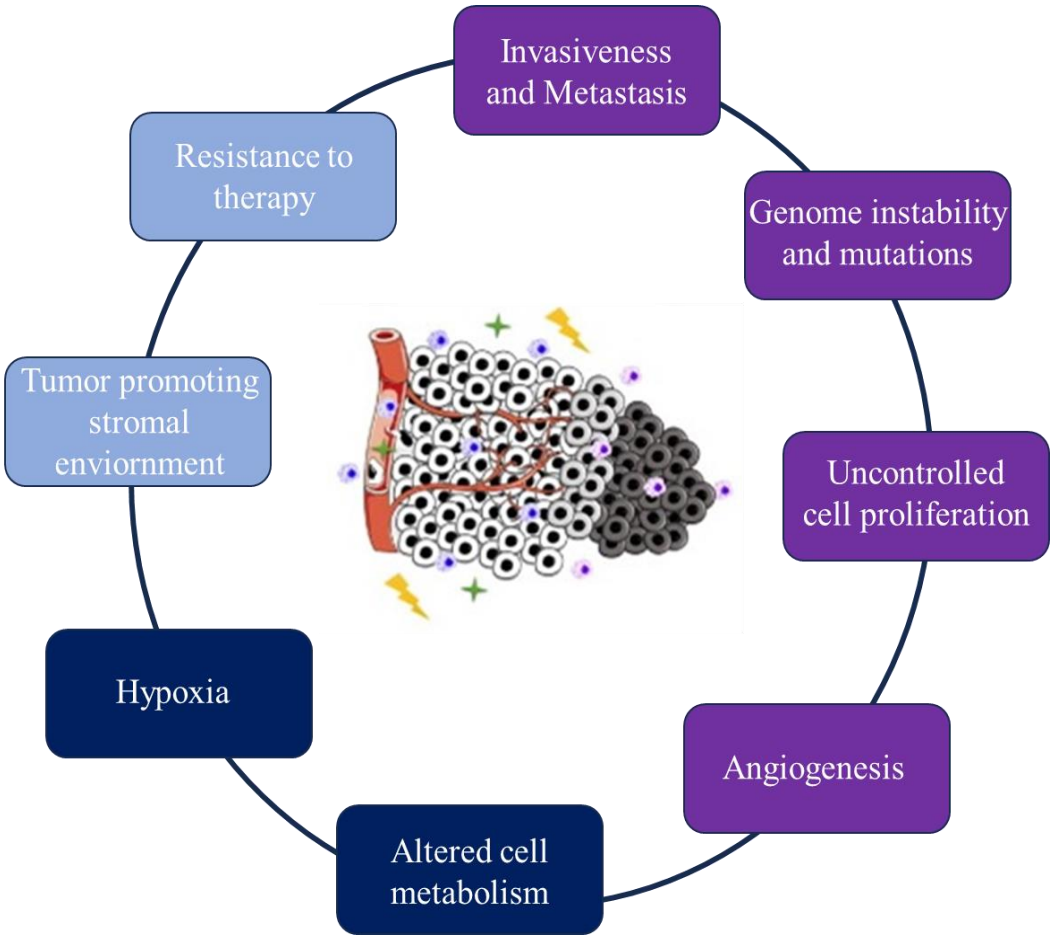

Figure 7: Major hallmarks of GBM: The cancer niche is a complex network of stromal, endothelial, and malignant cells of genomic traits that have evolved to enhance survival and encourage tumor cells to proliferate and metastasize uncontrollably [56].

Hypoxia favors the overall survival of tumors and the development of cancer, suggesting that hypoxia rises as the tumor develops; therefore, cells exposed to chronic hypoxia are more likely to proliferate and survive. Patients with chronic hypoxic tumors are linked to an aggressive phenotype and highly resistant

to therapy, suggesting the clinical importance of hypoxia [57]. Hypoxia-inducible factors (HIFs) are associated with hypoxic tumor microenvironments and frequently overexpressed in solid and metastatic tumors, including head and neck, breast, prostate, colon, lung, and pancreatic cancer. [58]. When oxygen levels are low, HIF-1 expression is induced and moves into the nucleus, acts as a transcription factor and binds to the HIF-1 sequence present in the numerous genes involved in the biology and metabolism of cancer, regulating the proliferative rate, metastasis, and aggressiveness of cancer cells [59, 60].

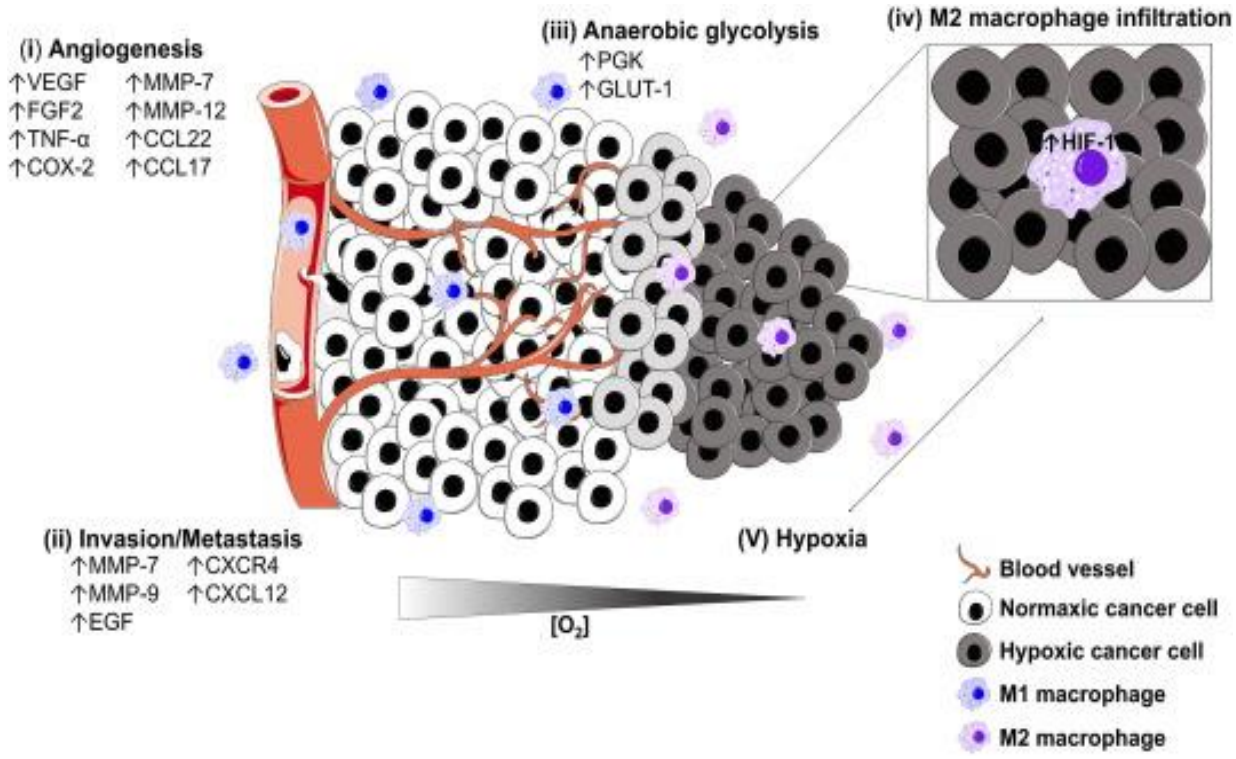

Figure 8: The hypoxic environment of tumor and role in oncogenesis: Deprivation of oxygen in the tumor core has been linked to tumor development and poor prognosis. Upregulation of HIF-1 has shown to enhance the expression of many cancer-related markers [37].

Glioblastoma tumors are highly vascular brain tumors with extremely dismal prognosis. Hypoxia is one of the significant characteristics of malignant GBM; the principal adaptive cellular response to a hypoxic environment is the upregulation of hypoxia-inducible transcription factors (HIFs). Similar to HIF1, HIF2 has also been extensively investigated in hypoxic cancer; HIF2 represents a more potentially targeted approach in glioblastoma due to their appearance in glioma stem cells. Expression and activation of

HIF2A display a role in stimulating angiogenesis signaling pathways through triggering oncogenes and suppressing tumor-suppressor genes in GBM [61, 62, 63, 64, 65, 66].

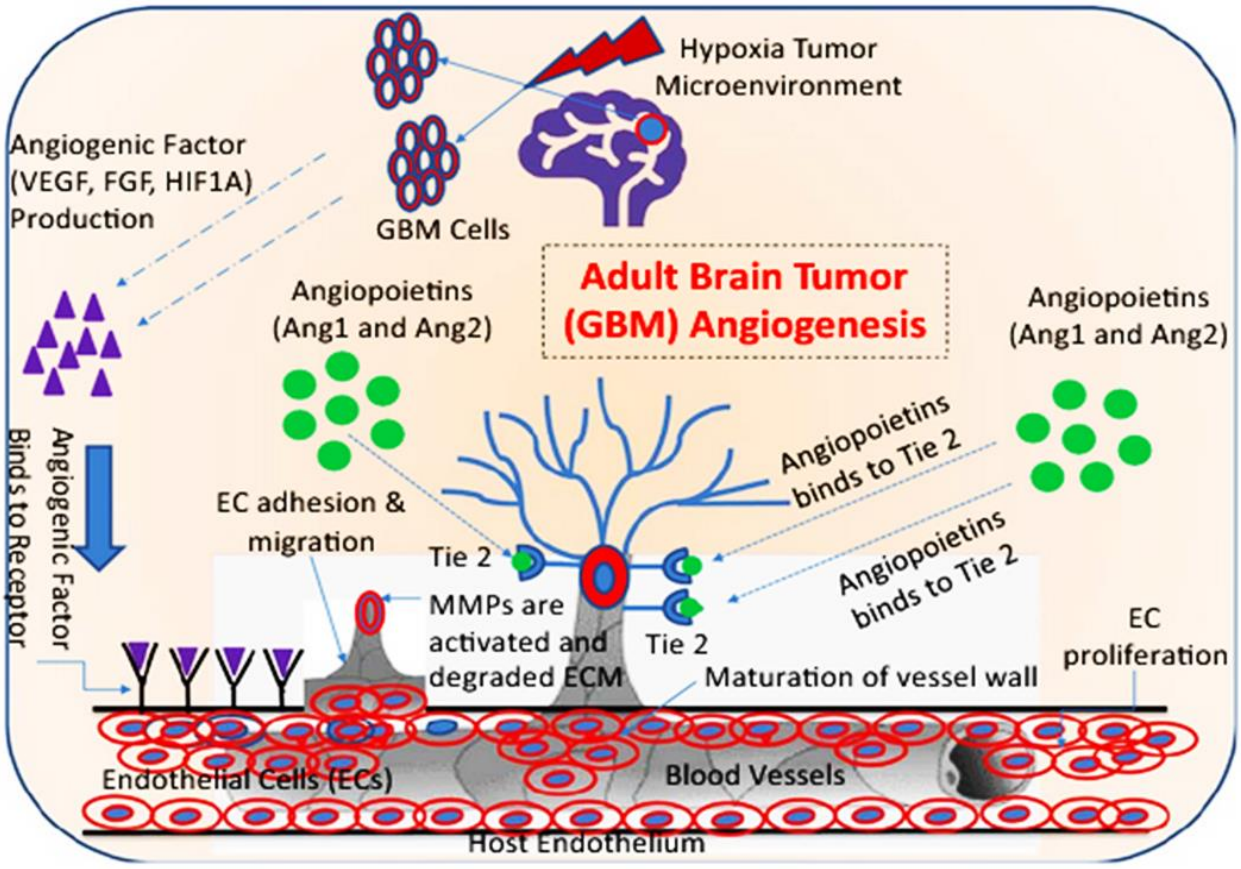

Figure 9: Schematic representation of angiogenic events in GBM: Angiogenesis processes are initiated by the angiogenic factors released from the GBM cells in the hypoxic tumor microenvironment [38].

1.3.2. RAP2B

RAP2B, a member of the Ras oncogene family known to induce tumorigenesis and are highly upregulated in various cancers [67]. The Rap family shares a 50–60% sequence homology with the Ras proto-oncogene family. RAP2B displayed approximately 50% identity with classical Ras proteins. It has three distinct regions: the effector domain responsible for interacting with downstream effector, a nucleotide-binding domain interacts with GTP and GDP, and the C-terminal contains a tetrapeptide motif responsible for sequential post-translational modification is required to trigger trans-localization to the plasma membrane. The Rap2 subfamily includes the members of RAP2A, RAP2B, and RAP2C [68].

RAP2A and RAP2B proteins have 90% and 70% of the same amino acid sequence [69]. RAP1B and RAP2B are the only two Rap family GTPases significantly expressed in circulating human platelets that encourage lung cancer and renal carcinoma cells to migrate, multiply, and invade [70, 71].

Figure 10: RAP2B structure: RAP2B is made up of three well-defined domains: the nucleotide-binding region (amino acids 11-148), the effector domain (amino acids 32-40), and the C-terminal CAAX motif (amino acids 179-183) [72].

1.3.2.1. RAP2B functions

RAP2B, a small guanosine 5′-triphosphate (GTP)-binding protein is widely up-regulated in many tumors. RAP2B activities GTPase is primarily controlled by guanine nucleotide exchange factors (GEFs) [72] that promote the GTP-bound active state and GTPase-activating proteins (GAPs) that enable the GDP-bound inactive state. The specific effects of RAP2B can affect multiple cancer-associated cellular processes, including cytoskeleton reorganization, proliferation, migration, and inflammation [73, 74, 71, 75]. RAP2B signaling is used FAK as a downstream target and stimulates FAK-phosphorylation to activate EMT and promote prostate cancer and hepatocellular carcinoma cells progression [72, 76, 77, 78]. RAP2B promotes lung cancer cell motility, invasion, and migration by enhancing the activity of the matrix metalloproteases-2 enzyme. RAP2B overexpression might increase the phosphorylation level of the extracellular signal-regulated protein kinases 1/2 [71]. RAP2B high expression contributes to lung carcinogenesis by activating the NF-κB pathway [79], suggesting that RAP2B may be a possible therapeutic target for various cancers.

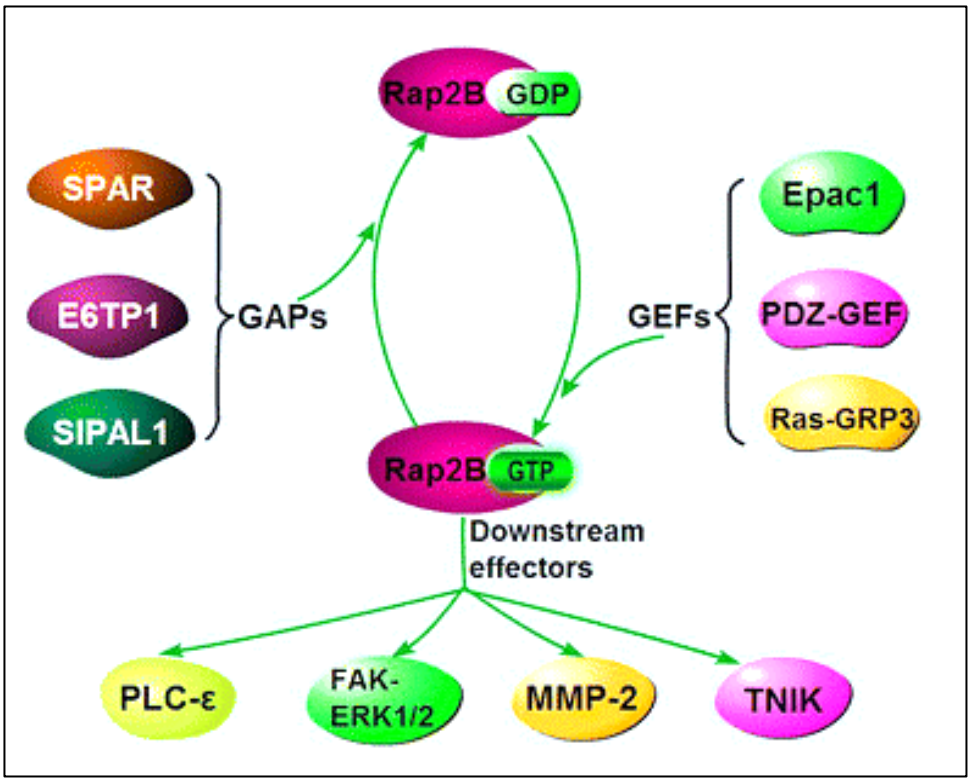

Figure 11: RAP2B activity is controlled by GTPase-activating proteins (GAPs), guanine nucleotide exchange factors (GEFs), and their downstream effectors.

1.3.3. HIF2A

HIF2A overexpression is significantly associated with high grades of astrocytoma and poor patients' survival [80]. HIF2A has a crucial role in the maintenance of hypoxia-driven stem cells, which support GIC self-renewal, growth, and tumorigenicity, and the expression of HIF2A is inversely correlated with glioma patient survival [81]. Hypoxia-regulated transcription factor HIF2A plays a role in stem cell maintenance [81]. The first HIF2 inhibitor, Welireg, is developed by Merck as a novel cancer medicine approved by US FDA for treating tumors linked to the VHL syndrome. There were no systemic treatments authorized for the treatment of VHL-related tumors before Welireg. Patients receiving Welireg for VHL-related tumors showed high response rates and long-lasting responses [82, 83]. The proliferation, metastasis, apoptosis, drug resistance, angiogenesis, stemness, and metabolism of gastric cancer cells are all controlled by HIF, which impacts how the disease progresses [84]. We eagerly await the day when researchers find HIF-targeting medications that could be clinically effective for treating cancer.

1.3.4. pFAK/pPYK2

pPYK2 is essential in developing multiple tumor types and crucial for cell migration and invasion [85], [86]. FAK/PYK2 as a downstream effector of the Rap GTPases [87], found in prostate cancer (PC3) and DU145 cells [88]. RAP2B plays an indispensable role in Rap-mediated cellular adhesion and migration. RAP2B overexpression increases the phosphorylation of FAK and promotes in prostate cancer (PCa) cells development. Correspondingly, inhibition of phosphorylated FAK was observed after RAP2B depletion in both PC3 and DU145 cell lines [89]. PYK2 activity correlates with glioma cell migration; however, the intrinsic mechanism of PYK2 activity remains unclear. FAK and PYK2 are associated with poorer overall survival, tumor cell invasion, and proliferation. FAK/PYK2 inhibitors may inhibit recurrent tumor growth after the postoperative phase. To better understand the involvement of RAP2B/HIF2A/PYK2 expression in contributing to EMT activation in GBM cell growth under hypoxia.

1.3.5. EMT Pathway:

Epithelial-to-mesenchymal transition (EMT) is a crucial regulator of this invasive condition in malignant gliomas which strongly linked to GBM malignancy. EMT is a complicated process controlled by multiple transcriptional factors interacting with various signaling pathways. These interactions form a network that enables cancer cells to develop invasive and infiltrative properties, creating a favorable environment for cancer growth [90]. Genetic and epigenetic changes make cancer cells more prone to EMT-inducing signals [91]. Myeloid cells that are either resident or circulatory (such as macrophages or microglia) may migrate into the tumor stroma in gliomas due to inflammatory processes or a hypoxic environment inside the tumor or the surrounding healthy tissues [92]. These cells release various growth factors, such as TGF-β, EGF, PDGF, and FGF-2, which can cause EMT through receptor tyrosine kinases (RTKs). These factors alter the levels of transcription factors required for the initiation of EMT and different proteases that increase invasiveness into the surrounding normal brain [92, 93]. The primary signaling cascade that RTKs can trigger in response to growth stimuli is RAS-RAF-MEK-ERK, generally known as MAPK kinase pathway. Activation of this pathway controls cell motility and invasion while inducing EMT by increasing the expression of EMT transcription factors. Under normal circumstances, glycogen synthase kinase three beta (GSK3β) easily phosphorylates (p) the cytoplasmic-located β-catenin, leading to ubiquitin-proteasome-mediated degradation. However, signaling pathways, including PI3K/AKT and wnt, cause mutations in GSK3β or decrease its activity in various types of cancer, resulting in β-catenin stabilizing and moving into the nucleus, where it binds forces with lymphocytes. Furthermore, the

chronic hypoxic tumor microenvironment can encourage EMT in glioma cells by activating the transcription factors Twist and Zeb through hypoxia-inducing factor (HIF-1) upregulation [90].

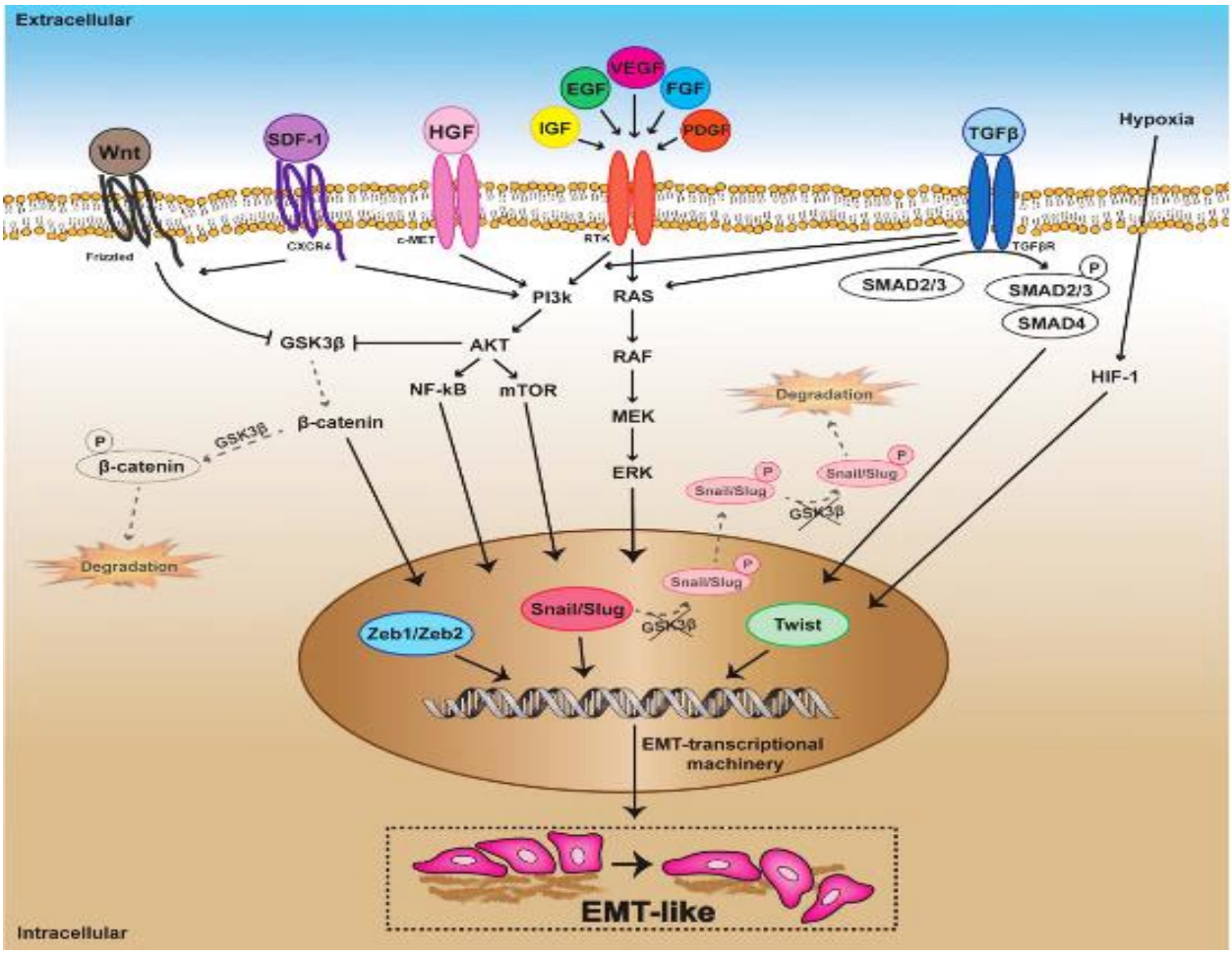

Figure 12: Activation of EMT signaling pathways play role in GBM progression [39].

1.4. Rationale of the present study

Gliomas are brain tumors that infiltrate the surrounding brain tissue profoundly. This fundamental shift is mainly attributable to recognizing that various genetic signatures are associated with multiple clinical outcomes. This represents the core idea of "precision medicine" [94] and demands alternative anticipations and treatment approaches. Glioblastomas develop very rarely in the cerebellum, brainstem, or spinal cord. Instead, they are mostly found in the brain's cerebral hemispheres, especially in the frontal and temporal lobes [48, 49, 50]. For instance, hypoxia impairs antitumor immune responses and

promotes resistance to traditional cancer therapy, which is the most dangerous factor in a GBM patient's life. Targeting hypoxia is thus a desirable approach for GBM treatment [51]. RAP1B and RAP2B are the only two Rap family GTPases significantly expressed in circulating human platelets that encourage lung cancer cells and renal carcinoma cells to migrate, multiply, and invade [70, 71]. Increased expression of RAP2B uses a downstream target of FAK, PYK2, NF-kB, ERK, and MMP-2 signaling activation. It plays a role in the proliferation and migration of prostate cancer, hepatocellular carcinoma cells, breast cancer, and lung cancer [72, 76, 77, 79]. RAP2B stimulates FAK phosphorylation and promotes the EMT process [78].

Additionally, RAP2B is a unique p53 target and contributes to the p53 pro-survival role. The silencing of RAP2B could make tumor cells more susceptible to apoptosis in response to DNA damage [95]. Knockdown of RAP2B increases the sensitivity of adriamycin and sensitizes HCT116 cells. Moreover, several drawbacks still limit the clinical application and targeted therapy in glioma; therefore, targeting RAP2B could be a therapeutic target for glioma treatment. The cellular response in hypoxia is regulated by transcription factors attributed to the hypoxia-inducible factor (HIF) family. Elevated HIF2A expression is associated with lower overall survival in non-small cell lung cancer (NSCLC) [96]. Although hypoxia, which primarily regulates HIF2A is fundamentally understood but the mechanisms behind hypoxia-induced tumor aggressiveness are still not fully understood [97, 98]. LRP1 triggers phosphorylation of PYK2 induced MMP-9 activation and promotes HVSMC migration and remodeling of blood vessels in response to hypoxia [99]. PYK2 plays a role in the pathogenesis of PH in hypoxia [100]. However, EMT, a biological process, enables stationary epithelial cells to transform into mobile mesenchymal phenotypes that are detachable and invasive [101]. This mechanism starts cancer metastasis in tumor cells by stimulating neo-angiogenesis, which increases migratory abilities, invasiveness, and resistance to apoptosis [102, 103]. We aimed to established the role of hypoxia-induced RAP2B/HIF2A expression that leads to EMT activation in GBM cell growth and migration. The class of synthetic tyrphostin compounds produced as a series of tyrosine kinase inhibitors with improved affinity for the tyrosine kinases, including epidermal growth factor receptor kinase, such as tyrphostin A9 [104]. In previous literature, Tyrphostin A9 attenuated hypoxia-induced HPASMC proliferation. PYK2 inhibition attenuated ERK½ activation as early as 24 hrs after the onset of hypoxia [105]. However, RAP2B expression and function are associated with various cancer malignancies [106, 107, 108]. Similarly, HIF2A is also associated with tumor malignancies and linked to poor overall survival [81, 109, 110], but its translational relevance is still needed. The report indicates the therapeutic relevance of HIF2A, PYK2, and EMT in hypoxia of various cancers [111] but nothing about glioblastoma. Previously

reported that the HAT1-HIF2A axis requires hypoxia-induced maintenance and reprogramming of cancer stem cells [98]. RAP2B expression, function, and correlation with HIF2A are unexplored in GBM under hypoxia. First time in the current study, we examined the hypoxia-responsive gene RAP2B, essential for HIF2A stabilization in GBM cell proliferation and migration under hypoxia vs normoxia. In the present study, we investigated the clinical and functional significance of RAP2B/HIF2A axis mediated activation of FAK/PYK2-EMT signaling pathway and its therapeutic relevance through chemical and molecular approaches, therefore indicating that RAP2B-HIF2A axis use as a potential therapeutic target.

1.5. References:

1. Lemmon, M.A. and J. Schlessinger, Cell signaling by receptor tyrosine kinases. Cell, 2010. **141**(7): p. 1117-34.
2. Witsch, E., M. Sela, and Y. Yarden, Roles for growth factors in cancer progression. Physiology (Bethesda), 2010. **25**(2): p. 85-101.
3. Hynes, N.E. and G. MacDonald, ErbB receptors and signaling pathways in cancer. Curr Opin Cell Biol, 2009. **21**(2): p. 177-84.
4. Patel, A., Benign vs Malignant Tumors. JAMA Oncol, 2020. **6**(9): p. 1488.
5. Maitra, A., Molecular envoys pave the way for pancreatic cancer to invade the liver. Nature, 2019. **567**(7747): p. 181-182.
6. Massague, J. and A.C. Obenauf, Metastatic colonization by circulating tumor cells. Nature, 2016. **529**(7586): p. 298-306.
7. Luzzi, K.J., *et al*., Multistep nature of metastatic inefficiency: dormancy of solitary cells after successful extravasation and limited survival of early micrometastases. Am J Pathol, 1998. **153**(3): p. 865-73.
8. Fares, J., *et al*., Molecular principles of metastasis: a hallmark of cancer revisited. Signal Transduct Target Ther, 2020—5 (1): p. 28.
9. Vargo, M., Brain tumor rehabilitation. Am J Phys Med Rehabil, 2011. **90**(5 Suppl 1): p. S50-62.
10. Vargo, M.M., Brain Tumors and Metastases. Phys Med Rehabil Clin N Am, 2017. **28**(1): p. 115-141.
11. Wrensch, M., *et al*., Epidemiology of primary brain tumors: current concepts and literature review. Neuro Oncol, 2002. **4**(4): p. 278-99.
12. Byun, Y.H. and C.K. Park, Classification and Diagnosis of Adult Glioma: A Scoping Review. Brain Neurorehabil, 2022. **15**(3): p. e23.
13. Weller, M. *et al*., EANO guidelines on diagnosing and treating diffuse gliomas of adulthood. Nat Rev Clin Oncol, 2021. **18**(3): p. 170-186.
14. Kang, H., *et al*., A Nationwide, Population-Based Epidemiology Study of Primary Central Nervous System Tumors in Korea, 2007-2016: A Comparison with United States Data. Cancer Res Treat, 2021. **53**(2): p. 355-366.

15. Cancer Genome Atlas Research, N., Comprehensive genomic characterization defines human glioblastoma genes and core pathways. Nature, 2008. **455**(7216): p. 1061-8.
16. Louis, D.N., *et al*., The 2021 WHO Classification of Tumors of the Central Nervous System: a summary. Neuro Oncol, 2021. **23**(8): p. 1231-1251.
17. Holland, E.C., Glioblastoma multiforme: the terminator. Proc Natl Acad Sci U S A, 2000. **97**(12): p. 6242-4.
18. Maher, E.A., *et al*., Malignant glioma: genetics and biology of a grave matter. Genes Dev, 2001. **15**(11): p. 1311-33.
19. Schwartzbaum, J.A., *et al*., Epidemiology and molecular pathology of glioma. Nat Clin Pract Neurol, 2006. **2**(9): p. 494-503; quiz 1 p following 516.
20. Agnihotri, S., *et al*., Glioblastoma, a brief review of history, molecular genetics, animal models and novel therapeutic strategies. Arch Immunol Ther Exp (Warsz), 2013. **61**(1): p. 25-41.
21. Brat, D.J., *et al*., cIMPACT-NOW update 5: recommended grading criteria and terminologies for IDH-mutant astrocytomas. Acta Neuropathol, 2020. **139**(3): p. 603-608.
22. Park, Y.W., *et al*., The 2021 WHO Classification for Gliomas and Implications on Imaging Diagnosis: Part 2-Summary of Imaging Findings on Pediatric-Type Diffuse High-Grade Gliomas, Pediatric-Type Diffuse Low-Grade Gliomas, and Circumscribed Astrocytic Gliomas. J Magn Reson Imaging, 2023. **58**(3): p. 690-708.
23. Yeole, B.B., Trends in the brain cancer incidence in India. Asian Pac J Cancer Prev, 2008. **9**(2): p. 267-70.
24. Jalali, R. and D. Datta, Prospective analysis of the incidence of central nervous tumors in a tertiary cancer hospital from India. J Neurooncol, 2008. **87**(1): p. 111-4.
25. Cha, Y.M., *et al*., Success of ablation for atrial fibrillation in isolated left ventricular diastolic dysfunction: a comparison to systolic dysfunction and normal ventricular function. Circ Arrhythm Electrophysiol, 2011. **4**(5): p. 724-32.
26. Aldape, K., *et al*., Glioblastoma: pathology, molecular mechanisms and markers. Acta Neuropathol, 2015. **129**(6): p. 829-48.
27. Park, Y.W., *et al*., The 2021 WHO Classification for Gliomas and Implications on Imaging Diagnosis: Part 1-Key Points of the Fifth Edition and Summary of Imaging Findings on Adult-Type Diffuse Gliomas. J Magn Reson Imaging, 2023. **58**(3): p. 677-689.
28. Ruda, R., *et al*., IDH wild-type grade 2 diffuse astrocytomas: prognostic factors and impact of treatments within molecular subgroups. Neuro Oncol, 2022. **24**(5): p. 809-820.
29. Miller, K.D., *et al*., Brain and other central nervous system tumor statistics, 2021. CA Cancer J Clin, 2021. **71**(5): p. 381-406.
30. Li, X.R. *et al*., Are Benign and Borderline Brain Tumors Underreported? J Registry Manag, 2016. **43**(4): p. 187-94.
31. Ostrom, Q.T., *et al*., CBTRUS Statistical Report: Primary Brain and Other Central Nervous System Tumors Diagnosed in the United States in 2014-2018. Neuro Oncol, 2021. **23**(12 Suppl 2): p. iii1-iii105.
32. McNeill, K.A., Epidemiology of Brain Tumors. Neurol Clin, 2016. **34**(4): p. 981-998.

33. Minniti, G., *et al*., Current status and recent advances in reirradiation of glioblastoma. Radiat Oncol, 2021. **16**(1): p. 36.
34. Marenco-Hillembrand, L., *et al*., Trends in glioblastoma: outcomes over time and type of intervention: a systematic evidence-based analysis. J Neurooncol, 2020. **147**(2): p. 297-307.
35. Stupp, R., *et al*., Radiotherapy plus concomitant and adjuvant temozolomide for glioblastoma. N Engl J Med, 2005. **352**(10): p. 987-96.
36. Gilbert, M.R., *et al*., A randomized trial of bevacizumab for newly diagnosed glioblastoma. N Engl J Med, 2014. **370**(8): p. 699-708.
37. Reardon, D.A., *et al*., Effect of Nivolumab vs Bevacizumab in Patients With Recurrent Glioblastoma: The CheckMate 143 Phase 3 Randomized Clinical Trial. JAMA Oncol, 2020. **6**(7): p. 1003-1010.
38. Jakola, A.S., *et al*., Surgical resection versus watchful waiting in low-grade gliomas. Ann Oncol, 2017. **28**(8): p. 1942-1948.
39. Lapointe, S., A. Perry, and N.A. Butowski, Primary brain tumors in adults. Lancet, 2018. **392**(10145): p. 432-446.
40. Ostrom, Q.T., S.S. Francis, and J.S. Barnholtz-Sloan, Epidemiology of Brain and Other CNS Tumors. Curr Neurol Neurosci Rep, 2021. **21**(12): p. 68.
41. Limam, S., *et al*., Investigation of simian virus 40 (SV40) and human JC, BK, MC, KI, and WU polyomaviruses in glioma. J Neurovirol, 2020. **26**(3): p. 347-357.
42. Rollison, D.E., *et al*., Investigation of human brain tumors for the presence of polyomavirus genome sequences by two independent laboratories. Int J Cancer, 2005. **113**(5): p. 769-74.
43. Neglia, J.P., *et al*., New primary neoplasms of the central nervous system in survivors of childhood cancer: a report from the Childhood Cancer Survivor Study. J Natl Cancer Inst, 2006. **98**(21): p. 1528-37.
44. Mathews, J.D., *et al*., Cancer risk in 680,000 people exposed to computed tomography scans in childhood or adolescence: data linkage study of 11 million Australians. BMJ, 2013. **346**: p. f2360.
45. Holick, C.N., *et al*., Prospective study of fruit, vegetables, and carotenoid intake and the risk of adult glioma. Am J Clin Nutr, 2007. **85**(3): p. 877-86.
46. Zhang, W., *et al*., Association Between Dietary Nitrite intake and Glioma Risk: A Systematic Review and Dose-Response Meta-Analysis of Observational Studies. Front Oncol, 2022. **12**: p. 910476.
47. Kuan, A.S., *et al*., Diet and risk of glioma: combined analysis of 3 extensive prospective studies in the UK and USA. Neuro Oncol, 2019. **21**(7): p. 944-952.
48. Nakada, M., *et al*., Aberrant signaling pathways in glioma. Cancers (Basel), 2011. **3**(3): p. 3242-78.
49. Hou, L.C., *et al*., Recurrent glioblastoma multiforme: a review of natural history and management options. Neurosurg Focus, 2006. **20**(4): p. E5.
50. Sherriff, J., *et al*., Patterns of relapse in glioblastoma multiforme following concomitant chemoradiotherapy with temozolomide. Br J Radiol, 2013. **86**(1022): p. 20120414.
51. Stupp, R., *et al*., Effects of radiotherapy with concomitant and adjuvant temozolomide versus radiotherapy alone on survival in glioblastoma in a randomized phase III study: 5-year analysis of the EORTC-NCIC trial. Lancet Oncol, 2009. **10**(5): p. 459-66.

52. Altorki, N.K., *et al*., Perioperative mortality and morbidity after sublobar versus lobar resection for early-stage non-small-cell lung cancer: a post-hoc analysis of an international, randomized, phase 3 trial (CALGB/Alliance 140503). Lancet Respir Med, 2018. **6**(12): p. 915-924.
53. Hanahan, D. and R.A. Weinberg, Hallmarks of cancer: the next generation. Cell, 2011. **144**(5): p. 646-74.
54. Yoshida, G.J., Beyond the Warburg Effect: N-Myc Contributes to Metabolic Reprogramming in Cancer Cells. Front Oncol, 2020. **10**: p. 791.
55. Maeda, H., *et al*., Tumor vascular permeability and the EPR effect in macromolecular therapeutics: a review. J Control Release, 2000. **65**(1-2): p. 271-84.
56. Silva, V.L. and W.T. Al-Jamal, Exploiting the cancer niche: Tumor-associated macrophages and hypoxia as promising synergistic targets for nano-based therapy. J Control Release, 2017. **253**: p. 82-96.
57. Casazza, A., *et al*., Tumor stroma: a complexity dictated by the hypoxic tumor microenvironment. Oncogene, 2014. **33**(14): p. 1743-54.
58. Dhani, N., *et al*., The clinical significance of hypoxia in human cancers. Semin Nucl Med, 2015. **45**(2): p. 110-21.
59. Zeng, W., *et al*., Hypoxia and hypoxia-inducible factors in tumor metabolism. Cancer Lett, 2015. **356**(2 Pt A): p. 263-7.
60. Bryant, J.L., *et al*., Targeting hypoxia in treating small cell lung cancer. Lung Cancer, 2014. **86**(2): p. 126-32.
61. El Hallani, S., *et al*., A new alternative mechanism in glioblastoma vascularization: tubular vasculogenic mimicry. Brain, 2010. **133**(Pt 4): p. 973-82.
62. Weller, M., Angiogenesis in glioblastoma: just another moving target? Brain, 2010. **133**(Pt 4): p. 955-6.
63. Takano, S., T. Yamashita, and O. Ohneda, Molecular therapeutic targets for glioma angiogenesis. J Oncol, 2010. **2010**: p. 351908.
64. Carmeliet, P., Angiogenesis in health and disease. Nat Med, 2003. **9**(6): p. 653-60.
65. Carmeliet, P., Angiogenesis in life, disease and medicine. Nature, 2005. **438**(7070): p. 932-6.
66. Ahir, B.K., H.H. Engelhard, and S.S. Lakka, Tumor Development and Angiogenesis in Adult Brain Tumor: Glioblastoma. Mol Neurobiol, 2020. **57**(5): p. 2461-2478.
67. Takashima, A. and D.V. Faller Targeting the RAS oncogene. Expert Opin Ther Targets, 2013. **17**(5): p. 507-31.
68. Paganini, S., *et al*., Identification and biochemical characterization of Rap2C, a new member of the Rap family of small GTP-binding proteins. Biochimie, 2006. **88**(3-4): p. 285-95.
69. Greco, F. *et al*., Rap2, but not Rap1 GTPase is expressed in human red blood cells and is involved in vesiculation. Biochim Biophys Acta, 2006. **1763**(3): p. 330-5.
70. Di, J.H. *et al*., Rap2B promotes migration and invasion of human suprarenal epithelioma. Tumour Biol, 2014. **35**(9): p. 9387-94.
71. Peng, Y.G. *et al*., Rap2b promotes proliferation, migration, and invasion of lung cancer cells. J Recept Signal Transduct Res, 2016. **36**(5): p. 459-64.

72. Zhu, Z., *et al*., Rap2B GTPase: structure, functions, and regulation. Tumour Biol, 2016. **37**(6): p. 7085-93.
73. Torti, M. *et al*., Rap1B and Rap2B translocation to the cytoskeleton by von Willebrand factor involves FcgammaII receptor-mediated protein tyrosine phosphorylation. J Biol Chem, 1999. **274**(19): p. 13690-7.
74. Di, J. *et al*., a p53 target gene Rap2B regulates the cytoskeleton and inhibits cell spreading. J Cancer Res Clin Oncol, 2015. **141**(10): p. 1791-8.
75. Li, J., *et al*., TMEM43 promotes pancreatic cancer progression by stabilizing PRPF3 and regulating RAP2B/ERK axis. Cell Mol Biol Lett, 2022. **27**(1): p. 24.
76. Pylayeva, Y. *et al*., Ras- and PI3K-dependent breast tumorigenesis in mice and humans requires focal adhesion kinase signaling. J Clin Invest, 2009. **119**(2): p. 252-66.
77. Zhang, L., H.B. Duan, and Y.S. Yang, Knockdown of Rap2B Inhibits the Proliferation and Invasion in Hepatocellular Carcinoma Cells. Oncol Res, 2017. **25**(1): p. 19-27.
78. Masalha, M. *et al*., MiR-199a-3p Induces Mesenchymal to Epithelial Transition of Keratinocytes by Targeting RAP2B. Int J Mol Sci, 2022. **23**(23).
79. Fu, G., *et al*., [Identification and Functional Analysis of A Novel Candidate Oncogene RAP2B in Lung Cancer.]. Zhongguo Fei Ai Za Zhi, 2009. **12**(4): p. 273-6.
80. Scrideli, C.A., *et al*., Prognostic significance of co-overexpression of the EGFR/IGFBP-2/HIF-2A genes in astrocytomas. J Neurooncol, 2007. **83**(3): p. 233-9.
81. Li, Z. *et al*., Hypoxia-inducible factors regulate tumorigenic capacity of glioma stem cells. Cancer Cell, 2009. **15**(6): p. 501-13.
82. Jonasch, E., *et al*., Belzutifan for Renal Cell Carcinoma in von Hippel-Lindau Disease. N Engl J Med, 2021. **385**(22): p. 2036-2046.
83. Kamihara, J., *et al*., Belzutifan, a Potent HIF2alpha Inhibitor, in the Pacak-Zhuang Syndrome. N Engl J Med, 2021. **385**(22): p. 2059-2065.
84. Li, M., *et al*., HIF in Gastric Cancer: Regulation and Therapeutic Target. Molecules, 2022. **27**(15).
85. Hoelzinger, D.B., *et al*., Gene expression profile of glioblastoma multiforme invasive phenotype points to new therapeutic targets. Neoplasia, 2005. **7**(1): p. 7-16.
86. Lipinski, C.A., *et al*., The tyrosine kinase pyk2 promotes migration and invasion of glioma cells. Neoplasia, 2005. **7**(5): p. 435-45.
87. Tse, K.W., *et al*., B cell receptor-induced phosphorylation of Pyk2 and focal adhesion kinase involves integrins and the Rap GTPases and is required for B cell spreading. J Biol Chem, 2009. **284**(34): p. 22865-77.
88. Di, J. *et al*., Rap2B promotes cell proliferation, migration and invasion in prostate cancer. Med Oncol, 2016. **33**(6): p. 58.
89. Carmona, G., *et al*., Role of the small GTPase Rap1 for integrin activity regulation in endothelial cells and angiogenesis. Blood, 2009. **113**(2): p. 488-97.
90. Iser, I.C., *et al*., The Epithelial-to-Mesenchymal Transition-Like Process in Glioblastoma: An Updated Systematic Review and In Silico Investigation. Med Res Rev, 2017. **37**(2): p. 271-313.
91. Charles, N.A., *et al*., The brain tumor microenvironment. Glia, 2011. **59**(8): p. 1169-80.

92. Ye, X.Z. *et al*., Tumor-associated microglia/macrophages enhance the invasion of glioma stem-like cells via the TGF-beta1 signaling pathway. J Immunol, 2012. **189**(1): p. 444-53.
93. Iwadate, Y., *et al*., Molecular classification and survival prediction in human gliomas based on proteome analysis. Cancer Res, 2004. **64**(7): p. 2496-501.
94. Perez, A. and J.T. Huse, The Evolving Classification of Diffuse Gliomas: World Health Organization Updates for 2021. Curr Neurol Neurosci Rep, 2021. **21**(12): p. 67.
95. Zhang, X., *et al*., Rap2b, a novel p53 target, regulates p53-mediated pro-survival function. Cell Cycle, 2013. **12**(8): p. 1279-91.
96. Kim, W.Y., *et al*., HIF2alpha cooperates with RAS to promote lung tumorigenesis in mice. J Clin Invest, 2009. **119**(8): p. 2160-70.
97. Grassi, E.S., V. Pantazopoulou, and A. Pietras, Hypoxia-induced release, nuclear translocation, and signaling activity of a DLK1 intracellular fragment in glioma. Oncogene, 2020. **39**(20): p. 4028-4044.
98. Kumar, N. *et al*., Histone acetyltransferase 1 (HAT1) acetylates hypoxia-inducible factor 2 alpha (HIF2A) to execute hypoxia response. Biochim Biophys Acta Gene Regul Mech, 2023. **1866**(1): p. 194900.
99. Revuelta-Lopez, E. *et al*., Hypoxia induces metalloproteinase-9 activation and human vascular smooth muscle cell migration through low-density lipoprotein receptor-related protein 1-mediated Pyk2 phosphorylation. Arterioscler Thromb Vasc Biol, 2013. **33**(12): p. 2877-87.
100. Fukai, K. *et al*., Pyk2 aggravates hypoxia-induced pulmonary hypertension by activating HIF-1alpha. Am J Physiol Heart Circ Physiol, 2015. **308**(8): p. H951-9.
101. Micalizzi, D.S., S.M. Farabaugh, and H.L. Ford, Epithelial-mesenchymal transition in cancer: parallels between normal development and tumor progression. J Mammary Gland Biol Neoplasia, 2010. **15**(2): p. 117-34.
102. Kalluri, R. and, E.G., Neilson, Epithelial-mesenchymal transition and its implications for fibrosis. J Clin Invest, 2003. **112**(12): p. 1776-84.
103. Kalluri, R. and R.A. Weinberg, The basics of epithelial-mesenchymal transition. J Clin Invest, 2009. **119**(6): p. 1420-8.
104. Gazit, A., *et al*., Tyrphostins I: synthesis and biological activity of protein tyrosine kinase inhibitors. J Med Chem, 1989. **32**(10): p. 2344-52.
105. Bijli, K.M. *et al*., Proline-rich tyrosine kinase 2 downregulates peroxisome proliferator-activated receptor gamma to promote hypoxia-induced pulmonary artery smooth muscle cell proliferation. Pulm Circ, 2016. **6**(2): p. 202-10.
106. Zhu, L. *et al*., Rap2B knockdown suppresses malignant progression of hepatocellular carcinoma by inactivating the PTEN/PI3K/Akt and ERK1/2 pathways. Mol Cell Biochem, 2020. **466**(1-2): p. 55-63.
107. Di, J. *et al*., Rap2B promotes angiogenesis via PI3K/AKT/VEGF signaling pathway in human renal cell carcinoma. Tumour Biol, 2017. **39**(7): p. 1010428317701653.
108. Guo, G., *et al*., The therapeutic potential of stem cell-derived exosomes in the ulcerative colitis and colorectal cancer. Stem Cell Res Ther, 2022. **13**(1): p. 138.

109. Shirvaliloo, M., LncRNA H19 promotes tumor angiogenesis in smokers by targeting anti-angiogenic miRNAs. Epigenomics, 2023. **15**(2): p. 61-73.
110. Kouri, F.M., C. Ritner, and A.H. Stegh, miRNA-182 and regulating the glioblastoma phenotype - toward miRNA-based precision therapeutics. Cell Cycle, 2015. **14**(24): p. 3794-800.
111. Yang, H. *et al*., Extracellular ATP promotes breast cancer invasion and epithelial-mesenchymal transition via hypoxia-inducible factor 2alpha signaling. Cancer Sci, 2019. **110**(8): p. 2456-2470.

1. Clinical significance and molecular mechanism of RAP2B connection with HIF2A in glioblastoma progression under hypoxia *vs* normoxia.

A. To demonstrate the expression and correlation of RAP2B and HIF2A in malignant astrocytoma.

B. Evaluating the role of RAP2B correlation with HIF2A in GBM progression under hypoxia vs normoxia.

2. To evaluate the combination of RAP2B knockdown and Tyrphostin A9 treatment: Inhibition on GBM progression in hypoxia.

3. Tyrphostin A9 attenuates glioblastoma growth by suppressing PYK2/EGFR-ERK signaling pathway.

4. To study Tyrphostin A9 anticancer potential and protective role in the cognitive assessment by targeting RAP2B/HIF2A/pPYK2-EMT signaling in glioma rats under hypoxia.

CHAPTER 2

Clinical significance and Molecular mechanism of RAP2B connection with HIF2A in Glioblastoma progression under hypoxia *vs* normoxia

Objective 1. Clinical significance and molecular mechanism of RAP2B connection with HIF2A in glioblastoma progression under hypoxia *vs* normoxia.

A. To demonstrate the expression and correlation of RAP2B and HIF2A in malignant astrocytoma.

B. Evaluating the role of RAP2B connection with HIF2A in GBM progression under hypoxia *vs* normoxia.

Abstract

Hypoxia is a crucial feature of malignant glioma which enhances tumor malignancy by triggering the epithelial-mesenchymal transition (EMT). RAP2B is one of the oncogenes belonging to the Ras family, and its function in cancer development. RAP2B and HIF2A overexpression found in malignant glioma; however, the link between hypoxia and RAP2B/HIF2A expression and their function in regulating EMT remains unknown. This objective investigated how RAP2B and HIF2A regulate EMT and promote GBM cell progression under hypoxia. PCR, RT-qPCR, western blot, and immunohistochemistry (IHC) were performed to evaluate RAP2B and HIF2A mRNA and protein expression in malignant astrocytoma tissues. Our results showed high mRNA and protein expression of RAP2B, HIF2A, EGFR, PYK2, pFAK, N-cadherin, and vimentin in malignant astrocytoma. High expression of RAP2B strongly correlated with IDH1/2 wildtype and associated with poor prognosis of GBM patients confirmed by correlation study. Increased expression of RAP2B and HIF2A positively correlated and associated with patients' poor survival in high-grade astrocytoma. *In vitro* we also found overexpressed RAP2B elevate mRNA and protein expression of RAP2B, HIF2A, EGFR, pFAK, pPYK2, and EMT signaling in both GBM cells under $CoCl_2$-induced hypoxia. MTT, clonogenic, and wound healing assays were employed to assess proliferation, growth, and migration in GBM cells under $CoCl_2$-induced hypoxia. Our study showed that overexpression of RAP2B increased proliferation and migration by activating HIF2A/pFAK/pPYK2-EMT signaling in both GBM cells under $CoCl_2$-induced hypoxia. Our results showed strong colocalization between RAP2B and HIF2A, in malignant astrocytoma and GBM cells. Similarly, we also observed strong colocalization between RAP2B and vimentin, GFAP, pPYK2 in LN18 and LN229 GBM cells under $CoCl_2$-induced hypoxia confirmed through immunofluorescence. The current research

showed that hypoxia-induced RAP2B and HIF2A could be EMT regulators and represent as a novel therapeutic avenue for GBM under hypoxia.

2.1. Introduction

Glioblastoma (GBM) is the major brain tumor of the central nervous system (CNS) that affects adult most commonly [1]. GBM comprises 14.5% overall brain CNS tumors and 48.6% of the aggressive types, despite being an uncommon tumor with an incidence rate of less than 5 cases per 100,000 individuals [2]. In a few instances, glioblastomas occur in cerebellum, brainstem and spinal cord but most cases, they are found in the cerebral hemispheres, particularly the frontal and temporal lobes [3]. Because of their infiltrative characteristics make it challenging to identify and distinguish a border zone between tumor and healthy brain. GBM treatment is difficult because of its invasive characteristics, heterogeneity, quick development of radio-chemotherapy resistance, and the existence of the blood-brain barrier (BBB); These are the main challenges in developing effective therapy [4]. Glioma cells undergo adaptive modifications, allowing them to survive in an advanced hypoxic microenvironment [5]. Hypoxia increases the potential stimulus for neovascularization, which is crucial for malignant gliomas to increase blood flow to provide nutrition and oxygen supply [6]. Hypoxia regulates gene expression in stem cell development, angiogenesis, migration, and metabolism, whereas tumor hypoxia is a detrimental factor that changes the tumor microenvironment [7].

The first time RAP2B identified, when a platelet cDNA library was screened in 1990 [8]. RAP2B is one of the Rap subfamily members which belongs to the Ras family; its expression is commonly elevated in a range of human tumors. RAP2B expression as well as function are well studied in tumors progression and associated with tumor malignancies [9]. RAP2B is highly upregulated and reported as a potential oncogene in lung cancer that contributes to carcinogenesis via NF-kB pathway [10]. RAP2B is a unique p53 target contributing to p53 pro-survival function [9]. Non-small cell lung cancer cell proliferation, invasion and migration are reportedly suppressed through miR-342-3p *via* targeting RAP2B [11]. RAP2B overexpression increases cell migration by enhancing matrix metalloproteinase-2 (MMP-2) protein expression in human suprarenal epithelioma [12]. Present study reported that high expression of RAP2B is strongly associated with hypoxic core region of malignant astrocytoma. Increased expression of RAP2B in hypoxia trigger activation of EMT by which GBM cells acquire proliferation and migration. Therefore, in the current study we investigating the association between hypoxia and RAP2B is essential for developing effective therapeutic approach against GBM.

Upregulation of the hypoxia-inducible factor (HIF) family is a characteristic of hypoxia-induced aggressive behavior of glioma cells [13]. HIF1 and HIF2 are two substantially homologous HIF proteins that binds to the related HRE sequences. Despite exhibiting a very limited expression pattern, HIF2A role in tumor development studied extensively [14]. A hypoxic environment can trigger the epithelial-mesenchymal transition (EMT) during glioma progression by regulating various pathways, including wnt/β-catenin [15], transforming growth factor (TGF-β) [16], and the Sonic Hedgehog (SHH) signaling pathway [17]. However, it is necessary to find an alternative mechanism through which hypoxia promotes glioma malignancy. HIF2A is the primary key player in the pathophysiology and prognosis of lung cancer [18], and it is also highly expressed in various cancer correlates with less survival, indicating that HIF2A could be an alternative marker for poor clinical outcome [19]. However, more investigation is still required to properly comprehend the precise mechanism through which hypoxia encourages glioma malignancy.

Recently reported that RAP2B positively regulate the development and metastasis of prostate cancer and also demonstrated that silencing of RAP2B significantly decrease the expression levels of FAK phosphorylation in HCC cells [20]. Proline-rich tyrosine kinase 2 (PYK2), a homolog of FAK, is a non-receptor tyrosine kinase that combines signals from cell surface receptors like receptor tyrosine kinases G-protein coupled receptors, and integrin adhesion receptors [21]. It is reported that PYK2 and FAK phosphorylation due to activation of Rap downstream of integrin interaction has been documented [22]. FAK is essential in developing various tumor types by connecting integrins and the dynamic actin cytoskeleton to regulate cell motility and invasion [23]. In earlier research, FAK is found to be a downstream effector of the Rap GTPases, and it is crucial for Rap-mediated cellular adhesion and migration [24]. PYK2 signaling has been linked to several cellular functions, including cell proliferation, survival, and migration. PYK2 is highly expressed in glioma and positively associated with glioma cell proliferation and migration [25]. RAP2B plays an essential role in various cancer progression, including glioma, but expression and correlation between RAP2B and HIF2A in glioma progression through pFAK/pPYK2-EMT pathway under $CoCl_2$-induced hypoxia remains unknown.

2.2. Materials and Methods:

2.2.1. Patient specimens

Surgically resected astrocytoma biopsies (n=90), including control biopsies (non-tumor, n=20), were collected from patients admitted for diagnosis and treatment in the Krishna Institute of Medical Sciences

(KIMS) Secunderabad Telangana, India. After collection of astrocytoma biopsies samples were further frozen in liquid nitrogen. Astrocytoma grading was performed for diagnosis using the WHO histopathological grading system [26]. This study examined 110 samples, including WHO grade 2 n=23, WHO grade 3 n=32, WHO grade 4 n=35, and adjacent temporal lobe epilepsy tissues as controls (non-tumor) n=20. Patients' clinicopathological data, including age and gender, survival rate, and family history, were kept up to date in the hospital registry. Written informed consent was obtained from the Department of Neurosurgery, KIMS Hospital for all patients who underwent surgery. This study was approved by the Institutional Ethics Committee (IEC) of the University of Hyderabad and the KFRC-Ethics Committee (KIMS) to use human tissues for experimental purposes.

2.2.2. Processing of astrocytoma biopsy samples for molecular and histopathological study

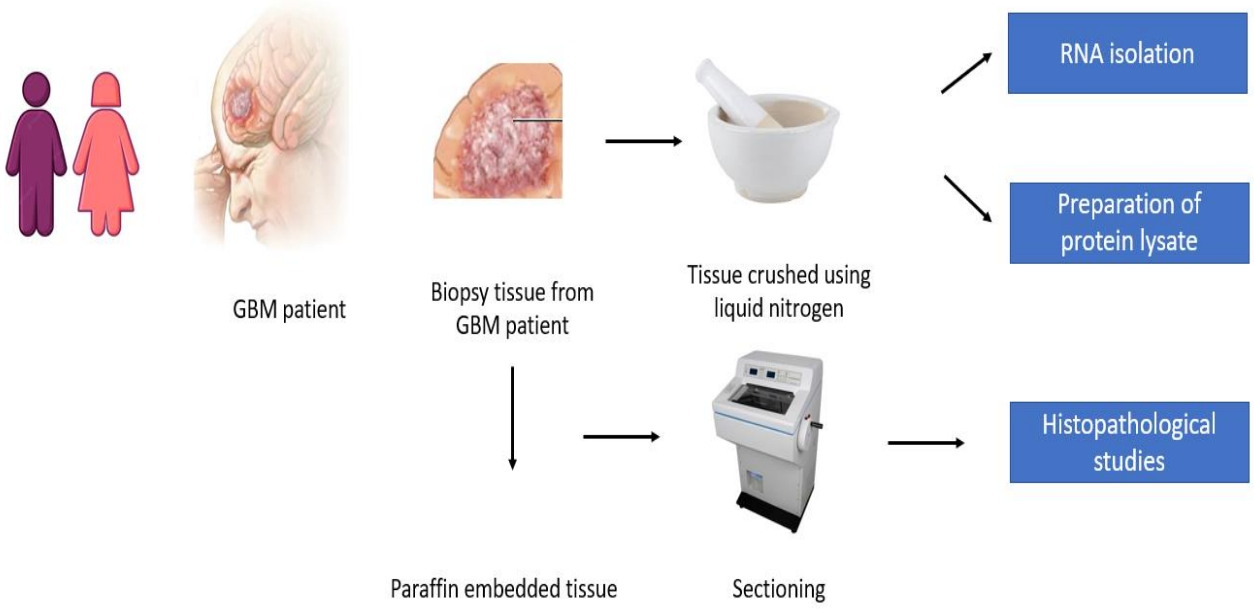

Figure 1: Diagrammatic representation of the experimental procedures for processing astrocytoma biopsies for PCR, western blot, and IHC staining.

2.2.3. RNA isolation and Polymerase chain reaction (PCR)/quantitative (RT-qPCR)

Total RNA was extracted from frozen astrocytoma tissues and GBM cell lines through the Trizol (sigma) method following manual instructions. The RNA quantification and purity were checked by Nanodrop spectrophotometer (Thermo-Scientific), and cDNA was prepared by PrimeScript^{TM} 1st strand cDNA

synthesis kit (TaKaRa, #6110). 1-5µg of RNA was used for cDNA preparation by following the manufacturer's instructions. PCR was performed using the Dream Taq Green DNA polymerase EmeraldAmp® GT PCR Master Mix (2X) (Cat# RR310) method. The PCR reactions (20µl) contain 2µl diluted cDNA (1:5), primers (5µM) 2µl each, Taq polymerase mix-10µl, and dH_2O to make the total 20µl volume. The PCR condition includes 94 ^{0}C for 3 minutes, 94 ^{0}C for 15 seconds, primer-specific annealing temperature 55-60 ^{0}C for 30 seconds, and 72 ^{0}C for 30 seconds for 25 cycles in an Applied Biosystems thermocycler PCR machine. The amplified product was detected by 1-2% EtBr agarose gel electrophoresis. The quantitative PCR was performed by TB Green^{tm} (Syber green) premix Ex Taq^{tm} II (Tli RNaseH Plus, #RRB20A) through manual instructions in an Applied Biosystems fast real-time PCR machine. The qPCR conditions include pre-denaturation 95 ^{0}C for 5 minutes, and final denaturation 95 ^{0}C for 15 seconds, primers-specific annealing tm 55-60 ^{0}C for 30 seconds, and extension at 72 ^{0}C for 15 seconds for 40 cycles. Each reaction was performed in triplicates and the melting curve was analyzed to detect reaction specificity. The mRNA expression was quantified using the procedure described earlier [40]. Gene-specific primers were enlisted in **Table S1 (Chapter 3)**. GAPDH was used as an internal control for both PCR and qPCR.

2.2.4. Western blotting

Whole-cell protein was extracted from the astrocytoma biopsy tissues and GBM cell lines using RIPA lysis buffer. Lysed tissues or cells were centrifuged at 12000 rpm for 20 minutes at 4 ℃ Protein was quantified by a Bradford reagent from Sigma (#B6916). Denatured proteins were separated by 8–12% SDS-PAGE and transferred into a nitrocellulose membrane (Amersham^{TM} #10600001). The nitrocellulose membrane was blocked with 5% nonfat milk (Himedia #GRM1254-500G) solution or bovine serum albumin (BSA) (Hychem Laboratories #97350) in 1XTBST and incubated for 1 hrs at room temperature (RT). After blocking, the membrane was probed with specific primary antibody names listed in **Table 3 (Chapter 3)** at 4 °C overnight on a shaker. On the following day after primary incubation, membranes were washed with 1XTBST and subsequently incubated with horseradish peroxidase (HRP)-conjugated secondary antibodies, detailed in **Table 3**. Chemiluminescence visualized immunoreactivity in a chemo-doc Touch detection system (Bio-Rad) imaging system. β-actin was used as an internal reference.

2.2.5. Immunohistochemistry (IHC) and Immunofluorescences (IF)

Astrocytoma biopsies tissues were used for molecular study. Similar tissue sections of each grade, like grade 2, grade 3, and grade 4, including control of 5-10 µm were prepared by microtome (LEICA-1850) collected from KIMS hospital and stored at room temperature for histopathological study. Before staining, tissue sections were dewaxed by heating on a slide warming table (YORCO Sales PVT. LTD.) at 100 °C for 20 min, subsequently dehydrated in xylene for 3 washes of 5 min each. Simultaneously rehydrated for 5 min washes in alcohol gradient 100, 95, 75, and 50% ethanol and then washed with distilled water. Slides were cooked for 20 minutes 3 cycles (5, 10, 5 minutes) called antigen retrieval with Tris/EDTA (pH 9.0) buffer, and immunohistochemical staining was performed as per the Bio-SB mouse/rabbit poly detector DAB HRP (#BSB 0003) KIT manual. The tissue sections were thoroughly washed with Tris-buffered saline (1XTBS) in each step, visualized with 3, 3'-diaminobenzidine tetrahydrochloride, and then counterstained with hematoxylin. Images were captured in 8 to 10 random fields from each sample in a Thermo-Fisher scientific microscope (EVOS M5000 Invitrogen). The previously described method quantified IHC on positively stained/unstained cells (Babu *et al*., 2021). The expression was classified as negative, low, moderate, and high in the following manner (0-5% stained cells- negative, >5-30% stained cells- low, >30-60% stained cells- moderate, and >50% stained cells- high). For immunofluorescence (IF) briefly, tissue sections followed the same procedure as described for IHC till primary antibody incubation, but the secondary antibody was tagged with FITC-conjugated Alexa Fluor™ 488 and Alexa Fluor™ 555 was incubated for one hour at RT in the dark. After secondary antibody incubations, sections were washed with 1XTBS and counterstained with a vecta-shield mounting medium (DAPI). Images were captured in 8–10 random fields in the confocal microscope (Carl Zeiss LSM 880) at 63X objective. Colocalization was analyzed using Fiji software.

2.3. Materials:

High glucose DMEM media (#AL007A-500ML), Fetal Bovine Serum (FBS) (#RM9955-500ML), Anti-anti (antibiotic and antimycotic) (#REF A002-20ML), and 0.25% trypsin-EDTA (#TCL049-100ML) were purchased from Himedia. RAP2B construct (pEGFP+RAP2B) was purchased from Addgene. Lipofectamine™ 2000 was obtained from Thermo-Fisher Scientific (Catalog number 11668027). Trizol reagent was purchased from Sigma (T9424-100ML). PrimeScript 1st strand cDNA Synthesis Kit (#6110A) and SYBR green (TB Green Premix Ex Taq II, #RR820A) were purchased from TaKaRa (Japan). Annexin V-fluorescein isothiocyanate (FITC)/propidium iodide (PI) apoptosis kit #V13241 was ordered from Thermo-Fisher Scientific. $CoCl_2$ (#232696-5G) was ordered from Sigma-Aldrich. RIPA

Lysis Buffer prepared recipes NaCl 150mM, EDTA 2mM, Tris-Base 50mM, Na-deoxycholic acid, NaF and Na-Benzoate from Himedia, Glycerol (G9012-500ML) and NP-40 IGEPAL® CA-630 (18896-50ML) from Sigma, Protease (#P0044-1ML) and Phosphatase (#P8340-1ML) Inhibitor Cocktail from Sigma. Primers were obtained from IDT, culture plates from Thermo-Scientific (Nunc). Matrigel® Matrix (REF 354230) was purchased from Corning. Pre-stained Protein Marker Tricolor PLUS (#786419), DNA ladder (#786853), and Femto-LUCENT^{TM} PLUS-HRP Chemiluminescent reagent (ECL) (#786003) developer was obtained from G-Biosciences.

2.4. Cell Treatment

2.4.1 Cell culture and transfection

Two LN18 and LN229 established GBM cell lines were procured from cell repository of NCCS Pune, India. In this study included GBM cell lines were authenticated and free from mycoplasma contamination. These GBM cell lines were cultured in a complete high glucose DMEM medium added with 10% FBS and 1X Anti-Anti (antibiotic and antimycotic) and grown in a 37 ºC humidified chamber 5% CO_2 incubator. GBM cells were seeded with approximately 70 to 80% confluency in six well-plates, and the next day, media was replaced with fresh incomplete DMEM without anti-anti and FBS. pEGFP empty vector (control) and pEGFP-RAP2B (RAP2B clone) were diluted in incomplete media. pEGFP empty vector and pEGFP-RAP2B construct were transfected into both GBM cell lines using Lipfectamine^{TM} 2000 (11668030) transfection reagent following the manufacturer's instructions. After 6 hrs of transfection incomplete media was replaced with complete DMEM media. Both GBM cells were exposed to a defined dose of $CoCl_2$ 150µM for LN18 and 200µM for LN229 after 24 hrs of transfection and further incubated for another 24 hrs. RNA and protein were extracted after 48 hrs of transfection. Plasmid construct for the ectopic expression of RAP2B, we used GFP-Rap2b, which was gifted from Philip Stork (Addgene plasmid #118321; http://n2t.net/addgene:118321;PRID:Addgene_118321) [41]. $CoCl_2$-induced chemical hypoxia is one of the most widely used models. $CoCl_2$ is a hypoxia imitative agent known to induce hypoxia and stabilize hypoxia-inducible factors 1α and 2α. Treatment with $CoCl_2$ known as hypoxia and without $CoCl_2$ treatment called as normoxia. Both GBM cells were first seeded and allowed them to reach 70 to 80% confluency. After transfection respective plasmid cells were allocated to the normoxia group (transfected with pEGFP and RAP2B without $CoCl_2$ treatment) cells cultured at the constant temperature of 37 ℃, and hypoxia (transfected cells with pEGFP and RAP2B cultured in the DMEM medium with 150µM and 200µM of $CoCl_2$ treatment) in an incubator at constant temperature 37 ℃ with 5% CO_2 incubator for 24 hrs to induced chronic hypoxia according to different

experimental condition. Cultured GBM cells were transfected with empty vector (pEGFP) and RAP2B clone in normoxia vs hypoxia and allocated with defined experimental conditions pEGFP, RAP2B, pEGFP+$CoCl_2$, RAP2B+$CoCl_2$ (RAP2B cloned in pEGFP vector). Various experiments were performed, such as MTT, clonogenic, and scratch wound healing assay, and expressions of genes and proteins were detected by RT-qPCR, western blot, and immunofluorescence.

2.4.2. MTT Assay

Cell viability test was performed using the MTT assay through 3-(4,5-dimethylthiazol-2-yl)-2,5-diphenyl-2H-tetrazolium bromide MTT method. LN18 and LN229 GBM cells were transfected with control and RAP2B. After 12 hrs of transfection GBM cells were trypsinzed and seeded at a density of 1×10^4 cells/well in 200 µl medium of 96-well plate. After 24 hrs of transfection, cells were exposed to 150µM and 200µM of $CoCl_2$ respectively incubated for another 24 hrs. MTT reagent 20 µl (5mg/ml) was added in each well at different time points 0, 24, 48, and 72 hrs and incubated at 37 ℃ in a 5% CO_2 incubator for 3 to 4 hrs. The supernatant was removed after 3 to 4 hrs of incubation, and 100 µl of DMSO was added in each well and shaken for 30 seconds. The optical density was measured at 570 nm using an ELISA plate reader. Media without cells were used as blank to normalize the experimental reading. Cell viability formula=control group-Experimental group/Control group×100.

2.4.3. Clonogenic assay

For the colony formation assay, 500-1000 cells were seeded in 6-well plates and transfected with empty vector and RAP2B construct with the help of transfection reagent lipofectamine 2000 in incomplete DMEM medium (without 10% FBS and anti-anti). After 6 hrs of transfection, incomplete media was replaced with fresh complete media. After 24 hrs of transfection GBM cells were exposed to 150 and 200 µM of $CoCl_2$ into a 6-well plate in 2 ml complete medium for another 24 hrs. Cell culture mediums were changed every 3 days and cultured at 37 ℃ humidified chambers in a 5% CO_2 incubator. Sustained culturing until the clones were visible; after that the medium was removed, and the cells were fixed for 15-20 minutes with a 4% paraformaldehyde solution. Following this, the clones were stained with 0.1% crystal violet, and the colonies were dried in the air for 1 hrs prior to being photographed and counted. Images were captured in the print scanner, and the number of clones was measured using Image J software.

2.4.4. Total RNA Extraction and RT-qPCR

LN18 and LN229 GBM cells were seeded at 70-80% of confluency and transfected with control and RAP2B exposed with 150 and 200 µM of $CoCl_2$ in respective GBM cell lines for 24 hrs incubation at 37 ℃ humidified chambers with 5% CO_2 incubator. Total RNA was extracted using the Trizol method (Sigma) followed manufacturer's instructions. RNA purity and concentration were checked with Nanodrop (Thermo-Scientific). 2 to 5µg of total RNA was transcribed into cDNA with cDNA synthesis kit (#6110A) TaKaRa as per manual instructions using specific primer oligodT reverse for cDNA synthesis. Semiquantitative PCR was performed using Dream Taq Emerald Amp® GT PCR Master Mix 2X (Code No. RR310A) (TaKaRa) as per manual suggestions in PCR machine (Applied Biosystems) under following conditions: pre-denaturation at 95 ℃ for 30 sec and final denaturation for 2 minutes at various annealing temperature at different target for 40 sec, pre-extension at 72 ℃ for 30 sec and final extension at 72 ℃ for 5 min for 25 to 30 cycles. GAPDH is used as an internal control. The data was analyzed using Image J software, and values were normalized by GAPDH.

2.4.5. Western Blot

LN18 and LN229 GBM cells were cultured in complete media and the next day media was replaced with incomplete DMEM (without 10% FBS and anti-anti). GBM cells were transfected with control vector and RAP2B clone, further exposed with $CoCl_2$ after 24 hrs of transfection and incubated for another 24 hrs hypoxia (with $CoCl_2$) and normoxia (without $CoCl_2$). The protein was extracted by RIPA lysis buffer from respective experimental conditions. Bradford reagent was used to quantify protein and separated in 8 to 10% SDS page gel electrophoresis at room temperature. Proteins were transferred to nitrocellulose membrane at 30 volts for 4 ℃ overnight. The nitrocellulose membrane was blocked with 5% skimmed milk or Bovine serum albumin (BSA) and further incubated with various targeted primary antibodies at 4 ℃ for overnight. The primary antibodies are listed in **Table 3 (Chapter 3)**; subsequently, after primary antibodies incubation, the secondary antibody labeled with horseradish peroxidase was incubated for 1 hrs at room temperature. The target protein was detected after using chemiluminescence (ECL). Here, β-actin was used as an internal control. Bands were quantified by image J software, analyzed value, and plotted graph in GraphPad Prism 9.3 version.

2.4.6. Wound healing assay

For scratch wound healing assay, GBM cells were grown to 80-90% of confluency and transfected with empty vector and RAP2B clone. Further treated with $CoCl_2$ (induced hypoxia) for 24 hrs to see RAP2B

expression and its effect on GBM cell migration in hypoxia. Transfected GBM cells with experimental condition pEGFP and RAP2B clone in normoxia and pEGFP+$CoCl_2$ and RAP2B+$CoCl_2$ in hypoxia formed monolayer, a scratch was made in the center of six-well plates in each well using 10 µl of microtip. Cells were washed with 1XPBS to remove dead cells and added fresh medium. Cells migration images were captured, and cell mobility was observed by measuring the movement of the cells toward the wound in each well. Images were captured at different time points: 0, 24, and 48 hrs. Here, we measured the wound length to monitor the migration rate by scale plate using Image J software. The formula was applied to calculate migration rate (MR) at different time points: MR= (Do-D')/Do mentioned in [42], where Do represents the wound at time 0, and D' represents the wound length at different time points. Each experiment was performed in triplicates.

2.4.6. Immunofluorescence

LN18 and LN229 GBM cells were transfected with pEGFP and RAP2B clones. After 12hrs of transfection, cells were trypsinized and seeded into coverslips. GBM cells were exposed to 150 µM and 200 µM of $CoCl_2$ to induce hypoxia and without $CoCl_2$ *i.e.*, normoxia. After 48 hrs of incubation saw effect of overexpressed RAP2B on HIF2A expression and their colocalization under hypoxic and normoxic condition. Cells were fixed with 4% PFA for 10 minutes, blocked with 5% goat serum, and incubated with the primary antibodies overnight at 4 ℃ and further incubated with the secondary antibodies Alexa Fluor™ 488 and Alexa Fluor™ 555 for 1 hrs at room temperature (RT) in the dark. Each coverslip was counterstained with DAPI and observed under a confocal microscope (Carl Zeiss LSM 880) at 63X magnification.

2.5. Statistical Analysis:

Graph Pad Prism version 9.3 was used for statistical analysis. One-way ANOVA was used to calculate the differences between the data sets, and the Sidak multiple comparison test and the student's t test were used to determine the differences between the two variables. The Kaplan-Meier curve was used to analyze the survival statistics with the Fischer exact and Chi-square tests to assess the clinicopathological associations with RAP2B and HIF2A expression and compared by Log-rank (Mantel-Cox) test. The Pearson correlation coefficient was used to examine the relationship between RAP2B/HIF2A and their downstream gene expression in various astrocytoma grades. A strong positive correlation was indicated by the correlation coefficient value $r^2 = +1$, a negative correlation by $r^2 = -1$ and no correlation was shown

by $r^2 = 0$. The mean ± SEM was used to represent the continuous data. Statistical significance indicates as *p≤0.05; **p≤0.01; ***p≤0.001; ***p≤0.0001; ns – not significant.

2.6. Results

2.6.1. RAP2B and HIF2A upregulations associated with astrocytoma malignancy and patient's poor survival:

We checked expression profiles of RAP2B, HIF2A, pFAK, pPYK2, and EMT-associated markers vimentin, β-catenin, VEGF, and GFAP in various grades of astrocytoma (n=90) and normal tissues (n=20). RAP2B, HIF2A, EGFR and PYK2 mRNA expression was evaluated through semiquantitative PCR in all grades of astrocytoma tissues and control **(Figure 2A)**. These results evidenced that high transcript level of RAP2B and HIF2A in malignant astrocytoma. Densitometry analysis results revealed that significant increased transcript levels of RAP2B (***p=0.0004), HIF2A (***p=0.0006), EGFR (**p=0.0037) and PYK2 (***p=0.0007) in higher grade astrocytomas as compared to lower-grades and control brain tissues **(Figure 2B)**. Subsequently, RT-qPCR results also evidenced that increased mRNA expression of RAP2B (**p=0.0012), (***p=0.0003) and HIF2A (***p=0.0001), (****p≤0.0001) in grade 3 and grade 4 respectively compared to low grade and control tissues **(Figure 2C, S6)**. The correlation study also indicated that increased mRNA expression of RAP2B and HIF2A were positively correlated r^2=0.978; *p=0.0107 **(Figure 2D)**, suggesting that increased mRNA expression pattern associated with malignant astrocytoma. Similarly, we also checked the protein expression of RAP2B and HIF2A through western blot in similar astrocytoma grades and control tissues used for RNA. This result indicated that increased protein expression of RAP2B and HIF2A in grade 3 and grade 4 compared to low-grade and control tissues **(Figure 3A)**. Densitometry analysis result revealed a significantly increased protein expression of both RAP2B (***p=0.0003) and HIF2A (***p=0.0005) in higher grades astrocytoma compared to lower grades and control tissues **(Figure 3B)**. This revealed that high expression positively associated with astrocytoma malignancies. The correlation studies suggested a positive correlation between RAP2B and HIF2A at protein levels r^2=0.98, *p=0.010 **(Figure 3C)**. We used TCGA (www.cancer.gov/ccg/research/genome-sequencing/tcga) and GEPIA (gepia.cancer-pku.cn) online available database and confirmed our results RAP2B and HIF2A increased transcripts expression in GBM tissues. These results evidenced that RAP2B and HIF2A expression significantly high in GBM tissues compared to normal tissue. The median survival of astrocytoma patients was affected by the increased protein expression and positive correlation between RAP2B and HIF2A, but their expressions and correlations were independent of the patient's age and gender **(Table 1)**. These results verify the

relationship between HIF2A and RAP2B in high-grade astrocytoma tissues. Astrocytoma tissues with high positive RAP2B expression also showed 86.5% HIF2A expression, indicating an association between RAP2B and HIF2A in astrocytoma malignancies **(Table S4)**.

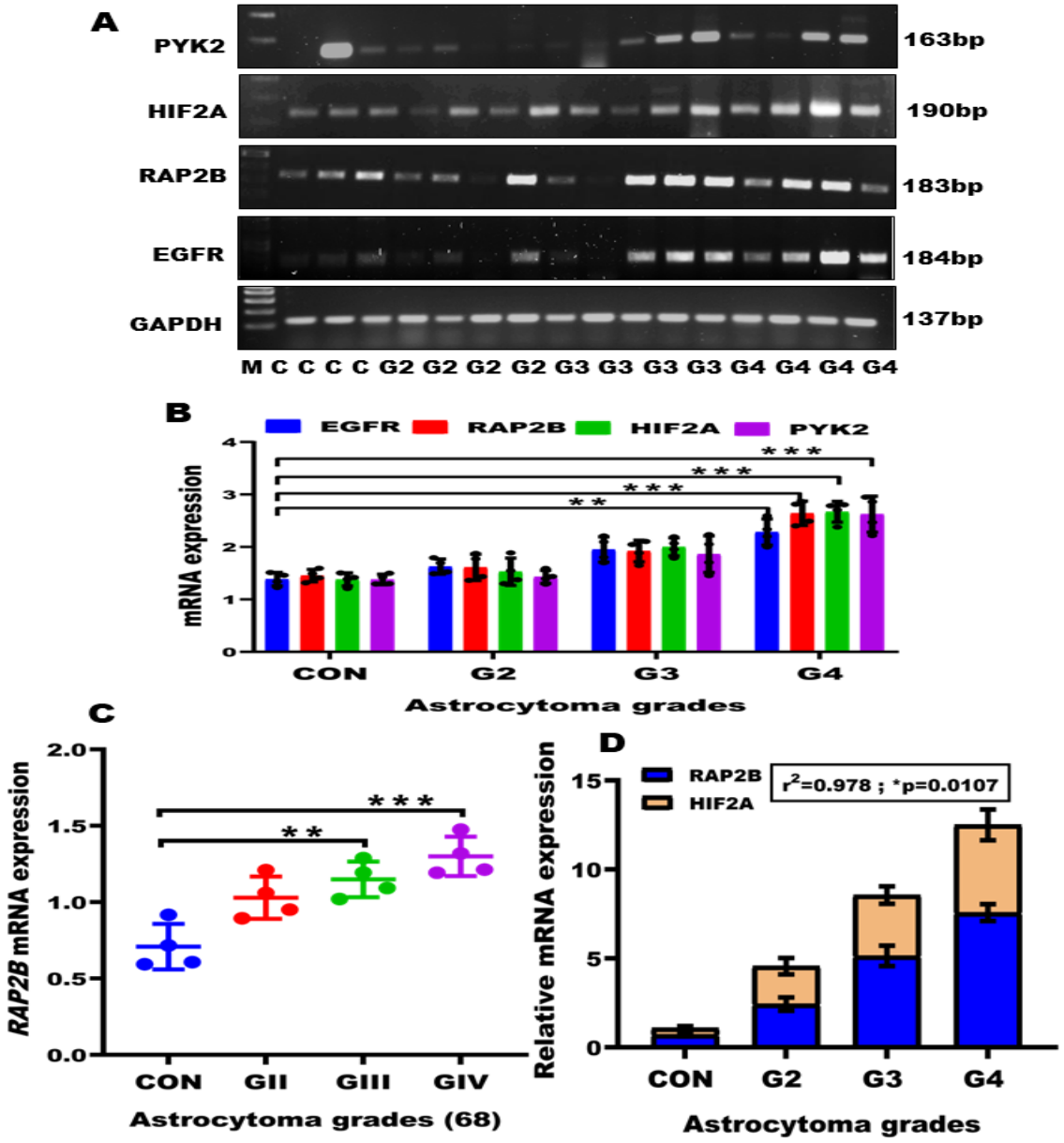

Figure 2: Upregulation of RAP2B in malignant astrocytoma: Astrocytoma cohort (n = 90) exhibiting **(A, B)**, PCR and densitometry result depicting more transcript expression of RAP2B, HIF2A, EGFR and PYK2 in GIII and GIV tissues compared to low-grade and control tissues. **(C)**, RT-qPCR results showed increased RAP2B transcript levels in grade 3 and grade 4 compared to the grade 2 and control. **(D)**, Correlation analysis found a positive correlation between RAP2B and HIF2A in malignant astrocytoma.

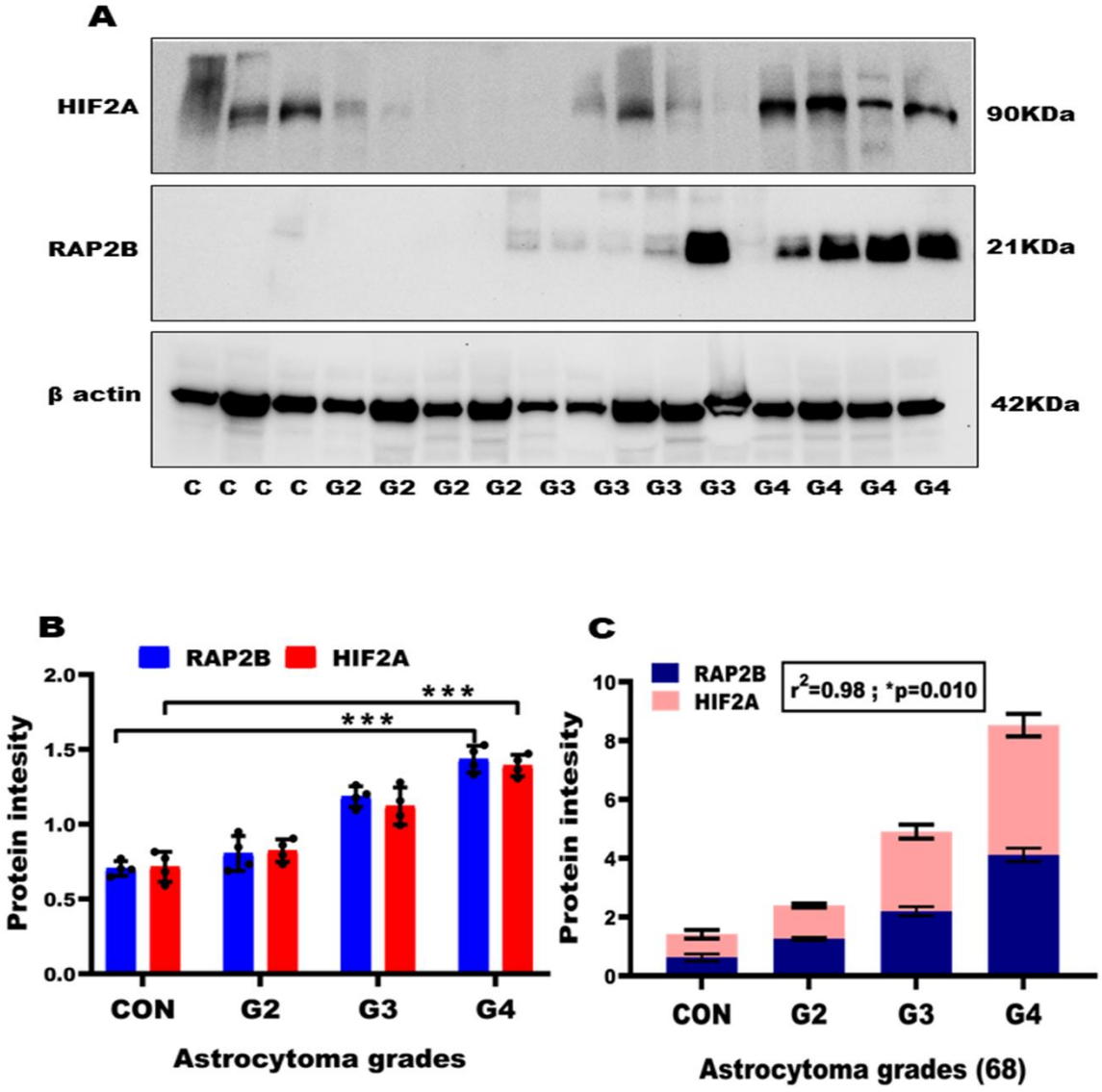

Figure 3: RAP2B expression elevated in malignant astrocytoma: (A, B), Western blot results and densitometry analysis show high protein expression of RAP2B (***p=0.0002) and HIF2A (***p=0.0003) in high grade astrocytoma tissues compared to low-grade and control tissues. **(C)**, The correlation study evidences a strong positive correlation between RAP2B and HIF2A at the protein level (r^2=0.98), (*p=0.010) in high-grade astrocytoma compared to low-grade and control.

2.6.2. Increased expression of RAP2B/HIF2A and pFAK/pPYK2-EMT signaling proteins associated with astrocytoma malignancies

We checked the protein expression of RAP2B and HIF2A with their downstream proteins EGFR, pFAK, pPYK2, and EMT markers in astrocytoma grades (n = 90) along with control brain tissues (n = 20) through western blot. Western blot results indicated increased protein expression of RAP2B, HIF2A, EGFR, GFAP, pFAK, pPYK2, N-cadherin and vimentin in grade 3 and grade 4 astrocytoma tissues compared to low grade and control **(Figure 4A)**. Densitometry analysis also showed significantly increased protein expression of RAP2B and HIF2A (****p<0.0001), and their downstream proteins EGFR (***p=0.0001), pPYK2 (***p<0.001), pFAK (***p=0.0003), EMT markers like vimentin (***p=0.0001), and N-cadherin (**p=0.0017) in higher grades of astrocytoma as compared to lower grades and control tissues **(Figure 4B)**. These results suggested that the upregulation of these protein markers strongly associated with astrocytoma malignancies. Further, we have examined mRNA and protein expression of RAP2B, HIF2A, and PYK2 in several GBM cell lines through PCR, RT-qPCR, Western blotting and densitometry result. The *in-vitro* data demonstrated the elevated differential expression patterns of RAP2B, HIF2A, and PYK2 at mRNA **(Figure 4C, D)** and protein **(Figure 4E, F)** levels. Based on their expression pattern and availability, we have selected three GBM cell lines, LN18, LN229, and U87 to validate our clinical data. Further, we verified RAP2B and HIF2A expression and role in GBM cell lines with $CoCl_2$ (hypoxia) *vs* without $CoCl_2$ (normoxia).

2.6.3. RAP2B and HIF2A expression positively correlated with astrocytoma grades:

We evaluated the correlation between RAP2B and HIF2A expression with several clinicopathological features, such as age, gender, and different grades of astrocytoma tissues. We found increased (positive) expression of RAP2B and HIF2A in 67 (74.44%) tissues and 23 (25.5%) tissues with negative expression of RAP2B and HIF2A out of a total 90 astrocytoma biopsies. High grade of astrocytoma significantly correlated with the overexpression of RAP2B (***p=0.0002) and HIF2A (***p=0.0004) compared to noncancer tissues. However, we also observed that there was no remarkable correlation among the RAP2B/HIF2A expressions and the patient's age ($p \leq 0.98$), ($p \leq 0.99$), gender ($p \leq 0.58$), ($p \leq 0.77$) represented in **Table 1**. In the total astrocytoma cohort, high-grade astrocytoma tissues showed positive expression of 77.7% GFAP, 83.3% β catenin, 94.4% vimentin, and 88.8% negative expression of E-cadherin shown in **Table S1**.

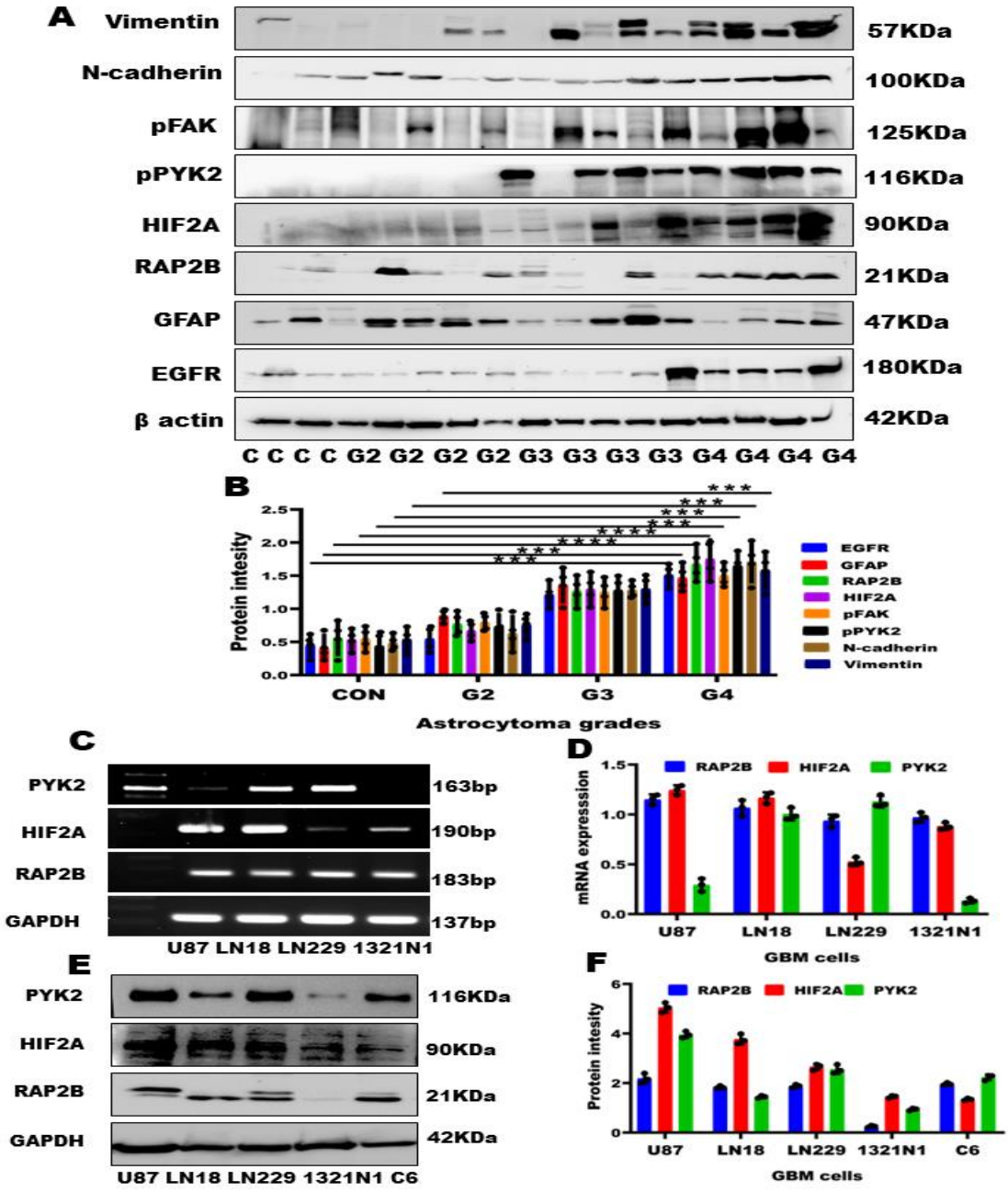

Figure 4: Enhanced RAP2B/HIF2A/pPYK2-EMT signaling proteins associated with astrocytoma malignancies: (A, B), Western blot and densitometry analysis depicts significantly increased protein expression of RAP2B, HIF2A, EGFR, GFAP, pPYK2, pFAK, N-cadherin and vimentin in high-grade astrocytoma tissues compared to low grade and control tissues. **(C**, **E)**, Representative PCR and western blot results showing differential mRNA and protein expression patterns of RAP2B, HIF2A, and pPYK2 in multiple GBM cell lines. **(D**, **F)**, Real time PCR and densitometry results representing mRNA and protein expression levels in multiple GBM cell lines.

Table 1: The correlation between RAP2B and HIF2A expression with various clinicopathological features.

Table 1: The correlation between RAP2B and HIF2A expression with various clinicopathological features.			
Features	**RAP2B expression profile (N = 90)**		**Chi-square test**
	Positive (n = 67)	**Negative (n = 23)**	
Gender			
Male (n = 67)	51 (76.1%)	16 (23.8%)	ns
Female (n = 23)	14 (60.8%)	9 (39.1%)	
Age			
≤40 (n = 37)	26 (70.2%)	11 (29.7)	ns
≥40 (n = 53)	41 (77.3%)	12 (22.6%)	
Histopathological Grades (WHO-2016, Classification System)			
GII (n = 23)	10	13	***p=0.0002
GIII (32)	25	7	
GIV (35)	32	3	
	HIF2A protein expression (n=90)		
Gender			
Male (n = 67)	48 (71.6%)	19 (28.3%)	ns
Female (n = 23)	13 (56.5%)	10 (43.4%)	
Age			
≤40 (n = 37)	22 (59.4%)	15 (40.5%)	ns
≥40 (n = 53)	37 (69.8%)	16 (30.1%)	
Histopathological Grades (WHO-2016, Classification System)			
GII (n = 23)	10	13	***p=0.0004
GIII (n = 32)	27	5	
GIV (n = 35)	30	5	

2.6.4. Positive relationship between RAP2B/HIF2A and EMT proteins in malignant astrocytoma

RAP2B is a small GTP-binding protein that acts as an oncogene in various cancers and its upregulation is associated with cancer malignancies, including glioma [1, 2]. In our study, Hematoxylin and Eosin (H&E) staining **(Figure 5A)** represented increased cellularity, nuclear atypia and multinucleation in malignant astrocytoma compared to lower grade and control. Now, we checked RAP2B with HIF2A expression, localization and colocalization in the tissue section of astrocytoma grades 2, 3, 4, and control through IHC and immunofluorescence (IF). HIF2A, nuclear expression is a marker for chronic hypoxia. IHC results showed strong positive nuclear staining of RAP2B (67.6%) and HIF2A (66.9%) in GIV as compared to GII (12.6%), (9.8%) and control (4.5%), (3.7%). Simultaneously, IHC staining showed increased expression of downstream protein EGFR (63.1%), pPYK2 (62.02%), and vimentin (64.9%) in high grade astrocytoma as compared to low-grade (12.3%), (6.6%), (4.6%) and control (3.71%), (2.32%), (2.75%) at tissues level **(Figure 5A)**. IHC staining also showed consistently positive RAP2B and HIF2A staining in high-grade astrocytoma at the tissue level supporting of previous results, PCR, RT-qPCR, and western blot. The densitometry results of IHC disclosed the expression pattern of RAP2B and HIF2A divided into four groups (negative, low positive, positive, and high positive) and significantly increased (RAP2B and HIF2A) ****$p \leq 0.0001$, EGFR, pPYK2 and vimentin (****$p \leq 0.0001$) in high grade astrocytoma compared to lower grade and control tissues **(Figure 5B, C, S1)**. We also observed that RAP2B expressed high-grade astrocytoma tissues showing strong positive staining of HIF2A and vimentin compared to low-grade and control tissues as represented in **Table S5**. Out of 90 astrocytoma tissues were found with high expression of 56.6% RAP2B, 50% HIF2A, 47.7% pPYK2, and 63.3% vimentin in high-grade astrocytoma in **Table S2**. High-grade astrocytoma tissues with elevated expression of RAP2B/HIF2A showed 83.3% positive vimentin expression, representing a strong association with mesenchymal property in malignant astrocytoma depicted in **Table S6**.

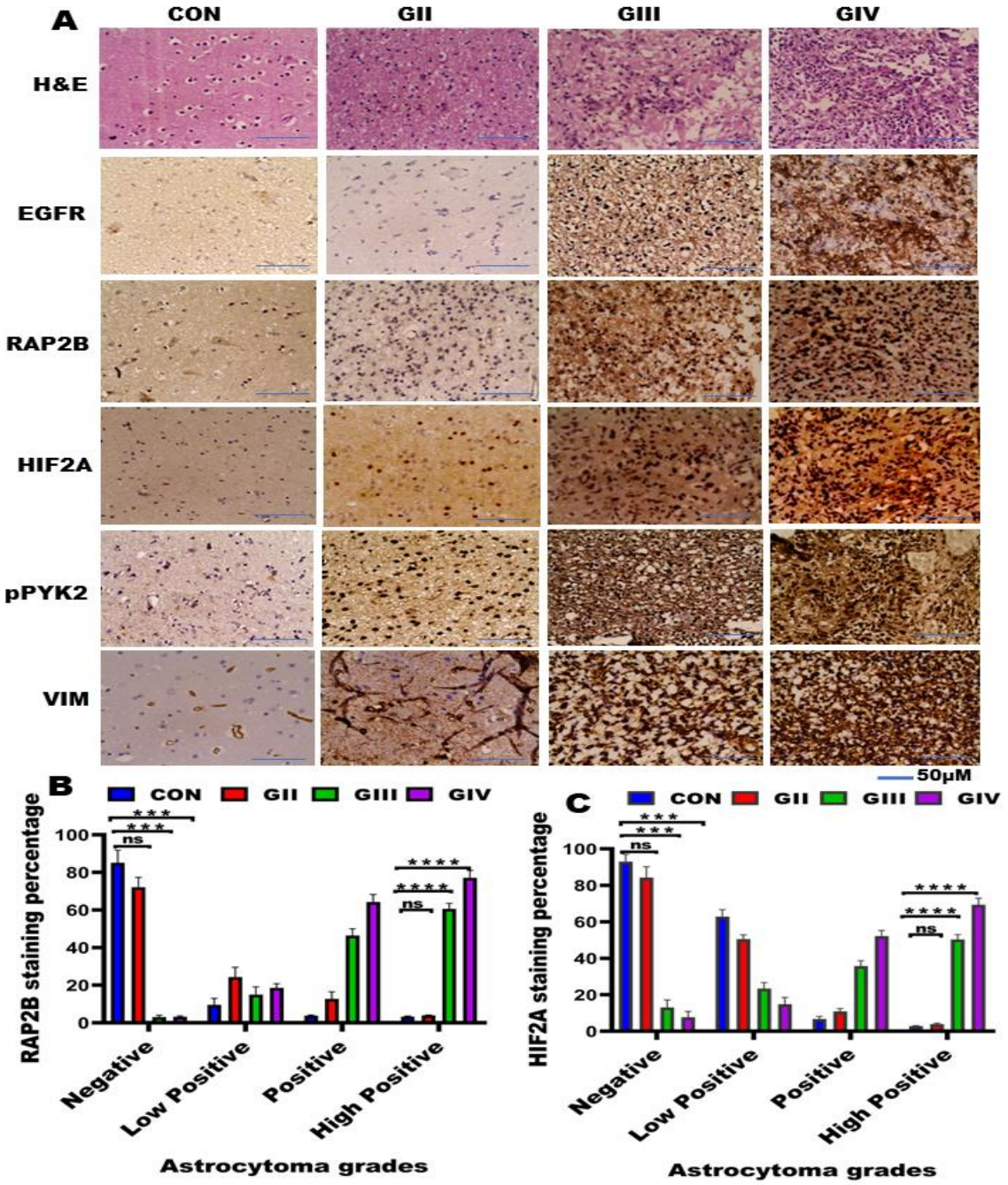

Figure 5: Increased expression of RAP2B and HIF2A linked to poor survival: (A) H&E and IHC results representing the pathological characteristics of various grades of astrocytoma and RAP2B, HIF2A, EGFR, pPYK2 and vimentin increased in higher grade astrocytoma. **(B, C)**, Densitometry analysis showed significantly high protein expression of RAP2B and HIF2A (****p<0.0001) in malignant astrocytoma compared to low-grade and control tissues.

2.6.5. High expression of RAP2B and HIF2A associated with astrocytoma malignancy and poor prognosis

To establish the clinical relevance of RAP2B and HIF2A in malignant astrocytoma tissues. Increased expression of RAP2B and HIF2A strongly associated with astrocytoma patients' poor survival. Kaplan-Meier survival statistics were examined for 79 cases out of the 90, because follow-up information was not obtained for the remaining 11 cases. The Kaplan-Meier curve evidenced that patient with elevated expression of both RAP2B and HIF2A had a worse prognosis **(Figure 6D)** than the patient with HIF2A and RAP2B alone **(Figure 6C, E)**. The hazard ratio of 4.9 (95% CI = 2.834 to 22.85) in the log-rank (Mantle-Cox) test indicated a noteworthy survival distribution (****$p<0.0001$) between the aforementioned groups, and the median survival of highly expressed RAP2B and HIF2A astrocytoma patients were 17 months. We performed immunofluorescence (IF) staining to confirm the positive staining and colocalization of RAP2B and HIF2A in high grades astrocytoma. IF images and densitometry results evidenced that increased RAP2B and HIF2A staining and colocalization in grade 3 and grade 4 as compared to low grade and control tissues **(Figure 6A, B)**. In our finding, target protein colocalization was calculated by Pearson's correlation coefficient represented by r through quantifying pixel intensity in the two channels of whole images. Pearson's correlation coefficient (PCC) in grade 3 r = 0.944, M1 = 0.213, M2 = 0.311 and in grade 4 r = 0.979, M1 = 0.242, M2 = 0.396 compared to grade 2 r = 0.88, M1 = 0.33, M2 = 0.429 and control r = 0.605, M1 = 0.623, M2 = 0.535. PCC represented strong colocalization between RAP2B and HIF2A in grade 3 and grade 4, suggesting that increased expression and colocalization of RAP2B/HIF2A might promote activation of pFAK/pPYK2-EMT signaling pathway that might be involved in astrocytoma malignancies. Additionally, the clinicopathological examination demonstrated that the expression of RAP2B, HIF2A, EGFR, pPYK2, GFAP, and vimentin linked with pathological grading but independent of age and gender in **Table 2**. Astrocytoma patients with positive expressions of RAP2B, HIF2A, vimentin (****$p<0.0001$), pPYK2 (***$p=0.0010$) and GFAP (***$p=0.0002$) positively correlated and associated with the worst prognosis. In this study, the relationship between elevated expression of RAP2B/HIF2A and positive correlation with EGFR, pPYK2, GFAP, and vimentin was investigated, this revealed that a strong association with malignant astrocytoma. This indicating that upregulation of RAP2B/HIF2A/EGFR/pPYK2-EMT signaling proteins involved in astrocytoma progression and poorer clinical outcomes and targeting RAP2B and HIF2A could improve astrocytoma malignancy and patient survival.

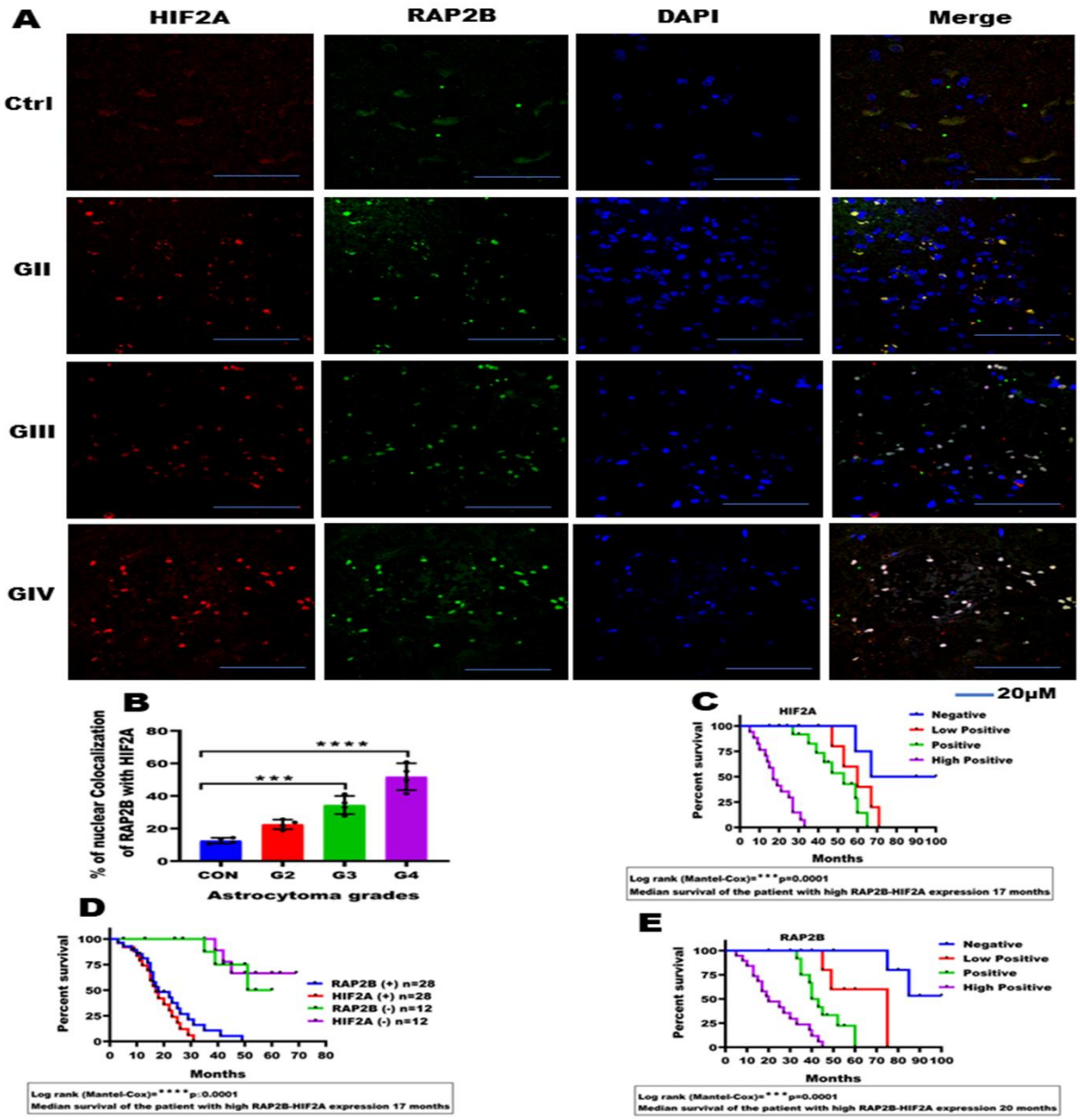

Figure 6: Increased RAP2B and HIF2A expression associated with poor patient survival: (A, B), Confocal images and densitometry analysis result showing increased nuclear colocalization between RAP2B and HIF2A in grade 3 (***p = 0.0002) and grade 4 (****p<0.0001) compared to grade 2 and control. **(C, D, E)**, The Kaplan-Meier survival graph results represent increased expression of RAP2B and HIF2A alone showed poor survival but increased expression of RAP2B and HIF2A together showed more dismal survival. The Log-rank test reveals significant survival difference (****p≤0.0001) compared to low or negative expression of RAP2B and HIF2A.

Table 2: Association between RAP2B, HIF2A, EGFR, pPYK2, GFAP and vimentin in different grades of astrocytoma.

The expression pattern of RAP2B, HIF2A, EGFR, GFAP, and vimentin proteins and follow-up information with various clinicopathological characteristics of astrocytoma patients								
S. No.	**Tumor grade**	**Age/Sex**	**RAP2B**	**pPYK2**	**HIF2A**	**GFAP**	**Vimentin**	**Follow-up time (months)**
			+ve/-ve	**+ve/-ve**	**+ve/-ve**	**+ve/-ve**	**+ve/-ve**	
1	CON	24/M	+ve	-ve	-ve	+ve	-ve	40 L
2	CON	20/M	-ve	-ve	-ve	+ve	-ve	56 L
3	CON	19/M	+ve	-ve	+ve	-ve	-ve	35 L
4	CON	39/M	-ve	+ve	-ve	-ve	-ve	43 L
5	CON	58/F	-ve	-ve	-ve	-ve	-ve	NA
6	CON	35/F	-ve	-ve	- ve	-ve	-ve	60 L
7	CON	13/M	+ve	+ve	-ve	+ve	-ve	48 L
8	CON	47/F	-ve	-ve	+ve	-ve	-ve	59 L
9	CON	43/M	-ve	-ve	-ve	-ve	-ve	NA
10	CON	35/M	+ve	+ve	+ve	-ve	+ve	NA
11	CON	51/F	-ve	-ve	-ve	-ve	-ve	65 L
12	CON	49/F	-ve	-ve	-ve	-ve	-ve	NA
13	CON	32/M	-ve	-ve	-ve	+ve	-ve	30 L
14	CON	29/F	-ve	-ve	-ve	-ve	-ve	52 L
15	CON	41/M	-ve	+ve	-ve	+ve	-ve	29 L
16	CON	55/M	-ve	-ve	-ve	+ve	-ve	32 L
17	CON	51/M	+ve	+ve	+ve	+ve	-ve	32 L
18	CON	43/M	+ve	+ve	-ve	+ve	-ve	38 L
19	CON	7/F	-ve	+ve	+ve	+ve	-ve	40 L
20	CON	23/F	+ve	-ve	+ve	-ve	-ve	22 L
21	Grade 2	37/M	-ve	-ve	-ve	+ve	-ve	27 L
22	Grade 2	33/M	-ve	+ve	-ve	+ve	+ve	15 D
23	Grade 2	30/M	+ve	-ve	+ve	+ve	+ve	10 D

24	Grade 2	29/F	-ve	+ve	-ve	+ve	-ve	17 D
25	Grade 2	10/M	+ve	-ve	+ve	+ve	+ve	12 D
26	Grade 2	53/M	+ve	-ve	+ve	+ve	+ve	19 D
27	Grade 2	40/F	-ve	-ve	+ve	+ve	-ve	30 L
28	Grade 2	45/M	+ve	-ve	-ve	+ve	+ve	16 D
29	Grade 2	36/F	-ve	-ve	-ve	+ve	-ve	22 L
30	Grade 2	44/M	+ve	-ve	+ve	+ve	-ve	18 L
31	Grade 2	42/M	+ve	-ve	-ve	-ve	-ve	34 D
32	Grade 2	30/F	+ve	-ve	-ve	+ve	-ve	27 D
33	Grade 2	39/M	+ve	+ve	+ve	+ve	-ve	25 D
34	Grade 2	54/M	+ve	-ve	-ve	+ve	-ve	13 D
35	Grade 2	51/M	-ve	+ve	-ve	+ve	-ve	20 D
36	Grade 2	59/M	+ve	+ve	+ve	-ve	+ve	19 D
37	Grade 2	77/F	+ve	-ve	-ve	+ve	-ve	28 D
38	Grade 2	51/M	-ve	-ve	-ve	+ve	-ve	52 D
39	Grade 2	31/M	-ve	+ve	-ve	+ve	-ve	15 D
40	Grade 2	11/F	-ve	+ve	-ve	-ve	-ve	14 D
41	Grade 2	50/M	+ve	+ve	+ve	-ve	+ve	16 L
42	Grade 2	42/M	-ve	-ve	-ve	+ve	+ve	19 D
43	Grade 2	32/F	-ve	+ve	+ve	+ve	-ve	22 D
44	Grade 3	27/F	+ve	-ve	-ve	+ve	-ve	28 L
45	Grade 3	21/F	-ve	+ve	-ve	-ve	+ve	20 L
46	Grade 3	38/F	-ve	+ve	-ve	+ve	+ve	10 D
47	Grade 3	43/M	+ve	+ve	+ve	+ve	+ve	15 D
48	Grade 3	46/M	+ve	-ve	+ve	-ve	-ve	23 D
49	Grade 3	54/M	+ve	+ve	+ve	+ve	+ve	19 L
50	Grade 3	17/M	-ve	+ve	-ve	+ve	-ve	NA
51	Grade 3	37/M	+ve	-ve	+ve	+ve	+ve	11 L
52	Grade 3	53/M	+ve	-ve	+ve	+ve	-ve	25 L
53	Grade 3	34/M	+ve	+ve	+ve	-ve	+ve	17 D

54	Grade 3	60/M	+ve	+ve	+ve	+ve	+ve	23 D
55	Grade 3	52/M	+ve	+ve	+ve	-ve	+ve	29 D
56	Grade 3	43/F	+ve	-ve	+ve	-ve	+ve	15 L
57	Grade 3	45/M	+ve	+ve	+ve	+ve	+ve	7 D
58	Grade 3	34/M	+ve	+ve	+ve	+ve	+ve	12 D
60	Grade 3	71/M	+ve	+ve	+ve	+ve	-ve	9 L
61	Grade 3	42/M	+ve	+ve	+ve	-ve	+ve	8 L
62	Grade 3	50/M	+ve	+ve	+ve	+ve	+ve	16 D
63	Grade 3	44/F	+ve	-ve	+ve	+ve	-ve	22 L
64	Grade 3	72/M	+ve	+ve	+ve	+ve	+ve	6 D
65	Grade 3	65/M	+ve	+ve	+ve	+ve	+ve	4 D
66	Grade 3	24/F	-ve	-ve	+ve	+ve	-ve	23 L
67	Grade 3	37/F	-ve	+ve	-ve	-ve	-ve	19 L
68	Grade 3	43/M	+ve	+ve	+ve	+ve	+ve	5 D
69	Grade 3	54/M	+ve	-ve	+ve	+ve	+ve	9 D
70	Grade 3	7/M	+ve	+ve	+ve	+ve	+ve	10 D
71	Grade 3	19/M	+ve	+ve	+ve	-ve	+ve	13 D
72	Grade 3	23/F	+ve	-ve	-ve	+ve	-ve	16 L
73	Grade 3	48/M	+ve	+ve	+ve	+ve	+ve	7 D
74	Grade 3	55/M	+ve	+ve	+ve	-ve	-ve	17 L
75	Grade 3	59/M	+ve	+ve	+ve	+ve	+ve	8 D
76	Grade 3	37/M	+ve	+ve	+ve	+ve	+ve	11 D
77	Grade 4	29/F	+ve	-ve	+ve	+ve	+ve	12 L
78	Grade 4	31/M	+ve	-ve	-ve	-ve	-ve	15 L
79	Grade 4	43/F	+ve	+ve	+ve	-ve	+ve	9 D
80	Grade 4	46/M	+ve	-ve	+ve	+ve	-ve	13 L
81	Grade 4	33/M	+ve	+ve	+ve	+ve	+ve	6 D
82	Grade 4	38/M	+ve	-ve	-ve	+ve	-ve	14 L
83	Grade 4	33/M	+ve	+ve	+ve	+ve	+ve	7 D
84	Grade 4	58/M	+ve	+ve	+ve	+ve	+ve	3 D

85	Grade 4	37/M	+ve	+ve	+ve	+ve	-ve	18 L
86	Grade 4	39/M	+ve	+ve	-ve	-ve	+ve	5 D
87	Grade 4	40/M	+ve	+ve	+ve	+ve	+ve	8 D
88	Grade 4	30/F	-ve	-ve	+ve	-ve	+ve	15 L
89	Grade 4	35/M	+ve	-ve	+ve	+ve	+ve	4 D
90	Grade 4	36/M	+ve	-ve	+ve	+ve	+ve	6 D
91	Grade 4	41/M	+ve	+ve	+ve	-ve	+ve	7 D
92	Grade 4	19/M	-ve	+ve	+ve	-ve	+ve	9 L
93	Grade 4	48/M	+ve	-ve	+ve	-ve	+ve	5 D
94	Grade 4	22/F	+ve	-ve	+ve	+ve	+ve	8 L
95	Grade 4	77/M	+ve	+ve	+ve	+ve	+ve	2 D
96	Grade 4	52/M	-ve	+ve	+ve	+ve	-ve	10 L
97	Grade 4	37/F	+ve	-ve	-ve	+ve	-ve	14 L
98	Grade 4	41/M	-ve	-ve	+ve	+ve	+ve	9 L
99	Grade 4	45/M	-ve	+ve	+ve	+ve	+ve	3 D
100	Grade 4	51/M	+ve	+ve	+ve	+ve	+ve	4 L
101	Grade 4	65/M	-ve	-ve	-ve	-ve	+ve	14 D
102	Grade 4	59/M	+ve	-ve	-ve	+ve	-ve	17 L
103	Grade 4	49/M	-ve	-ve	-ve	+ve	+ve	11 D
104	Grade 4	54/M	+ve	+ve	+ve	+ve	+ve	5 D
105	Grade 4	67/M	+ve	-ve	+ve	+ve	+ve	4 D
106	Grade 4	49/M	-ve	+ve	-ve	+ve	-ve	15 L
107	Grade 4	65/F	-ve	+ve	-ve	+ve	-ve	13 L
108	Grade 4	40/F	+ve	+ve	-ve	+ve	-ve	10 L
109	Grade 4	62/M	+ve	-ve	+ve	-ve	+ve	9 D
110	Grade 4	53/F	+ve	+ve	+ve	+ve	+ve	7 D
111	Grade 4	36/M	+ve	+ve	+ve	+ve	+ve	3 L

+ve and -ve represent the presence and absence of protein respectively, L; Live, D; Dead, NA; not applicable (still alive)

2.7. Overexpression of RAP2B in GBM cells and its expression increased by $CoCl_2$.

LN18 and LN229 GBM cell lines were transfected with pEGFP empty vector (control) and RAP2B clone (Cloned RAP2B in pEGFP vector, *i.e.*, pEGFP-RAP2B). After transfection, cells were exposed to 150µM and 200µM of $CoCl_2$ treatment for 24 hrs to mimic hypoxia and another group without $CoCl_2$, *i.e.*, normoxia. We found that 60 to 70% of LN18 and LN229 GBM cells were transfected with RAP2B. RAP2B expression was detected in both GBM cell lines by fluorescence microscopy **(Figure 7C)** and western blot **(Figure 7A, B)**. Western blot results evidenced that increased RAP2B expression in overexpressed RAP2B but enhanced when exposed with $CoCl_2$ compared to control. We assured RAP2B overexpression through fluorescence microscopy and western blot every time before performing our other experiments.

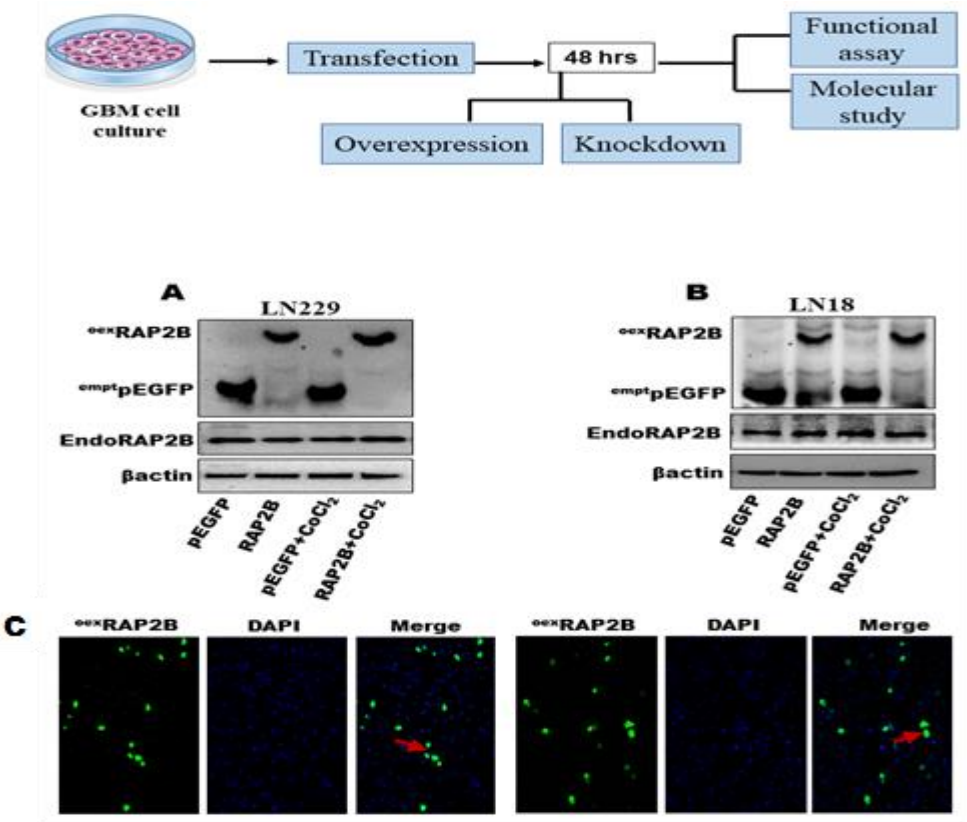

Figure 7: RAP2B expression in LN18 and LN229 GBM cells transfected with RAP2B clone: (A, B), Western blot result showing elevated ectopic RAP2B expression after 48 hrs of transfection with $CoCl_2$ (to mimic hypoxia) and without $CoCl_2$ (normoxia) exposure. **(C)**, Fluorescence microscopy images reveals overexpression of RAP2B denoted by red arrow after 48 hrs of transfection.

2.7.1. Overexpression of RAP2B promotes proliferation and colony-forming ability enhanced by $CoCl_2$-induced hypoxia in GBM cells.

To provide additional evidence supporting an oncogenic role of RAP2B in the survival and growth of GBM cells under hypoxic conditions. LN18 and LN229 GBM cells were transiently transfected with pEGFP (empty vector) and RAP2B construct (cloned in pEGFP vector). After 12 hrs of transfection cells were trypsinized and seeded for MTT and clonogenic assays, exposed with and without $CoCl_2$ treatment such as hypoxia vs. normoxia after 24 hrs of transfection. MTT assay result demonstrated that overexpressed RAP2B effect on GBM cell proliferation under both hypoxia and normoxia. Our result demonstrated that increased cell proliferation in overexpressed RAP2B (**p = 0.0038, **p = 0.0043), pEGFP+$CoCl_2$ treated (**p = 0.0041, *p = 0.023) but significantly enhanced cell proliferation in RAP2B+$CoCl_2$ (***p = 0.0002, ***p = 0.0001) as compared to pEGFP in both GBM cells **(Figure 8A, B)**. This suggesting that $CoCl_2$-induced hypoxia resulted more proliferation compared to normoxia similar to previous study [46]. MTT assay graph results showed 9.8-fold, 8.1-fold increased mean of the OD values in overexpressed RAP2B (**p = 0.0029), (**p = 0.0043), 6.8fold, 4.5-fold increase in pEGFP+$CoCl_2$ (**p = 0.0074), (*p = 0.021) but significantly increased 13.4-fold, 11.9-fold in RAP2B+$CoCl_2$ (***p = 0.0002), (***p = 0.0005) compared to pEGFP in both GBM cells. Further, we checked the expression of GFAP, a marker of glial cell proliferation. Western blot and densitometry results revealed increased expression in RAP2B and pEGFP+$CoCl_2$ but elevated in RAP2B+$CoCl_2$ **(Figure 10, A, B, C)** in both GBM cells under hypoxia *vs* normoxia. These results suggested that overexpression of RAP2B under hypoxia promotes more GBM cell proliferation.

To investigate overexpressed RAP2B effects on one of the most critical cancer cell characteristics, colonies forming ability from a single cell under hypoxia *vs* normoxia. We performed a clonogenic assay following the above-mentioned experimental conditions for MTT assay. Clonogenic assay results showed that increased colony number in overexpressed RAP2B and pEGFP+$CoCl_2$ but significantly increased colony number in RAP2B+$CoCl_2$ compared to pEGFP (normoxia) **(Figure 8C, E)**. Densitometry analysis results demonstrated that increased number of colonies 25.2%, 35% in overexpressed RAP2B (**p = 0.0041), (**p = 0.00176), 21.9%, 27% in pEGFP+$CoCl_2$ (*p = 0.0137), (*p = 0.025), and significantly increased colonies number 47%, 52% in RAP2B+$CoCl_2$ (***p = 0.0005), (***p = 0.0003) compared to pEGFP (normoxia), in LN18 and LN229 GBM cell lines **(Figure 8D, F)**. This result suggests that overexpression of RAP2B under hypoxia has a significant role in GBM cell growth.

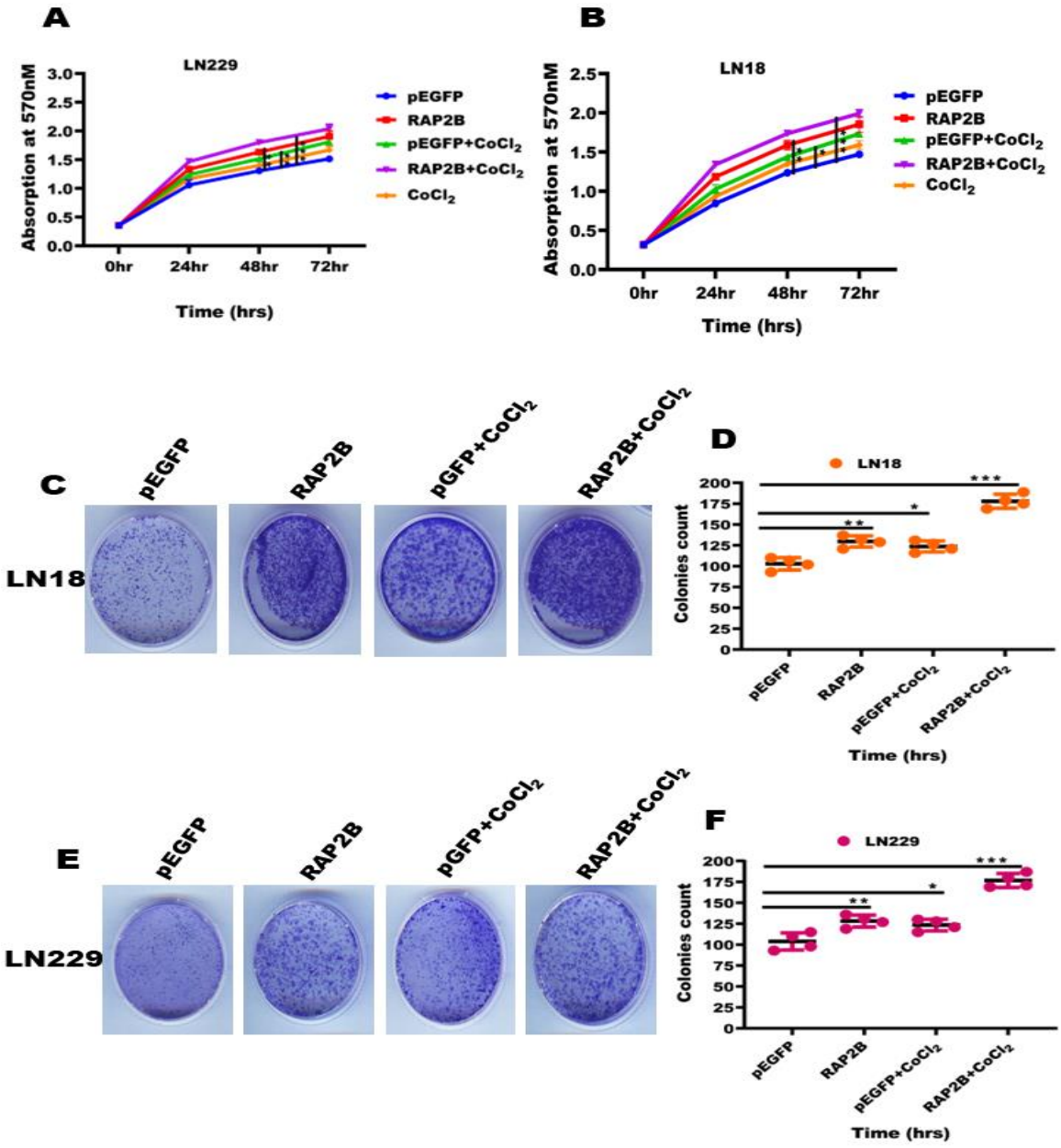

Figure 8: Upregulation of RAP2B/HIF2A promotes GBM cell proliferation and growth under $CoCl_2$ induced hypoxia: (A, B), MTT assay results demonstrating significant increased cell proliferation in RAP2B+$CoCl_2$ compared to pEGFP (***p = 0.0002, ***p = 0.0001). **(C, D, E, F)**, Clonogenic assays result and densitometry analysis represent a significantly increased colonies number in RAP2B+$CoCl_2$ compared to pEGFP (***p = 0.0005), (***p = 0.0003) hypoxia *vs* normoxia in both GBM cells.

2.7.2. Overexpression of RAP2B increases MMP-9 and VEGF expression and promotes GBM cell migration through HIF2A/pFAK/pPYK2-EMT pathway in GBM cells under $CoCl_2$-induced hypoxia.

We performed a scratch wound healing assay to investigate the effect of overexpressed RAP2B in GBM cell migration under hypoxia. Both GBM cells were transfected with pEGFP, RAP2B without $CoCl_2$ (normoxia), pEGFP+$CoCl_2$, and RAP2B+$CoCl_2$ with $CoCl_2$ (hypoxia). We found that overexpressed RAP2B in hypoxia increased the migration of GBM cells compared to normoxia **(Figure 9A, B)**. The wound healing assay images were captured at three time points 0, 24, and 48 hrs after the wound was made. We measured the mean length between migrated cells in all experimental groups. The mean value of migrated cells was increased 6.8-fold, 7.5-fold in overexpressed RAP2B, 4.4-fold, 5.1-fold in pEGFP+$CoCl_2$ but significantly increased 12.6-fold, 15.9-fold in RAP2B+$CoCl_2$ compared to pEGFP in both GBM cells. Densitometry analysis results also showed increased percent migrated cells 53%, 58.2% in overexpressed RAP2B (**p = 0.004), (**p = 0.0032) and 47.5%, 51.9% pEGFP+$CoCl_2$ (*p = 0.032), (**p = 0.0072) but significantly increased percent migration 81.4%, 86% in RAP2B+$CoCl_2$ (***p = 0.0003), (****p≤0.0001) compared to pEGFP in LN18 and LN229 GBM cells **(Figure 9C, D)**. Subsequently, we also checked the molecular markers involved in migration, like MMP-9 and VEGF in both GBM cells. Western blot and densitometry results represented the increased protein expression in overexpressed RAP2B, pEGFP+$CoCl_2$ but enhanced expression in RAP2B+$CoCl_2$ compared to pEGFP normoxia **(Figure 10A, B, C)**. These results suggested that overexpression of RAP2B in hypoxia plays a significant role in GBM cell migration through activation of MMP-9 and VEGF.

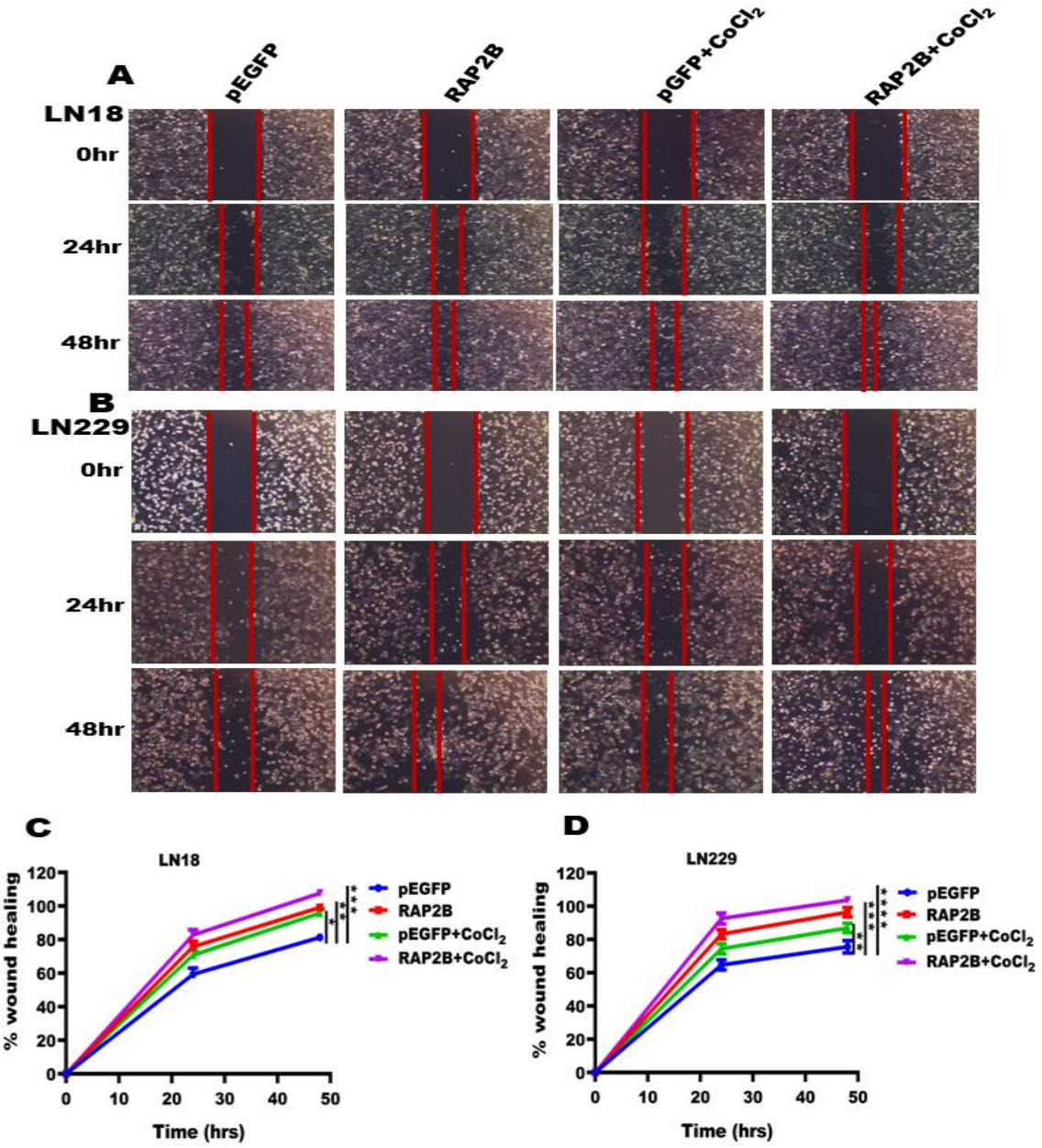

Figure 9: Upregulation of RAP2B/HIF2A promotes GBM cell migration under $CoCl_2$-induced hypoxia: (A, B), The scratch wound healing assay images showing migration in LN18 and LN229 GBM cells. **(C, D)**, Densitometry results depicting increased migration in RAP2B, pEGFP+$CoCl_2$ and significantly increased in RAP2B+$CoCl_2$ compared to pEGFP (***p = 0.0003), (****p≤0.0001) in both GBM cells.

2.7.3. Overexpressed RAP2B enhances activation of HIF2A/pFAK/pPYK2-EMT signaling in GBM cells under $CoCl_2$-induced hypoxia.

To explore the molecular mechanism of RAP2B-induced activation of HIF2A/pFAK/pPYK2-EMT signaling enhance proliferation and migration of GBM cells under hypoxia. We examined that overexpressed RAP2B increased HIF2A expression and their positive correlation involved in activating the EGFR/pFAK/pPYK2-EMT signaling pathway in GBM cells with and without $CoCl_2$. HIF2A is a potential marker for chronic hypoxia induction [47]. Our PCR and densitometry results demonstrated that increased mRNA expressions of RAP2B, HIF2A, EGFR, PYK2, GFAP, CTNNB1, VEGF, CDH2, and VIM in overexpressed RAP2B, pEGFP+$CoCl_2$ but high expression in RAP2B+$CoCl_2$ compared to pEGFP **(Figure 10D, E, F)**. Subsequently, we also performed Western blot to check the protein expression level after overexpression of RAP2B in hypoxia *vs* normoxia. Western blot and densitometry result also evidenced that increased protein expression of RAP2B, HIF2A and their downstream proteins EGFR, pFAK, pPYK2, β-catenin, N-cadherin, vimentin, snail, and slug in overexpressed RAP2B and pEGFP+$CoCl_2$, but enhanced expression in RAP2B+$CoCl_2$ compared to pEGFP **(Figure 10G, H, I)**. We also demonstrated IF between overexpressed RAP2B and HIF2A, GFAP and vimentin. Our IF results revealed that overexpressed RAP2B increased staining and colocalization of HIF2A, GFAP and vimentin in RAP2B, pEGFP+$CoCl_2$ but enhanced in RAP2B+$CoCl_2$ in both GBM cells **(Figure S2-S4)**. **Figure S5** represented epithelial to mesenchymal property. This finding suggested that overexpression of RAP2B acts as an oncogene, and its oncogenicity increased more when exposed with $CoCl_2$-induced hypoxic microenvironment. These promoted GBM cell growth and malignancy by enhancing the activation of HIF2A/EGFR/pFAK/pPYK2-EMT signaling pathway in both GBM cells. Overexpression of RAP2B enhanced the expression of vimentin and N-cadherin in hypoxia; these are the most important molecular markers of EMT induction. This confirmed that hypoxic exposure could be the cause of RAP2B mediated EMT activation in GBM cells. This finding revealed that increased expression of RAP2B/HIF2A induced the activation of pPYK2 and EMT, indicating that RAP2B/HIF2A acts as an oncogene promoter for EMT induction in both LN18 and LN229 GBM cells under hypoxia.

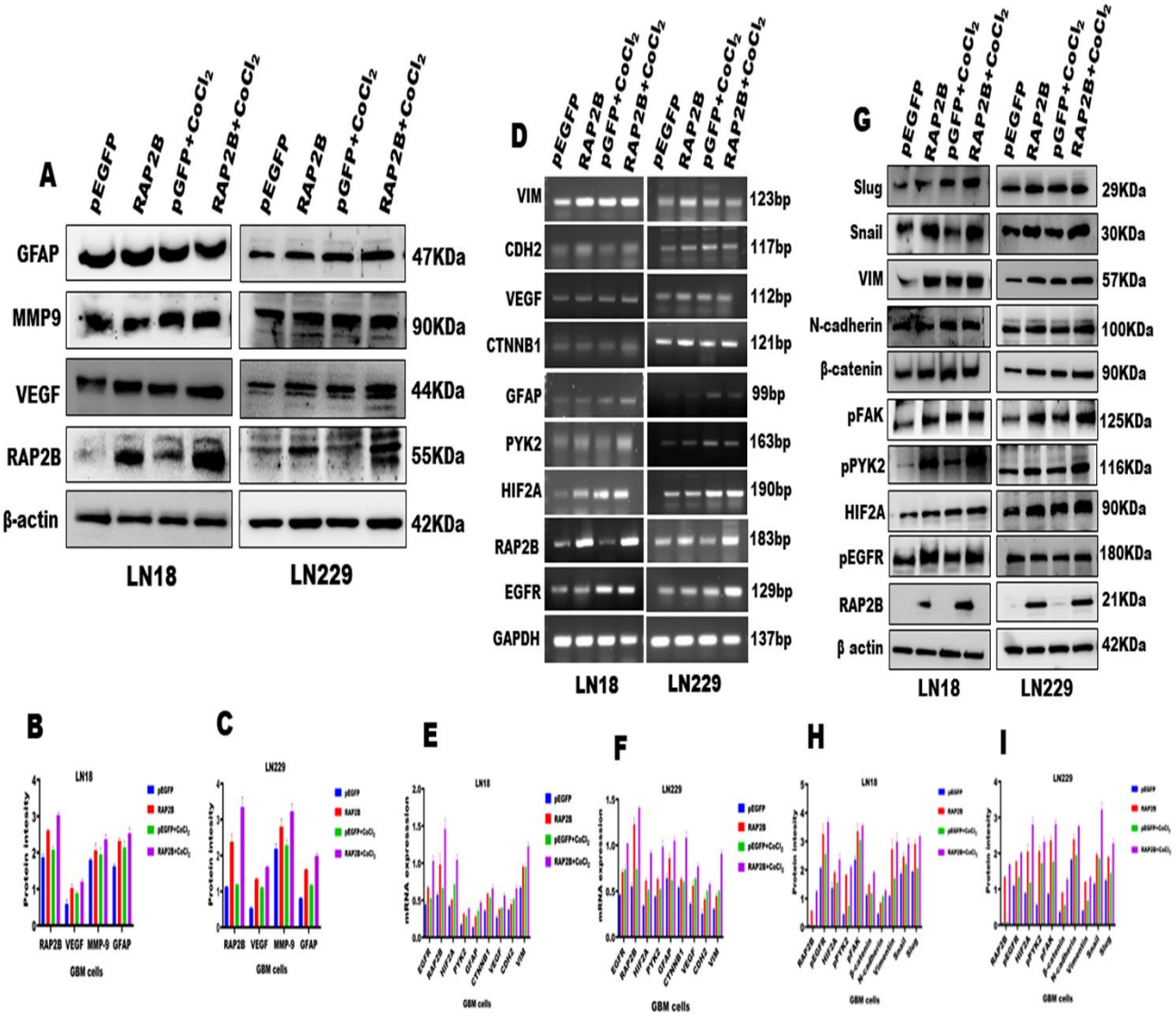

Figure 10: Upregulation of RAP2B/HIF2A activates pFAK/pPYK2-EMT signaling pathway in both GBM cells under hypoxia: (A, B, C), Western blot and densitometry results representing increased protein expression of GFAP, MMP-9 and VEGF in RAP2B, pEGFP+$CoCl_2$ but enhanced in RAP2B+$CoCl_2$ compare to pEGFP. **(D, E, F, G, H, I)**, PCR, western blot and their densitometry results depicting increased mRNA and protein expression of RAP2B, HIF2A, EGFR, PYK2, GFAP, CTNNB1, VEGF, CDH2, and VIM in RAP2B, pEGFP+$CoCl_2$ but higher in RAP2B+$CoCl_2$ compared to pEGFP in both GBM cells.

2.8. Discussion

The metastasis of cancer is the most critical event that impacts patient prognosis. Molecular research has enabled us to examine the causes of tumor resistance to established clinical therapies and shed light on the possible mechanism of cancer progression [27]. Studying the relationship between RAP2B and HIF2A expression in malignant astrocytoma tissues and GBM cells is critical. Previous research found that $CoCl_2$ (a hypoxia-mimicking agent) induces hypoxia in different cancers and promotes cancer cell proliferation and migration in a time or concentration-dependent manner. The current work developed an *in vitro* hypoxia model exposed with $CoCl_2$ to induced hypoxic microenvironment in support of the previous study [28]. It established a positive association between RAP2B and HIF2A to see their effect on GBM cell proliferation and migration. Previously reported that a hypoxic tumor microenvironment significantly alters the oxygen balance in various solid tumor tissues [29]. The presence of hypoxia may cause a variety of biological changes in solid tumors, and these alterations may be the fundamental cause of resistance to radiation and chemotherapy [30].

Ras protein controls gene expression and involved in cell proliferation, death, differentiation, and cytoskeletal rearrangement [31]. RAP2B, a small GTP-binding protein, found to be highly expressed in numerous types of tumors and acts as an oncogene including glioma [32], but limited information is explored. However, no one has reported RAP2B expression and function in GBM cell progression under hypoxia. The current study examined the expression correlation between RAP2B and HIF2A and their clinical and functional significance in malignant astrocytoma tissues. Our finding revealed that increased mRNA and protein expression of RAP2B and HIF2A in high grades astrocytoma tissues (grade 3 and grade 4) compared to low-grade (grade 2) and control. Interestingly, in the present study, we explored the increased expression of RAP2B positively correlated with HIF2A, suggesting that upregulation of RAP2B and HIF2A were associated with astrocytoma malignancy. The current study showed that increased expression of RAP2B and HIF2A significantly associated with high-grade astrocytoma (****$p<0.0001$) and positively associated with patient's poor survival but independent of patient age and gender shown in Table 1 supporting previous report [32]. Surprisingly, the correlation analysis exhibited that increased expression of RAP2B and HIF2A were positively correlated and associated with dismal survival compared to low grade and control. EMT is a progressive program associated with carcinogenesis and provides malignant properties in cancer cells by boosting mobility, invasion, and resistance to apoptotic stimuli [33]. Downstream protein expressions of pFAK, pPYK2 GFAP, vimentin, β-catenin, and N-cadherin were also highly upregulated in high-grade astrocytoma tissues, showing a

positive association with RAP2B/HIF2A in malignant astrocytoma. Moreover, understanding the relationship between RAP2B and HIF2A-mediated EMT activation in malignant astrocytoma could be highly significant. Here, we also performed IHC and IF; these results showed significantly more positive nuclear staining of RAP2B and HIF2A and colocalization in higher-grades astrocytoma compared to lower grades and noncancer tissues. Increased expression and colocalization between RAP2B and HIF2A positively associated with the high expression of pPYK2 and EMT proteins; suggesting that the RAP2B/HIF2A axis could be involved in the activation of pPYK2 and EMT in malignant astrocytoma. Furthermore, the transcript and protein expression data evidenced that activation of RAP2B/HIF2A/pFAK/pPYK2-EMT signaling in malignant astrocytoma, suggesting that these signaling pathway might be involved in GBM pathogenesis. We also compared our results of RAP2B and HIF2A transcript expression of malignant astrocytoma tissues positively correlated with gene expression data of RAP2B and HIF2A in GBM tissues from the online available databases TCGA and GEPIA. This indicated that clinicopathological analysis and etiological correlation between RAP2B and HIF2A in GBM malignancy and patients' poor survival emphasize its clinical significance. This indicated that targeting RAP2B and HIF2A could be a potential biomarker against glioma.

Previous reports suggested that RAP2B promotes cancer metastasis by affecting cell migration, invasion, angiogenesis, and cytoskeleton rearrangement [34]. Previously existing literature indicated that RAP2B, is a novel p53 target involved in Ca^{2+}-dependent FAK-ERK1/2 signaling, wnt signaling, c-Jun N-terminal kinase (JNK), and nuclear factor NF-kB signaling pathways, which regulate cell growth, differentiation, bacterial autophagy, synaptic transmission, and neuronal shape [35]. Herein, we provided insight into the expression and function of RAP2B under hypoxia through HIF2A/pFAK/pPYK2-EMT pathway in GBM cell progression. The present study demonstrated the differential mRNA and protein expression of RAP2B, HIF2A, and pPYK2 in C6, U87, LN18, LN229, and 1321N1 GBM cell lines. HIF2A is a hypoxia-inducible marker involved in cancer progression, and malignancies regulate various signaling pathways [36]. In the current study, we demonstrated that overexpression of RAP2B increased mRNA expression of RAP2B, HIF2A, VIM, EGFR, VEGF, PYK2, GFAP and proteins expressions of RAP2B, HIF2A, EGFR, β-catenin, vimentin, GFAP, VEGF, pFAK, pPYK2, snail and slug but enhanced expression in overexpressed RAP2B under hypoxia confirmed through PCR and western blot. In our finding, first time we showed overexpression of RAP2B increased expression and stabilized HIF2A in normoxia *vs* hypoxia. Increased expression of RAP2B/HIF2A axis enhanced the expression of MMP-9 and VEGF a proof of their role in migration under hypoxia, supporting previous studies [23]. Previously

reported that RAP2B unique function alter various cancer-related cellular processes, including inflammation, proliferation and migration [37]. Therefore, we performed *in vitro* functional assays and molecular studies to support our clinical outcome and investigated the impact of overexpressed RAP2B on GBM cell proliferation and migration under hypoxia. Several studies reported that overexpression of RAP2B and its oncogenic status promotes proliferation and migration through ERK, pFAK, AKT, and EMT pathways in various cancers, including glioma [32]. Likewise, HIF2A is also highly expressed in hypoxia and promotes tumorigenesis in multiple cancers through NF-kB, EGFR, p38/MAPK, Ras/MAPK, PI3K/AKT and EMT signaling pathways [38]. In the present study, we performed various cell-based assays like MTT, clonogenic, and scratch wound healing assay *in vitro* under hypoxia vs normoxia. Our finding demonstrated that overexpression of RAP2B increased proliferation, colony number, and migration but enhanced its effects when exposed to $CoCl_2$ for 24 hrs in both GBM cells. Thus, suggesting that overexpressed RAP2B oncogenicity increased in hypoxia and enhanced the proliferation and migration of GBM cells. Further, we performed immunofluorescence to confirm the colocalization between RAP2B and HIF2A, vimentin, GFAP, pPYK2. Our present study demonstrated that increased RAP2B and HIF2A staining strongly colocalized in the nucleus in overexpressed RAP2B in normoxia but enhanced expression and colocalization in LN18 and LN229 GBM cells under hypoxia. Likewise, overexpressed RAP2B increased vimentin, GFAP and pPYK2 staining as well as colocalization in normoxia and enhanced under hypoxia in both GBM cells. These suggested that overexpression of RAP2B increased HIF2A expression, and indicating that RAP2B/HIF2A-dependent activation of pFAK/pPYK2-EMT signaling could involve in GBM cell proliferation and migration in normoxia but enhanced their effects in hypoxia. Therefore, we strongly believe that apart from other oncogenic targets, RAP2B/HIF2A could be one of the most important oncogenic promoters for PYK2-EMT activation in GBM cell progression under hypoxia *vs* normoxia. These suggesting their clinical importance as a potential biomarker in malignant astrocytoma and established an oncogenic role of RAP2B/HIF2A in hypoxia.

2.9. Conclusion

Overall, the current study confirmed that increased expression of RAP2B/HIF2A in malignant astrocytoma associated with patients' worst survival. Furthermore, we verify our clinical data with *in vitro*, increased expression of the RAP2B/HIF2A axis positively enhanced pFAK/pPYK2-EMT signaling under hypoxia *vs* normoxia in GBM cells. Activation of RAP2B/HIF2A/pFAK/pPYK2-EMT signaling enhanced proliferation and migration in overexpressed RAP2B under hypoxia *vs* normoxia GBM cells.

These findings provided compelling evidence that increased RAP2B/HIF2A protein expression might play a role in the pathogenesis of gliomas and could be an essential target against GBM under hypoxia.

2.10. Additional Information

Study Approval

All procedures performed in the study involving human participants were approved by the Institutional Ethics Committee (IEC), University of Hyderabad, Hyderabad; Telangana (TS), with IEC reference number UH/IEC/2016/18. The written informed consent was obtained from all participants included in the study.

Supporting Information

To determine the association between RAP2B/HIF2A and IDH in malignant astrocytoma. High-grade astrocytoma tissues with increased expression of RAP2B showed 58.2% IDH mutant and 65.6% IDH wild type, but negative RAP2B represented 41.7% IDH mutant and 34.3% IDH wild type. Similarly, positive HIF2A tissues showed 62.6% IDH mutant and 59.7% in IDH wild type, but HIF2A negative tissues showed 37.3% IDH mutant and 40.2% IDH wild type shown in **Table S3**. The correlation study indicated the negative and positive association of GFAP, vimentin, and N-cadherin with RAP2B, as depicted in **Table S7**. To identify the relationship between RAP2B and HIF2A in high-grade astrocytoma tissues. Astrocytoma tissues with high positive RAP2B expression showed 86.5% HIF2A expression, indicating the association between RAP2B and HIF2A in astrocytoma malignancies represented in **Table S4**.

Supplementary Tables:

Table S1. EMT proteins associated with human astrocytoma grades

Astrocytoma grades	Grade 2 (n = 16)	Grade 3 (n = 16)	Grade 4 (n = 18)	Total (n = 50)
GFAP (+)	9 (56.25%)	13 (81.25%)	14 (77.7%)	36 (72%)
β-catenin (+)	11 (68.75%)	14 (87.5%)	15 (83.3%)	40 (80%)
Vimentin (+)	7 (43.75%)	13 (81.25%)	17 (94.4%)	37 (74%)
E-cadherin (-)	6 (37.5%)	13 (81.25)	16 (88.8%)	35 (70%)

EMT signaling activation involves EMT biomarkers at protein levels; (+ve/-ve) represents the presence/absence of protein expression.

Table S2: RAP2B/HIF2A association with EMT marker in different grades of astrocytoma

Tissues	CON (n = 7)	GII (n = 12)	GIII (n = 17)	GIV (n = 24)	Total (n = 53)
RAP2B (+)	4 (57.1%)	11 (91.6%)	15 (88.2%)	22 (91.6%)	48 (86.6%)
HIF2A (+)	3 (42.8)	9 (75%)	14 (82.3%)	23 (95.8%)	46 (83.3%)
Vimentin (+)	1 (14.2%)	5 (41.6)	15 (88.2%)	20 (83.3%)	40 (68.3%)

Table S3: Expression correlation between RAP2B/HIF2A and IDH mutant and wild-type status in human astrocytoma grades.

IDH status	RAP2B staining (n = 67)		p-value
	Positive	Negative	
IDH–mutant type	39 (58.2%)	28 (41.7%)	
IDH–wildtype	44 (65.6%)	23 (34.3%)	**p = 0.0056
	HIF2A staining (n = 67)		p-value
	Positive	Negative	
IDH–mutant type	42 (62.6%)	25 (37.3%)	
IDH–wildtype	40 (59.7%)	27 (40.2%)	**p = 0.0095

Co-expression of RAP2B and HIF2A in a hypoxic tumor microenvironment worsens astrocytoma malignancy and survival.

Table S4: Association between RAP2B and HIF2A in astrocytoma (n = 90)

	RAP2B expression profile		p-value
	(+)	(-)	
HIF2A (+)	(58) 86.5 %	(9) 13.4%	****p<0.0001
HIF2A (-)	(13) 19.4%	(54) 80.5%	

The relationship between RAP2B and HIF2A was examined in astrocytoma tissues (n=67) by using Fisher's exact test, which is represented by positive (+) or negative (-).

Table S5: IHC staining for RAP2B, HIF2A, and Vimentin in astrocytoma tissues.

Astrocytoma grades	No. of individuals with positive staining	RAP2B	HIF2A	Vimentin
Grade 2	10	+	++	+
Grade 3	17	+	+++	+++
Grade 4	20	+	++++	++++
Non tumor (Control)	5	+	-	+

This table represents the strong positive RAP2B stained astrocytoma tissue associated with HIF2A and vimentin positive and strong positive staining.

Table S6: Expression of RAP2B, HIF2A, pPYK2 and vimentin in astrocytoma grades and normal brain tissues (n = 110).

Groups	No of cases	Negative staining (%)	Moderate staining (%)	High (%) staining	p-value
RAP2B					
Astrocytoma	90	13 (14.4%)	32 (35.5%)	45 (50%)	****p<0.0001
Normal	20	15 (75%)	5 (25%)	0 (0%)	
HIF2A					
Astrocytoma	90	9 (10%)	30 (33.3%)	51 (56.6%)	****p<0.0001
Normal	20	17 (85%)	2 (10%)	1 (5%)	
pPYK2					
Astrocytoma	90	12 (13.3%)	35 (38.8%)	43 (47.7%)	****p<0.0001
Normal	20	14 (70%)	3 (15%)	3 (15%)	
Vimentin					
Astrocytoma	90	5 (5.5%)	28 (31.1%)	57 (63.3%)	****p<0.0001
Normal	20	19 (95%)	1 (5%)	0 (0%)	

The association between RAP2B, HIF2A, pPYK2 and vimentin for determining clinical outcome of astrocytoma patients.

Table S7: Clinical correlation between RAP2B and EMT proteins in human astrocytoma (70).

	RAP2B expression profile		Fischer's exact test
	(+)	(-)	
GFAP (+)	40	10	**p = 0.0080
GFAP (-)	9	11	
	RAP2B expression profile		
	(+)	(-)	
Vimentin (+)	42	8	***p = 0.0001
Vimentin (-)	7	13	
	RAP2B expression profile		
	(+)	(-)	
N-cadherin (+)	39	10	***p=0.0003
N-cadherin (-)	7	14	

RAP2B association with GFAP, vimentin, and N-cadherin were examined in astrocytoma grades using Fischer's exact test denoted by positive (+) or negative (-) protein expression.

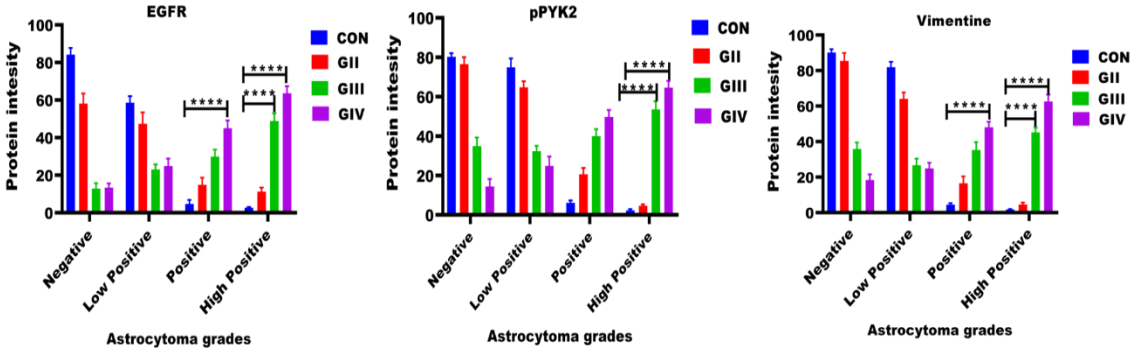

Figure S1: Densitometry analysis results show significantly elevated protein expression of EGFR, pPYK2 and vimentin (****p<0.0001) in malignant astrocytoma compared to lower grade and control tissues.

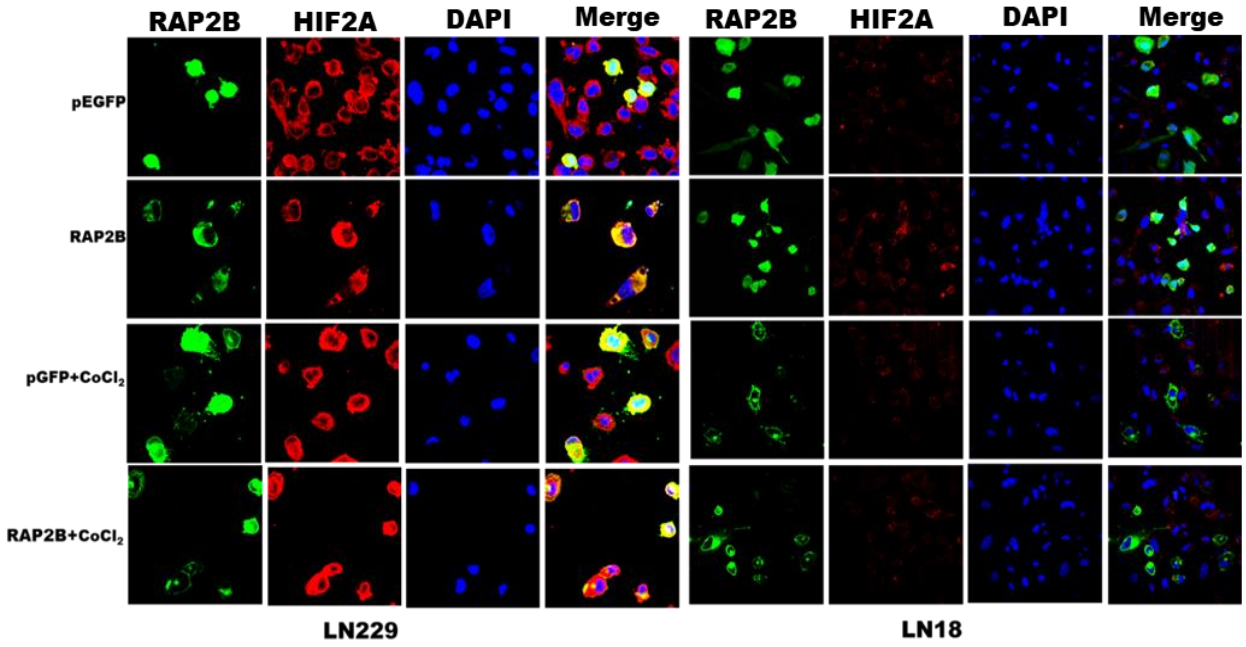

Figure S2: The IF images indicating over-expression of RAP2B increased RAP2B/HIF2A nuclear staining and colocalization in GBM cells under hypoxia *vs* normoxia.

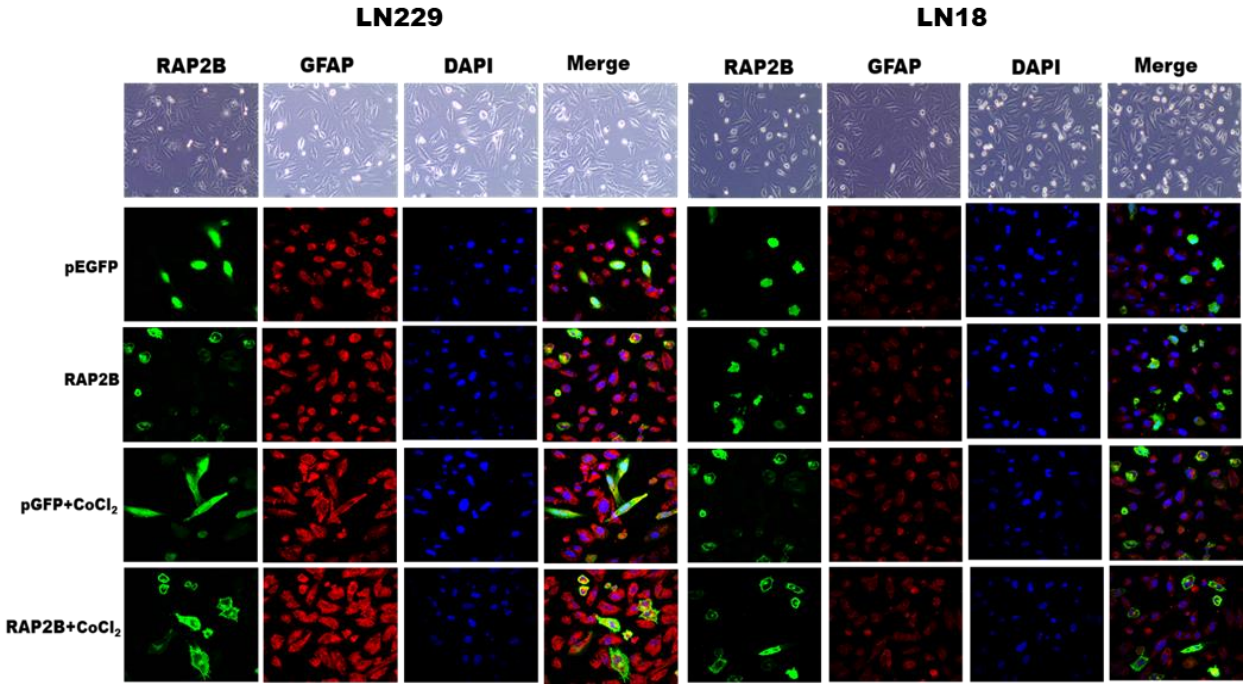

Figure S3: Representative IF images showing over-expression of RAP2B increased RAP2B/GFAP expression and colocalization in GBM cells under hypoxia *vs* normoxia.

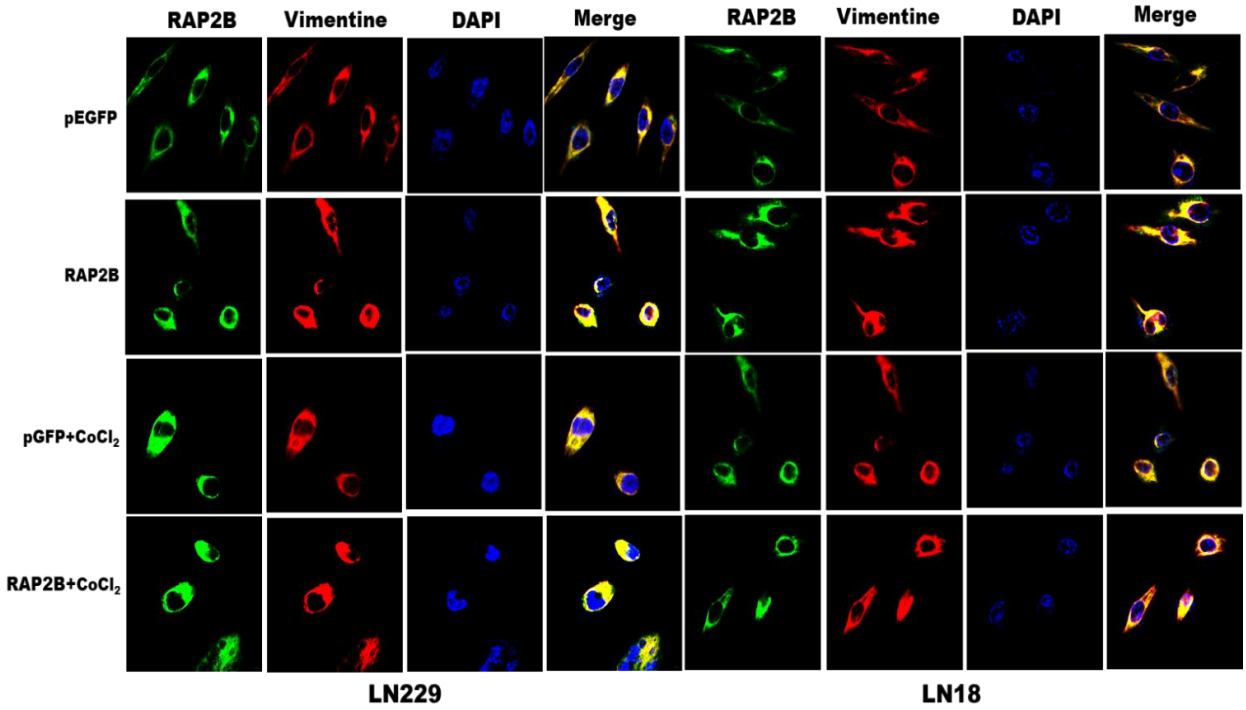

Figure S4: The IF images demonstrating the over-expression of RAP2B increased vimentin expression and colocalization with RAP2B in GBM cells under hypoxia compared to normoxia.

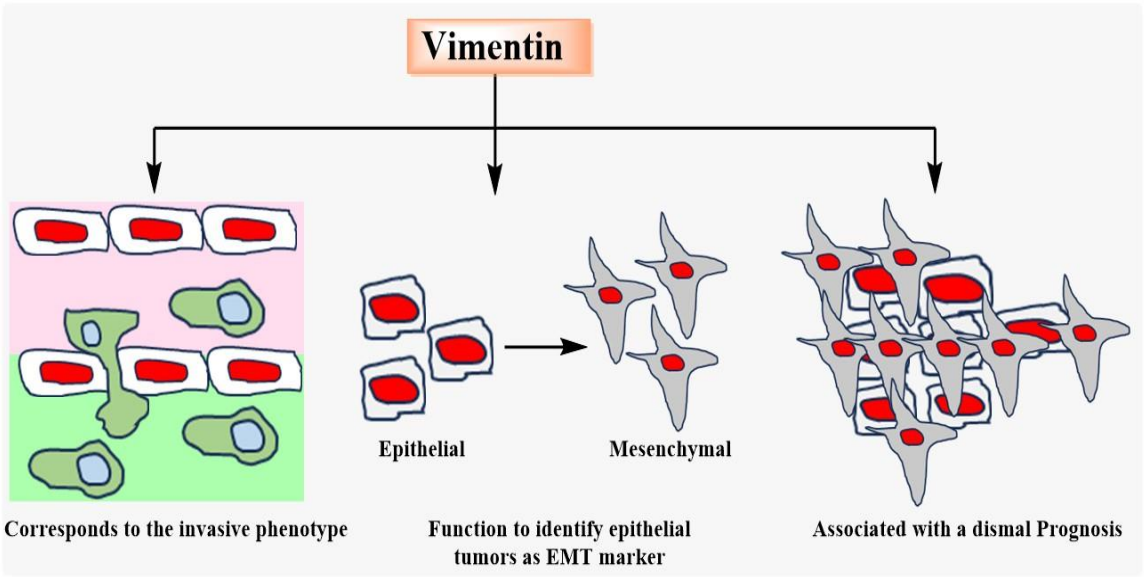

Figure S5: A schematic illustration showing the overexpression of vimentin, which is mainly associated with EMT in the progression of GBM [39].

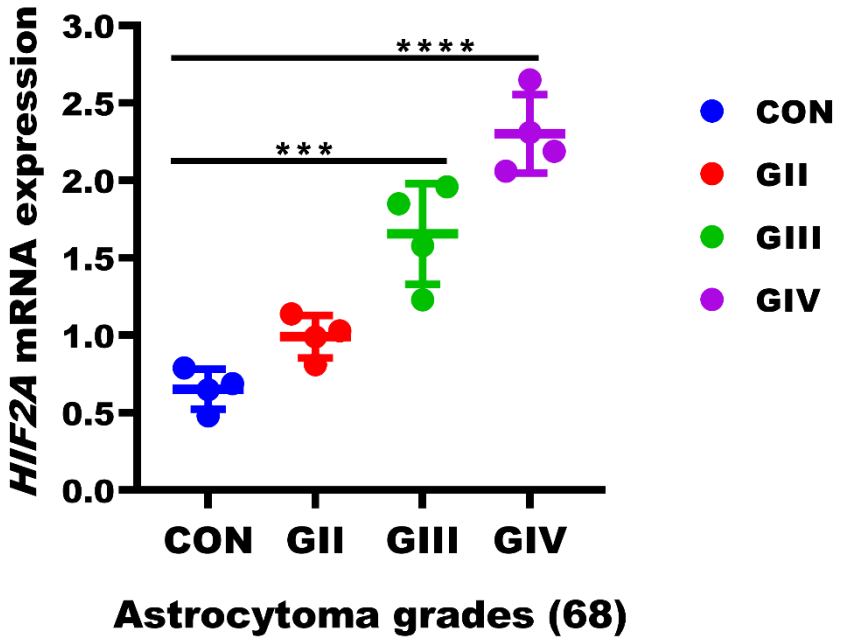

Figure S6: This result depicting increased transcript expression of HIF2A in grade 3 and grade 4 astrocytoma tissues compared to low grade and control. HIF2A mRNA significantly increased in grade 3 (***p=0.0001) and grade 4 (****p<0.0001) compared to low grade and control.

2.11. References:

1. Thakkar, J.P., *et al*., Epidemiologic and molecular prognostic review of glioblastoma. Cancer Epidemiol Biomarkers Prev, 2014. **23**(10): p. 1985-96.
2. Ostrom, Q.T., *et al*., CBTRUS Statistical Report: Primary Brain and Other Central Nervous System Tumors Diagnosed in the United States in 2014-2018. Neuro Oncol, 2021. **23**(12 Suppl 2): p. iii1-iii105.
3. Nakada, M., *et al*., Aberrant signaling pathways in glioma. Cancers (Basel), 2011. **3**(3): p. 3242-78.
4. (a) Hou, L.C., *et al*., Recurrent glioblastoma multiforme: a review of natural history and management options. Neurosurg Focus, 2006. **20**(4): p. E5. (b) Sherriff, J., *et al*., Patterns of relapse in glioblastoma multiforme following concomitant chemoradiotherapy with temozolomide. Br J Radiol, 2013. **86**(1022): p. 20120414.
5. Persano, L., *et al*., Glioblastoma cancer stem cells: role of the microenvironment and therapeutic targeting. Biochem Pharmacol, 2013. **85**(5): p. 612-622.
6. Mongiardi, M.P., Angiogenesis, and hypoxia in glioblastoma: a focus on cancer stem cells. CNS Neurol Disord Drug Targets, 2012. **11**(7): p. 878-83.

7. Harris, A.L., Hypoxia--a key regulatory factor in tumor growth. Nat Rev Cancer, 2002. **2**(1): p. 38-47.
8. Ohmstede, C.A., *et al*., RAP2B: a RAS-related GTP-binding protein from platelets. Proc Natl Acad Sci U S A, 1990. **87**(17): p. 6527-31.
9. Zhang, X., *et al*., Rap2b, a novel p53 target, regulates p53-mediated pro-survival function. Cell Cycle, 2013. **12**(8): p. 1279-91.
10. Fu, G., *et al*., [Identification and Functional Analysis of A Novel Candidate Oncogene RAP2B in Lung Cancer.]. Zhongguo Fei Ai Za Zhi, 2009. **12**(4): p. 273-6.
11. Xie, X., et al., miR-342-3p targets RAP2B to suppress proliferation and invasion of non-small cell lung cancer cells. Tumor Biol, 2015. **36**(7): p. 5031-8.
12. Di, J.H. *et al*., Rap2B promotes migration and invasion of human suprarenal epithelioma. Tumour Biol, 2014. **35**(9): p. 9387-94.
13. Luo, Z. *et al*., Silencing of HIF-1alpha enhances the radiation sensitivity of human glioma growth in vitro and in vivo. Neuropharmacology, 2015. **89**: p. 168-74.
14. Covello, K.L. *et al*., HIF-2alpha regulates Oct-4: effects of hypoxia on stem cell function, embryonic development, and tumor growth. Genes Dev, 2006. **20**(5): p. 557-70.
15. Liu, Z.J. *et al*., TIPE2 Inhibits Hypoxia-Induced Wnt/beta-Catenin Pathway Activation and EMT in Glioma Cells. Oncol Res, 2016. **24**(4): p. 255-61.
16. Iwadate, Y. *et al*., Transforming growth factor-beta and stem cell markers are highly expressed around necrotic areas in glioblastoma. J Neurooncol, 2016. **129**(1): p. 101-7.
17. Bhuria, V. *et al*., Hypoxia-induced Sonic Hedgehog signaling regulates cancer stemness, epithelial-to-mesenchymal transition and invasion in cholangiocarcinoma. Exp Cell Res, 2019. **385**(2): p. 111671.
18. Swinson, D.E. *et al*., Carbonic anhydrase IX expression, a novel surrogate marker of tumor hypoxia, is associated with a poor prognosis in non-small-cell lung cancer. J Clin Oncol, 2003. **21**(3): p. 473-82.
19. Giatromanolaki, A., *et al*., Relation of hypoxia-inducible factor 1 alpha and 2 alpha in operable non-small cell lung cancer to angiogenic/molecular profile of tumors and survival. Br J Cancer, 2001. **85**(6): p. 881-90.
20. Zhang, L., H.B. Duan, and Y.S. Yang, Knockdown of Rap2B Inhibits the Proliferation and Invasion in Hepatocellular Carcinoma Cells. Oncol Res, 2017. **25**(1): p. 19-27.
21. (a) Schaller, M.D., Cellular functions of FAK kinases: insight into molecular mechanisms and novel functions. J Cell Sci, 2010. **123**(Pt 7): p. 1007-13. (b) Avraham, H., et al., RAFTK/Pyk2-mediated cellular signaling. Cell Signal, 2000. **12**(3): p. 123-33.
22. McLeod, S.J. *et al*., The Rap GTPases regulate integrin-mediated adhesion, cell spreading, actin polymerization, and Pyk2 tyrosine phosphorylation in B lymphocytes. J Biol Chem, 2004. **279**(13): p. 12009-19.
23. (a) Chen, J.S. *et al*., FAK is involved in the invasion and metastasis of hepatocellular carcinoma. Clin Exp Metastasis, 2010. **27**(2): p. 71-82. (b) Schaller, M.D. et al., Autophosphorylation of the focal adhesion kinase, pp125FAK, directs SH2-dependent binding of pp60src. Mol Cell Biol, 1994. **14**(3): p. 1680-8.

24. Carmona, G., *et al*., Role of the small GTPase Rap1 for integrin activity regulation in endothelial cells and angiogenesis. Blood, 2009. **113**(2): p. 488-97.
25. Hoelzinger, D.B., *et al*., Gene expression profile of glioblastoma multiforme invasive phenotype points to new therapeutic targets. Neoplasia, 2005. **7**(1): p. 7-16.
26. Louis, D.N., *et al*., The 2007 WHO classification of central nervous system tumors. Acta Neuropathol, 2007. **114**(2): p. 97-109.
27. Chen, R. et al., Glioma Subclassifications and Their Clinical Significance. Neurotherapeutics, 2017. **14**(2): p. 284-297.
28. (a) Chu, C.Y. *et al*., CA IX is upregulated in $CoCl_2$-induced hypoxia and associated with cell invasive potential and a poor prognosis of breast cancer. Int J Oncol, 2016. **48**(1): p. 271-80. (b) Liu, J. et al., NKAP functions as an oncogene, and its expression is induced by CoCl(2) treatment in breast cancer via the AKT/mTOR signaling pathway. Cancer Manag Res, 2018. **10**: p. 5091-5100.
29. Cho, J. *et al*., Cobalt chloride-induced estrogen receptor alpha down-regulation involves hypoxia-inducible factor-1alpha in MCF-7 human breast cancer cells. Mol Endocrinol, 2005. **19**(5): p. 1191-9.
30. Mego, M. *et al*., CXCR4-SDF-1 interaction potentially mediates trafficking of circulating tumor cells in primary breast cancer. BMC Cancer, 2016. **16**: p. 127.
31. Bourne, H.R., D.A. Sanders, and F. McCormick, The GTPase superfamily: a conserved switch for diverse cell functions. Nature, 1990. **348**(6297): p. 125-32.
32. Shi, G. and Z. Zhang, Rap2B promotes the proliferation and migration of human glioma cells via activation of the ERK pathway. Oncol Lett, 2021. **21**(4): p. 314.
33. Mittal, V., Epithelial Mesenchymal Transition in Tumor Metastasis. Annu Rev Pathol, 2018. **13**: p. 395-412.
34. Neglia, J.P., *et al*., New primary neoplasms of the central nervous system in survivors of childhood cancer: a report from the Childhood Cancer Survivor Study. J Natl Cancer Inst, 2006. **98**(21): p. 1528-37.
35. Torti, M., *et al*., Association of the low molecular weight GTP-binding protein rap2B with the cytoskeleton during platelet aggregation. Proc Natl Acad Sci U S A, 1993. **90**(16): p. 7553-7.
36. Di, J. *et al*., Rap2B promotes proliferation, migration, and invasion of human breast cancer through calcium-related ERK1/2 signaling pathway. Sci Rep, 2015. **5**: p. 12363.
37. Peng, Y.G. *et al*., Rap2b promotes proliferation, migration, and invasion of lung cancer cells. J Recept Signal Transduct Res, 2016. **36**(5): p. 459-64.
38. Semenza, G.L., Pharmacologic Targeting of Hypoxia-Inducible Factors. Annu Rev Pharmacol Toxicol, 2019. **59**: p. 379-403.
39. Neglia, J.P., *et al*., New primary neoplasms of the central nervous system in survivors of childhood cancer: a report from the Childhood Cancer Survivor Study. J Natl Cancer Inst, 2006. **98**(21): p. 1528-37.

CHAPTER 3

To evaluate the cumulative therapeutic effect of RAP2B knockdown and Tyrphostin A9 treatment: Inhibition on GBM progression

Objective 2: To evaluate the cumulative therapeutic effect of RAP2B knockdown and Tyrphostin A9 treatment: Inhibition on GBM progression

Abstract

RAP2B is a novel p53 target, because of its high expression and oncogenic potential contributes to the development of various cancers as well as glioma. One of the essential characteristics of malignant gliomas is that EMT promotes tumor malignancy induced by hypoxia. The relationship between RAP2B and HIF2A as well as their therapeutic approach in GBM cells under hypoxia remains unknown. Herein, first time we investigated the linked between RAP2B and HIF2A expression, function as well as therapeutic approach in hypoxia. RAP2B/HIF2A role in activation of pFAK/pPYK2-EMT signaling promotes GBM cell proliferation and migration after 24 hrs of $CoCl_2$ exposure. In the present study, we evaluated the anticancer efficacy of a nontoxic dose of TYR A9 after RAP2B silencing in GBM cells under hypoxia. We observed that combination therapeutic approach of RAP2B knockdown and TYR A9 nontoxic dose showed better anticancer effect on GBM cells. We performed PCR, western blot, and immunofluorescence. PCR and western blot results proved that decreased mRNA and protein expression of RAP2B, HIF2A, EGFR, pFAK, pPYK2, β-catenin, N-cadherin, vimentin, snail, slug, MMP-9, VEGF and GFAP in siRAP2B, $CoCl_2$+siRAP2B and $CoCl_2$+TYR A9 treatment but diminished their expressions in combination of siRAP2B+TYR A9 treatment induced by pretreatment of $CoCl_2$ for 24 hrs in both GBM cells. siRAP2B, $CoCl_2$+siRAP2B and $CoCl_2$+TYR A9 treatment decreased RAP2B and HIF2A protein expression and their colocalization but abolished in combination of siRAP2B and TYR A9 induced by pretreatment of $CoCl_2$ for 24 hrs. We performed various cell-based experiments, MTT, clonogenic and wound healing assay, AO/EtBr, and annexin V staining to assess proliferation, migration, and apoptosis in GBM cells under hypoxia vs normoxia. Interestingly, our study evidenced that RAP2B knockdown increased the sensitivity of TYR A9 nontoxic dose inhibited proliferation, migration and sensitized GBM cells to induced apoptosis under hypoxia. However, combination treatment of siRAP2B and TYR A9 attenuated RAP2B and HIF2A mediated activation of pFAK/pPYK2-EMT signaling pathway and inhibited GBM cell progression under hypoxia. This suggests that RAP2B knockdown increased the anticancer efficacy of TYR A9 even at nontoxic doses, collectively evidencing that a combination of siRAP2B and TYR A9 could provide a strong promising therapeutic approach against glioma.

3.1. Introduction

Gliomas is the major malignant tumors of the central nervous system, have a poor prognosis. The median survival time for glioblastoma (WHO grade 4) is less than two years [1]. Therefore, it is crucial to understand the mechanism of glioma growth and identify new molecular targets for glioma treatment. However, despite several therapeutic efforts to target different signaling pathways or potential driver mutations, significant improvement has yet to be found with the addition of temozolomide (TMZ) or radiation as early therapy. RAP2B is predominantly 80% upregulated in several cancers, and additionally, it is a unique target of p53 and contributes to p53-mediated pro-survival function. Inhibition of RAP2B could make tumor cells more susceptible to apoptosis in response to DNA damage [2].

Tyrosine kinases and the downstream signaling proteins are inhibited by tyrosine kinase inhibitors [3]. Tyrphostin A9 is a member of the group of synthetic tyrphostin substances that are a series of tyrosine kinase inhibitors with improved affinity for epidermal growth factor receptor kinase domain [4]. A few selected tyrosine kinase inhibitors, such as AG1478 and AG1417, are being studied as possible anticancer drugs in preclinical models [5]. Tyrphostin A9 inhibits activated PYK2 (Tyr402 phosphorylation) and also reduced hypoxia-induced human pulmonary artery smooth-muscle (HPASM) cell proliferation. PYK2 expression is linked to the increased expression of HIF-1α and are involved in pulmonary vascular wall cell proliferation [6].

Overexpressed RAP2B promotes the proliferation, migration, and invasion in prostate cancer, breast cancer, human suprarenal epithelioma, and HCC cancers by regulating various signaling pathways [7]. Despite earlier reports on RAP2B expression and function in human glioma, but the relationship between RAP2B and HIF2A expression and their function under hypoxia remains unknown. Therefore, this objective aimed to understand the positive correlation between RAP2B and HIF2A that contributes to GBM cell progression under hypoxia. Downregulation of RAP2B makes HCT116 colorectal cancer cells more susceptible to apoptosis caused by Adriamycin (Adr), indicating that RAP2B increases Adr resistance in cancer cells [2]. It is reported that siRNA-mediated knockdown of RAP2B and FAK inhibitors blocks the EMT process by targeting RAP2B and FAK, showing treatments for cutaneous squamous cell carcinoma (CSCC) [8]. Previous findings motivated us to evaluate the anticancer efficacy of TYR A9 nontoxic dose treatment after RAP2B knockdown against GBM cells under hypoxia. In the current study, we found that RAP2B knockdown enhanced the sensitivity of TYR A9 and increased the susceptibility of GBM cells to apoptosis under hypoxia. In the present study, we demonstrated that the knockdown of RAP2B decreased HIF2A expression and abolished it after a combination of siRAP2B

and TYR A9 treatment. Interestingly, we investigated PYK2 expression and function inhibited by TYR A9 in GBM cells under hypoxia. First time, we showed $CoCl_2$ treatment increased expression of RAP2B, HIF2A and GFAP, VEGF, MMP-9 together with EMT protein levels and phosphorylation levels of EGFR, FAK, PYK2 promotes GBM cell progression after 24 hrs of treatment. Our results showed RAP2B knockdown or TYR A9 treatment decreased the expression of RAP2B/HIF2A/pFAK/pPYK2-EMT signaling proteins and VEGF, MMP-9, GFAP but attenuated by combination of RAP2B knockdown and TYR A9 nontoxic dose in hypoxia. Combined treatment of RAP2B knockdown and TYR A9 nontoxic dose inhibited RAP2B/HIF2A axis suppressed GBM cell proliferation and migration by inhibiting the activation of the pFAK/pPYK2-EMT signaling pathways. RAP2B knockdown and TYR A9 treatment induces apoptosis but enhanced more apoptosis induction in combination of siRAP2B and TYR A9 nontoxic dose in GBM cells under hypoxia. Therefore, this study indicated that RAP2B/HIF2A axis may serve as a potential novel regulator of PYK2-EMT signaling in GBM under hypoxia.

3.2. To developed therapeutic approaches against GBM cell progression under hypoxia by inhibition of RAP2B/HIF2A axis

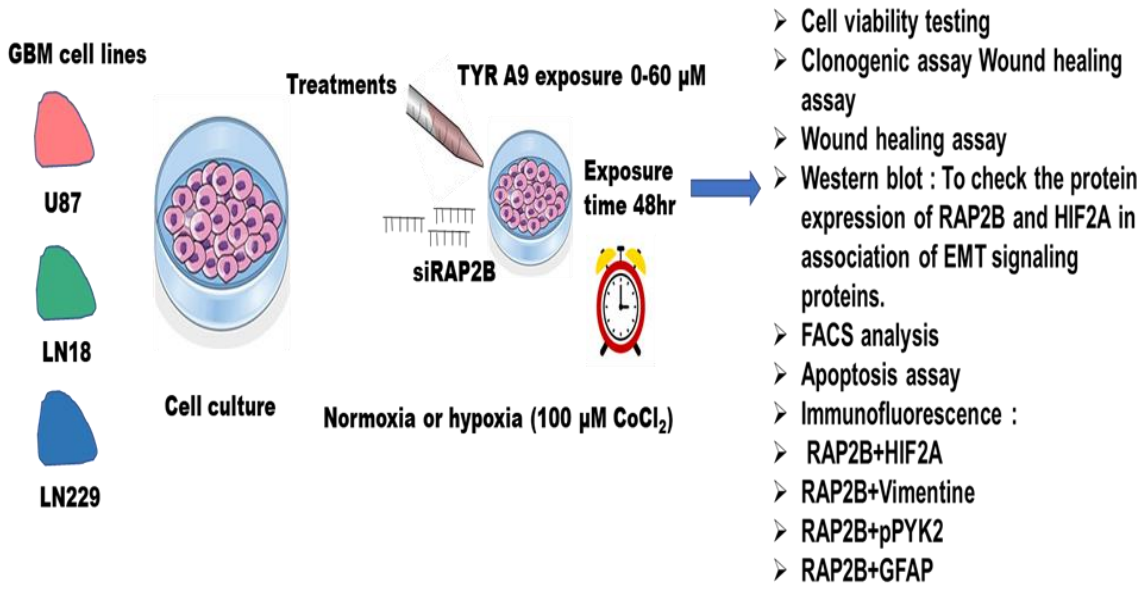

Figure 1: The experimental procedure showing in above diagram represents therapeutic approach by transfection of siRAP2B and TYR A9 treatment in both GBM cells under hypoxia (100 µM, 150 µM and 200 µM of $CoCl_2$) *vs* normoxia (without $CoCl_2$).

3.3. Material and Methods

3.3.1. Materials

DMEM, FBS, Anti-Anti (antibiotic and antimycotic) and trypsin, Trizol reagent, cDNA synthesis kit, Premix Dream Taq, and SYBR premix Ex Taq II, RIPA Lysis buffer recipes, Protease and Phosphatase cocktail, Bradford reagent, primers used as **objective 1**, Protein marker, enhanced chemiluminescent (ECL) following details refer to **objective 1** with mentioned modified experimental conditions siRNA for RAP2B was purchased from Genex; Lipofectamine 2000 was obtained from Thermo-Fisher Scientific. Annexin V- fluorescein isothiocyanate (FITC)/Propidium iodide (PI) apoptosis kit purchased from Thermo-Fisher Scientific. Tyrphostin A9 was purchased from TCI; for details refer to **objective 3**.

3.4. Cell culture and transfection

Two established GBM cell lines, U87 and LN18, were procured from NCCS Pune, India. These cells were maintained in a complete DMEM medium with 10% FBS, 1X anti-anti (antibiotic and antimycotic) at 37 ℃ humidified chambers in 5% CO_2 incubator. GBM cells were seeded with approximately 70 to 80% confluency in six well-plates and, the next day, replaced media with fresh incomplete DMEM without anti-anti and FBS. Further diluted siRNA target for RAP2B and negative control siNC (scramble siRNA) in incomplete medium and incubated for 20 minutes at room temperature. To knockdown RAP2B expression in U87 and LN18 GBM cells were transfected with 30nmol siRNA targeted for RAP2B (siRAP2B) and scrambled siRNA non targeted (Negative control) when cells reached 70% confluency using Lipofectamine™ 2000 (Invitrogen; Thermo-Fisher Scientific, Inc.) for 6 hrs in incomplete DMEM. After 6hr of incubation, incomplete media was replaced with complete DMEM and normally grew for 24 hrs before subsequent experimentation. siRNA sequences were given: A scrambled RNA (siNC) was used as a negative control for RAP2B in GBM cells. Experimental group in this study siNC (scramble siRNA), siRAP2B (RAP2B targeted siRNA), $CoCl_2$ treatment for 24 hrs (To induce hypoxia), $CoCl_2$+siRAP2B, $CoCl_2$+TYR A9, $CoCl_2$+siRAP2B+TYR A9. GBM cells were transfected with siRAP2B for 24 hrs of incubation, $CoCl_2$+siRAP2B cells were pretreated with $CoCl_2$ for 24 hrs and then transfected with siRAP2B, $CoCl_2$+siRAP2B+TYR A9 Firstly, treated with $CoCl_2$ for 24 hrs and transfected with siRAP2B and then TYR A9 nontoxic dose (10 µM for U87 and 20 µM for LN18 below IC_{50} value) treatment for another 24 hrs, $CoCl_2$+TYR A9 cells were pretreated with $CoCl_2$ and then treated with 20 µM and 40 µM (IC_{50} value) of TYR A9 in respective GBM cell lines.

3.4.1. Transfection of siRNA in GBM cells

siRNA is a powerful technique to knockdown RAP2B (Sense sequence: 5'-CCA-UGA-GAG-AGU-ACA-AAG-U55-3') and (Antisense sequence: 5'-ACU-UUG-UAC-UCU-CUC-AUG-G56-3') were designed and synthesized from Eurogentec Belgium (SR-NP001-004-siRNA Duplex SePOP 40nmol). Commercially available scrambled siRNA was purchased from Qiagen (#1022076). According to the manual instructions, scramble siRNA and RAP2B target siRNA transfection was performed using Lipofectamine®2000 reagent (1mg/ml) (Catalog No. 11668030) purchased from Invitrogen. The maximum transfection efficiency was determined at 30 nmol of RAP2B targeted siRNA. RAP2B knockdown was confirmed at both mRNA and protein levels after 48 hrs of siRNA transfection.

3.4.1.1 RNA isolation and quantitative real-time PCR (RT-qPCR)

U87 and LN18 GBM cell lines were used for RNA isolation and PCR followed the mentioned experimental conditions. Experimental groups used in this study such as GBM cells were treated with defined dose (100 μM and 150 μM) of $CoCl_2$ treatment for 24 hrs. GBM cells were transfected with scrambled siRNA (control), siRAP2B, $CoCl_2$+siRAP2B pretreated defined dose of $CoCl_2$ for 24 hrs and then transfected with siRAP2B, $CoCl_2$+TYR A9 pretreated defined dose of $CoCl_2$ for 24 hrs treated with TYR A9 treatment (IC50 dose) and $CoCl_2$+siRAP2B+TYR A9 pretreated $CoCl_2$ for 24 hrs transfected with siRAP2B and then treated with TYR A9 nontoxic dose. GBM cells with above mentioned experimental conditions total RNA was extracted from both GBM cells through the Trizol method. For cDNA synthesis, reverse transcribes to cDNA synthesis using the first strand cDNA synthesis KIT, semiquantitative PCR, and RT-qPCR were performed using a similar procedure detailed refer to **objective 1**. Genes used for this study detailed mentioned in **Table S1**. Each gene was normalized with GAPDH, and relative quantification was performed using the $2^{-\Delta\Delta Ct}$.

3.4.1.2 Western blot and antibodies

Above mentioned experimental condition for RNA isolation, same experimental conditions were used for western blot in U87 and LN18 GBM cell lines. Followed procedure for protein isolation, quantification, and SDS page information provided in **objective 1** applied to this objective—antibodies details mentioned in below given **Table 3**.

Table 3 Antibodies' details are listed below:

Name of Antibody	Company Name	Catalog	WB dilutions	IHC dilutions	IF dilution
β- Actin	Sigma Aldrich	A3854	1:25000		
EGFR	CST	2220S	1:1000	1:100	
RAP2B	Abcam	ab101369	1:3000	1:250	1:100
HIF2A	Novus Biological	NB100-132SS	1:2000	1:250	1:100
pPYK2	Invitrogen	#44-618G	1:1000	1:250	1:100
PYK2	Santa Cruz	sc-393181	1:500	1:50	
pFAK	CST	#8556T	1:1000	1:250	1:100
β-catenin	CST D10A8	#8480T	1:1000	1:250	
N-cadherin	CST D4R1H	#13116T	1:1000		
Vimentin	CST D21H3	#5741T	1:2000	1:250	1:100
Slug	CST C19G7	#9585T	1:1000		
Snail	CST C15D3	#3879T	1:1000		
MMP-9	Santa Cruz 2C3	sc-21733	1:1000		
VEGF	Gene Tex	GTX102643	1:1000		
GFAP	Abcam	#ab7260	1:3000	1:250	1:100
Ki-67	CST D2H10	#9027		1:250	
PCNA	Santa Cruz PC10	sc-56	1:1000		
pERK1/2	CST	#4377	1:2000	1:250	1:100
tERK1/2	CST	#9102	1:1000		
pSRC	CST Tyr416	#6943	1:2000		
FAK	CST	#3285T	1:1000		
Cleaved caspase-3	CST (D175)	#9664T	1:1000	1:100	
Caspase-3	CST	#9662S	1:1000		
Cleaved Caspase-9	CST	7237T	1:1000		
PARP both	CST	9542T	1:1000		
GFP	G-1544	Sigma Aldrich	1:3000		

Bcl2	CST	4223 T	1:1000		
Bax	CST	2772 T	1:1000		
Bad	CST	9292 T	1:1000		
Cytochrome-C	Santacruz	sc-13560	1:1000		
P53	Abcam	Ab131442	1:3000		
Anti-rabbit	GeNei Lab	(#1140380011730)	1:10000		
anti-mouse	GeNei Lab	(#1140680011730)	1:10000		

3.4.1.3. MTT assay

MTT assay was performed to see the inhibition of GBM cell proliferation in above mentioned experimental conditions for RNA isolation. U87 and LN18 GBM cells were counted and seeded 1×10^4 cells/well of 96 well plates allowed them to grow for overnight. Both GBM cell lines transfected with scrambled siRNA, siRAP2B, $CoCl_2$ treatment of defined dose 100 µM and 150 µM for 24 hrs (to induce hypoxia) of respective cells, $CoCl_2$+siRAP2B pretreated with $CoCl_2$ for 24 hrs transfected with siRAP2B incubated for another 24 hrs. $CoCl_2$+TYR A9, pretreated $CoCl_2$ treated with TYR A9 (IC50 dose) for another 24 hrs and $CoCl_2$+siRAP2B+TYR A9, pretreated $CoCl_2$ GBM cells transfected with siRAP2B and then treated with TYR A9 nontoxic dose for another 24 hrs. Both GBM cells were incubated and added MTT reagent at different time points 0, 24, 48 and 72 hrs. MTT assay was performed following the procedure mentioned in **objective 1** refer to **page no 33**.

3.4.1.4. Clonogenic assay

Followed above all experimental conditions mentioned for MTT assay and used methodology details provided in **objective 1** refer to **page no 33**.

3.4.1.5. Scratch wound healing assay

To perform wound healing assay, both GBM cells were seeded 80 to 90% confluency for each experimental condition as mentioned above for MTT assay. Followed procedure, capturing images and calculated % of migrated cells mentioned in **objective 1** applied for this objective also.

3.4.1.6. Flow cytometry for apoptosis detection

Annexin V-FITC apoptosis assay was performed to see induction of apoptosis in both GBM cells under hypoxia *vs* normoxia. U87 and LN18 GBM cells were seeded at density of 5×10^6 in each 60 mm dish and transfected with siNC, siRAP2B, $CoCl_2$+siRAP2B, $CoCl_2$+TYR A9 and $CoCl_2$+siRAP2B+TYR A9.

Pretreated with and without $CoCl_2$ of 100 µM and 150 µM defined dose for respective GBM cells (to mimic hypoxia) for 24 hrs. After 24 hrs of transfection, both GBM cells were trypsinized and washed with pre-chilled 1XPBS. Cells were centrifuged at 2000 rpm for 3 minutes and supernatant was removed carefully, further resuspended in 100µl of annexin V binding buffer. Cells suspension was incubated with 5 µl of annexin V/FITC and 1 µl of propidium iodide for 15 minutes at room temperature in the dark. After incubation, additionally added 400 µl of binding buffer (as per manual instructions) before detecting apoptosis through flow cytometry. Further, samples were analyzed using FACS BD caliber instrument. Rate of apoptosis and statistical analysis was performed using Flow Jo software. Experiments are repeated twice independently.

3.4.1.7. Immunofluorescence

Both U87 and LN18 GBM cell lines were seeded on coverslip and grown overnight at 37 ℃ humidified chambers in 5% CO_2 incubator. Next day, cells were washed with 1X PBS added incomplete media and transfected with siNC, siRAP2B without $CoCl_2$, (normoxia), $CoCl_2$+siRAP2B, $CoCl_2$+TYR A9 (IC_{50} dose) and $CoCl_2$+siRAP2B+TYR A9, pretreated with 100 µM and 150 µM of $CoCl_2$ (to mimic hypoxia) respectively for 24 hrs transfected with siRAP2B and treated with TYR A9 at dose IC_{50} value and below IC_{50}. 100 µM and 150 µM of $CoCl_2$ treatment without transfection for 24 hrs (induce hypoxia). After 48 hrs of incubation performed immunofluorescence staining following methodology mentioned in **objective 1** applied for this also. Each sample at least 30 to 50 cells were counted and analyzed. Fluorescence intensity represented the quantitative protein expression. On the other hand, the results of colocalization between RAP2B and HIF2A, vimentin showed quantitatively in the term of the colocalization factor, which was quantified using the Fiji image J software. The co-localization factor is calculated as [(fraction of co-localized cells) × (fraction of colocalized foci per cell) ×100].

3.5. Statistical analysis

In this study, all experiments were performed more than two times. GraphPad prism 9.3 software was used to analyze all experimental data. The comparison between experimental groups and control performed One way ANOVA and Two-way ANOVA test depending on the number of groups analyzed using Sidak's multiple comparisons test. Differences were considered significant at $p<0.05$.

3.6. Results

3.6.1. RAP2B knockdown enhanced TYR A9 sensitivity inhibits GBM cell proliferation and growth in $CoCl_2$-induced hypoxia

We attempted to understand whether the knockdown of RAP2B involved in inhibiting GBM cell proliferation and growth under hypoxia. We confirmed knockdown of RAP2B mRNA and protein levels detected through PCR and western blot **(Figure 4D, G)** in both GBM cells under hypoxia *vs* normoxia. Uncontrolled proliferation and growth are the fundamental characteristics of cancer cells. Therefore, we evaluated the role of RAP2B knockdown and TYR A9 treatment alone and combination of both RAP2B knockdown and TYR A9 nontoxic dose on cell proliferation and growth confirmed by MTT and clonogenic assay. MTT assay results **(Figure 2A, B)** showed that decreased cell proliferation in RAP2B knockdown (siRAP2B) compared to nontarget siRNA (siNC) without $CoCl_2$ (**p = 0.0052), (**p = 0.0038). Similarly, $CoCl_2$+siRAP2B, $CoCl_2$+TYR A9 treatment also reduced cell proliferation, however significantly inhibited cell proliferation in combination of $CoCl_2$+siRAP2B+TYR A9 (nontoxic dose) compared to $CoCl_2$ (**p = 0.0028), (**p = 0.0012), (***p = 0.0004), (***p = 0.0001) and (****p≤0.0001) in both GBM cells. These results suggested that the knockdown of RAP2B increased TYR A9 anticancer efficacy significantly inhibited proliferation in GBM cells. Likewise, clonogenic assay **(Figure 2C, E)** and densitometry analysis results **(Figure 2D, F)** demonstrated that decreased colony number in siRAP2B compared to siNC (**p = 0.0035) (**p = 0.0027). Similarly, $CoCl_2$+siRAP2B, $CoCl_2$+TYR A9 treatment also reduced number of colonies but significantly repressed in combination of $CoCl_2$+siRAP2B+TYR A9 (nontoxic dose) compared to $CoCl_2$ (**p = 0.0041), (**p = 0.0022), (***p = 0.0006), (***p = 0.0008) and (****p≤0.0001). Interestingly, these results indicated that RAP2B knockdown and TYR A9 treatment decreased colony-forming ability but combination of silenced RAP2B and TYR A9 nontoxic dose significantly inhibited colony-forming ability of GBM cells under hypoxia. This suggesting that silenced RAP2B increased anticancer efficacy of TYR A9 even at nontoxic dose. Simultaneously we also checked molecular markers involved in proliferation like GFAP, protein level detected by western blot. Western blot and densitometry results **(Figure 4A, B, C)** demonstrated that GFAP protein levels were decreased in siRAP2B compared to siNC (normoxia). Similarly, $CoCl_2$+siRAP2B, $CoCl_2$+TYR A9 treatment also reduced GFAP protein level but diminished in $CoCl_2$+siRAP2B+TYR A9 compared to $CoCl_2$ treated (hypoxia) in both GBM cells.

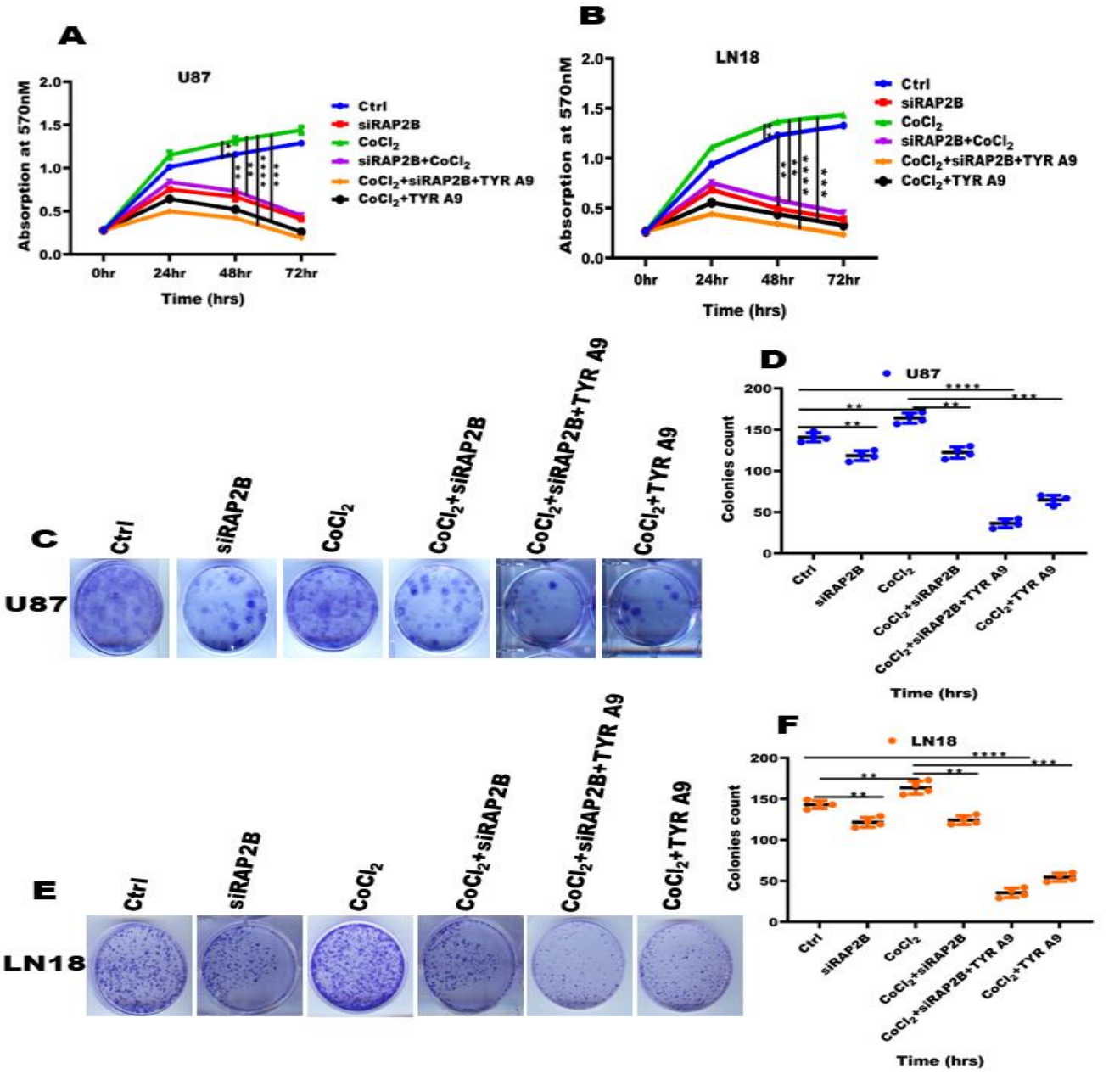

Figure 2: Knockdown of RAP2B enhanced sensitivity of TYR A9 non-toxic dose in GBM cells: (A, B), MTT assay results indicates decrease cell proliferation in siRAP2B (normoxia), $CoCl_2$+siRAP2B and $CoCl_2$+TYR A9 (IC_{50}) but inhibited in $CoCl_2$+siRAP2B+TYR A9. **(C, E)**, Clonogenic assay images represent number of colonies were detected in all experimental groups in both GBM cells. **(D, F)**, Densitometry analysis results showing decreased no. of colonies in siRAP2B, CoCl2+siRAP2B, $CoCl_2$+TYR A9 but significantly reduced in $CoCl_2$+siRAP2B+TYR A9 compared to $CoCl_2$ (****$p \leq 0.0001$).

3.6.2. RAP2B downregulation increases TYR A9 sensitivity significantly inhibited cell migration by regulating VEGF and MMP-9 level in GBM cells.

The impact of RAP2B knockdown and TYR A9 treatment at (nontoxic dose) (10 µM for U87 and 20 µM for LN18) was examined on cell migration using scratch wound healing assay in both GBM cell lines. The effect of knockdown RAP2B, TYR A9 treatment and combination of both knockdown RAP2B and TYR A9 nontoxic treatment on cell migration without $CoCl_2$ (normoxia) and with $CoCl_2$ (hypoxia) in both GBM cells. Scratch wound healing assay images and densitometry analysis results **(Figure 3A, B, C, D)**, evidenced that reduced migration in RAP2B knockdown (siRAP2B) compared to control (siNC) normoxia (**p = 0.0013), (**p = 0.0021). Similarly, $CoCl_2$+siRAP2B, $CoCl_2$+TYR A9 treatment also decreased migration but significantly inhibited migration in combination of $CoCl_2$+siRAP2B+TYR A9 (nontoxic dose) compared to $CoCl_2$ (hypoxia) (**p = 0.0024), (**p = 0.0041), (***p = 0.0005), (***p = 0.0003) and (****p<0.0001) in both GBM cells. Densitometry analysis results **(Figure 3C, D)** showed 67% decreased migration in siRAP2B compared to control (siNC). Likewise, decreased migration 66% in $CoCl_2$+siRAP2B, 72% in $CoCl_2$+TYR A9, but significantly inhibited 87% migration in $CoCl_2$+siRAP2B+TYR A9 compared to $CoCl_2$ treated (hypoxia). Simultaneously we also checked molecular markers involved in migration like MMP-9 and VEGF protein levels were detected by western blot. Western blot and densitometry results **(Figure 4A, B, C)** demonstrated that MMP-9 and VEGF protein levels were decreased in siRAP2B compared to siNC (normoxia). Similarly, $CoCl_2$+siRAP2B, $CoCl_2$+TYR A9 treatment also reduced MMP-9 and VEGF protein levels but diminished in $CoCl_2$+siRAP2B+TYR A9 compared to $CoCl_2$ treated (hypoxia) in both GBM cells. These results suggested that RAP2B knockdown and TYR A9 decreased migration in normoxia *vs* hypoxia. RAP2B knockdown enhanced anticancer potential of TYR A9 even at nontoxic dose and combination of both inhibited cell migration in both GBM cell lines under hypoxia.

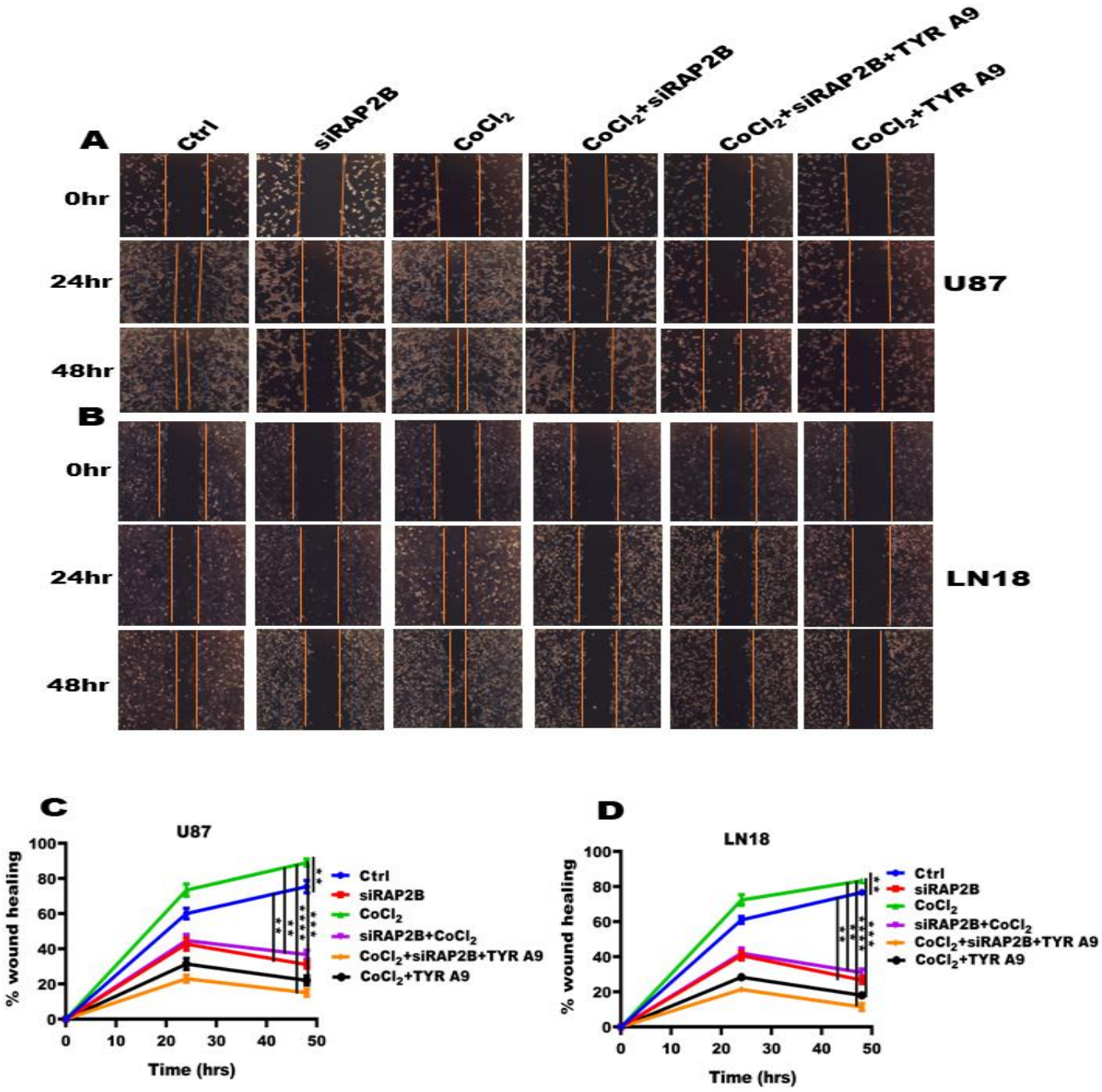

Figure 3: siRAP2B enhanced inhibitory effect of TYR A9 nontoxic dose in GBM cells: (A, B) Scratch wound healing assay indicates inhibition of cell migration in both GBM cells under hypoxia *vs* normoxia. **(C, D)** Densitometry analysis representing percent of wound width closer efficiency inhibition in siRAP2B $CoCl_2$+siRAP2B, $CoCl_2$+TYR A9 and $CoCl_2$+siRAP2B+TYR A9 compared to $CoCl_2$ and siNC.

3.6.3. Cumulative therapeutic effect of RAP2B knockdown and TYR A9 nontoxic dose attenuate activation of HIF2A/pFAK/pPYK2-EMT signaling pathway in GBM cells under hypoxia

The pFAK/pPYK2 signaling pathways are a conventional cell survival involved in the cell proliferation, differentiation, aggressiveness, metastasis and apoptosis. Previously reported that pFAK/pPYK2 signaling pathway is activated by RAP2B oncoprotein in the several type of cancer [21]. In present study we verified that combination therapeutic approach by RAP2B knockdown along with TYR A9 treatment in both U87 and LN18 GBM cell lines under hypoxia **(Figure S1)**. Semi-quantitative PCR, western blot and densitometry results demonstrated that decreased mRNA and protein expression of RAP2B, HIF2A, EGFR, pPYK2, pFAK, β-catenin, N-cadherin, vimentin, snail and slug in siRAP2B compared to siNC (control normoxia). Likewise, $CoCl_2$+siRAP2B, $CoCl_2$+TYR A9 treatment also decreased these mRNA and proteins expression but abolished in $CoCl_2$+siRAP2B+TYR A9 (nontoxic dose) compared to $CoCl_2$ (hypoxia) in both GBM cells **(Figure 4D, E, F and G, H, I)**. Simultaneously, we were also interested to check their localization, therefore we performed immunofluorescence in U87 GBM cell line under hypoxia vs normoxia. Immunofluorescence results revealed that decreased RAP2B, HIF2A and vimentin staining and their colocalization in siRAP2B, $CoCl_2$+siRAP2B, $CoCl_2$+TYR A9, but inhibited in $CoCl_2$+siRAP2B+TYR A9 compared to $CoCl_2$ (****$p<0.0001$) and siNC (***$p = 0.0003$), (***$p = 0.0008$) **(Figure 5A)** in U87 GBM cell. Further, colocalization was calculated by Pearson's correlation coefficient of each identified object for the pixel intensities in the two channels of whole image-based intensity correlation (r) when reach to 1.0 represented strong colocalization. Pearson's correlation coefficient showed weak colocalization between RAP2B and HIF2A $r = 0.321$, RAP2B and vimentin $r=0.386$ in siRAP2B compared to siNC $r = 0.771$, $r = 0.601$. Similarly, PCC showed less colocalization in $CoCl_2$+siRAP2B $r = 0.407$, $r = 0.331$, in $CoCl_2$+TYR A9 $r = 0.292$, $r = 0.309$ but inhibited in $CoCl_2$+siRAP2B+TYR A9 $r = 0.0109, 0.105$ compared to $CoCl_2$ treated $r = 0.967$, $r = 0.846$ in U87 GBM cells under hypoxia. These results showing that PCC (r) values very close to 1 represents strong colocalization in $CoCl_2$ and control and combination of RAP2B knockdown and TYR A9 nontoxic dose treatment inhibited expression, colocalization and RAP2B/HIF2A/pFAK/pPYK2-EMT signaling pathway induced by $CoCl_2$ after 24 hrs of treatment in both GBM cells.

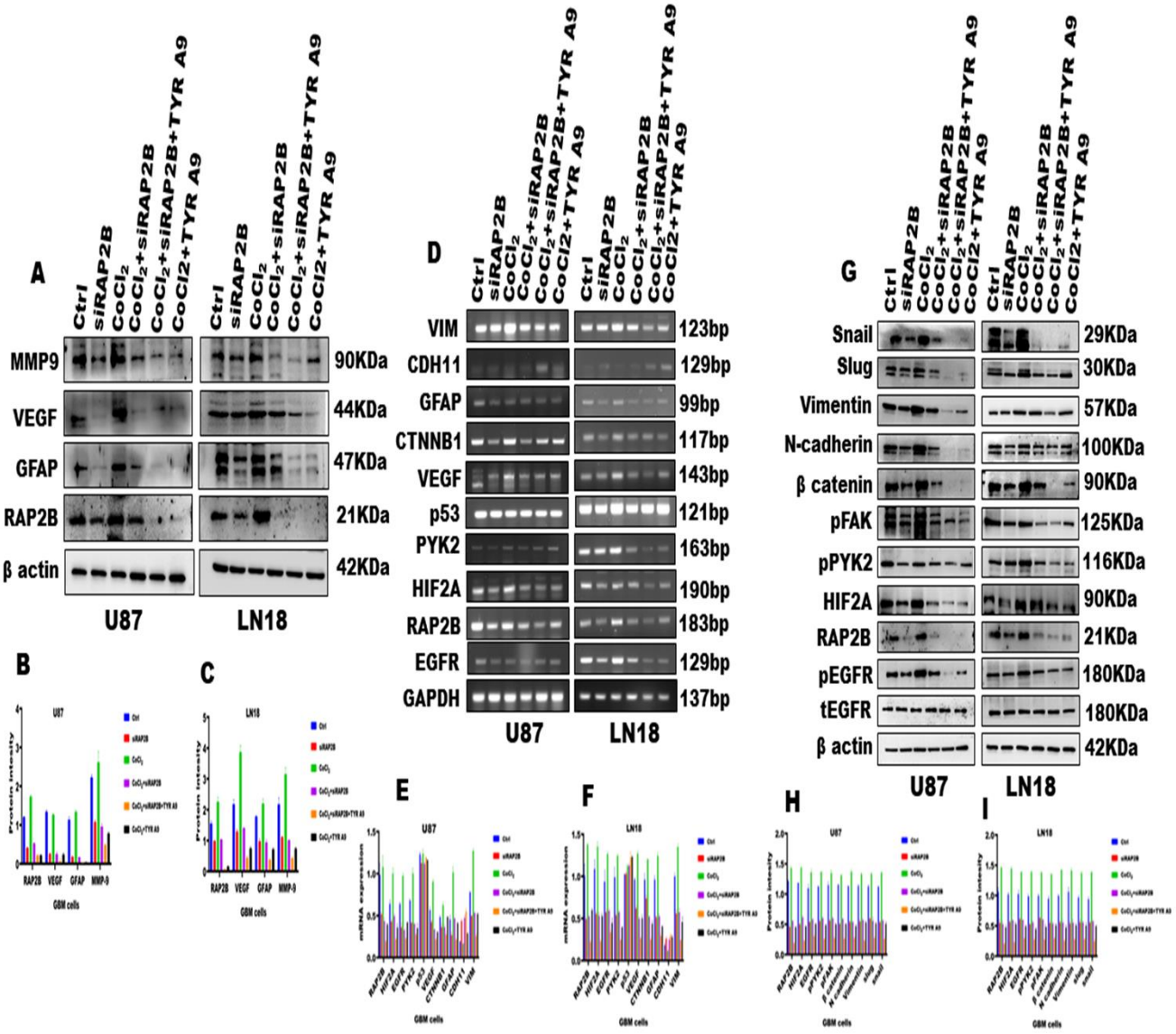

Figure 4: RAP2B knockdown enhanced anticancer effect of TYR A9 (nontoxic dose) in GBM cells: (A, B, C), Western blot and densitometry results showing decreased protein expression of RAP2B, GFAP, VEGF and MMP-9 in siRAP2B, $CoCl_2$+siRAP2B, $CoCl_2$+TYR A9 but inhibited in $CoCl_2$+siRAP2B+TYR A9. **(D, E, F and G, H, I)**, PCR and western blot along with densitometry results representing decreased mRNA and protein expression of RAP2B, HIF2A, EGFR, PYK2, GFAP, CTNNB1, VEGF, CDH2 and VIM in siRAP2B, $CoCl_2$+siRAP2B, $CoCl_2$+TYR A9 but abolished in $CoCl_2$+siRAP2B+TYR A9. These experiments were repeated twice independently.

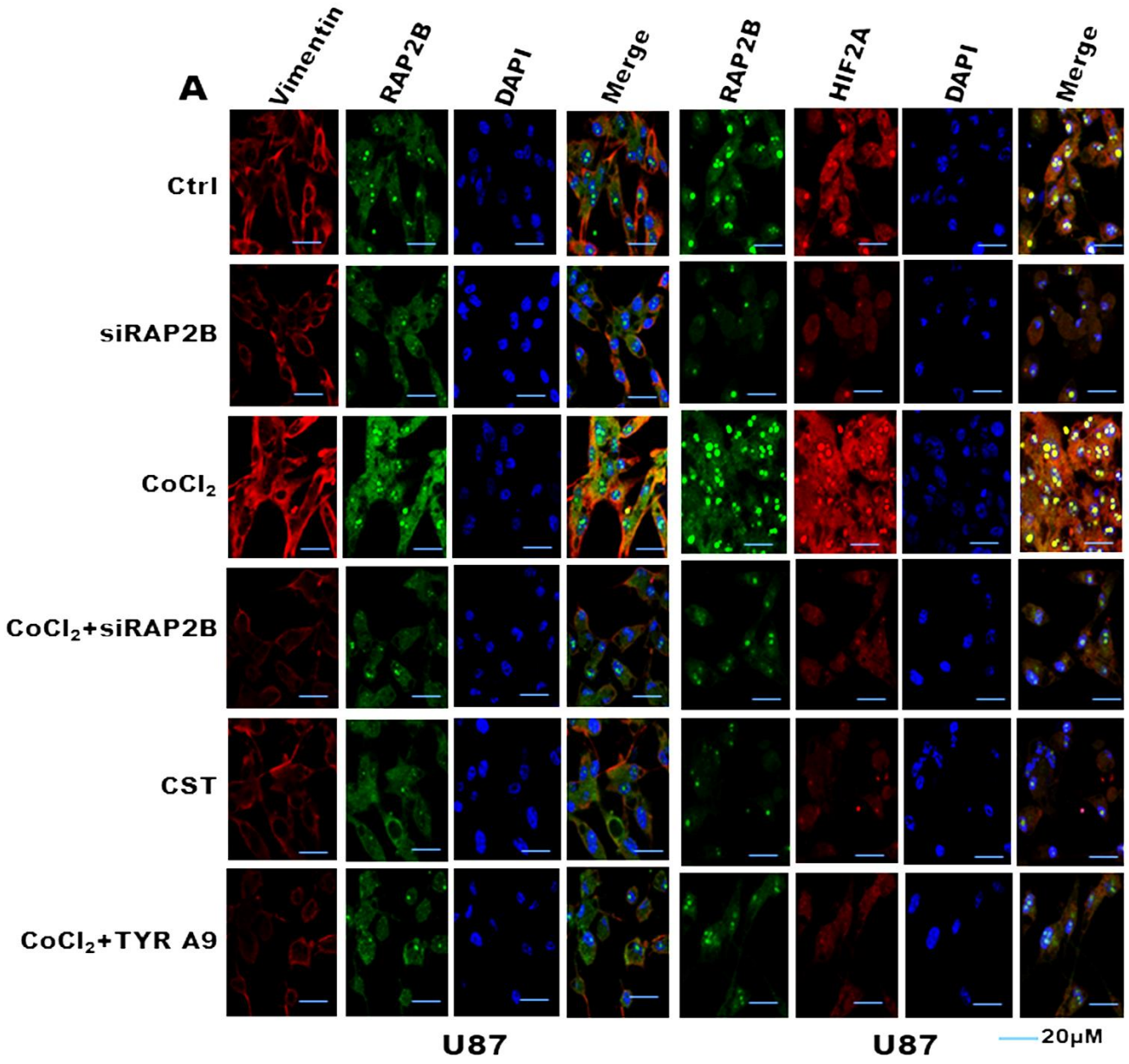

Figure 5: Enhanced sensitivity of TYR A9 (nontoxic dose) after RAP2B silencing in GBM cells: (A), Confocal images representing decreased colocalization between RAP2B and HIF2A, RAP2B and vimentin in siRAP2B compared to control. Similarly reduced colocalization in $CoCl_2$+siRAP2B, $CoCl_2$+TYR A9 but inhibited in $CoCl_2$+siRAP2B+TYR A9 compared to $CoCl_2$. Pearson's correlation coefficient was calculated for both red and green channel intensity r = 0.0109, 0.105 in $CoCl_2$+siRAP2B+TYR A9 U87 GBM cell line.

3.6.4. RAP2B silencing enhanced anticancer potential of TYR A9 and promotes apoptosis induction in GBM cells under hypoxia

We performed flow cytometry to examine the effect of RAP2B knockdown along with TYR A9 nontoxic treatment on apoptosis induction in LN18 and U87 GBM cell lines under hypoxia *vs* normoxia. In the present study we demonstrated that increased annexin V staining in siRAP2B compared to siNC. Similarly, $CoCl_2$+siRAP2B, $CoCl_2$+TYR A9 treatment also increased annexin V staining but enhanced in $CoCl_2$+siRAP2B+TYR A9 (CST) compared to $CoCl_2$ detected through flow cytometry **(Figure 6A, B)** in both GBM cells. Densitometry analysis showed (31%), (28%) increased annexin V staining in siRAP2B, evidenced that induced apoptosis compared to siNC (*p = 0.027), (*p = 0.039). Moreover, increased annexin V staining (26%), (24%) in $CoCl_2$+siRAP2B and (47%), (36%) in $CoCl_2$+TYR A9 but significantly increased annexin V staining (52%), (66%) in $CoCl_2$+siRAP2B+TYR A9 compared to $CoCl_2$ (*p = 0.025), (*p = 0.037), (**p = 0.0023), (**p = 0.0035) and (****p<0.0001) **(Figure 6C, D)** in both GBM cells. Flow cytometry results were analyzed by FlowJo 7.1 software and also calculated percent of apoptosis, suggesting that inhibition of RAP2B/HIF2A role in apoptosis. Interestingly, we also checked the expression of apoptosis related markers through western blot showed in **(Figure 8)**. Western blot and densitometry results showed RAP2B knockdown increased the expression of pro-apoptotic proteins like caspase 9, cleaved caspase 3, Bax, Bad, p53 cleaved PARP and reduced expression of anti-apoptotic protein Bcl-2 compared to siNC. Similarly, $CoCl_2$+siRAP2B, $CoCl_2$+TYR A9 treatment also increased pro-apoptotic proteins expression and deceased anti-apoptotic protein expression but enhanced pro-apoptotic proteins expression and abolished antiapoptotic protein expression in combination of both $CoCl_2$+siRAP2B+TYR A9 compared to $CoCl_2$ treatment in both GBM cells **(Figure 8A, B & C)**. Simultaneously we also performed acridine orange and EtBr staining to confirm apoptosis in both GBM cells. Fluorescence images **(Figure 7A)** were showed uniform green color represented healthy cells, concentrated one side accumulated green color and orange color depicted early and late apoptotic cells. Densitometry analysis in **(Figure 7B, C)** showed that 19%, 13% increased EtBr staining in siRAP2B compare to siNC (*p = 0.023), (*p = 0.042). Similarly, 17%, 11% increased EtBr staining in $CoCl_2$+RAP2B and 25%, 21% in $CoCl_2$+TYR A9, but 42%, 36% significantly increased in $CoCl_2$+siRAP2B+TYR A9 compared to $CoCl_2$ (*p = 0.031), (*p = 0.035), (**p = 0.0066), (**p = 0.0092) and (***p = 0.0002), (***p = 0.0006) in both GBM cells under hypoxia. This evidencing that RAP2B knockdown and TYR A9 treatment induced apoptosis but combination of siRAP2B+TYR A9 nontoxic treatment significantly increased apoptosis in LN18 and U87 GBM Cells under hypoxia.

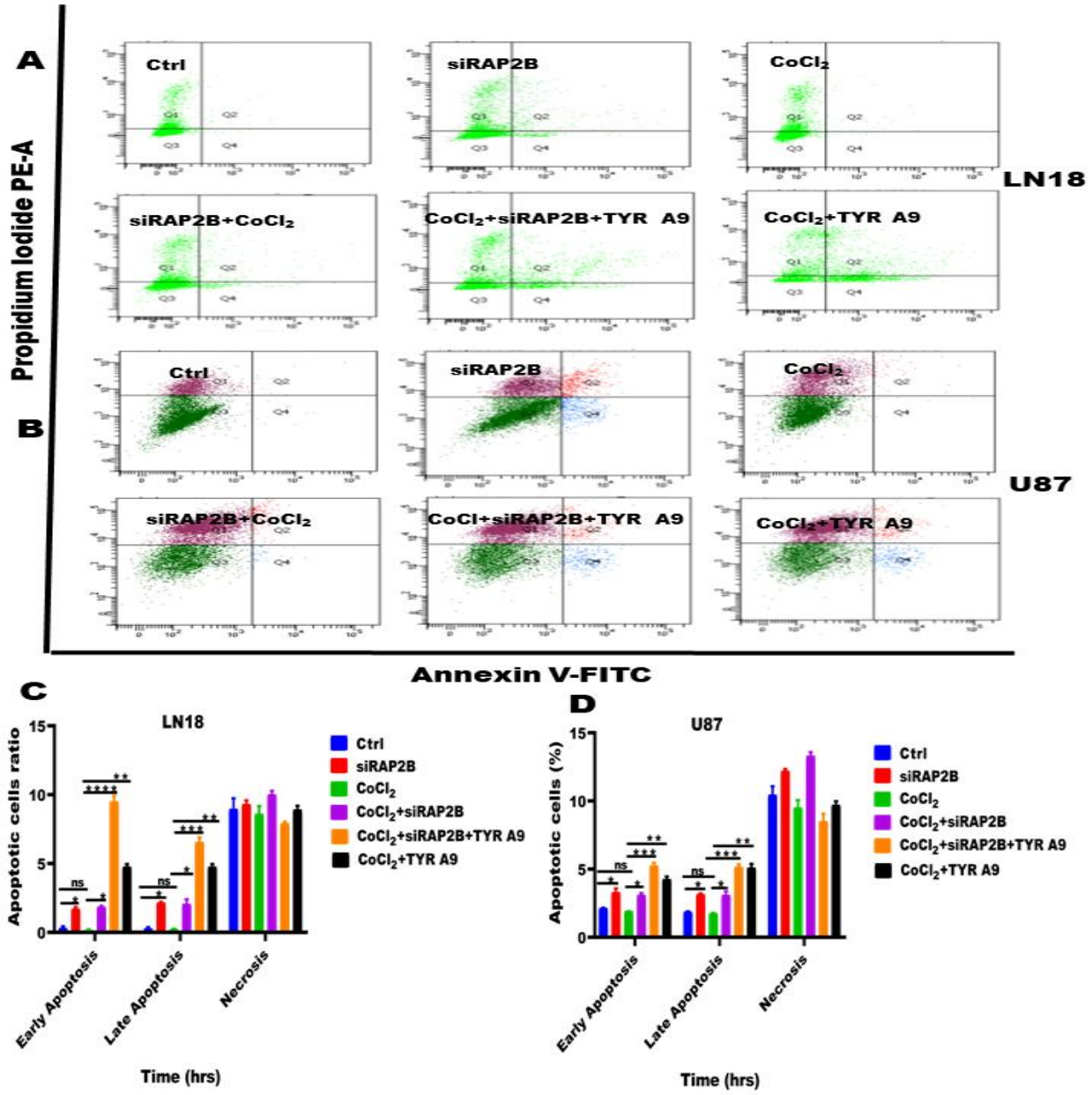

Figure 6: Knockdown of RAP2B increased TYR A9 toxicity and enhanced apoptotic cell death in GBM cells: (A, B), Flow cytometry results representing FITC-conjugated annexin-V positive cells and propidium iodide (PI) staining of all experimental groups in both GBM cells. **(C, D)**, Densitometry analysis results represent increase apoptotic cells in siRAP2B, $CoCl_2$+siRAP2B and $CoCl_2$+TYR A9 but increased high number of apoptotic cells in $CoCl_2$+siRAP2B+TYR A9 compared to $CoCl_2$ treated and siNC.

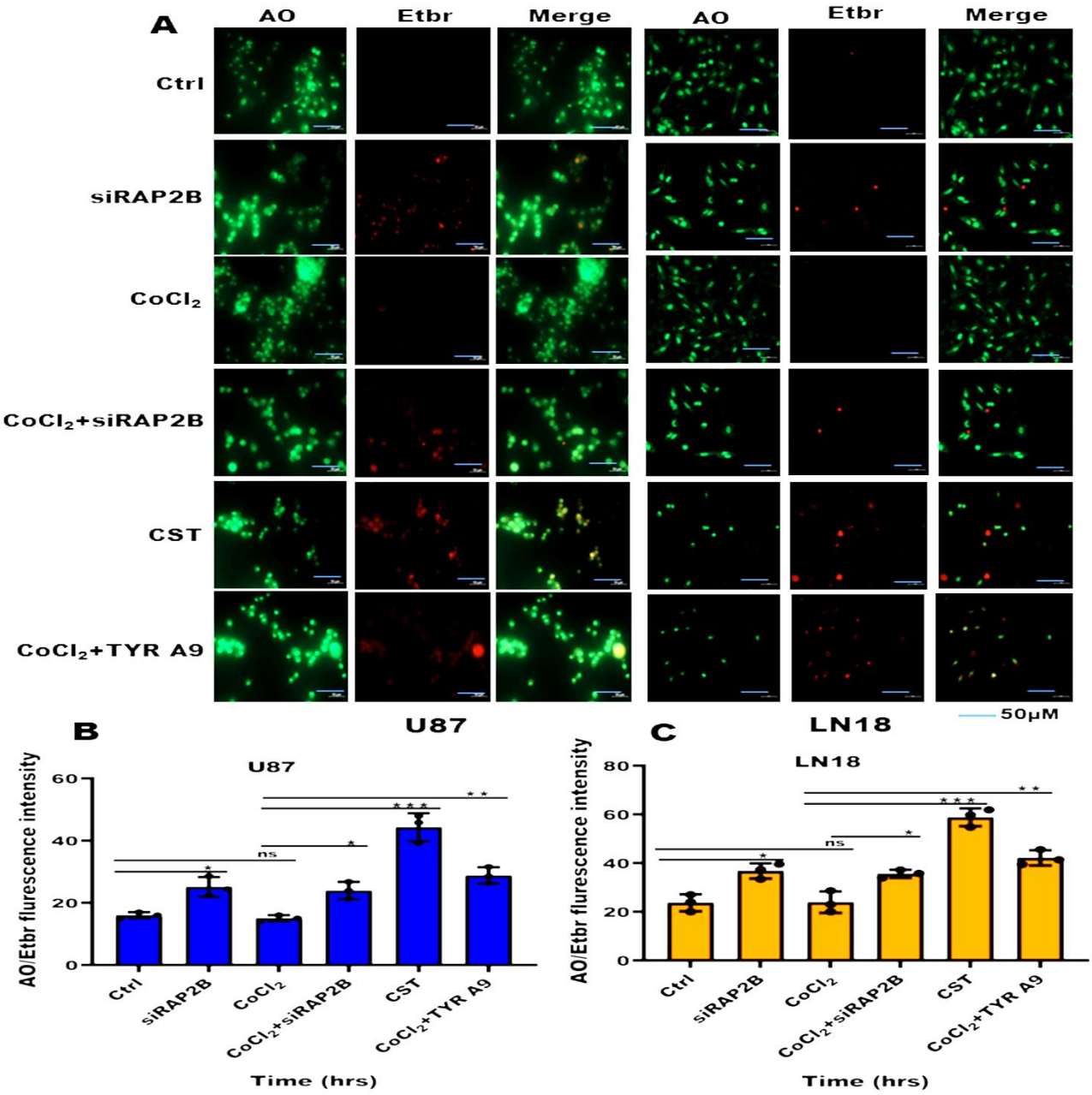

Figure 7: RAP2B knockdown enhanced anticancer efficiency of TYR A9 nontoxic dose in GBM cells: (A), Fluorescence images with dark green concentrated at one side, orange and red color representing early, late apoptotic cells and necrotic cells of both GBM cells in all experimental groups. **(B, C)**, Densitometry analysis results representing increased apoptotic cells in siRAP2B, $CoCl_2$+siRAP2B and $CoCl_2$+TYR A9 but more apoptotic cells in $CoCl_2$+siRAP2B+TYR A9 (CST) compared to $CoCl_2$ treated and siNC.

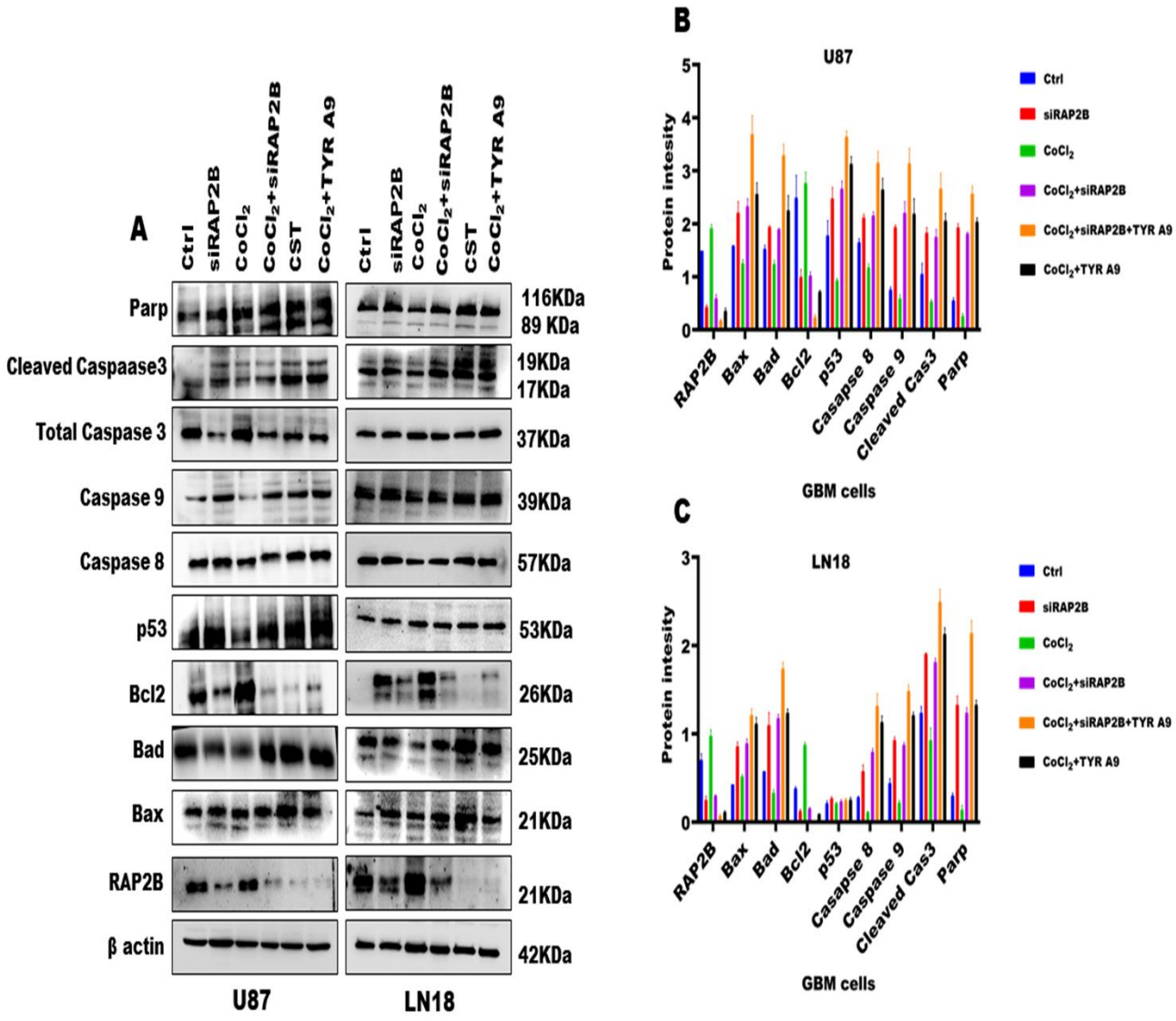

Figure 8: Combination of RAP2B knockdown and TYR A9 nontoxic dose treatment induces apoptosis in both GBM cells: (A, B, C), Western blot and densitometry results showing increased expression of pro-apoptotic protein markers and decreased antiapoptotic protein marker in siRAP2B, $CoCl_2$+siRAP2B, $CoCl_2$+TYR A9 but enhanced more pro-apoptotic proteins expression and inhibited antiapoptotic protein expression in $CoCl_2$+siRAP2B+TYR A9 (CST) compared to $CoCl_2$ and siNC in both U87 and LN18 GBM cells. β actin used as a loading control.

3.7. Discussion

Glioblastoma is a molecularly heterogeneous brain tumor with limited treatment options and a dismal prognosis [9], although molecular characteristics have been extensively studied [10]. As a result, identifying the main biomarkers and targets that influence prognosis is critical for improving the clinical outcome of glioma patients. Previous studies reported that hypoxia is known to be a primary cause of glioma development and resistance to treatment particularly common in malignant astrocytoma that have always higher necrosis and microvascular proliferation. Existing studies reported that RAP2B belongs to the Ras superfamily members predominately elevated in a various cancer [11a, 11b, 11c], also reported as a potential oncogene in glioma [12a, 12b] and lung cancer development by activating the NF-kB pathway [13a, 13b]. Previously explored that VEGF and MMP-9 play role in vascular endothelial cell proliferation and promote angiogenesis, which is essential for new blood vessels formation. MMP-9 helps in extracellular matrix degradation and promote cell migration [14]. The relation and expression correlation between RAP2B and HIF2A as well as their therapeutic relevance in hypoxia is still unknown in glioma. As previously reported that high grade of glioma coincides with high deficiency of oxygen and its aggressive behavior [15a, 15b]. In support of previous study, the present study evidenced that increased expression of RAP2B and HIF2A in high grade astrocytoma might be associated with ubiquitous hypoxic microenvironment in malignant astrocytoma tissues. Furthermore, we verify our clinical outcome with *in vitro*, we used $CoCl_2$ exposure for 24 hrs to mimic hypoxic microenvironment in GBM cells. We investigated the relationship between hypoxia and RAP2B/HIF2A axis expression and function in GBM cells proliferation and migration. Herein, we observed increased mRNA and protein expression of RAP2B after 24 hrs of $CoCl_2$ exposure in both GBM cells. This is first study we found that RAP2B, a novel hypoxia responsive gene along with increased HIF2A expression after 24 hrs of $CoCl_2$ (mimic hypoxia) treatment in U87 and LN18 GBM cells. This evidencing that increased expression of RAP2B and HIF2A positively correlated and enhanced their expressions and correlation in hypoxia. Simultaneously, we also demonstrated their downstream signaling, we observed that increased expression of RAP2B/HIF2A axis positively correlated with expressions of EGFR, pFAK, pPYK2, GFAP, MMP-9, VEGF, vimentin, N-cadherin, β catenin, snail and slug. These evidencing that $CoCl_2$-induced hypoxia increased RAP2B/HIF2A expression and activation of pFAK/pPYK2-EMT signaling pathway, this might involve in GBM cell progressions supporting previous study [16]. First time our finding revealed that increased RAP2B and HIF2A expression positively correlated with malignant astrocytoma as well as in GBM cell lines. In the current study we also examined that increased RAP2B

and HIF2A expression and their positive correlation triggered proliferation and migration in both GBM cells under hypoxia *vs* normoxia. Furthermore, our aim to develop siRNA mediated therapeutic approach against GBM cells under hypoxia. small interference RNA (siRNA) is an extremely powerful method for assessing targeted gene function by transcriptional gene silencing through mRNA degradation. However, many factors limit the clinical application of siRNA-based therapies. Several previous reports suggested that the use of combination treatment in many cancers that share a common pathway to inhibit cancer growth. Previous study reported that knockdown of RAP2B increased sensitivity of adriamycin against GBM [17]. In the present study GBM cells were transfected with siRNA specific to RAP2B to confirmed RAP2B knockdown (siRAP2B) and then treated with TYR A9 nontoxic dose for 24 hrs in pretreated $CoCl_2$. We observed that RAP2B knockdown increased anticancer potential of TYR A9 at nontoxic dose and increased its inhibitory effect on GBM cell progression under $CoCl_2$-induced hypoxia. Previously reported that RAP2B knockdown repressed expressions of various downstream signaling and blocked cancer progression in addition of inhibitor [11]. In the current study, first time we demonstrated that RAP2B knockdown increased anticancer efficacy of TYR A9 even at nontoxic dose (below IC_{50} value) in GBM cells under hypoxia. Surprisingly, in the current study we found that RAP2B knockdown or TYR A9 treatment decreased mRNA and protein expression of RAP2B and HIIF2A along with their downstream EGFR, pFAK, pPYK2, MMP-9, GFAP, VEGF, vimentin, N-cadherin, β catenin, snail and slug but inhibited in combination of both RAP2B knockdown and TYR A9 (nontoxic dose) treatment induced by pretreated $CoCl_2$ after 24 hrs of exposure in both GBM cells. Interestingly, we found that decreased mRNA and protein expression of HIF2A after RAP2B knockdown proved that HIF2A is not stabilized under hypoxia in both GBM cells, indicating that HIF2A not present at upstream of RAP2B. However, the total protein levels of FAK, EGFR and PYK2 were not changed in siRAP2B, $CoCl_2$+siRAP2B, $CoCl_2$+TYR A9 and $CoCl_2$+siRAP2B+TYR A9 treatment in normoxia vs hypoxia. Increased mRNA and protein expressions of RAP2B and HIIF2A along with their downstream EGFR, pFAK, pPYK2, MMP-9, GFAP, VEGF, vimentin, N-cadherin, β catenin, snail and slug were confirmed through PCR and western blot in both GBM cells without and with $CoCl_2$ treatment after 24 hrs. We demonstrated that knockdown of RAP2B and TYR A9 treatment decreased proliferation and migration in GBM cells but abolished in combination of siRAP2B and TYR A9 nontoxic dose treatment in both GBM cells under hypoxia. After confirming RAP2B and HIF2A inhibition simultaneously we performed multiple cell-based assays like MTT, clonogenic and scratch wound healing assay. We observed that decreased cell proliferation, colony forming ability and migration in siRAP2B, $CoCl_2$+siRAP2B, $CoCl_2$+TYR A9 but diminished in combination of both compared to control (normoxic) and $CoCl_2$

treated (hypoxic) GBM cells. EMT process occurs during tumorigenesis and progression of high-grade glioma [18]. This finding suggested that knockdown of RAP2B or TYR A9 treatment reduced proliferation, migration and activation of RAP2B/HIF2A/pPYK2-EMT signaling whereas attenuated in combination of siRAP2B+TYRA9 nontoxic dose treatment in both GBM cells under hypoxia. This study indicating that RAP2B/HIF2A axis is a master regulator of hypoxia and involved in activation of pFAK/pPYK2-EMT pathway in GBM cells proliferation and migration. Targeting RAP2B/HIF2A axis prevented EMT signaling and blocked the transition from epithelial to mesenchymal in support of previous report [19]. Our finding revealed that targeting RAP2B/HIF2A axis inhibited pFAK/pPYK2-EMT signaling pathway and GBM cells proliferation, migration in hypoxia. This evidencing that combination of RAP2B knockdown and TYR A9 nontoxic dose treatment could be more effective therapy against GBM.

These findings indicated that RAP2B mediated HIF2A involved in the activation of pFAK/pPYK2-EMT signaling pathways in glioma progression under $CoCl_2$ induced hypoxia after 24 hrs of treatment. In agreement of RAP2B staining we also performed immunofluorescence to see their colocalization with HIF2A and vimentin through confocal microscopy. RAP2B knockdown decreased RAP2B, HIF2A, GFAP and pPYK2 staining and their colocalization compared to control. Similarly, $CoCl_2$+siRAP2B, $CoCl_2$+TYR A9 treatment also decreased RAP2B, HIF2A, GFAP and pPYK2 staining as well as their colocalization but inhibited in $CoCl_2$+siRAP2B+TYR A9 compared to $CoCl_2$ in both GBM cells. According to accumulating evidence apoptosis plays a crucial role in inhibition of tumorigenesis and malignancy. As previously reported, glioma cell death and the prognosis of the patient were predicted by the apoptosis associated gene signature [20]. Therefore, in the present study RAP2B knockdown increased expression of proapoptotic markers like Caspase 9, Bax, Bak, cleaved Caspase 3 and cleaved PARP and reduced expression of antiapoptotic marker Bcl-2 compared to control. Likewise, $CoCl_2$+siRAP2B, $CoCl_2$+TYR A9 treatment also increased expression of proapoptotic markers and reduced expression of antiapoptotic marker, but combination of siRAP2B+TYR A9 nontoxic enhanced more expression of pro-apoptotic proteins and inhibited antiapoptotic protein expression compared to $CoCl_2$. Additionally, we observed that increased annexin V and EtBr staining positive cells evidenced that increased apoptosis in siRAP2B, $CoCl_2$+siRAP2B, $CoCl_2$+TYR A9 but enhanced more annexin V and EtBr staining proved high apoptosis induction in $CoCl_2$+siRAP2B+TYR A9 compared to $CoCl_2$ and control in U87 and LN18 GBM cells. Collectively, our results demonstrate that RAP2B knockdown and

TYR A9 treatment induced apoptosis but combination therapy led to more apoptotic cells in both GBM cells.

3.8. Conclusion

Altogether, the correlation and their positive association between hypoxia and RAP2B/HIF2A axis provide a strong, effective approach for predicting the prognosis of malignant astrocytoma. Further, we confirmed our clinical data with an *in vitro* by establishing an oncogenic role of RAP2B/HIF2A axis in $CoCl_2$-induced hypoxia. Indeed, our study demonstrated that $CoCl_2$ induced hypoxia increased expression of RAP2B/HIF2A and activation of the pPYK2-EMT signaling pathway which promotes GBM cells proliferation and migration. We developed combination therapeutic approach by siRAP2B and TYR A9 nontoxic treatment and found significantly inhibited proliferation and migration by attenuating the RAP2B/HIF2A/pPYK2-EMT signaling pathway in both GBM cells under hypoxia. We concluded that RAP2B/HIF2A could be a new regulator of EMT and a promising target for developing combination therapy may provide an effective and potential therapeutic approach against GBM under hypoxia.

3.9. Additional Information

Supplementary Figure:

Proposed signaling involved in glioblastoma progression and its regulation by siRAP2B and TYR A9:

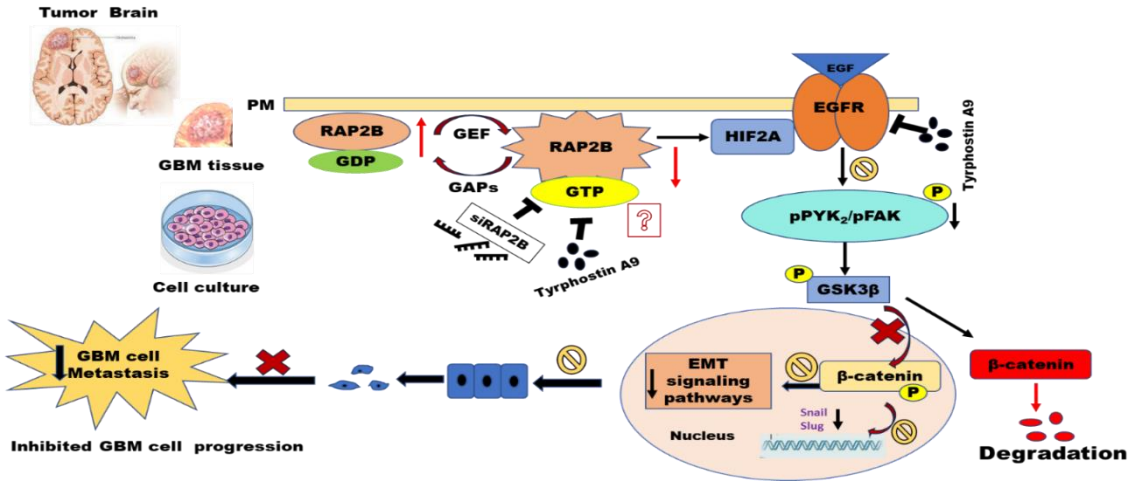

Figure S1: Proposed model of the study: Schematic diagram illustrating the clinical significance and therapeutic approach of RAP2B inhibition in relation to HIF2A-mediated EMT in GBM cells.

Supplementary Tables:

Table S1: Real-time PCR primer sequences			
S. No	**Primers**	**Primer Sequences (5'-3')**	**Tm**
1.	RAP2B Forward primer	5'-GAGAAGTACGACCCGACCATCG-3'	59.1
	RAP2B Reverse primer	5'-GAGGCTGTAGACCAGGATGAAGC-3'	59.2
2.	EGFR Forward primer	5'-GCGTCCGCAAGTGTAAGAAGTG-3'	62.2
	EGFR Reverse primer	5'-GAGATCGCCACTGATGGAGG-3'	59.9
3.	HIF2A Forward primer	5'-AAGCCTTGGAGGGTTTCATT-3'	50
	HIF2A Reverse primer	5'-TCATGAAGAAGTCCCGCTCT-3'	52
4.	PYK2 Forward primer	5'-CGAGCTCCTAGAAAAGGAAGTG-3'	55.0
	PYK2 Reverse primer	5'-GGCGAGAGTGTTGAAGAAC-3'	53.5
5.	p53 Forward primer	5'-GTACTCCCCTGCCCTCAACAAG-3'	60.5
	P53 Reverse primer	5'-ACCATCGCTATCTGAGCAGC-3'	59
6.	VEGF Forward primer	5'-AAGGAGGAGGGCAGAATCAT-3'	52
	VEGF Reverse primer	5'-ATCCGCATAATCTGCATGGT-3'	50
7.	CTNNB1 Forward primer	5'-TGTAGAAGCTGGTGGAATGC-3'	57.3
	CTNNB1 Reverse primer	5'-CCTTCCTGTTTAGTTGCAGC-3'	57.3
8.	GFAP Forward primer	5'-AGCAGATGAAGCCACCCTG-3'	58.8
	GFAP Reverse primer	5'-AACCTCCTCCTCGTGGATC-3'	58.8
9.	CDH11 Forward primer	5'-CCAATGTGGGAACGTCAG-3'	55.9
	CDH11 Reverse primer	5'-GATACCTGTCTGTGCTTCC-3'	56.6
10.	VIM Forward primer	5'-GACAGGATGTTGACAATGCG-3'	57.3
	VIM Reverse primer	5'-GCTCCTGGATTTCCTCTTC-3'	56.6
11.	GAPDH Forward primer	5'-TGACAACTTTGGTATCGTGGAAGG-3'	56
	GAPDH Reverse primer	5'-AGGCAGGGATGATGTTCTGGAGAG-3'	59

3.10. References:

1. Lara-Velazquez, M., *et al*., Advances in Brain Tumor Surgery for Glioblastoma in Adults. Brain Sci, 2017. **7**(12).
2. Zhang, X., *et al*., Rap2b, a novel p53 target, regulates p53-mediated pro-survival function. Cell Cycle, 2013. **12**(8): p. 1279-91.
3. Hartmann, J.T., *et al*., Tyrosine kinase inhibitors - a review on pharmacology, metabolism, and side effects. Curr Drug Metab, 2009. **10**(5): p. 470-81.
4. Gazit, A., *et al*., Tyrphostins I: synthesis and biological activity of protein tyrosine kinase inhibitors. J Med Chem, 1989. **32**(10): p. 2344-52.
5. Iida, K. *et al*., EGFR gene amplification is related to adverse clinical outcomes in cervical squamous cell carcinoma, making the EGFR pathway a novel therapeutic target. Br J Cancer, 2011. **105**(3): p. 420-7.
6. Fukai, K. *et al*., Pyk2 aggravates hypoxia-induced pulmonary hypertension by activating HIF-1alpha. Am J Physiol Heart Circ Physiol, 2015. **308**(8): p. H951-9.
7. Di, J. *et al*., Rap2B promotes proliferation, migration, and invasion of human breast cancer through calcium-related ERK1/2 signaling pathway. Sci Rep, 2015. **5**: p. 12363.
8. Masalha, M. *et al*., MiR-199a-3p Induces Mesenchymal to Epithelial Transition of Keratinocytes by Targeting RAP2B. Int J Mol Sci, 2022. **23**(23).
9. Gusyatiner, O. and M.E. Hegi, Glioma epigenetics: From subclassification to novel treatment options. Semin Cancer Biol, 2018. **51**: p. 50-58.
10. Reifenberger, G., *et al*., Advances in the molecular genetics of gliomas - implications for classification and therapy. Nat Rev Clin Oncol, 2017. **14**(7): p. 434-452.
11. (a) Guo, G., *et al*., The therapeutic potential of stem cell-derived exosomes in the ulcerative colitis and colorectal cancer. Stem Cell Res Ther, 2022. **13**(1): p. 138. (b) Di, J., *et al*., Rap2B promotes cell proliferation, migration and invasion in prostate cancer. Med Oncol, 2016. **33**(6): p. 58. (c) Ferlay, J., *et al*., Estimates of worldwide burden of cancer in 2008: GLOBOCAN 2008. Int J Cancer, 2010. **127**(12): p. 2893-917.
12 (a) Miao, F. *et al*., Rap2B promotes cell adhesion, proliferation, migration, and invasion of human glioma. J Neurooncol, 2019. **143**(2): p. 221-229. (b) Miao, Y. *et al*., Adaptive Immune Resistance Emerges from Tumor-Initiating Stem Cells. Cell, 2019. **177**(5): p. 1172-1186 e14.
13 (a) Fu, G., *et al*., [Identification and Functional Analysis of A Novel Candidate Oncogene RAP2B in Lung Cancer.]. Zhongguo Fei Ai Za Zhi, 2009. **12**(4): p. 273-6. (b) Brosch, T. *et al*., The impact of emotion on perception, attention, memory, and decision-making. Swiss Med Wkly, 2013. **143**: p. w13786.
14. Xue, Q. *et al*., High expression of MMP9 in glioma affects cell proliferation and is associated with patient survival rates. Oncol Lett, 2017. **13**(3): p. 1325-1330.
15. (a) Evans, S.M. *et al*., Hypoxia is important in the biology and aggression of human glial brain tumors. Clin Cancer Res, 2004. **10**(24): p. 8177-84. (b) Colwell, N., *et al*., Hypoxia in the glioblastoma microenvironment: shaping the phenotype of cancer stem-like cells. Neuro Oncol, 2017. **19**(7): p. 887-896.

16. Zeng, W., *et al*., Hypoxia and hypoxia-inducible factors in tumor metabolism. Cancer Lett, 2015. **356**(2 Pt A): p. 263-7.
17. Ding, L., R. Sun, and X. Zhang, Rap2b siRNA significantly enhances the anticancer therapeutic efficacy of adriamycin in a gold nanoshell-based drug/gene co-delivery system. Oncotarget, 2017. **8**(13): p. 21200-21211.
18. Liu, J., *et al*., Hypoxia induced ferritin light chain (FTL) promoted epithelia mesenchymal transition and chemoresistance of glioma. J Exp Clin Cancer Res, 2020. **39**(1): p. 137.
19. Lu, Y.B. *et al*., Targeting the Epithelial-to-Mesenchymal Transition in Cancer Stem Cells for a Better Clinical Outcome of Glioma. Technol Cancer Res Treat, 2020. **19**: p. 1533033820948053.
20. Valdes-Rives, S.A., *et al*., Apoptotic Signaling Pathways in Glioblastoma and Therapeutic Implications. Biomed Res Int, 2017. **2017**: p. 7403747.
21. Naser, R., *et al*., Endogenous control mechanisms of FAK and PYK2 and their relevance to cancer development. Cancers, 2018. **10**(6): p. 196.

CHAPTER 4

Tyrphostin A9 attenuates glioblastoma growth by suppressing PYK2/ EGFR-ERK signaling pathway

Objective 3: Tyrphostin A9 attenuate glioblastoma growth by suppressing PYK2/ EGFR-ERK signaling pathway

Abstract

The primary brain tumor known as glioblastoma (GBM) is lethal and has very poor clinical outcome. Tyrosine kinase inhibitors (TKIs) have anticancer efficacy in GBM and other cancers with restricted therapeutic outcomes. In our ongoing research, we planned to explore the clinical impact of phosphorylated proline-rich tyrosine kinase-2 (PYK2) and epidermal growth factor receptor (EGFR) in GBM and assess its draggability using a synthetic TKI called Tyrphostin A9 (TYR A9). The expression profiles of phosphor-PYK2 and EGFR were evaluated in astrocytoma biopsies (n=48) and GBM cell lines using qPCR, western blot and immunohistochemistry. The clinical correlation of phospho-PYK2 and EGFR were examined with several clinicopathological features and the Kaplan-Meier survival curve. The drugability of phospho-PYK2 and EGFR along with the ensuing anticancer efficacy of TYR A9, were assessed in GBM cell lines and intracranial C6 glioma model. We observed that elevated phospho-PYK2 and EGFR expression, which worsens the malignancy of astrocytomas and linked with the patient's poor survivability. The mRNA and protein correlation data revealed that positive relationship between phospho-PYK2 and EGFR in GBM tissues. *In vitro* results showed that TYR A9 decreased GBM cell growth, migration as well as induce apoptosis by diminishing PYK2/EGFR-ERK signaling. *In-vivo* studies demonstrated that TYR A9 treatment significantly decreased glioma growth and increasing animal survival through suppressing PYK2/EGFR-ERK signaling pathways. The findings of our study collectively indicate that a poor prognosis was linked to elevated phospho-PYK2 and EGFR expression in astrocytomas. The translational effect of TYR A9 through inhibition of PYK2/EGFR-ERK signaling pathway was highlighted *in-vitro* and *in-vivo* evidence.

4.1. Introduction

In Glioblastoma (GBM), approximately 30-60% of intracranial tumors are highly malignant primary brain tumors [1]. GBM's elaborate molecular and cellular heterogeneity causes unrestricted cell growth, invasion, and chemoresistance, aggravating patients' poor survivability (14–15 months) [1-3]. In fact, due to the diffuse infiltrative behavior of GBM extensive vascularization, high toxicity or low efficacy, and drug resistance of currently available chemotherapeutics, the current standard of care, which includes surgical resection followed by chemotherapy or radiotherapy, often fails [3-5]. A better understanding of the molecular etiology of GBM and the investigation of alternative therapeutic options have been spurred by increased incidences of GBM and dismal prognosis.

Advancements in genomics have revealed diverse genetic modifications in receptor tyrosine kinases (RTKs) in cancer, which disrupt multiple cellular functions such as cell proliferation, survival, apoptosis etc [6, 7]. As a driver oncogene, the epidermal growth factor receptor (EGFR) is most frequently amplified RTK or mutated (kinase domain) in a variety of cancers, including GBM [8, 9]. Proline-rich tyrosine kinase-2 (PYK2) is a non-receptor cytoplasmic tyrosine kinase protein widely dispersed across the central nervous system. It is a member of the family of tyrosine kinase [10]. Focal adhesion kinase (FAK), a non-receptor tyrosine kinase that exhibits strong sequence homology and a comparable domain is structurally similar to it. It is also participated in the regulation of cytoskeleton dynamics, cell survival, and cell growth [11]. Selective activation of the PYK2 cascade occurs either by autophosphorylation at Tyr402 or through Ca^{2+}/Calmodulin-dependent protein kinase II (CAMKII) signaling pathways [12, 13]. Phospho-PYK2 (pPYK2) is highly expressed and activates multiple signaling pathways, including PI3K/STAT3, Src/GPCR/RhoA, ERK/MAPK etc [14-16]. In various cancers, activation of these pathways promotes immune cell polarization and adhesion and increases cell migration, invasion, and proliferation [11, 17-21]. Gliomas have not yet been investigated for the connectivity of pPYK2 and EGFR in mitogen-activated protein kinase (MAPK) signaling despite reports of this relationship in several malignancies [15, 22]. Previous studies have demonstrated the function of p-PYK2 in the migration and proliferation of glioma cells [18, 23]. More research is necessary to understand the molecular mechanisms of PYK2 in GBM progression and malignancy as the clinical and therapeutic significance of pYK2 in GBM is currently lacking. The current study explored the expression of activated PYK2 and the clinical correlation with the EGFR-mediated extracellular receptor kinase (ERK) signaling pathway in GBM.

It has demonstrated clinical significance to target RTKs in different cancers using TKIs or molecular scissors [24, 25]. Tyrphostin A9 (TYR A9) is a small (282.38 g/mol) synthetic tyrosine kinase inhibitor that has been shown to specifically inhibit PYK2, VEGF, and the receptor for platelets-derived growth factor (PDGFR) [26-29]. Neuroblastoma and breast cancer cell lines show that TYR A9 has anti-migratory and cell death potential 28, 30], apart from its low toxicity TYR A9 ability to cross the blood-brain barrier (BBB) [5] led us to assess its anticancer effectiveness in GBM. Here, we also aim to determine whether the rationale for using a TKI (TYR A9) to inhibit the dual tyrosine kinases PYK2 and EGFR could effectively block downstream ERK signaling [31, 32].

The results of the present investigation showed that EGFR and activated PYK2 influenced ERK signaling in malignant astrocytomas and its translational impact by TYR A9. We showed that elevated expression of pPYK2, and EGFR was positively associated with astrocytoma malignancy and patients' poor survival. In GBM, there is a positive correlation between pPYK2, EGFR, and pERK½, according to the correlation analysis. Subsequently, the inhibition of PYK2 and EGFR-modulated ERK signaling pathway by TYR A9 reduced the growth of GBM cells and triggered apoptosis *in vitro* and *in vivo*.

4.2. Materials and methods

4.2.1. Astrocytoma Biopsies

We have collected resected astrocytoma tissues (n = 48) and non-tumor control (temporal epilepsy tissues n = 12) from Krishna Institute of Medical Sciences (KIMS) Secunderabad surgically. Astrocytoma biopsies were histopathologically classified into different grades such as diffused astrocytoma-Grade 2 (n = 14), anaplastic astrocytoma-Grade 3 (n = 14), and Glioblastoma (GBM)-Grade 4 (n = 20) by pathologists at KIMS hospital according to the World Health Organization (WHO) defined 2016 classification scheme [33]. All astrocytoma and control biopsies were snap-frozen in liquid nitrogen and stored at −80 °C. The clinicopathological information of patients, such as age/gender, survival, and family history, was maintained in the hospital registry. Written informed consent was obtained from each patient or their relatives to use clinical biopsies and clinicopathological information in the study. The study was approved by the Institutional Ethics Committee (IEC), University of Hyderabad, India.

4.2.2. Cell cultures

Rat glioma cell line C6 and human GBM cell line U87 and LN18 were obtained from the National Centre for Cell Sciences (NCCS), Pune, India. Cell maintenance information was provided in **objective 1** that is applicable to this objective.

4.2.3. Reagents and Chemicals

Details provided in **objective 1** refer **page no 31**.

4.2.4. Isolation of RNA and Polymerase chain reaction (PCR)/quantitative PCR

Total RNA was extracted using the Trizol reagent method from frozen astrocytoma tissues or GBM cell lines according to Trizol method (sigma) manual instructions. The mRNA expression was calculated using the procedure described earlier [34]. Gene-specific primers were enlisted in **Table S1 (page no 127)**. GAPDH was used as an internal control for both PCR and qPCR. Following procedure, refer to **objective 1, page no 34**.

4.2.5. Western blotting

The general information provided for **objective 1** is also applicable to this objective. Refer to **page no 34**.

4.2.6. Haemotoxylin and Eosin and Immunohistochemistry (H&E and IHC) staining.

Astrocytoma tissue sections of different grades, such as grade 2, grade 3, and grade 4, including control tissues, were obtained from KIMS hospital. All histological staining, such as Haemotoxylin and Eosin (H&E), Immunohistochemistry (IHC), and Immunofluorescence (IF), were performed by following protocol optimized in our laboratory [35, 36]. The following procedure provided for objective 1 is also applied in this chapter refer to **page no 31**.

4.2.7. MTT [3-(4,5 Dimethyl-2 thiazolyl)-2,5-diphenyl-2- tetrazolium bromide] cell proliferation assay

The MTT assay was performed following the previously described method [37]. Briefly, GBM cell lines C6, U87, and LN18 were trypsinized and seeded 1×10^4 cells/well in 96 well plates and kept for overnight growth at 37 °C in a 5% CO_2 incubator. After overnight incubation, cells were treated with different micromolar concentrations, *viz*. 5 µM, 10 µM, 15 µM, 20 µM, 30 µM, 40 µM of TYR A9 and vehicle control (DMSO 0.01%) for 24 hrs. After 24 hrs of treatment, MTT (5mg/ml) was added to each well and incubated for 3 hrs in the dark in a CO_2 incubator. Subsequently, the MTT solution was removed, and DMSO 100 µl/well was added to dissolve formazan crystals. Absorbance was taken at 570 nm by a microtiter ELISA plate reader (TECAN). All experiments were repeated three times, and results were presented as mean ± SEM.

4.2.8. Clonogenic assay

C6, U87, and LN18 GBM cells were seeded at a density of 1000 cells/well in six-well plates and kept in a CO_2 incubator for overnight growth at 37 °C. Cells were treated with a range of concentrations (10 µM, 20 µM, and 40 µM) of TYR A9 and vehicle control for 24 hrs. After 24 hrs of treatment, fresh media was added every three days until the colonies formed. The colonies were fixed with 4% paraformaldehyde (PFA) and stained with 0.5% crystal violet. Colony counting and analysis were done using the method described earlier [35, 38].

4.2.9. Cell migration (scratch wound healing) assays

Cell migration was evaluated using the scratch wound healing assay. The GBM cells C6, U87 and LN18 were seeded in 6-well plates at density of 1×10^5 cells/well and incubated for 24 hrs at 37 °C in a CO_2 incubator. Upon reaching 80% confluency, a wound scratch was made using a 10 µl tip. Dead cells were promptly removed by washing them twice with 1XPBS before adding 2ml of complete medium. The cells were exposed to different concentrations of TYR A9 (5 µM, 10 µM, 15 µM, and 20 µM) as well as a vehicle control for 24 hr. At 4 x magnification, images were taken using an inverted phase-contrast microscope (Leica DFC 300 FX) at various time intervals 0, 6, 12, and 24 hr. The wound-healing width ratio was used to estimate the wound-healing percentage at each time point. All experiments were repeated thrice, and results were presented as mean ± SEM.

4.2.10. Cell cycle and annexin V staining and analysis through fluorescence-activated cell sorting (FACS)

To study the effect of TYR A9 in the cell cycle distribution of C6 and U87, a density of 1×10^5 GBM cells were seeded in 60 mm dishes and kept for overnight growth in a CO_2 incubator. Both GBM cell lines were treated with different concentrations of TYR A9 (10 µM, 20 µM, and 40 µM) and vehicle control for 24 hrs. Cells were trypsinized with 0.25% 1X trypsin EDTA, twice washed with 1XPBS, and fixed with 70% ethanol for 4 hrs at 4 ^{0}C. After incubation, the fixed cells were washed twice with 1XPBS and incubated with propidium iodide (PI) solution containing PI (50µg/ml), RNase A (50 µg/ml), and 1% triton-X100 or with annexin V-fluorescent tag antibody in the dark for 30 minutes for 1hr as mentioned in earlier studies [39, 40]. The PI-stained cells were used for cell cycle analysis, and annexin V-stained cells were used to detect apoptosis through flow cytometry (FACS Calibur-BD Biosciences). We use the flowJo v10.7.1 software to analyze data.

4.2.11. Intracellular reactive oxygen species (ROS) levels

The 2′7′-Dichlorofluorescin diacetate (DCFDA, #D6883-**S**igma) method was used for ROS estimation. C6 and U87 GBM cells were trypsinized and seeded 10000 cells in each well of 96-well plates and grown overnight in a CO_2 incubator. Cells were treated with different concentrations of TYR A9 (5 µM, 10 µM, 15 µM, 20 µM, and 40 µM) and vehicle for 24 hrs. After 24hr of TYR A9 exposure, cells were washed with 1XPBS and incubated with 20µM DCFDA in the dark for 30 minutes in a CO_2 incubator at 37 ℃. An ELISA micro-plate reader measured the fluorescence with excitation and emission wavelengths of 485 and 530 nm. All experiments were repeated three times, and results were presented as mean ± SEM.

4.2.12. Mitochondrial membrane potential ($\Delta\Psi m$)

The mitochondrial membrane potential was determined by tetramethyl rhodamine methyl ester (JC-1) upon TYR A9 exposure. JC-1 dye can bind specifically to the polarized mitochondria and is widely used to study $\Delta\Psi m$ [41]. In a 35mm dish, C6 and U87 cells (1×10^5) were seeded and allowed to grow overnight in a 5% CO2 incubator. For a full day, the cells were exposed to various concentrations of TYR A9 (10 µM, 20 µM, and 40 µM) and vehicle control. Following the treatment, the cells were stained with 5 µM of JC-1 dye for 30 minutes in the dark in a 5% CO_2 incubator, following the manufacturer's instructions. Cells were washed with 1XPBS. Using a Zeiss fluorescence microscope, the fluorescence was measured at a 20x magnification to determine the $\Delta\Psi$m.

4.3. Intracranial-C6 glioma model and TYR A9 treatment

We bought male Wistar rats weighing 180–230 grams from Jiva Life Sciences in Hyderabad. Every animal was kept in pathogen-free conditions in animal house facilities at the University of Hyderabad for a minimum of two weeks with a 12-hour light/dark cycle. Using stereotaxic surgery, the C6 glioma cell line was intracranially allografted [42, 43]. Before starting stereotaxic surgery, rats were deeply anesthetized by intraperitoneal (i.p.) injection of xylazine (15 mg/kg body weight) and ketamine (80 mg/kg body weight). Anesthetized rats were fixed on stereotaxic apparatus with the help of ear bars, and a midline scalp incision was made on the head to expose the skull and visualized the bregma point. Using striatum coordinates (0.5mm posterior; 3mm lateral), the skull was thinned with a 1mm diameter dental drilling machine. C6 glioma cells (2×10^6) were resuspended in a 6:4 (v/v) mixture of culture media and matrigel [44] and injected into the right striatum at a 6mm depth by microinjector with a speed of 5µl/min. After stabilizing cells in the striatum, the syringe was removed, and the incision was covered with dental

cement. Animals were kept back in the cage and maintained under aseptic conditions. After 7 days of stereotaxic surgery, animals were randomly selected and categorized into two groups with eight animals each. The vehicle control (0.1%DMSO) or TYR A9 (1.5mg/kg body weight) groups were treated intraperitoneally (i.p.) daily for 10 days. TYR A9 non-toxic dose and treatment route was selected according to the previous report [45]. The animal procedures followed the Institutional Animal Ethics Committee guidelines (UH/IAEC/PPB/2021-22/22) of the University of Hyderabad.

4.3.1. Tissue sample collection and histopathological analysis

All animals were sacrificed and perfused intra-cordially with 0.9% saline buffer followed by 4% paraformaldehyde (PFA) for histopathological evaluation. The rat's brain was removed and fixed in 4% PFA for 24 hrs, then dehydrated in ethanol and embedded in paraffin. Fixed brain tissues were sectioned with microtome (5-um thick) and collected on silane (3-aminopropyl triethoxysilane) coated glass slides for further histopathological analysis. After deparaffinization and rehydration, sections were used for H&E and IHC staining as described above, and tumor area or volume was calculated using formula: $(V)=4/3\ \pi\ (L/2\times W/2\times H/2)$.

4.4. Statistical analysis

All results were analyzed through statistical software Sigma Plot 11.0 or GraphPad Prism 9. The median or mean were used to evaluate central tendency and presented as median or mean ± SEM. The statistical significance was calculated by One-way ANOVA (Holm-Sidak method) for multiple groups or student t-tests (Mann-Whitney U) for two groups, and $p \leq 0.05$ is considered significant. The Pearson correlation was performed to study the correlation between the experimental groups. Survival data was analyzed using the Kaplan-Meier survival curve and compared using the Log-rank (Mantel-Cox) test. All experiments were performed in four replicates and repeated at least thrice. The graphical illustration represents mean values, and the bar represents SEM; the p-value ≤ 0.05 was considered statistically significant and described as not significant (ns) if $P > 0.05$; * $P \leq 0.05$; ** $P \leq 0.01$, *** $P \leq 0.001$; **** $P \leq 0.0001$.

4.5. Results

4.5.1. Upregulated expression of PYK2 and EGFR associated with astrocytoma malignancy and patients' poor survival

The *PYK2* and *EGFR* transcripts expression was evaluated through qPCR in different grades of astrocytoma tissues (n = 48) and control tissues (n = 12). Results showed increased *PYK2* transcript levels in grade 3 ($p = 0.003$) and grade 4 ($p = 0.009$) as compared to control brain tissues **(Figure 1A)**. The increased *PYK2* transcript level was positively correlated with *EGFR* mRNA ($r^2 = 0.98$; $P = 0.007$) expression, and the increased expression pattern was increased with astrocytoma progression **(Figure 1B)**. The pPYK2 and EGFR protein expression analysis in different grades of astrocytoma (n=48, including n = 12 control tissues) through western blot indicated increased pPYK2 and EGFR expression in grade 3 and grade 4 compared to the grade 2 and control tissue **(Figure S1)**. The representative IHC staining in astrocytoma (n = 3, each grade) tissue sections displayed high total and phospho form of PYK2 and EGFR protein in grade 3 and grade 4 compared to the grade 2 and control tissue **(Figure 1C)**. The pPYK2 and EGFR protein correlation analysis using densitometry values of western blot revealed a significant positive correlation between pPYK2 and EGFR ($r^2 = 0.91$; $P = 0.04$) **(Figure 1D)**. The positive expression of pPYK2 and EGFR was not significantly associated with the patient's age and gender; however, their positive expression considerably affected the median survival of astrocytoma patients **(Table 1)**. The increased pPYK2 expression was significantly ($p = 0.0279$) correlated with astrocytoma grades **(Table 1)**. Patients' survival analysis through the Kaplan Meier curve showed that positive pPYK2 expression was associated with patients' poor survival (Log-rank test $p \leq 0.047$) **(Figure S2)**. Noticeably, the patients with both pPYK2 and EGFR expression revealed dismal patients' survival (Log-rank test $p \leq 0.0128$) with a hazard ratio of 4.20 (95% CI 1.403 to 17.25) **(Figure 1E)**, suggesting that the increased expression of pPYK2 and EGFR aggravate astrocytoma malignancy and patients' poor survival.

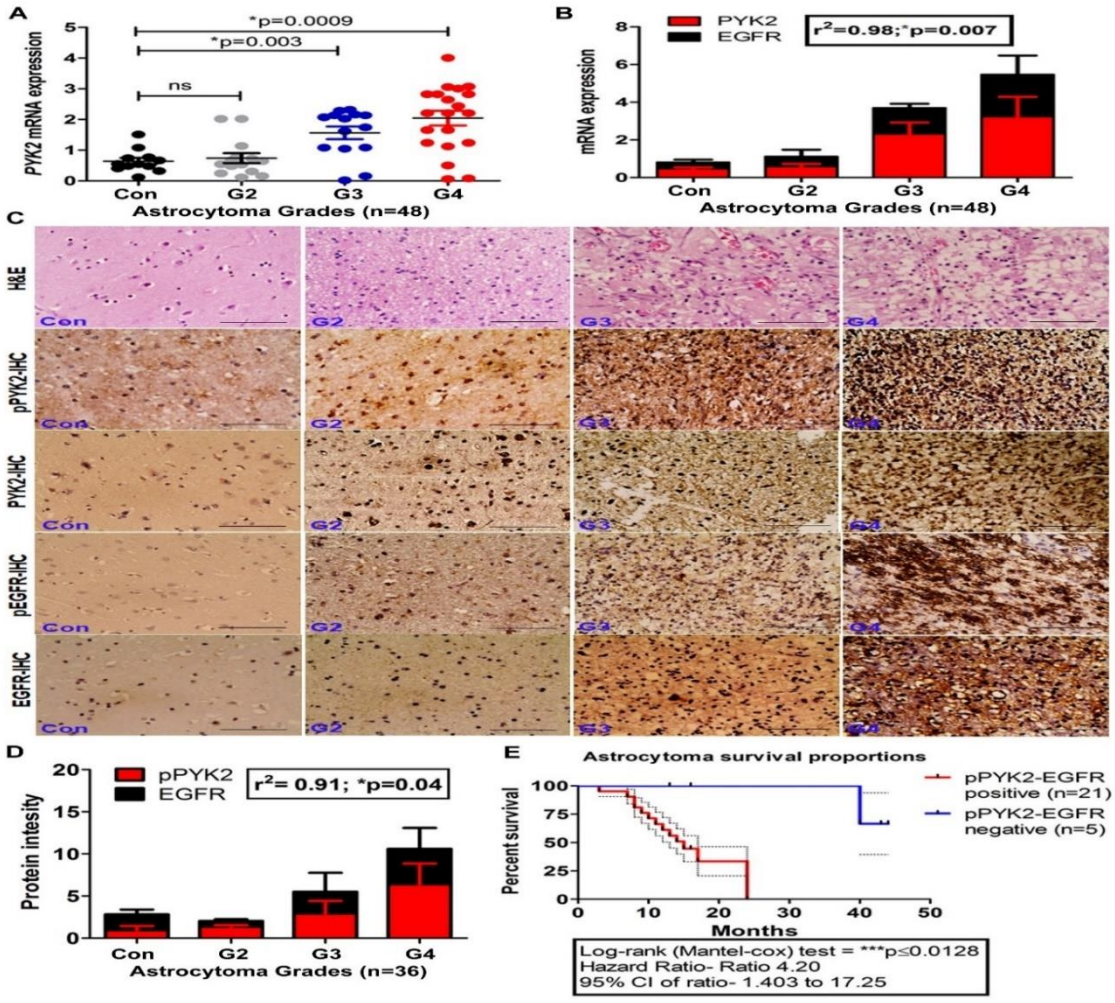

Figure 1: Upregulated PYK2-EGFR levels in astrocytomas (**A**), The qPCR mRNA expression analysis of PYK2 in astrocytoma tissues (n = 48) shows that, in comparison to the control (n = 12), PYK2 mRNA levels were significantly higher in grade 3 (n = 14) p = 0.003 and grade 4 (n = 20) p = 0.0009. (**B**), PYK2 and EGFR have a positive expression correlation, according to the correlation analysis (r^2 = 0.98; p = 0.007). (**C**), H&E images display pathological features of different grades of astrocytoma, and the representative IHC images show that grade 3 (n = 3) and grade 4 (n = 3) have stronger pPYK2 and EGFR staining than grade 2 (n = 3) and the control (n = 3). (**D**), pPYK2 and EGFR protein correlation analysis using normalized densitometry values of western data show a significant positive correlation between pPYK2 and EGFR (r^2 = 0.91, p = 0.04). **(E)**, The survival graph indicates a worse survival proportion of patients with positive pPYK2 and EGFR proteins; the Log-rank test reveals significant survival statistics (p≤0.0128) with a hazard ratio of 4.20 (95% CI 1.403 to 17.25).

Table 1: Clinicopathological association of pPYK2 and EGFR in astrocytoma			
Parameters	**pPYK2 protein expression (n = 48)**		
	Positive	Negative	Chi-square test
Age			
<35 (n = 21)	17	4	p = 0.61
>35 (n = 27)	19	8	
Gender			
Male (n = 30)	23	7	p = 1.00
Female (n = 18)	13	5	
Astrocytoma grades (WHO-2016, Classification system)			
GII (n = 14)	7	7	*p = 0.0279
GIII (n = 14)	11	3	
GIV (n = 20)	18	2	
Median survival age	**24 months**	**35 months**	
	EGFR protein expression (n = 48)		
	Positive	Negative	
Age			
<35 (n = 21)	16	5	p=0.82
>35 (n = 27)	21	6	
Gender			
Male (n = 30)	23	7	p=0.79
Female (n = 18)	14	4	
Astrocytoma grades (WHO-2016, Classification system)			
GII (n = 14)	9	5	p=0.362
GIII (n = 14)	11	3	
GIV (n = 20)	17	3	
Median survival age	**18 months**	**30 months**	
Median survival age	**15 months for both pPYK2 and EGFR-positive patients**		

4.5.2. Activated PYK2/EGFR-ERK signaling and pPYK2 druggability by TYR A9 in GBM

The mRNA expression of PYK2 and EGFR, along with its downstream ERK2 and ERK1, were in astrocytoma biopsies using qPCR (n = 50, including control brain tissue n = 10) and PCR (n = 16, including control brain tissue n = 4). The PCR and qPCR results showed significantly increased mRNA expression of PYK2 ($p = 0.023$), EGFR ($p = 0.0013$), and MAPK3/ERK1 ($p<0.0001$) in grade 4 compared to the control tissues **(Figure 2A, S3 A)**. Similarly, the protein expression through western blot revealed elevated levels of pPYK2, EGFR, pEGFR, and its downstream pERK½ in astrocytoma grades compared to the control tissues **(Figure 2B)**. Densitometry analysis results revealed significantly higher levels of pPYK2 ($p = 0.006$), EGFR ($p = 0.005$), and pERK½ ($p = 0.018$) in grade 4 compared to the control tissues **(Figure S3 B)**. A pairwise Pearson correlation map representing a strong positive correlation between pPYK2, EGFR, and pERK½ in astrocytoma tissues was created using the normalized densitometry values to create a correlation matrix **(Figure S4)**. The pERK½ IHC staining in astrocytoma tissue sections (n = 3, each grade) showed an increased pERK½ expression level in grade 3 and grade 4 compared to the grade 2 and control tissues **(Figure S5)**. We also performed immunofluorescence (IF) staining to confirm that pPYK2 and pERK$^{1/2}$ are co-localized. According to the IF results, increased expression and co-localization of pPYK2 and pERK½ in grade 4 compared to the control tissues **(Figure S6)**, which suggested that activated pPYK2/EGFR-pERK½ signaling axis in malignant astrocytoma might be associated with astrocytoma malignancy. We further examined PYK2 expression in several GBM cell lines using qPCR and western blotting. The results showed differential expression patterns of *PYK2* at mRNA **(Figure S7)** and protein (activated or pPYK2) levels **(Figure 2C)**. To evaluate pPYK2 druggability by TYR A9, based on pPYK2 expression, we selected three GBM cell lines, C6, U87, and LN18 **(Figure 2N)**. Interestingly, we found dose-dependent pPYK2 inhibition upon 24hrs of TYR A9 exposure in these cell lines (Figure. 2D). To study the anticancer efficacy of TYR A9, we treated C6, U87, and LN18 cells at multiple doses. We observed a significant dose-dependent inhibition of C6, U87 and LN18 cell proliferation after 24 hrs of TYR A9 treatment compared to the vehicle control (0.01% DMSO) **(Figure 2E-G)**. The half-effective concentration (EC_{50}) of TYR A9 was calculated by a nonlinear fit equation. The estimated EC_{50} dose was 20±2 µM for both the C6 and U87 cell lines and 38±2 for the LN18 cell line **(Figure S8)**. We used half EC_{50} (10 µM), EC_{50} (20 µM), and 2X EC_{50} (40 µM) doses of TYR A9 for the further in-vitro experiments. Time-dependent inhibition in cell growth of C6, U87, and LN18 cell lines was observed upon TYR A9 exposure (**Figure S9**), indicating dose and time-dependent antiproliferative efficacy of TYR A9. The proliferating cell nuclear antigen (PCNA) estimation with western blot indicated dose-dependent inhibition in both GBM cell lines compared to

the vehicle control **(Figure S10)**. To find out the long-term effect of TYR A9 on C6, U87, and LN18, we performed a colony assay, which showed significantly reduced colonies growth in terms of size and number in the C6 cell line at 10 µM ($p = 0.023$) 20 µM ($p = 0.0003$) and 40 µM ($p<0.0001$) of TYR A9 concentrations as compared to the vehicle control **(Figure 2H, I)**. Similarly, a dose-dependent reduced colonies formation was also observed in U87 and LN18 GBM cell lines at 20 µM ($p = 0.001$) and 40 µM ($p = 0.0001$) of TYR A9 concentrations as compared to the vehicle control **(Figure 2J-M)**.

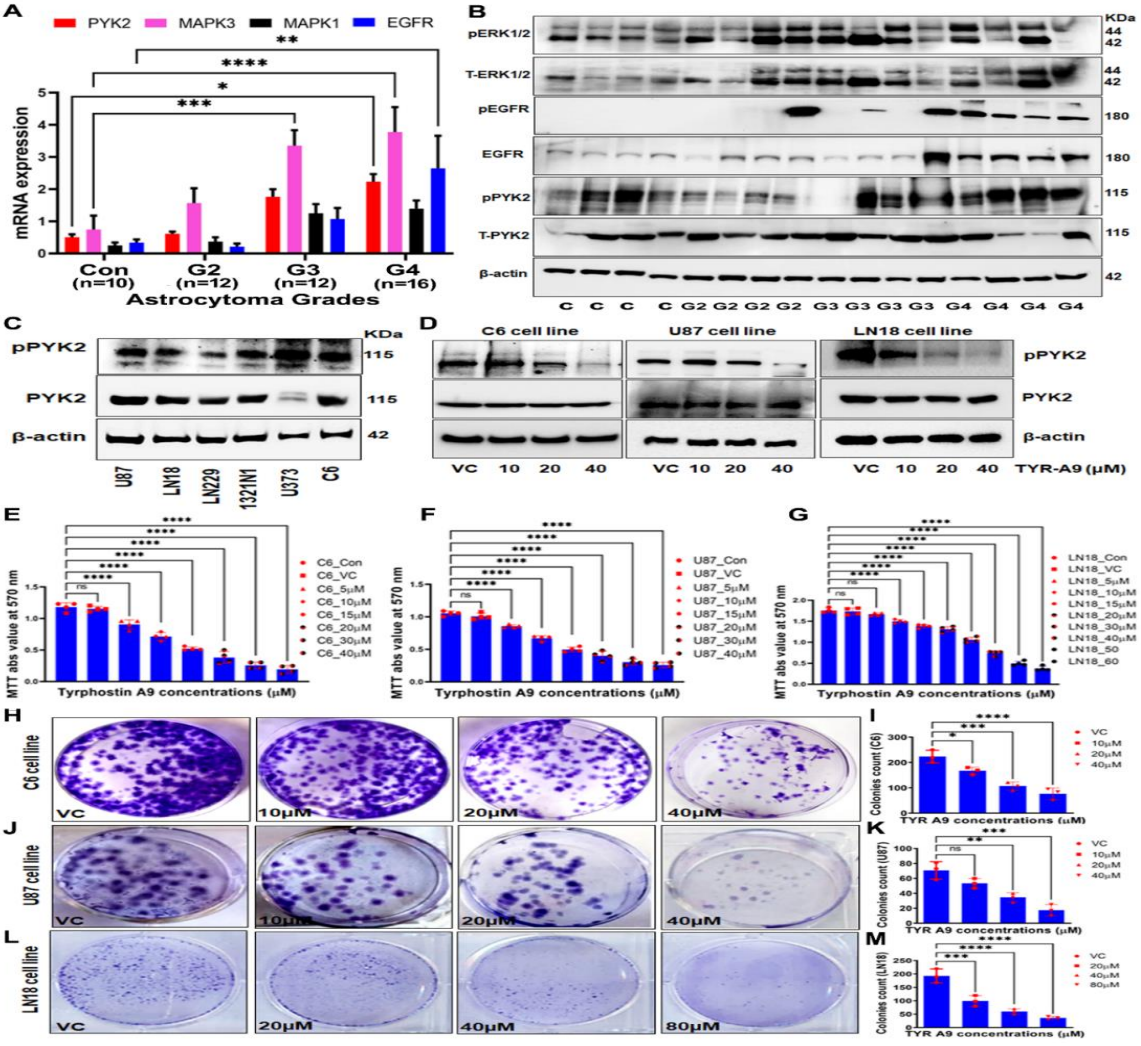

Figure 2: Activated PYK2-EGFR induced ERK signaling pathway and pPYK2 draggability by TYR A9 in GBM: (A), The mRNA levels of *PYK2* and *EGFR*, along with its downstream *ERK* by PCR and qPCR analysis, indicate an increased mRNA expression of *PYK2* ($p = 0.023$), *EGFR* ($p = 0.0013$) and *MAPK3/ERK1* ($p<0.0001$) in grade 4 ($n = 16$) as compared to the control tissues ($n = 10$). **(B)**, The representative western blot shows that grade 4 ($n = 4$) tissues have higher levels of PYK2, EGFR, and

pERK½ protein expression than do the control tissues (n = 4). **(C)**, Showing differential protein expression of total and pPYK2 in GBM cell lines. **(D)**, Dose-dependent inhibition of pPYK2 by TYRA9 in C6, U87, and LN18 cell lines. **(F, G, E)**, The cell proliferation assay showed inhibited cell proliferation in a dose-dependent manner upon TYR A9 exposure in C6, U87, and LN18 cell lines. **(H-M)**, The dose-dependent reduced colonies formation in the C6 cell line at TYR A9 doses of 10 µM ($p = 0.023$), 20 µM ($p = 0.0003$), 40 µM ($p<0.0001$) compared to the vehicle control, together with U87 and LN18 cell line showing significant reduction at 20 µM and 40 µM TYR A9 doses compared to the vehicle control.

Activation of pPYK2/EGFR-ERK signaling pathway in glioblastoma progression

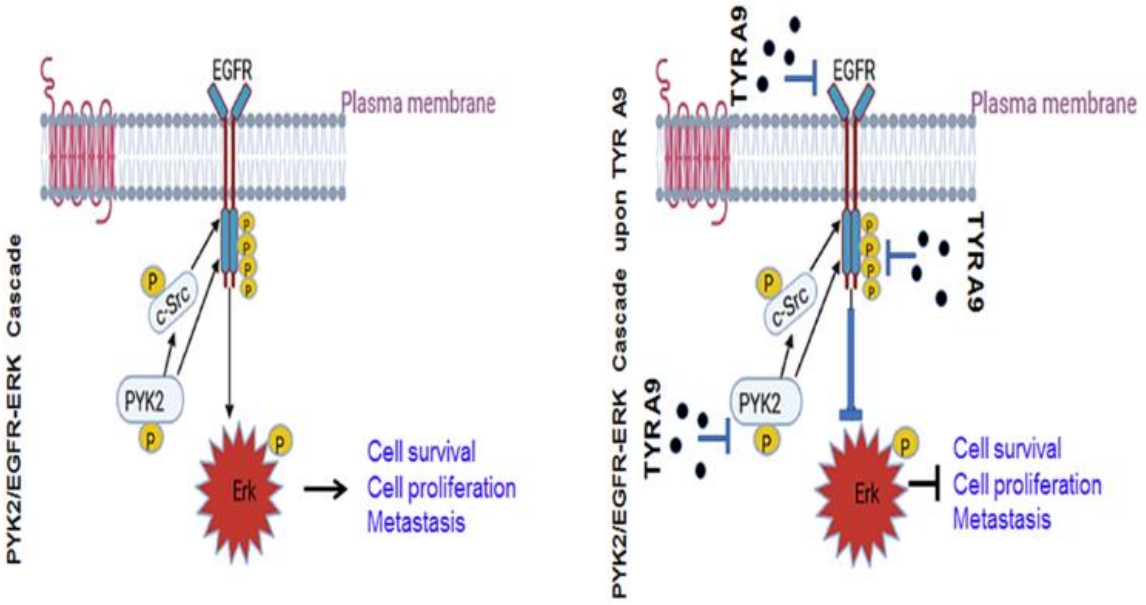

Figure 2N: The schematic diagram displayed proof of concept of the current study indicating TYR A9 treatment attenuates GBM cell proliferation and migration and induces GBM cell death by inhibiting PYK2 and EGFR-induced ERK activation.

4.5.3. TYR A9 treatment altered cell cycle distribution, induced apoptosis, and depolarized mitochondria.

To investigate, if TYR A9 can cause cell death and inhibit GBM cell growth, Phase-contrast microscopic evaluation showed altered C6 and U87 cell morphology with an indication of cell death upon TYR A9 exposure **(Figure S11)**. Trypan blue dye exclusion staining confirmed cell death with increased TYR A9

concentrations compared to the vehicle control in C6 and U87 cell lines **(Figure S12)**. To find out the cell cycle distribution and mode of cell death, we stained C6 and U87 cells with PI after TYR A9 and vehicle exposure and analyzed them through FACS. The cell cycle analysis showed TYR A9 treatments arrested the cell cycle at G0/G1 cyclic phase at 10µM and 20µM of TYR A9 concentrations compared to the vehicle control **(Figure 3A and S13)**. Simultaneously, annexin V staining **(Figures 3B)** and acridine orange/ethidium bromide (AO/EB) staining **(Figures S14)** showed an increased annexin V levels or AO/EB ratio respectively after TYR A9 treatment than the vehicle control, indicating apoptosis induction in both cell lines **(Figures 3B, S14)**. Western blot results showed increased levels of apoptotic proteins like cleaved PARP and cleaved caspase3 after treatments with 10µM and 20µM of TYR A9 in both the C6 and U87 cell lines **(Figure 3C)**. Additionally, TYR A9 dose-dependent exposure increased pro-apoptotic mitochondrial protein BAX and BAK; and decreased anti-apoptotic protein Bcl_2 compared to the vehicle control **(Figure 3C)**. These findings demonstrated that TYR A9 treatment induced apoptosis cell death in GBM cell lines. One of the main causes of apoptosis is further disruption of the mitochondrial membrane potential ($\Delta\Psi m$) [28, 39]. The JC-1 fluorescent dye is used to identify variations in $\Delta\Psi m$. It forms J-aggregates upon binding to the mitochondrial membrane and emits red-orange fluorescence, indicating polarized mitochondria with high $\Delta\Psi m$. However, in depolarized mitochondria with low $\Delta\Psi m$, it emits green fluorescence and forms J-monomers. To determine the $\Delta\Psi m$ using the red/green fluorescence intensity ratio [41]. TYR A9 treatment in C6 **(Figure 3D)** and U87 **(Figure 3E)** cells showed decreased red and increased green fluorescent intensity at 20µM and 40µM concentrations compared to the vehicle control. The quantified graph showed a remarkable decrease in red/green fluorescence ratio with increasing TYR A9 dose in C6 (10 µM, 20 µM, 40 µM; $p<0.0001$) and U87 (10 µM; $p = 0.008$, 20 µM and 40 µM; $p<0.0001$) compared to vehicle control **(Figure 3F, G)**, indicating deceased $\Delta\Psi m$. Besides, western blots showed increased cytosolic cytochrome-c protein levels after TYR A9 treatment compared to the vehicle control in C6 and U87 cell lines **(Figure 3H)**, proving mitochondrial depolarization. Emerging reports raise concern about drug toxicity and chemoresistance, particularly anticancer drugs with ROS-inducing potentials [46]. Considering this point, we also examined TYR A9 effect on ROS production and checked the expression level of a key enzyme NOX2 involved in ROS/NOS production. We observed significantly low ROS levels at TYR A9 dose 10 µM, $p = 0.008$, and 15 µM, $p = 0.0002$, compared to the vehicle control in the C6. Similarly, significant ROS inhibition was also observed in the U87 cell line at 10µM ($p = 0.0004$) and 15µM ($p = 0.0001$) of TYR A9 concentrations as compared to the vehicle control after 24hrs of TYR A9 exposure **(Figure S15A)**.

Western blots revealed lower NOX2 protein levels in TYR A9 treated cells compared to the vehicle control **(Figure S15B)**, suggesting TYR A9 mediated cell death response is independent of ROS levels.

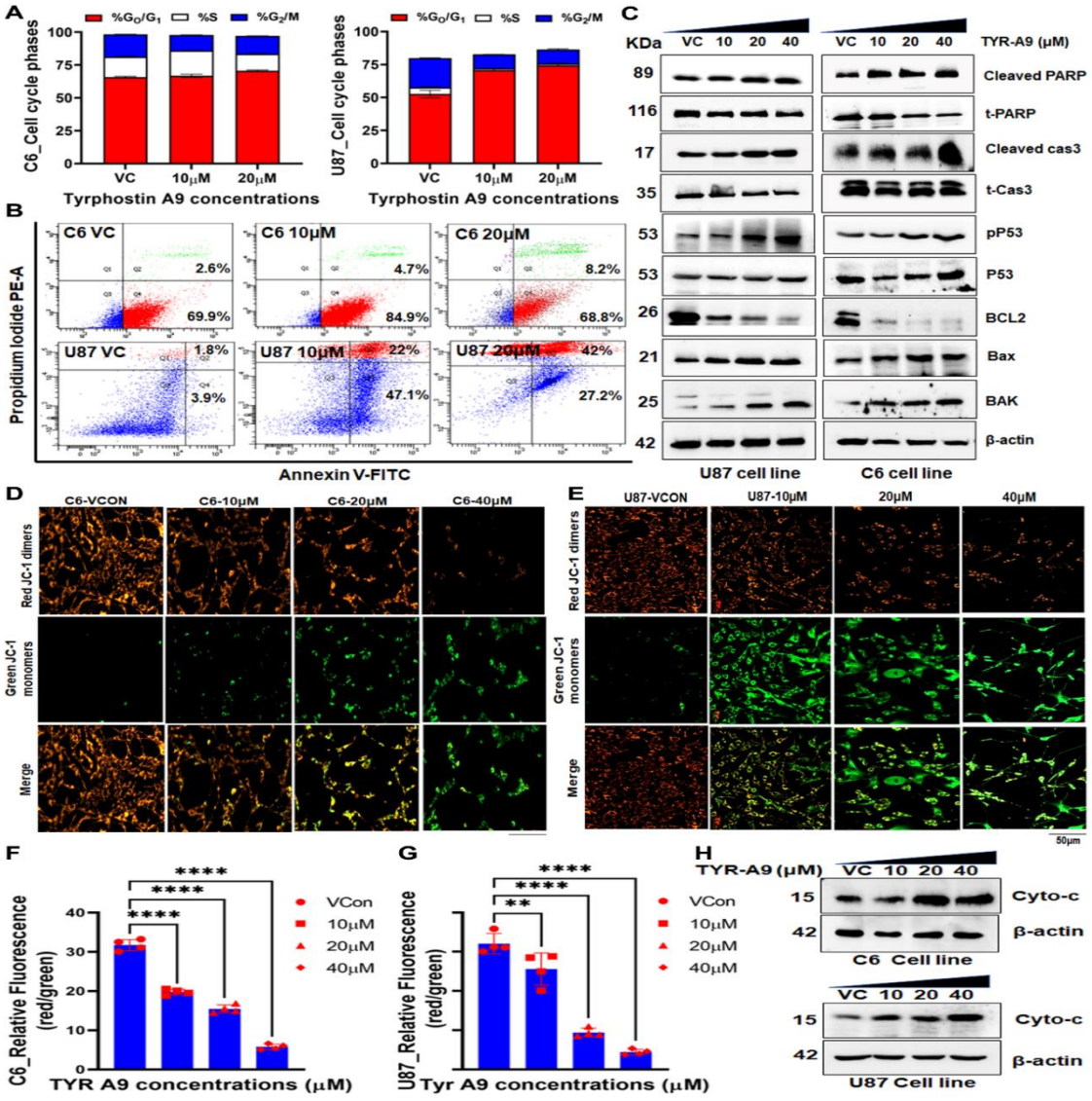

Figure 3: TYR A9 treatment altered the cell cycle, induced apoptosis, and depolarized mitochondria: (A), The cell cycle distribution graph shows G0/G1 cyclic arrest at 10 µM and 20 µM of TYR A9 dose in C6 and U87 cell lines compared to the vehicle control. **(B)**, FACS analyzed the dot plot, which exhibits increased Annexin V staining after TYR A9 treatment in C6 and U87 cell lines. **(C)**, Apoptosis-associated proteins evaluated by western blot show increased cleaved PARP and Caspase 3 together with mitochondrial pro-apoptotic (total and phospho p53, BAX, and BAK) and decreased anti-apoptotic protein BCL2 upon TYR A9 exposure compared to the vehicle control in both cell lines. **(D, E)**, JC-1-stained cells images and **(F, G)**, quantified red/green fluorescence intensity indicate a significant

decrease with increasing TYR A9 dose in C6 (10 µM, 20 µM, 40 µM; $p<0.0001$) and U87 (10 µM; $p=0.008$, 20 µM and 40 µM; $p<0.0001$) compared to vehicle control. **(H)**, Increased cytochrome C levels in dose dependent manner in both GBM cells. All experiments were performed in four replicate and repeated three times.

4.5.4. TYR A9 reduced GBM cell migration and sensitized TMZ resistance by suppressing pPYK2/EGFR modulated ERK½ signaling in GBM cell lines.

In C6, U87, and LN18 cells, the wound healing migration assay at half EC50 and EC50 dose of TYR A9 revealed slow wound closure compared to the vehicle control **(Figure 4A and S16)**. The relative cell migration graph showed significantly inhibited cell migration of C6 ($p = 0.0002$) and U87 ($p = 0.0007$) cell lines at half EC_{50} (10µM) TYR A9 dose as compared to the vehicle control **(Figure 4B, C)**. Similarly, significant inhibition in cell migration was also observed in the LN18 cell line at 20 µM of TYR A9 dose **(Figure S16)**. Further, to demonstrate the clinical relevance of TYR A9 in GBM, specifically in temozolomide (TMZ) resistance GBM cells [65, 107], we evaluated the synergistic effect of TYR A9 and TMZ in C6, U87, and LN18 cell lines by using previously indicate TMZ doses 50 µM and 100 µM [95]. Interestingly, we observed attenuated cell proliferation of C6, U87, and LN18 cells, treated in combination with TYR A9 (EC_{50}) plus TMZ (50 µM or 100 µM) as compared to the TMZ alone **(Figure S17)**; this effect was more intense after 48hr of TYR A9 plus TMZ (50 µM or 100 µM) exposure. Eventually, no statistical significance was observed when combined doses, TYR A9 plus TMZ (50 µM or 100 µM) were compared with TYR A9 (EC_{50}) **(Figure S17)**. Similarly, the colony formation assay showed a significant reduction in colony formation of C6 and LN18 cells in combined doses, TYR A9 plus TMZ (50 µM or 100 µM) as compared to the TMZ 50 µM and 100 µM alone **(Figure 4D-E)**. Note LN18 is a TMZ-resistant cell line [50] and showed considerable difference in terms of colony size and number in combined doses of TYR A9 40 µM plus TMZ (50 µM or 100 µM) as compared to the TYR A9 (40 µM) and TMZ 50 µM or 100 µM alone **(Figure 4F, G)**. To evaluate the molecular mechanisms, we exposed C6, U87, and LN18 cells with TYR A9 at half EC50 and EC50 and double EC50 concentrations. We observed repressed phosphorylation of PYK2, EGFR, FAK, Src, and ERK together with EGFR protein in C6, U87 and LN18 cell lines **(Figure 4H)**. Additionally, to verify TYR A9 attenuated phosphorylation of PYK2, we induced phosphorylation of PYK2 by TNF-α in notion with previous evidence [22] and simultaneously treated with TYR A9. The western blot and quantified protein intensity analysis showed dose-dependent inhibition of TNF-α induced PYK2 phosphorylation in U87 cells at 20 µM and 40 µM of TYR A9 concentrations as compared to the TNF-α **(Figure S18)**.

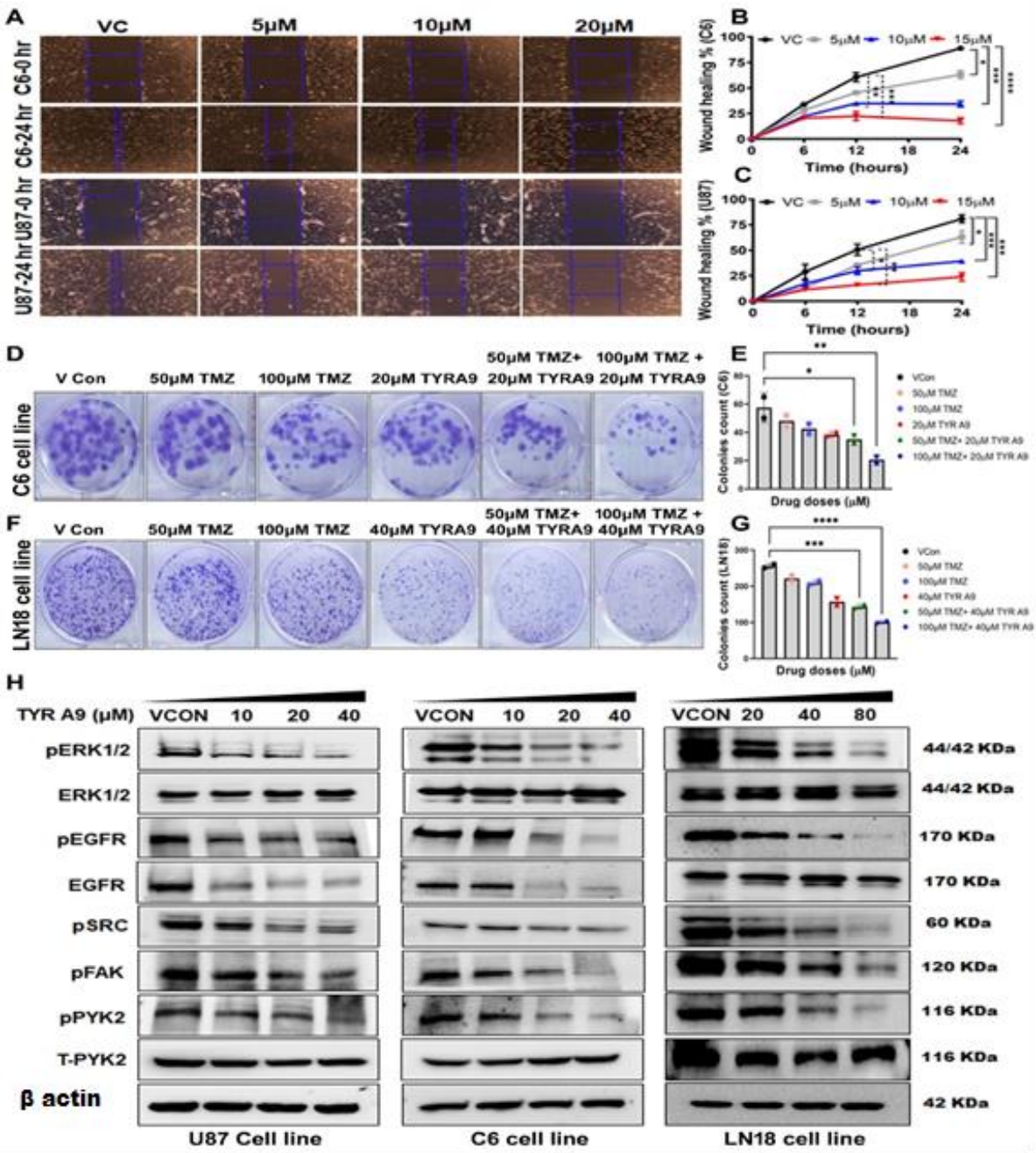

Figure 4: TYR A9 reduced GBM cell migration and sensitized TMZ resistance by suppressing PYK2/EGFR modulated ERK½ signaling pathways: (A–C), The scratch wound healing migration assay reveals significant inhibition of cell migration after 24 hrs of TYR A9 exposure at 10 μM dose in C6 ($p = 0.0002$), and U87 ($p = 0.0007$) compared to the vehicle control. **(D–G)**, Colony assay shows a significant reduction in colony formation in combined doses of TYR A9 plus TMZ compared to TMZ or TYRA9 alone in both C6 and LN18 cells. **(H)**, The representative western blot depicts repressed

phosphorylation of PYK2, EGFR, FAK, Src, and ERK with total EGFR protein upon dose-dependent TYR A9 exposure in GBM cell lines.

4.5.5. TYR A9 restricted tumor growth and improved animal survival by suppressing PYK2/EGFR-ERK signaling with induced apoptosis in *in-vivo*

We grafted C6 cells into Wistar rats to create an intracranial glioma model to evaluate the anticancer efficacy of TYR A9 formally. In comparison to the vehicle control (0.1% DMSO), we observed that TYR A9 (1.5 mg/kg body weight) treatment for ten days at intervals of 24hrs significantly reduced glioma growth ($p = 0.002$) **(Figure 5A, B)**. To verify the anticancer efficacy of TYR A9 in glioma rats, we performed a histopathological study after TYR A9 treatments. Our histological H&E and Ki67-IHC staining on TYR A9 and vehicle-treated glioma rats revealed significantly fewer tumor cells in TYR A9-treated glioma rats ($p = 0.0004$) than in the vehicle-treated glioma rats **(Figure 5C, D)**. We also evaluated the impact of TYR A9, including drug toxicity and animal survival for 60 days of post-TYR A9 treatment. We notice there was no weight loss in TYR A9 treated glioma rats compared to the vehicle-treated glioma rat **(Figure 5E)**. The Kaplan-Meier survival curves indicated TYR A9 treated glioma rats showed significantly improved survival by Log-rank (Mantel-Cox) test ($p=0.0144$) as compared to the vehicle-treated glioma rats **(Figure 5F)**. TYR A9 treated glioma rats had a longer median survival of 45 days compared to the vehicle-treated rats 15-20 days. IHC staining with phospho PYK2, pEGFR, and pERK1/2 showed considerably low positive pPYK2 ($p = 0.0008$), pEGFR ($p = 0.0028$) and pERK½ ($p = 0.0027$) **(Figure 5G-J)** in TYR A9 treated glioma rats compared to the vehicle-treated glioma rats. Subsequently, cleaved caspase 3 staining showed a significantly high positive level of cleaved caspase 3 cells in TYR A9 treated glioma rats ($p = 0.0012$) compared to the vehicle-treated glioma rats **(Figure 5G, K)**. These *in-vivo* data corroborate *in-vitro* evidence advocating the anticancer potential of TYR A9 by suppressing PYK2/EGFR-ERK signaling pathways.

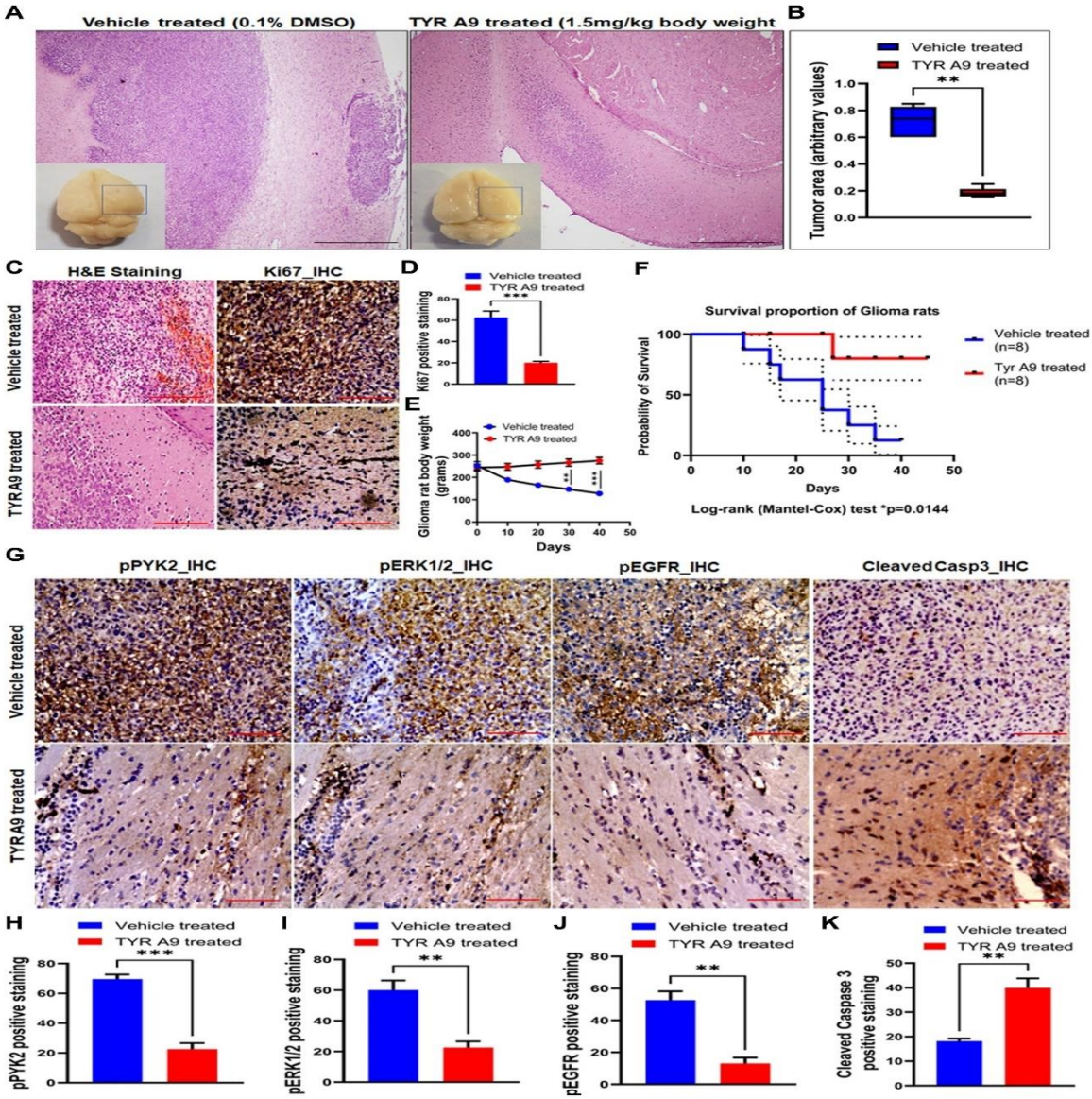

Figure 5: TYR A9 attenuated tumor growth with improved animal survival by suppressing PYK2/EGFR-ERK signaling and inducing apoptosis: (A, B), Histological evaluation by H&E and total tumor area estimation demonstrates significantly reduced tumor growth upon TYR A9 treatments ($p = 0.002$) compared to the vehicle (0.1% DMSO) treated glioma rats. **(C, D)**, H&E and Ki67-IHC staining indicate significantly decreased tumor cells in TYR A9 treated glioma rats ($p = 0.0004$) compared to the vehicle-treated glioma rats. **(E)**, TYR A9 treated glioma rats exhibit no weight loss compared to vehicle-treated glioma rats. **(F)**, The Kaplan-Meier survival curves reveal TYR A9 treatment significantly improved survival by Log-rank (Mantel-Cox) test ($p = 0.0144$) compared to the vehicle-treated glioma rats. **(G–J)**, IHC images and quantified graphs show significantly low positive staining of H pPYK2 ($p = 0.0008$), I pERK ($p = 0.0027$), and pEGFR ($p = 0.0028$) in TYR A9 treated compared to

the vehicle-treated glioma rats. **(G, K)**, IHC staining for cleaved Caspase 3 reveals considerably high cleaved caspase 3 positive cells in TYR A9 ($p = 0.0012$) compared to vehicle-treated glioma rats**.**

4.6. Discussion

To prevent GBM-associated mortality, more translational research is necessary because the complex cellular and molecular etiology of GBM engenders resistance against the current standard of care [108, 109]. Indeed, the molecular-based grading and present therapeutic regimen, including surgery combined with radio and chemotherapy, improved GBM prognosis. However, drug resistance and GBM reoccurrence impose low clinical outcomes [5, 33, 25], implying that developing therapeutic approaches for GBM is desperately needed.

Emerging studies disclosed that the receptor tyrosine kinases (RTKs) modulated signaling pathways could elicit cancer progression and malignancy [6, 7, 25]. Altered expression and activity of PYK2 and EGFR are reported in several cancers, including glioma [8, 11, 17, 18, 20, 21]. In the current study, we found that high grade 3 and grade 4 of astrocytoma associated with GBM malignancy had upregulated levels of pPYK2 and EGFR, supporting the findings of the earlier study [23]. Interestingly, we observed that the increased pPYK2 expression was positively correlated with EGFR protein expression in astrocytoma grades. The increased pPYK2 and EGFR expression in astrocytoma grades were positively associated with patients' poor survival in agreement with previous reports indicating activated PYK2 might be a key trans-activator of EGFR, which initiates Ras/MEK/ERK signaling cascade [21, 22]. Simultaneously, we identified activated PYK2/EGFR-ERK signaling pathways in malignant astrocytoma (grade 3 and grade 4), suggesting the involvement of this signaling axis in GBM pathogenesis. Moreover, the clinicopathological analysis revealed an etiological association between pPYK2 and EGFR in GBM malignancy and the patient’s poor survival [20, 23, 50], showing its clinical significance.

To verify the druggability of pPYK2 and EGFR modulated ERK signaling in GBM and its phenotypic consequences, we used TYR A9, a known TKI which is an efficient inhibitor of PYK2, PDGF, and VEGF [26-29]. We found that TYR A9 treatment suppressed pPYK2 expression and significantly reduced cell proliferation and cell survival at EC50 of TYR A9 in C6, U87, and LN18 cell lines. Our long-term cell proliferation and cell survival through clonogenic assay indicated significantly reduced colony formation at different doses of TYR A9 in C6, U87, and LN18 GBM cell lines, supporting the antiproliferative properties of TYR A9 [28, 30]. Cell proliferation is regulated by the cell cycle; we sought to evaluate whether TYR A9 could affect cyclic distributions of GBM cells in notion with a previous report [31]; our cell cycle data revealed G0/G1 cyclic phase arrest upon TYR A9 treatment in both C6 and U87 GBM

cell lines also an indication of apoptosis induction. Eventually, cellular staining with an apoptosis marker annexin V after TYR A9 treatment confirmed apoptotic cell death in both C6 and U87 cell lines. Similarly, our western blotting data showed increased expression levels of apoptosis stimulators, including p53, Bax, cleaved caspase3, and cleaved PARP, and reduced anti-apoptosis BCl_2 protein upon TYR A9 treatment in C6 and U87 cell lines, validating apoptosis stimulating efficacy of TYR A9 [28]. We further measured mitochondrial membrane potential ($\Delta\Psi m$) through JC-1 staining, which revealed TYR A9 treatment decreased mitochondrial membrane potential in both GBM cell lines, coincides with the fact that the decreased $\Delta\Psi m$ is associated with the mitochondrial permeabilization that leads to the cytochrome-c release in the cytosol and increases Bax protein levels. Our western blotting data confirmed increased cytochrome-c protein upon TYRA9, indicating TYR A9 induces mitochondrial-dependent apoptosis in agreement with the earlier reports [28, 51, 52]. Tyrphostin A9 also acts as a mitochondrial uncoupler [53]; mechanistically, mitochondrial uncoupling proteins (UCPs) impede oxidative phosphorylation and reduce mitochondrial ROS production [52]. Several UCPs have been identified with their therapeutic implication in various diseases, including cancer [53, 54]. In agreement with previous reports [55-57], this is the first study where, in addition to the anticancer efficacy of TYR A9 in GBM cell lines, we showed TYR A9 significantly reduced ROS levels and NOX2 protein orthogonally verifies TYR A9 repressing potentials of PYK2 phosphorylation, as pPYK2 can trigger ERK½ mediated ROS generation [58]. Cancer cell migration and invasion are enhanced upon integrin binding to the ECM and recruitment of FAK and PYK2 activation, which initiates phosphorylation of various downstream effectors involved in cell proliferation and migration [10, 59]. Accordingly, our cell-based wound-healing assay results showed significant inhibition in C6, U87 and LN18 cell migration.

In agreement with the existing literature suggesting drug resistance is critical in limiting the usage of TKIs in therapeutic interventions [60], we sought to evaluate whether TYR A9 can sensitize TMZ efficacy or resistance in GBM cells [47, 61]. Besides, TYR A9 is most potent among 51 tyrosine kinase inhibitors, and various reports have demonstrated that TYR A9 can potentially target MAP kinases (ERK and JNK) and NF-κB pathways [27, 28, 45, 53] are known signaling pathways regulating TMZ resistance. Intriguingly, combined treatment of TYR A9 and TMZ reduced cell proliferation and cell growth of GBM cell lines, including TMZ resistance LN18 cells. However, an in-depth study with an appropriate chemoresistance model is required to demonstrate the synergistic or TMZ sensitization effect of TYR A9 in GBM.

Further, our western data indicating TYR A9 treatment attenuated protein levels of pPYK2, pEGFR, pFAK, pSRC, pERK, and total EGFR in C6, U87 and LN18 GBM cell lines, suggesting suppressed ERK signaling cascade, which is a key molecular pathway that regulates cell survival, cell migration and chemoresistance (TMZ) [10, 59, 61]. Conversely, we also showed TYR A9 efficacy in suppressing TNF-α induced PYK2 phosphorylation, together presenting a strong druggable effect of TYR A9 and restricted cell migration potential in agreement with earlier studies [10, 23, 26].

We assessed the anticancer efficacy of TYR A9 in the intracranial C6 glioma model in order to support our in-vitro data. Our histopathological analysis by H&E and Ki67-IHC staining showed that TYR A9 treatment significantly reduced tumor growth with augmented animal survival. Toxicity of TKIs is the major concern in the therapeutic intervention of cancer [60]. Similarly, we evaluated the toxic effect of TYR A9 in glioma rats. We found no weight loss or any abnormalities in skin coat or fur loss in TYR A9-treated glioma rats, suggesting TYRA9 could be a safer therapeutic drug for glioma. Further, IHC staining displayed considerably low cellular positivity of pPYK2, pEGFR, and pERK½. It significantly increased cleaved caspase 3 cellular staining in TYR A9 treated glioma rats compared to the vehicle-treated glioma rats corroborating *in-vitro* data, and advocating anticancer potential of TYR A9 by suppressing PYK2/EGFR-ERK signaling pathways.

4.7. Conclusion

Overall, the present study demonstrated that an upregulated pPYK2 and EGFR in GBM aggravate disease malignancy and dismal patient survival. The *in-vitro* and *in-vivo* study showed that TYR A9 treatment significantly reduced GBM cell growth and induced apoptosis. Additionally, TYR A9 exposure suppressed pPYK2 and EGFR-modulated ERK signaling cascades, suggesting TYR A9 can be used as a pharmacological inhibitor of PYK2 phosphorylation (Tyr-402) and EGFR-triggered ERK signaling cascade in GBM.

4.8. Additional Information

Ethical approval

The study's use of clinical biopsies and clinicopathological information was approved by the Institutional Ethics Committee (UH/IEC/2016/180), University of Hyderabad, India. All animal procedures followed the Institutional Animal Ethics Committee guidelines (UH/IAEC/PPB/2021-22/22) of the University of Hyderabad.

Supporting Information

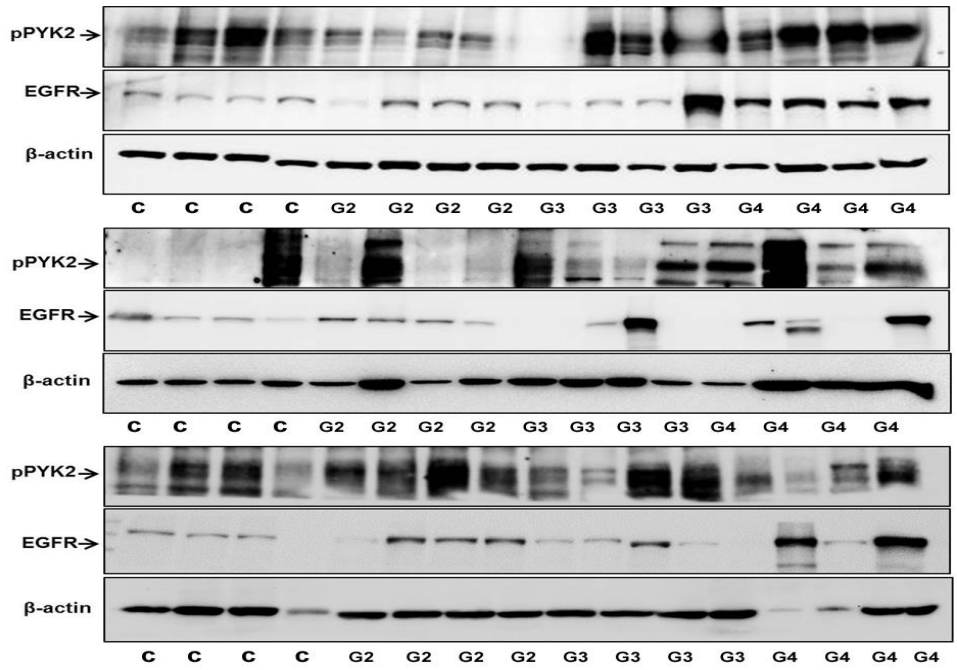

Figure. S1: The pPYK2 and EGFR protein expression by western blot in different grades of astrocytoma (n=48, including n=12 control tissues) show increased pPYK2 and EGFR protein levels in astrocytoma grades as compared to the control tissues

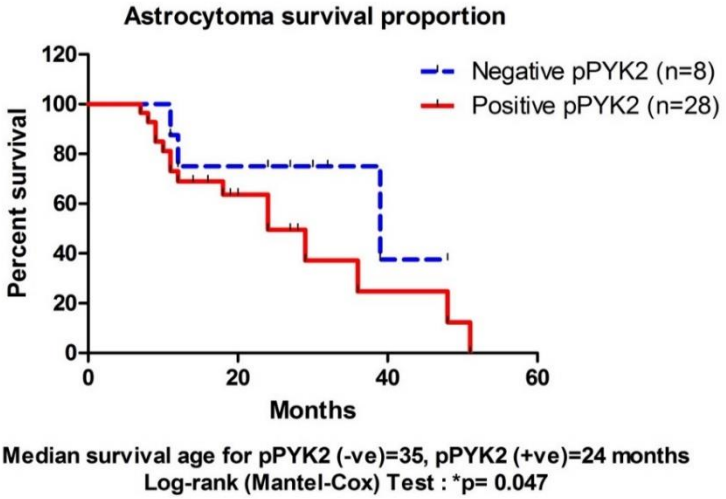

Figure. S2: The survival curve indicates pPYK2 positive patients exhibit poor survival compared to the negative pPYK2 patients. The Log-rank test showed significant survival statistics (p≤0.047).

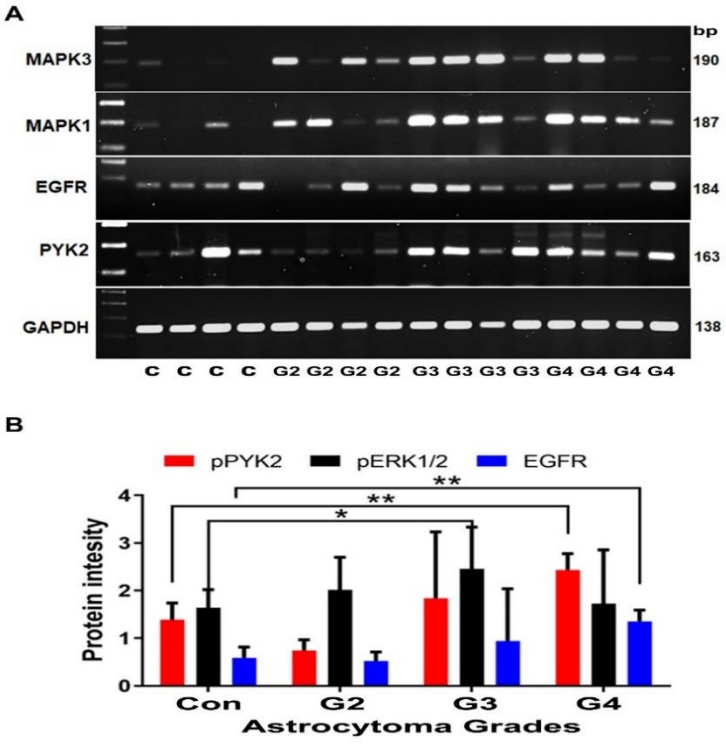

Figure. S3: The mRNA expression by PCR-gel analysis indicated an increased mRNA expression of *PYK2*, *EGFR,* and *MAPK3/ERK1* in high grades of astrocytoma as compared to the low and control

tissues. Protein quantification shows significantly increased pPYK2 ($p = 0.006$), EGFR ($p = 0.005$), and pERK½ ($p = 0.018$) in grade 4 ($n = 4$) compared to the control tissues ($n = 4$).

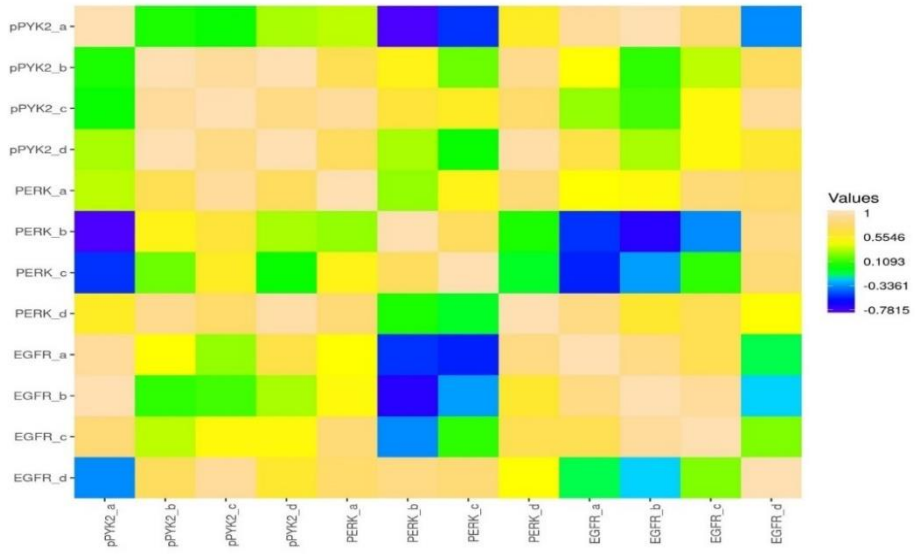

Figure. S4: The correlation matrix (a pair-wise Pearson correlation map) showing a significant positive correlation of pPYK2, EFGR, and pERK½ in astrocytoma grades (a-Con, b-G2, c-G3, and d-G4).

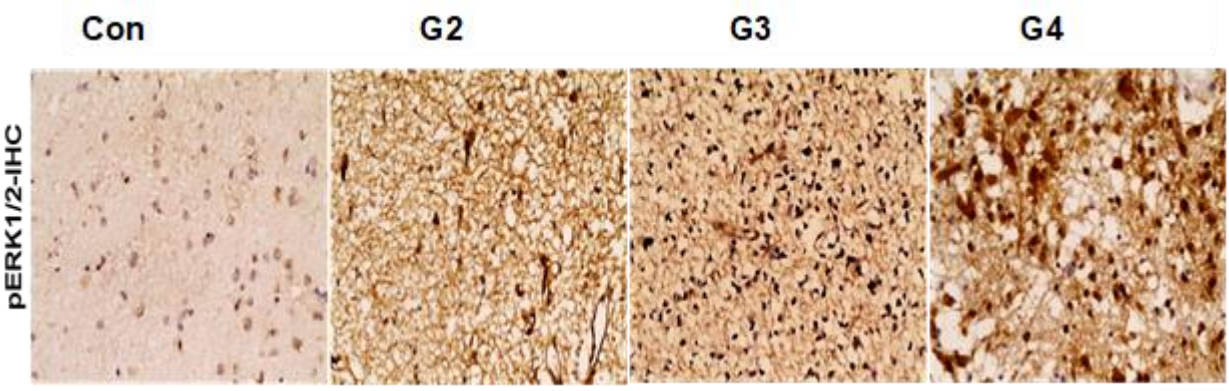

Figure. S5: The representative IHC image indicates increased cellular staining $pERK^{1/2}$ in G3 and G4 compared to the G2 and control brain tissues.

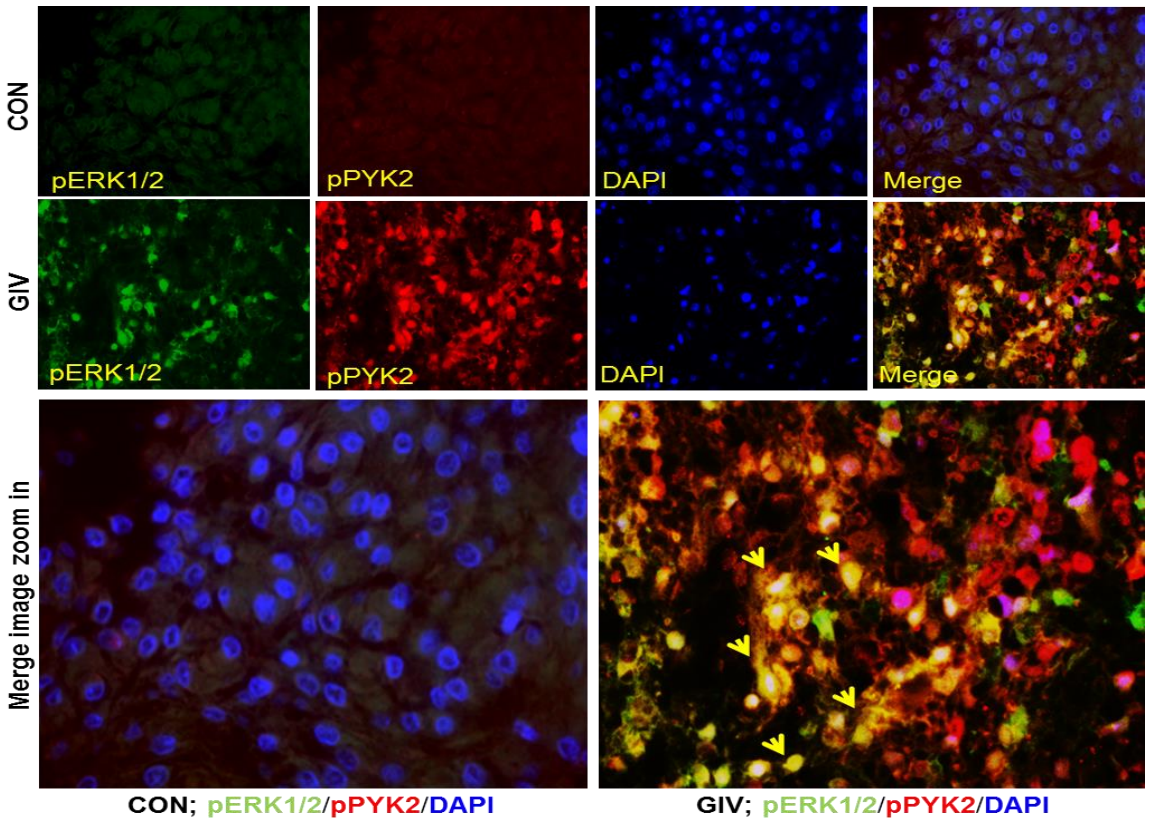

Figure. S6: The IF image shows increased expression and co-localization of pPYK2 and pERK1/2 in G4 compared to the control brain tissues, the zoom-in images with arrowheads showing co-localization of pPYK2 and pERK1/2 in G4.

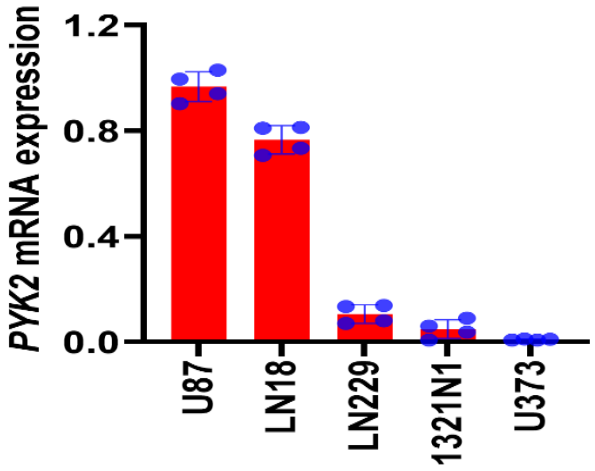

Figure. S7: q-RTPCR analysis showing differential mRNA expression of *PYK2* in GBM cell lines.

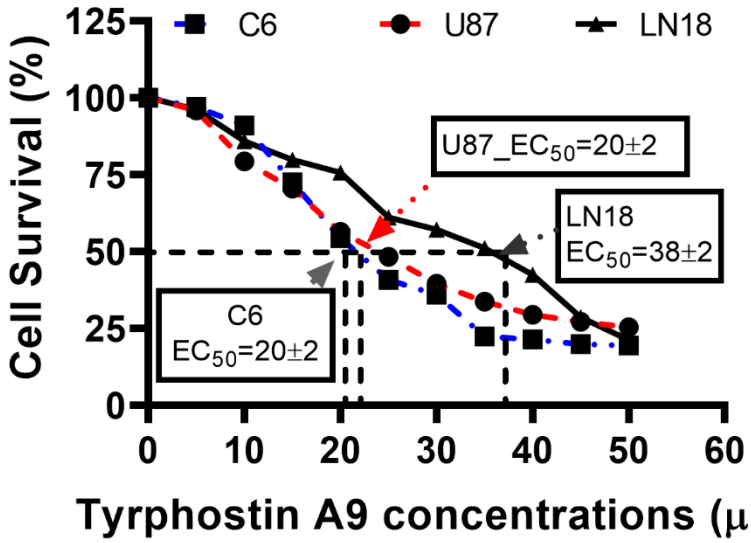

Figure. S8: The half-effective concentration (EC50) estimation of TYR A9 in C6, U87, and LN18 GBM cell lines by nonlinear fit equation.

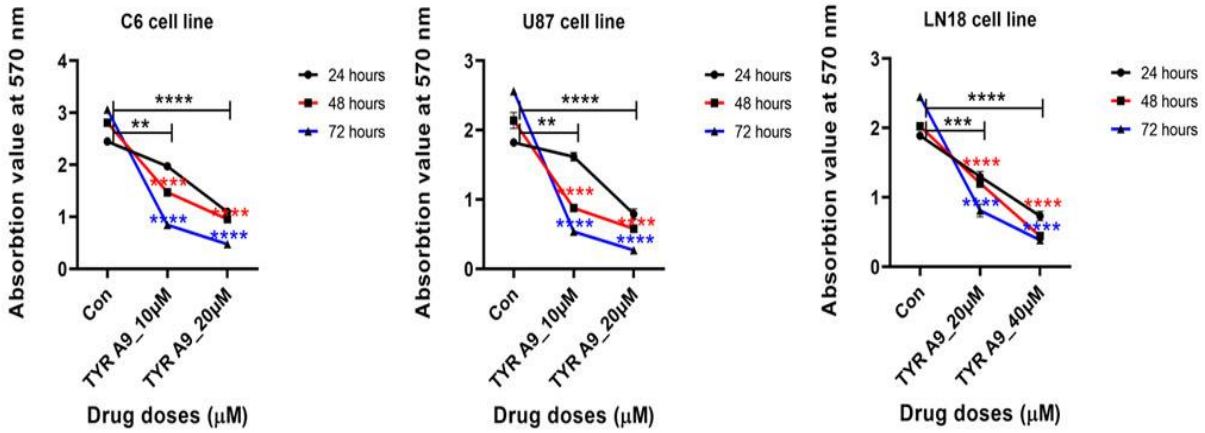

Figure. S9: MTT cell proliferation assay evaluates time-dependent inhibition in cell proliferation of C6, U87, and LN18 cells.

Figure. S10: The dose-dependent inhibition of PCNA protein levels upon TYR A9 exposure in C6 and U87 cell lines.

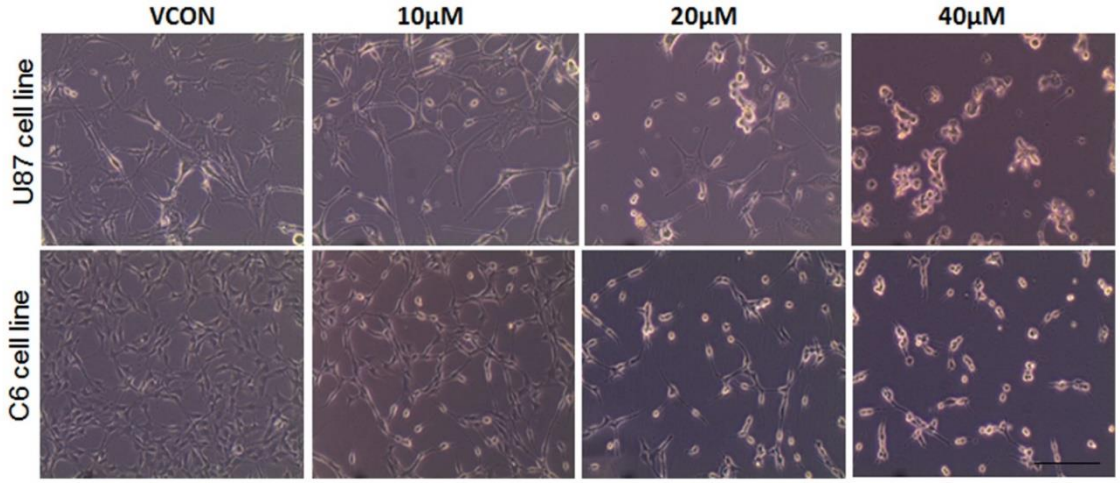

Figure. S11: The microscopic images indicate altered cell morphology and cell death upon TYR A9 doses compared to the vehicle treatment in both cell lines.

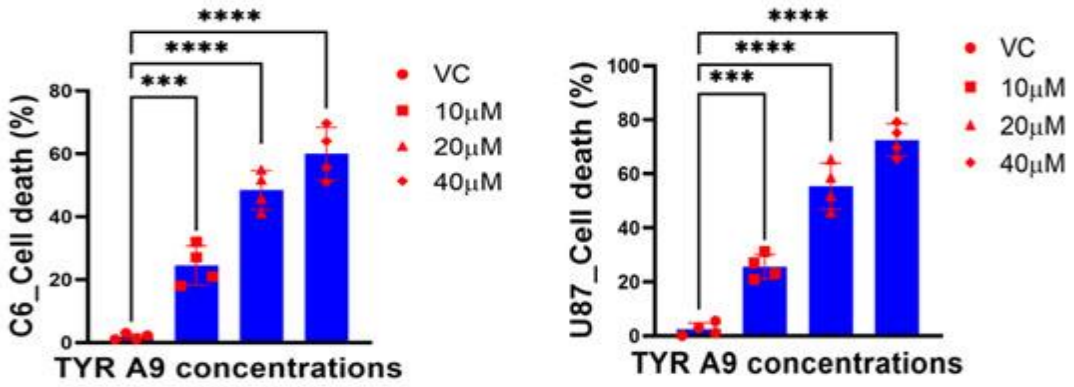

Figure. S12: The cell death analysis by trypan blue dye exclusion test indicates TYR A9 exposure-induced cell death compared to the vehicle control in both lines.

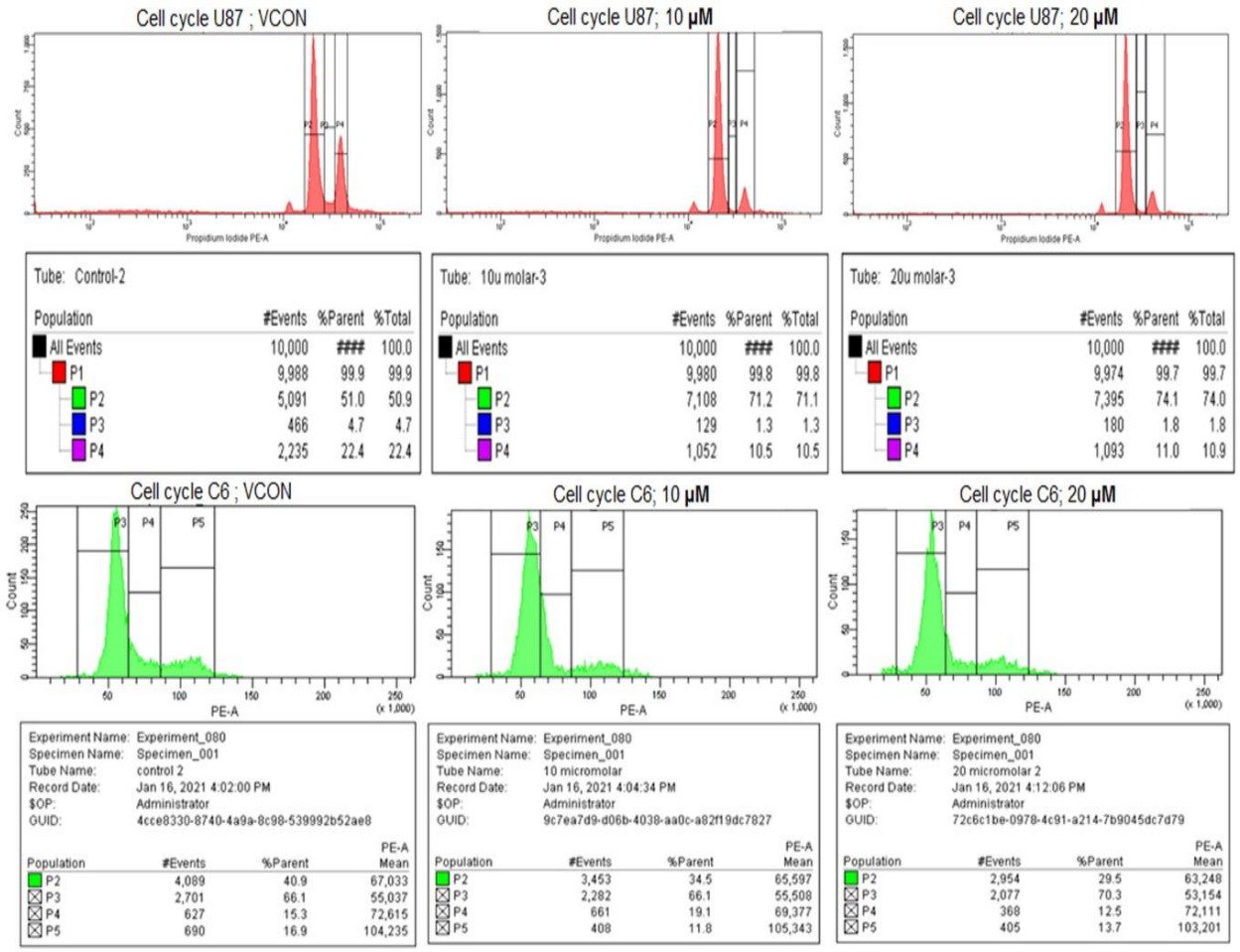

Figure. S13: Cell cycle histograms indicate G0/G1 cyclic arrest at 10 and 20µM TYR A9 dose compared to the vehicle control in both cell lines.

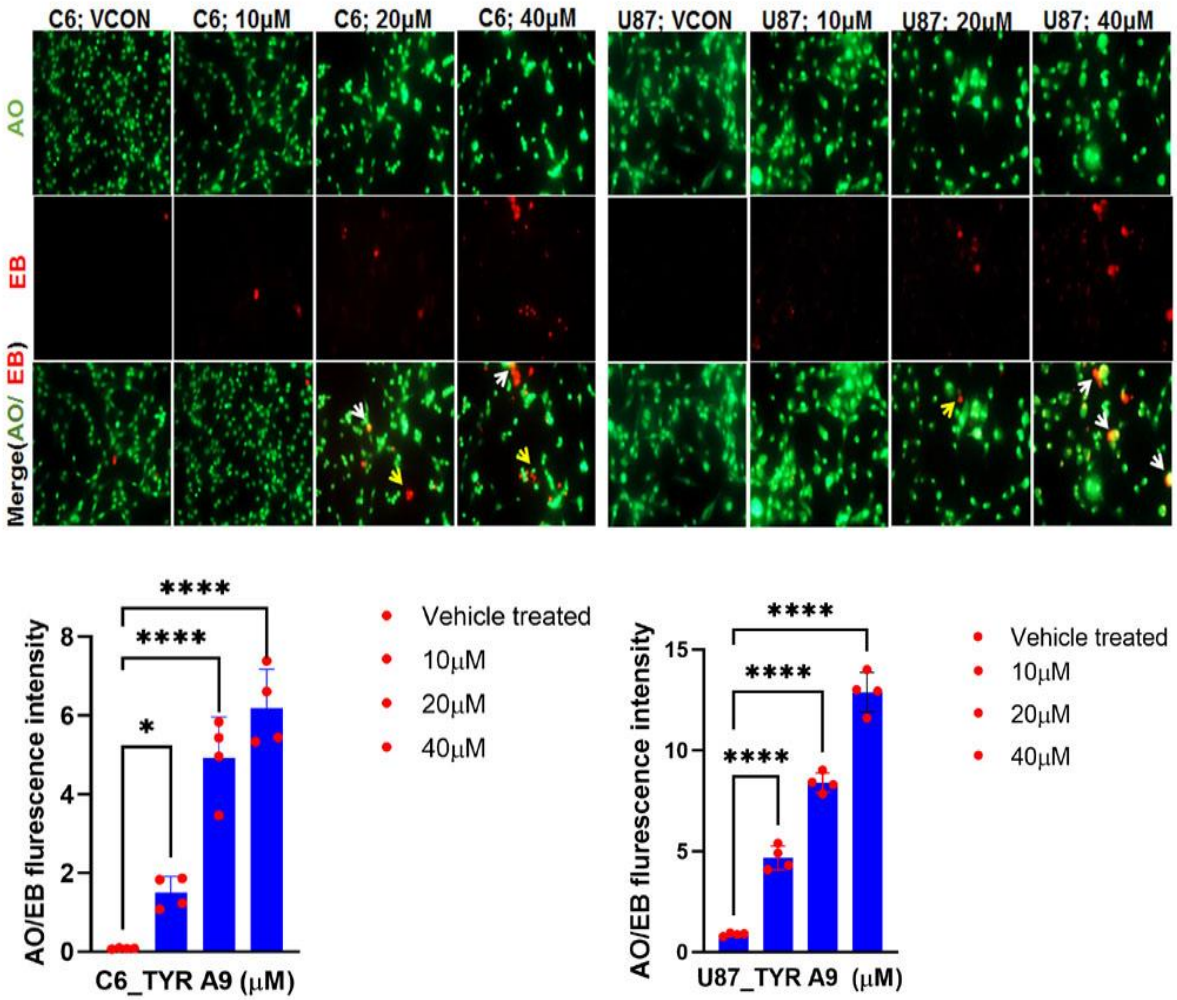

Figure. S14: Acridine orange (AO)/ethidium bromide (EB) stained IF images display early (orange staining-white arrow) and late apoptotic (red staining-yellow arrow) cell bodies upon TYR A9 exposure in both GBM cell lines. The bar graphs showing quantified AO/EB ratio indicate significant apoptosis in C6 at 10 μM ($p = 0.048$), 20 μM ($p<0.00001$), 40 μM ($p<0.00001$) of TYR A9 dose compared to the vehicle control. U87 cell lines also show similar dose-dependent effects at 10 μM ($p<0.00001$), 20 μM ($p<0.00001$), and 40 μM ($p<0.00001$) of TYR A9 dose compared to the vehicle control.

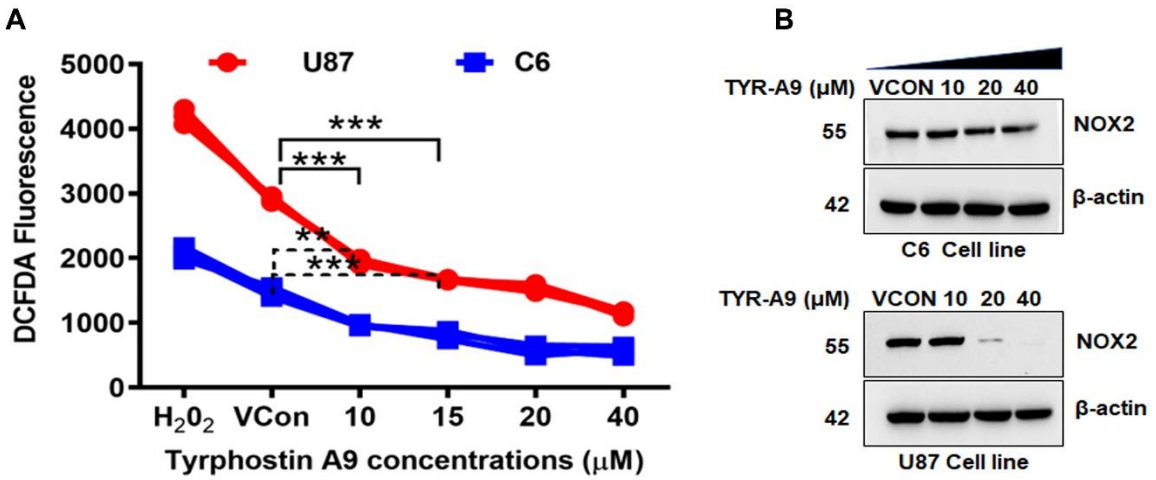

Figure. S15: (A) TYR A9 exposure significantly decreased ROS level at TYR A9 dose 10μM, p = 0.008 and 15 μM, p = 0.0002 compared to the vehicle control in the C6. Likewise, in the U87 cell line at 10 μM (p = 0.0004) and 15μM (p = 0.0001) of TYR A9 concentrations compared to the vehicle control. **(B)** Western blot analysis shows decreased NOX2 levels in TYR A9 treated cells compared to the vehicle control.

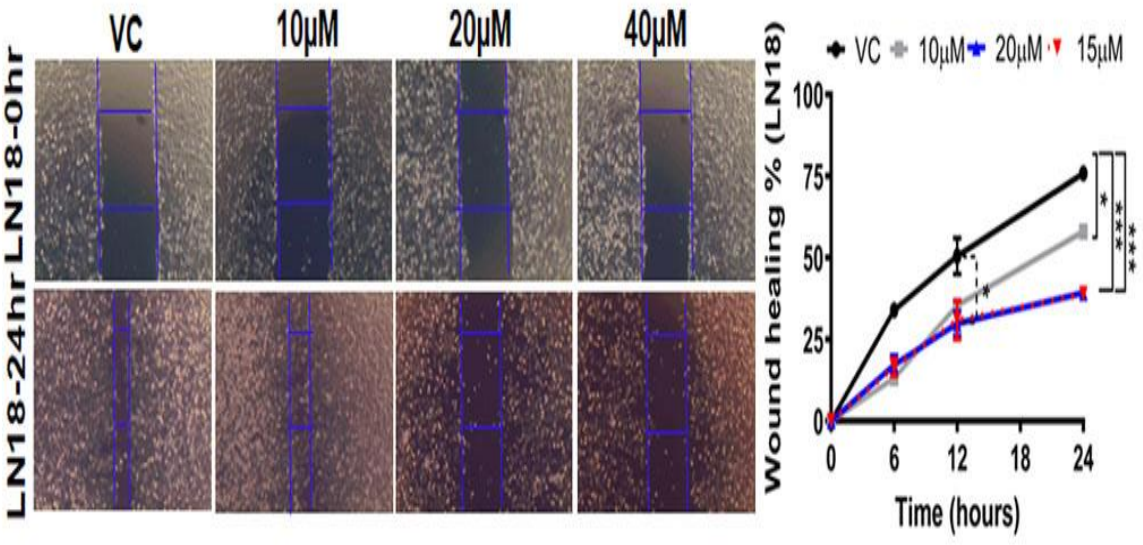

Figure. S16: Wound healing assay shows inhibited cell migration of LN18 cells upon TYR A9 exposure compared to the vehicle control.

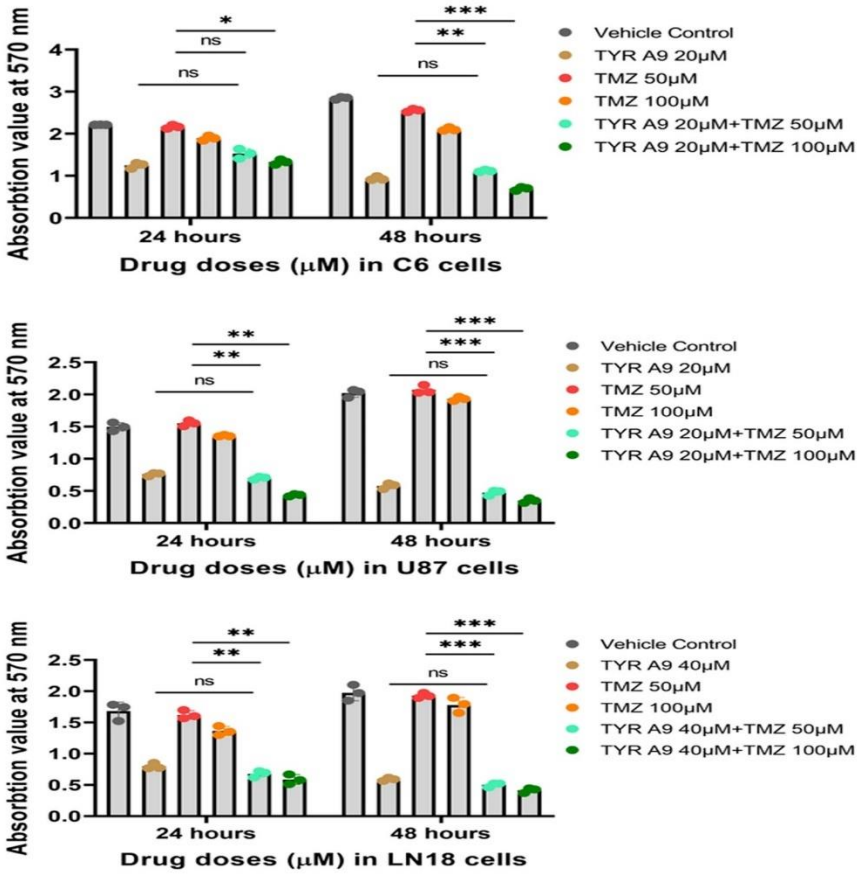

Figure. S17: MTT cell proliferation assay shows the combined effect of TYR A9 and TMZ in C6, U87, and LN18 cells. Combined doses of TYR A9 plus TMZ showed a significant difference as compared to TMZ alone; however, no significant difference was observed when compared with TYR A9.

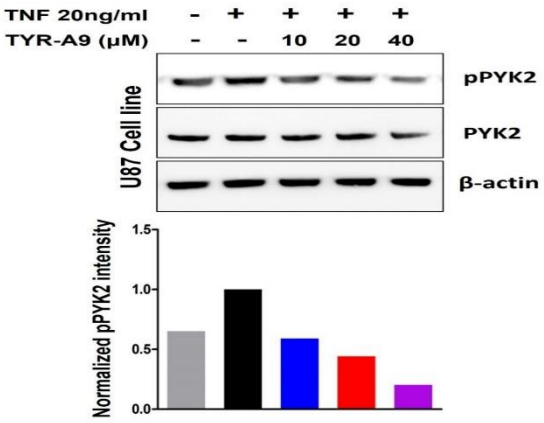

Figure. S18: The western blot and quantified protein intensity analysis show dose-dependent inhibition of TNF- α induced PYK2 phosphorylation in the U87 cell line.

Supplementary Tables:

Table S1: PCR and q-RT-PCR primers			
S. No	**Primer Sequences**	**Primer Sequences (5'--3')**	**Tm**
1	PYK2 Forward primer	CGAGCTCCTAGAAAAGGAAGTG	55.0
	PYK2 Reverse primer	GGCGAGAGTGTTGAAGAAC	53.5
2	EGFR Forward primer	GCGTCCGCAAGTGTAAGAAGTG	56.7
	EGFR Reverse primer	GAGATCGCCACTGATGGAGG	55.9
3	ERK2 Forward primer	CTCAAGATCTGTGACTTTGGCC	59.25
	ERK2 Reverse primer	GAAAGATGGGCCTGTTAGAAAG	59.8
4	ERK1 Forward primer	GAACTCCAAGGGCTATACCAAG	59
	ERK1 Reverse primer	GTAGTTTCGGGCCTTCATGTTG	58.9
5	GAPDH Forward primer	AAG GCT GGG GCT CAT TTG CAG	56.3
	GAPDH Reverse primer	GCA GGA GGC ATT GCT GAT C	56.7

4.9. References

1. Ostrom, Q.T., *et al*., CBTRUS Statistical Report: Primary Brain and Other Central Nervous System Tumors Diagnosed in the United States in 2012-2016. Neuro Oncol, 2019. **21**(Suppl 5): p. v1-v100.
2. Bondy, M.L., *et al*., Brain tumor epidemiology: consensus from the Brain Tumor Epidemiology Consortium. Cancer, 2008. **113**(7 Suppl): p. 1953-68.
3. Ohgaki, H. and P. Kleihues, Epidemiology and etiology of gliomas. Acta Neuropathol, 2005. **109**(1): p. 93-108.
4. Ramirez, Y.P., *et al*., Glioblastoma multiforme therapy and resistance mechanisms. Pharmaceuticals (Basel), 2013. **6**(12): p. 1475-506.
5. Minniti, G., *et al*., Chemotherapy for glioblastoma: current treatment and future perspectives for cytotoxic and targeted agents. Anticancer Res, 2009. **29**(12): p. 5171-84.
6. Du, Z., and C.M. Lovly, Mechanisms of receptor tyrosine kinase activation in cancer. Mol Cancer, 2018. **17**(1): p. 58.
7. McDonell, L.M., *et al*., Receptor tyrosine kinase mutations in developmental syndromes and cancer: two sides of the same coin. Hum Mol Genet, 2015. **24**(R1): p. R60-6.
8. Lemmon, M.A., J. Schlessinger, and K.M. Ferguson, The EGFR family: not so prototypical receptor tyrosine kinases. Cold Spring Harb Perspect Biol, 2014. **6**(4): p. a020768.
9. Eskilsson, E., *et al*., EGFR heterogeneity and implications for therapeutic intervention in glioblastoma. Neuro Oncol, 2018. **20**(6): p. 743-752.
10. Avraham, H., *et al*., RAFTK/Pyk2-mediated cellular signalling. Cell Signal, 2000. **12**(3): p. 123-33.
11. Zhu, X., *et al*., Proline-Rich Protein Tyrosine Kinase 2 in Inflammation and Cancer. Cancers (Basel), 2018. **10**(5).
12. Ginnan, R. and H.A. Singer, CaM kinase II-dependent activation of tyrosine kinases and ERK1/2 in vascular smooth muscle. Am J Physiol Cell Physiol, 2002. **282**(4): p. C754-61.
13. Park, S.Y., H. Li, and S. Avraham, RAFTK/Pyk2 regulates EGF-induced PC12 cell spreading and movement. Cell Signal, 2007. **19**(2): p. 289-300.
14. Behmoaram, E. *et al*., Focal adhesion kinase-related proline-rich tyrosine kinase 2 and focal adhesion kinase are co-overexpressed in early-stage and invasive ErbB-2-positive breast cancer and cooperate for breast cancer cell tumorigenesis and invasiveness. Am J Pathol, 2008. **173**(5): p. 1540-50.
15. Selitrennik, M. and S. Lev, PYK2 integrates growth factor and cytokine receptors signaling and potentiates breast cancer invasion via a positive feedback loop. Oncotarget, 2015. **6**(26): p. 22214-26.
16. Zhang, B. *et al*., Nir1 promotes invasion of breast cancer cells by binding to chemokine (C-C motif) ligand 18 through the PI3K/Akt/GSK3beta/Snail signaling pathway. Eur J Cancer, 2013. **49**(18): p. 3900-13.
17. Gutenberg, A., *et al*., Expression of tyrosine kinases FAK and Pyk2 in 331 human astrocytomas. Acta Neuropathol, 2004. **108**(3): p. 224-30.

18. Lipinski, C.A., *et al*., Differential role of proline-rich tyrosine kinase 2 and focal adhesion kinase in determining glioblastoma migration and proliferation. Mol Cancer Res, 2003. **1**(5): p. 323-32.
19. Miao, L., *et al*., Hydrogen Sulfide Recruits Macrophage Migration by Integrin beta1-Src-FAK/Pyk2-Rac Pathway in Myocardial Infarction. Sci Rep, 2016. **6**: p. 22363.
20. Okigaki, M. *et al*., Pyk2 regulates multiple signaling events crucial for macrophage morphology and migration. Proc Natl Acad Sci U S A, 2003. **100**(19): p. 10740-5.
21. Shen, T. and Q. Guo, Role of Pyk2 in Human Cancers. Med Sci Monit, 2018. **24**: p. 8172-8182.
22. Shen, T. and Q. Guo, EGFR signaling pathway occupies an important position in cancer-related downstream signaling pathways of Pyk2: cell Biol Int, 2019.
23. Lipinski, C.A., *et al*., The tyrosine kinase pyk2 promotes migration and invasion of glioma cells. Neoplasia, 2005. **7**(5): p. 435-45.
24. Hojjat-Farsangi, M., Small-molecule inhibitors of the receptor tyrosine kinases: promising tools for targeted cancer therapies. Int J Mol Sci, 2014. **15**(8): p. 13768-801.
25. Tilak, M., *et al*., Receptor Tyrosine Kinase Signaling and Targeting in Glioblastoma Multiforme. Int J Mol Sci, 2021. **22**(4).
26. Fuortes, M., *et al*., Role of the tyrosine kinase pyk2 in the integrin-dependent activation of human neutrophils by TNF. J Clin Invest, 1999. **104**(3): p. 327-35.
27. Levitzki, A., *et al*., Inhibition of protein-tyrosine kinases by tyrphostins. Methods Enzymol, 1991. **201**: p. 347-61.
28. Park, S.J., *et al*., A receptor tyrosine kinase inhibitor, Tyrphostin A9 induces cancer cell death through Drp1 dependent mitochondria fragmentation. Biochem Biophys Res Commun, 2011. **408**(3): p. 465-70.
29. Thyberg, J., Tyrphostin A9 and wortmannin perturb the Golgi complex and block the proliferation of vascular smooth muscle cells. Eur J Cell Biol, 1998. **76**(1): p. 33-42.
30. Joy, M.E. *et al*., A high-content, multiplexed screen in human breast cancer cells identifies profilin-1 inducers with anti-migratory activities. PLoS One, 2014. **9**(2): p. e88350.
31. Block, E.R., M.A. Tolino, and J.K. Klarlund, Pyk2 activation triggers epidermal growth factor receptor signaling and cell motility after wounding sheets of epithelial cells. J Biol Chem, 2010. **285**(18): p. 13372-9.
32. Tan, A.C., S. Vyse, and P.H. Huang, Exploiting receptor tyrosine kinase co-activation for cancer therapy. Drug Discov Today, 2017. **22**(1): p. 72-84.
33. Louis, D.N., *et al*., The 2016 World Health Organization Classification of Tumors of the Central Nervous System: a summary. Acta Neuropathol, 2016. **131**(6): p. 803-20.
34. Livak, K.J. and T.D. Schmittgen, Analysis of relative gene expression data using real-time quantitative PCR and the 2(-Delta Delta C(T)) Method. Methods, 2001. **25**(4): p. 402-8.
35. Babu, D. *et al*., Rabeprazole has efficacy per se and reduces resistance to temozolomide in glioma via EMT inhibition. Cell Oncol (Dordr), 2021. **44**(4): p. 889-905.
36. Sareddy, G.R., *et al*., Activation of Wnt/beta-catenin/Tcf signaling pathway in human astrocytomas. Neurochem Int, 2009. **55**(5): p. 307-17.
37. van Meerloo, J., G.J. Kaspers, and J. Cloos, Cell sensitivity assays: the MTT assay. Methods Mol Biol, 2011. **731**: p. 237-45.

38. Franken, N.A., *et al*., Clonogenic assay of cells in vitro. Nat Protoc, 2006. **1**(5): p. 2315-9.
39. Geeviman, K., D. Babu, and P. Prakash Babu, Pantoprazole Induces Mitochondrial Apoptosis and Attenuates NF-kappaB Signaling in Glioma Cells. Cell Mol Neurobiol, 2018. **38**(8): p. 1491-1504.
40. Kim, K.H. and J.M. Sederstrom, Assaying Cell Cycle Status Using Flow Cytometry. Curr Protoc Mol Biol, 2015. **111**: p. 28 6 1-28 6 11.
41. Kimata, M. *et al*., p53 and TIGAR regulate cardiac myocyte energy homeostasis under hypoxic stress. Am J Physiol Heart Circ Physiol, 2010. **299**(6): p. H1908-16.
42. Smilowitz, H.M., *et al*., Orthotopic transplantation of v-src-expressing glioma cell lines into immunocompetent mice: establishment of a new transplantable in vivo model for malignant glioma. J Neurosurg, 2007. **106**(4): p. 652-9.
43. Babu, D. *et al*., Rabeprazole has efficacy per se and reduces resistance to temozolomide in glioma via EMT inhibition. Cell Oncol (Dordr), 2021.
44. Mey, U., [Foundations of the diagnosis and therapy of hemolytic anemias]. Z Gesamte Inn Med, 1978. **33**(9): p. 265-70.
45. Camacho, A. *et al*., Tyrphostin AG17 inhibits adipocyte differentiation in vivo and in vitro. Lipids Health Dis, 2018. **17**(1): p. 128.
46. Kim, S.J., H.S. Kim, and Y.R. Seo, Understanding of ROS-Inducing Strategy in Anticancer Therapy. Oxid Med Cell Longev, 2019. **2019**: p. 5381692.
47. Happold, C., *et al*., Distinct molecular mechanisms of acquired resistance to temozolomide in glioblastoma cells. J Neurochem, 2012. **122**(2): p. 444-55.
48. Tan, A.C., *et al*., Management of glioblastoma: State of the art and future directions. CA Cancer J Clin, 2020. **70**(4): p. 299-312.
49. Rajaratnam, V., *et al*., Glioblastoma: Pathogenesis and Current Status of Chemotherapy and Other Novel Treatments. Cancers (Basel), 2020. **12**(4).
50. Gong, J. *et al*., Microparticles Mediate the Intercellular Regulation of microRNA-503 and Proline-Rich Tyrosine Kinase 2 to Alter the Migration and Invasion Capacity of Breast Cancer Cells. Front Oncol, 2014. **4**(220).
51. Garrido, C., *et al*., Mechanisms of cytochrome c release from mitochondria. Cell Death Differ, 2006. **13**(9): p. 1423-33.
52. Cadenas, S., Mitochondrial uncoupling, ROS generation, and cardioprotection. Biochim Biophys Acta Bioenerg, 2018. **1859**(9): p. 940-950.
53. Sagara, Y. *et al*., Tyrphostins protect neuronal cells from oxidative stress. J Biol Chem, 2002. **277**(39): p. 36204-15.
54. Baffy, G., Mitochondrial uncoupling in cancer cells: Liabilities and opportunities. Biochim Biophys Acta Bioenerg, 2017. **1858**(8): p. 655-664.
55. Childress, E.S., *et al*., Small Molecule Mitochondrial Uncouplers and Their Therapeutic Potential. J Med Chem, 2018. **61**(11): p. 4641-4655.
56. Li, S.Z. *et al*., MicroRNA-34a induces apoptosis in the human glioma cell line, A172, through enhanced ROS production and NOX2 expression. Biochem Biophys Res Commun, 2014. **444**(1): p. 6-12.

57. Sullivan, P.G., *et al*., Mitochondrial uncoupling as a therapeutic target following neuronal injury. J Bioenerg Biomembr, 2004. **36**(4): p. 353-6.
58. Lysechko, T.L., S.M. Cheung, and H.L. Ostergaard, Regulation of the tyrosine kinase Pyk2 by calcium is through the production of reactive oxygen species in cytotoxic T lymphocytes. J Biol Chem, 2010. **285**(41): p. 31174-84.
59. Xu, C.-S., *et al*., Induction of proline-rich tyrosine kinase 2 activation-mediated C6 glioma cell invasion after anti-vascular endothelial growth factor therapy. Journal of translational medicine, 2014. **12**: p. 148.
60. Yang, Y., *et al*., Protein tyrosine kinase inhibitor resistance in malignant tumors: molecular mechanisms and future perspective. Signal Transduct Target Ther, 2022—7 (1): p. 329.
61. Singh, N., *et al*., Mechanisms of temozolomide resistance in glioblastoma - a comprehensive review. Cancer Drug Resist, 2021. **4**(1): p. 17-43.

CHAPTER 5

To study the anticancer efficacy and protective role of TYR A9 in the cognitive assessment by targeting RAP2B/HIF2A/pPYK2-EMT signaling in glioma rat hypoxia *vs* normoxia

Objective 4: To study the anticancer efficacy and protective role of TYR A9 in the cognitive assessment by targeting RAP2B/HIF2A/pPYK2-EMT signaling in glioma rat hypoxia *vs* normoxia.

Abstract

Glioma rats have hypoxia-induced cognitive impairment because of its invasive behavior and high tumor load. C6 glioma cells were implanted in the Wistar rat brain to develop a glioma model that plays a role in neurological disorders, cerebral inflammation, and memory loss. TYR A9 has a protective role, anticancer, antioxidant and anti-inflammatory effect against neuroinflammation. The anticancer effects and mechanism by which TYR A9 maintains cognitive function and prevents glioma rat growth in hypoxia *vs* normoxia remains unknown. In hereto, first time we examined TYR A9 anticancer effects and neuroprotective role in vehicle and $CoCl_2$-treated glioma rats. Hematoxylin and eosin (H&E) staining result showed that decreased cellularity and nuclear atypia, necrosis and microvascular proliferation compared vehicle and $CoCl_2$-treated glioma rats. In our finding, TYR A9 and $CoCl_2$+TYR A9 treatment increased survivability compared to $CoCl_2$ and vehicle-treated glioma rats. Glioma-bearing rats increased expression of RAP2B, HIF2A, EGFR, pPYK2, Ki-67, and vimentin proteins but enhanced in $CoCl_2$-treated glioma rats. TYR A9 and CoCl2+TYR A9 treated glioma rats decreased the expression of RAP2B, HIF2A, EGFR, pPYK2, Ki-67, and vimentin confirmed through IHC staining. These results evidenced that decreased staining of Ki-67 reduced glioma growth in TYR A9 and $CoCl_2$+TYR A9 treated glioma rats. TYR A9 treatment protected cognitive function and increased survivability by inhibiting RAP2B/HIF2A/pPYK2-EMT signaling pathway without and with $CoCl_2$ treated glioma rats. TYR A9 and $CoCl_2$+TYR A9 treated glioma rats increased the cleaved caspase-3 level, this evidencing a proof of apoptosis induction. This suggests that apoptosis might be the reason for the reduction of tumor load in TYR A9 and $CoCl_2$+TYR A9 treated glioma rats.

5.1. Introduction

Cerebral gliomas account for 40% to 60% of primary brain tumors. Mass-reduction surgery is currently used as a treatment method, followed by radiation and chemotherapy. Despite surgery, radiation, and chemotherapy, patients with gliomas have a poor prognosis due to their aggressive and invasive properties [1]. Chemotherapy improves the prognosis of patients with malignant gliomas by increasing life expectancy compared to surgery and radiation [2, 3]. However, chemotherapy for glioma has some drawbacks, including treatment failure due to improper distribution and the blood-brain barrier that causes low or limited drug absorption in the brain tumor. Establishing an experimental animal model is crucial to comprehend the biological characteristics of glioma [4]. The determination of humane endpoints is particularly challenging for models of rapidly growing brain tumors such as gliomas [5]. Human endpoints are described imprecisely or not in experimental rats focused on the etiology of brain tumors; Kaplan-Meier curve survival analysis is used for survival rates [6]. The frequency of anxiety, depression, and cognitive impairment in glioma patient has been extensively investigated [7]. The most frequent side effects of treatment include behavioral symptoms like sadness, anxiety, and cognitive impairment [8].

Tyrphostin A9 (TYR A9), a tyrosine kinase inhibitor, is an innovative anticancer drug used to treat various cancers [9, 10], including glioma [11]. In a previous paper, we reported that TYR A9 treatment inhibits glioma cell proliferation and increases the median survival of glioma rats [11]. In the current study, we sought to understand Tyrphostin A9 restricted tumor growth and increased survivability in $CoCl_2$-treated glioma rats. Furthermore, we hypothesized that TYR A9 might have a protective role and maintain cognitive function in glioma rats without and with $CoCl_2$ treatment. The present study investigated the effects of TYR A9 on the inhibition of RAP2B/HIF2A/pFAK/pPYK2-EMT signaling that might contribute to the hippocampus-dependent cognitive impairment induced by C6 glioma cells implantation and enhanced by $CoCl_2$.

5.2. Material and Methods:

5.2.1. Cell Culture

The C6 rat glioma cell line was procured from NCCS Pune. Cells were cultured in complete high glucose DMEM supplemented with 10% fetal bovine serum (FBS) and 1X Anti-Anti (antibiotic and antimycotic) purchased from Himedia. Cells were trypsinized and grown at 37 ℃ humidified chambers in a 5% CO_2 incubator.

5.2.2. Animals housing

All trials employed adult male rats with weights between 250 and 300 g. The animals were housed in standard laboratory conditions with unlimited food and water provided to them all the time. All experiments were performed according to International Guiding Principles for Biomedical Research Involving Animals. The Committee for the Care and Use of Laboratory Animals at the University of Hyderabad approved the experimental procedure. Total 24 Wistar rats were divided into the 4 groups vehicle control (n = 6), $CoCl_2$ (n = 6), TYR A9 (n = 6) and $CoCl_2$+TYR A9 (n = 6). The Kaplan-Meier curve was used to examine animal survival rates to assess the impact of $CoCl_2$ and the therapeutic effect of TYR A9.

5.2.3. C6 rat glioma cell implantation and treatment

C6 cells were intracranially implanted in the striatum region of the cerebral hemisphere to create the C6 glioma model. In each group, 8-12 weeks old, 4 to 6 Wistar rats were used. Before performing surgery, animals were acclimatized in an animal house facility for 15 days at the University of Hyderabad. Before performing stereotaxic surgery, animals were anesthetized using ketamine 80 mg/kg of body weight and xylazine 15 mg/kg of body weight. The bregma was exposed by making a small incision using stereotaxic apparatus 1 mm AP and 3 mm to the LV of the bregma, and 3mm depth burr hole was drilled. A density of 5×10^4 C6 glioma cells suspension was injected in the striatum region of the rat brain through a Hamilton syringe and left in place for three minutes after the injection to prevent reflux. A drilled burr hole was filled with dental cement. Analgesia was given to the animals and kept on a heating pad until they recovered. After seven days of implantation, rats were randomly divided into 4 groups based on the experiment conditions. Treatment was started after 10 days of implantation. **Group 1:** 10% DMSO vehicle treatment, **Group 2:** $CoCl_2$ treatment 50 mg/kg of body weight, **Group 3:** TYR A9 1.5mg/kg of body weight, and **Group 4:** $CoCl_2$+TYR A9 (pretreatment of $CoCl_2$) 50 mg/kg of body weight for 5 days and after 24 hrs of interval started TYR A9 treatment 1.5 mg/kg body weight every 24 hrs of interval for 10 days. Animals' examination started after fifteen days of implantation, like neurological disorders, body weight, and behavior of animals compared with negative control (1XPBS) treated rats. All procedures that involved rats were approved by the Animal Care and Use Committee guidelines (UH/IAEC/PPB2021-22/22) of the Central University of Hyderabad.

5.2.4. Rat brain extraction

Before the test, 2 to 3 rats were randomly sacrificed, and extracted brains were used to assess the expression of molecular markers associated with GBM progression. After completion of treatment from each group, vehicle treated with 10% DMSO, $CoCl_2$, TYR A9, and $CoCl_2$+TYR A9, rats were

anesthetized and performed the heart perfusion using 0.9% saline solution and then fixed by 4% PFA. All groups were sacrificed and harvested brain, the extracted brain was fixed in 4% PFA for histopathological study to determine the levels of EGFR, RAP2B, HIF2A, pPYK2, and vimentin.

5.3. Development of C6 rat glioma model and treatments

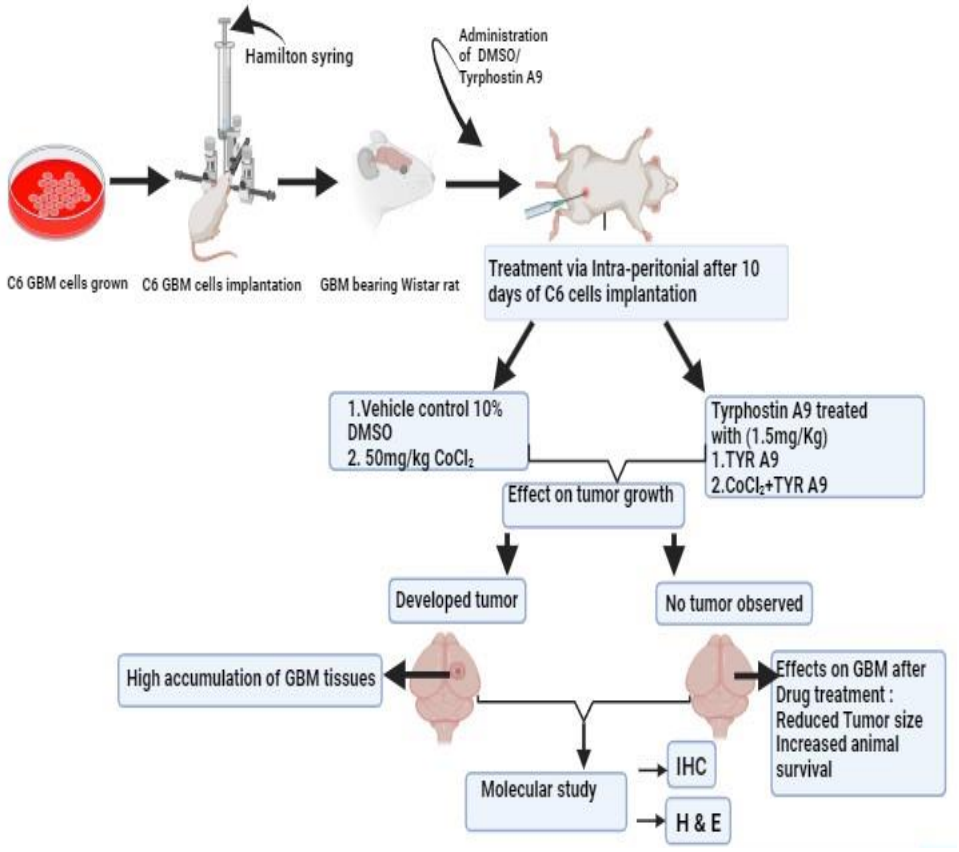

Figure 1. The schematic diagram represents stereotaxic surgery and implantation of C6 to develop a rat glioma model. Therapeutic approach for treating rat glioma and explored histopathology (Diagram made using Bio-render).

5.4. Methodology and experimental plans:

We chose the spontaneous movement test because it allows us to assess the rat's exploratory and working memory after completion of TYR A9 treatment compared to vehicle and $CoCl_2$-treated glioma rats. We trained all experimental rats for a brief time regarded as the acquisition for all cognitive test. The percentage of correct and incorrect alterations for each experimental rat were calculated based on the selection of its alteration.

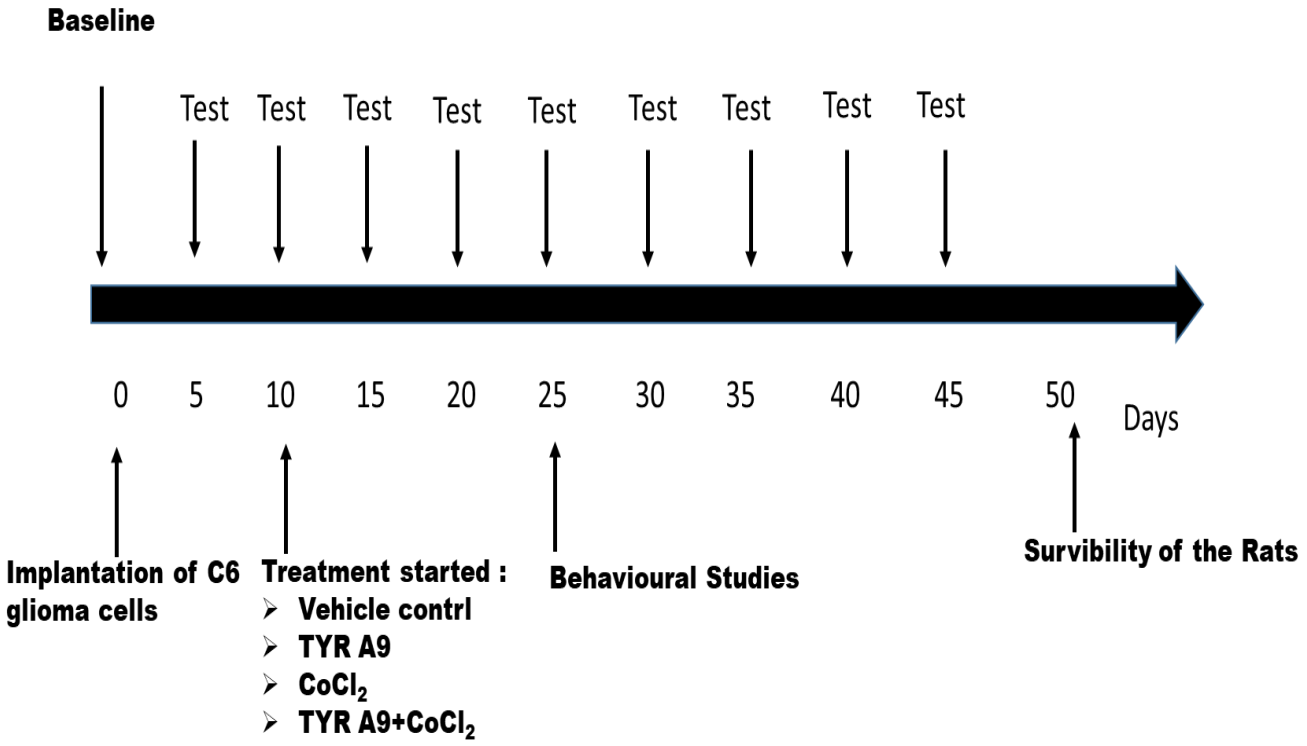

Figure 2: Experimental timeline for the treatment, behavioral test and survivability.

5.4.1. Cylinder Test

Each animal from the experimental group's: vehicle control, $CoCl_2$, TYR A9, and $CoCl_2$+TYR A9 was put inside a spotless, clear, open-top cylinder (26 cm in height; 16 cm in diameter), which was used to record video for three minutes. Each rat's rears the position at which it stands upright on its hind limbs were counted. After each trial, the cylinder was frequently sanitized with 70% alcohol. The typical number of rears and grooming time was calculated for each group of animals.

5.4.2. Beam Balance Test

To evaluate the motor deficiencies after observing glioma symptoms for three days and conduct tests every day. Every animal from all four experimental conditions, rats were trained to walk from one end of a beam to opposite end. In a beam balance test, a one-meter beam with a 25 mm width stands 60 cm above the ground. Each experimental rat was trained by placing it at one end and allowing it to move toward the other end. Each group rat's scoring paw slips and the time it takes to walk the beam are calculated. After each experimental rat, the beam was cleaned using 70% alcohol and dry paper, and the rats' droppings were removed from the beam.

5.4.3. Barnes Maze test

This test used to assess glioma rats' long-term spatial memory and cognitive functions. A circular platform with 20 evenly placed holes lengthwise its edge the test's physical component (100 cm in diameter). One of the holes has an escape platform underneath it, and the remaining 19 holes are empty, the escape hole position is maintained at a constant place. Each animal was led for four days from the maze's center to a platform that might be used to escape (acquisition phase). After each test, 70% alcohol was used to clean the escape platform and the maze. On day five, the escape platform was removed, and then animals were put on a probing trial to assess the reference memory. The number of holes entered prior to the escape hole i.e. primary error and the time it took to locate the escape hole, the primary latency was calculated. Rat videos were documented and tested individually with ANY-maze behavioral tracking software version 6.1, Stoelting Co, Wood Dale, USA.

5.4.4. Rotarod test motor function assessment

Rotarod test was performed to assess coordinated motor function after 10 days of intracranial implantation of C6 glioma cells in Wistar rats. We used four groups: vehicle control, $CoCl_2$, TYR A9, and $CoCl_2$+TYR A9. For each experiment, the rotarod speed was gradually accelerated from 0 to 15 rpm for each trial. Four rats from each group were trained for 5 days, and a timer switch was turned on at the same time the cylinder was made to rotate. When the rat fell off the rotating rod, a photosensitive switch was tripped, and the timer stopped for that compartment and immediately noted that time. The Rotarod test was performed twice after five days of training on days 7, 8, and 9, consisting of four trials in a day with 10-minute intervals between each trial. The elapsed time was recorded in seconds at 10 and 15 rpm, respectively.

5.5. Statistical analysis

The statistical study was carried out using Graph Pad Prism version 9.3. All data are expressed as mean and SEM of four samples. Sidak’s multiple comparisons test was used in One-way ANOVA data analysis for multiple groups. The differences were determined significant at *$p<0.05$; **$p<0.01$; ***$p<0.001$; ****$p<0.0001$; ns not significant.

5.6. Results:

5.6.1. TYR A9 reduces tumor growth and maintained body weight in rat glioma hypoxia *vs* normoxia

Our finding showed histopathological analysis by H&E staining. Hematoxylin and Eosin (H&E) staining represented high cellularity and nuclear atypia, multinucleation in the $CoCl_2$ and vehicle-treated glioma rat compared to TYR A9 and $CoCl_2$+TYR A9 **(Figure 3A)**. $CoCl_2$ and vehicle-treated glioma rats exhibited multilayer arrangement and necrosis areas. Morphological assessments were performed after 10 days doses of TYR A9 1.5 mg/kg of body weight. TYR A9 and $CoCl_2$+TYR A9 showed improved physiology like fur density and brain structure compared to $CoCl_2$ and vehicle-treated glioma rats. We also analyzed the tumor volume of TYR A9 and $CoCl_2$+TYR A9 vs $CoCl_2$ and vehicle control. After 10 days of treatment every 24 hrs of interval, TYR A9 and $CoCl_2$+TYR A9 treatment significantly reduced tumor volume $0.413mm^3 \pm 0.039$, $0.462mm^3 \pm 0.056$ compared to vehicle $1.052mm^3 \pm 0.062$ and $CoCl_2$ $1.442mm^3 \pm 0.076$ **(Figure 3B)**, this indicating that inhibited tumor growth. We also evaluated the body weight of vehicle, $CoCl_2$, TYR A9 and $CoCl_2$+TYR A9 treated glioma rats. In our findings we found that $CoCl_2$ and vehicle-treated glioma rats began to significantly decreased body weight with increased tumor load but TYR A9 and $CoCl_2$+TYR A9 (****$p<0.0001$) treated glioma rats maintained their body weight with reduced tumor growth **(Figure 3C)**.

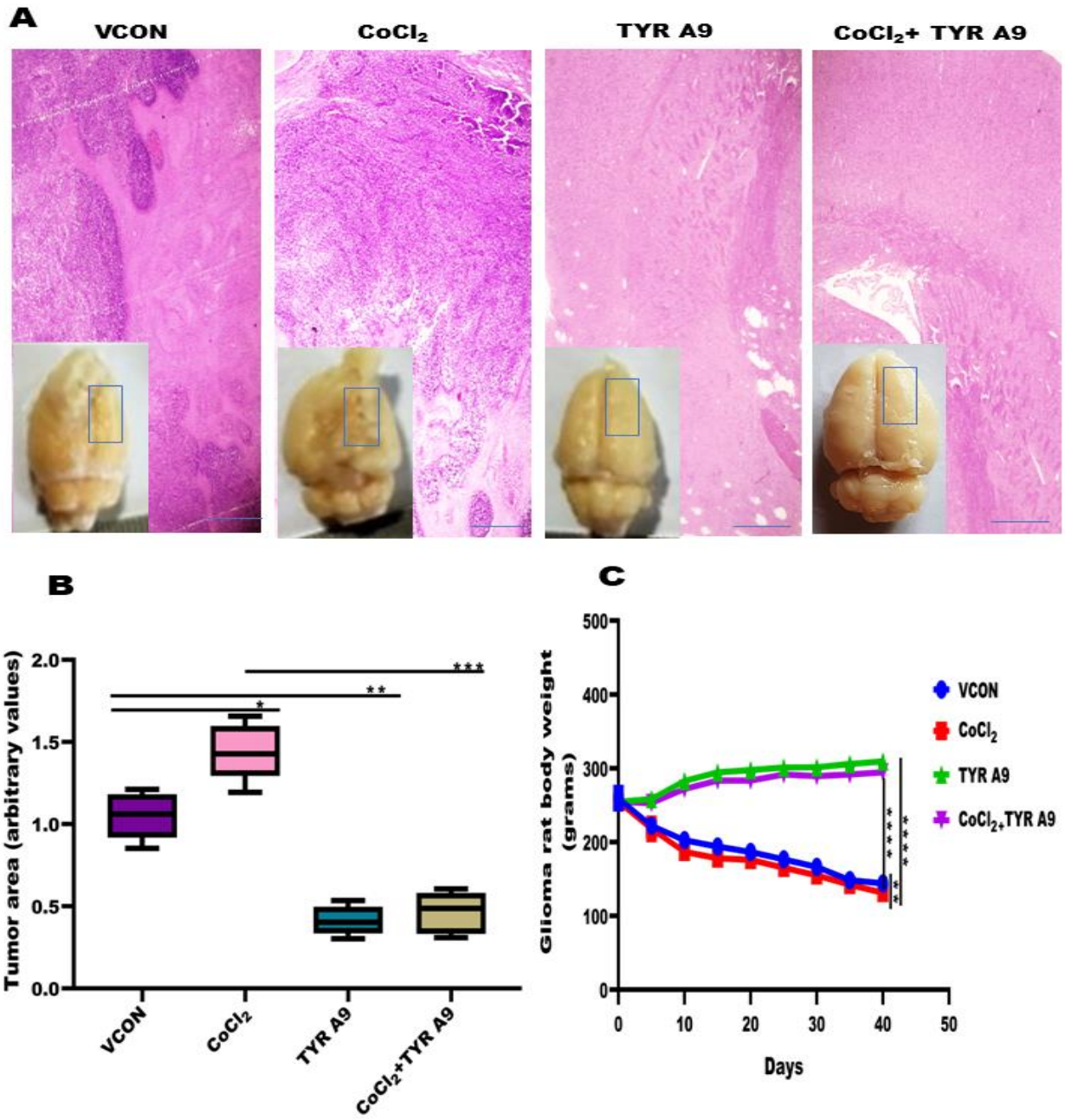

Figure 3: TYR A9 and $CoCl_2$+TYR A9 treatment effects on tumor growth and body weight: (**A, B)**, The results of histopathological analysis (H&E) represent TYR A9 and $CoCl_2$+TYR A9 treatments significantly reduced cellularity and reduced tumor volume compared to $CoCl_2$ and vehicle (***p = 0.0002) treated glioma rats. (**C)**, Vehicle and $CoCl_2$ treated glioma rats showed weight loss, but not in TYR A9 and $CoCl_2$+TYR A9 (****p<0.0001) treated glioma rats. Statistical significance represented as **p<0.01, **p<0.001, ****p<0.0.0001.

5.6.2. TYR A9 treatment improved median survival and inhibited RAP2B/HIF2A/pPYK2-EMT pathway in glioma rats under hypoxia vs. normoxia

In our finding, H&E staining **(Figure 4A)** showed restricted tumor growth with clearly defined boundaries of glioma striatum in TYR A9 and $CoCl_2$+TYR A9 treated glioma rats compared to $CoCl_2$ and vehicle-treated glioma rats. IHC results represented weaker Ki-67 staining in TYR A9 and $CoCl_2$+TYR A9 treated glioma rats compared to $CoCl_2$ and vehicle-treated glioma rats **(Figure 4B)**, suggesting that TYR A9 and $CoCl_2$+TYR A9 inhibited glioma growth. Densitometry analysis result evidenced that significantly decreased Ki-67 staining in TYR A9 and $CoCl_2$+TYR A9 compared to $CoCl_2$ and vehicle-treated glioma rat (***p = 0.0001), (***p = 0.0002) **(Figure 4C)**. Further, we analyzed the TYR A9 effect on the survival of vehicle and $CoCl_2$-treated glioma rats. Kaplan Meier curve analysis showed that improved median survival of 30 to 50 days of TYR A9 and $CoCl_2$+TYR A9 treated glioma rats showed by long rank (Mantel-Cox) survival curve evidenced significant difference (****p<0.0001) compared to $CoCl_2$ and vehicle-treated glioma rats **(Figure 4D)**. In our observation, 3 to 4 rats out of 8 survived more than 50 to 60 days from TYR A9 and $CoCl_2$+TYR A9 treated groups, but 4 to 5 rats out of 8 died before 15 to 20 days from $CoCl_2$ and vehicle-treated glioma rats, only 2 to 3 rats were survived up to defined 20 to 30 days **(Figure 4D)**. Immunohistochemistry (IHC) results revealed that decreased expression of RAP2B, HIF2A, EGFR, pPYK2, and vimentin in TYR A9 and $CoCl_2$+TYR A9 treated glioma rats as compared to $CoCl_2$ and vehicle-treated glioma rats. **(Figure 5A)**. Densitometry results indicated that significantly decreased expression of RAP2B, HIF2A, EGFR, pPYK2, and vimentin in TYR A9 and $CoCl_2$+TYR A9 compared to vehicle and $CoCl_2$-treated glioma rats **(Figure 5B, C, D, E, F, G)**. Increased expression of RAP2B, HIF2A, EGFR, and pPYK2 in cancer tumorigenesis and vimentin expression is a key EMT regulator in cancer progression [12a].

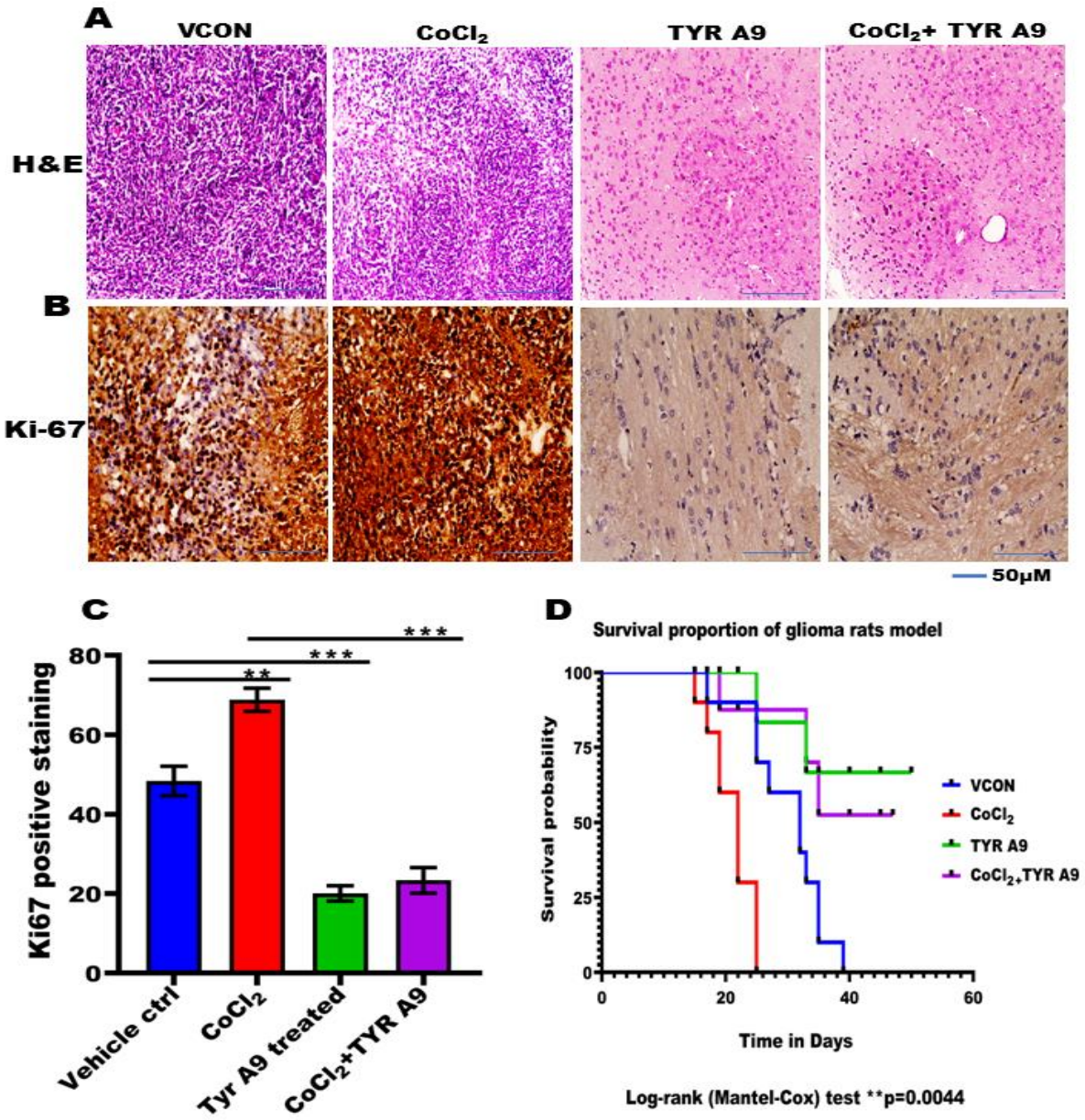

Figure 4: TYR A9 therapeutic effect on tumor growth inhibition in glioma rat treated with $CoCl_2$: (A, B), H&E, and Ki67-IHC staining show reduced tumor growth in TYR A9 and $CoCl_2$+TYR A9 as compared to $CoCl_2$ and vehicle-treated glioma rats. **(C)**, Densitometry analysis represents a significantly decreased Ki-67 in TYR A9 and $CoCl_2$+TYR A9 compared to $CoCl_2$ and vehicle control. **(D)**, Using the Log-rank (Mantel-Cox) test, the Kaplan-Meier survival curves show increased survivorship in TYR A9 and $CoCl_2$+TYR A9 compared to $CoCl_2$ and vehicle-treated glioma rats. Statistical significance is represented as **p<0.01, ***p<0.001.

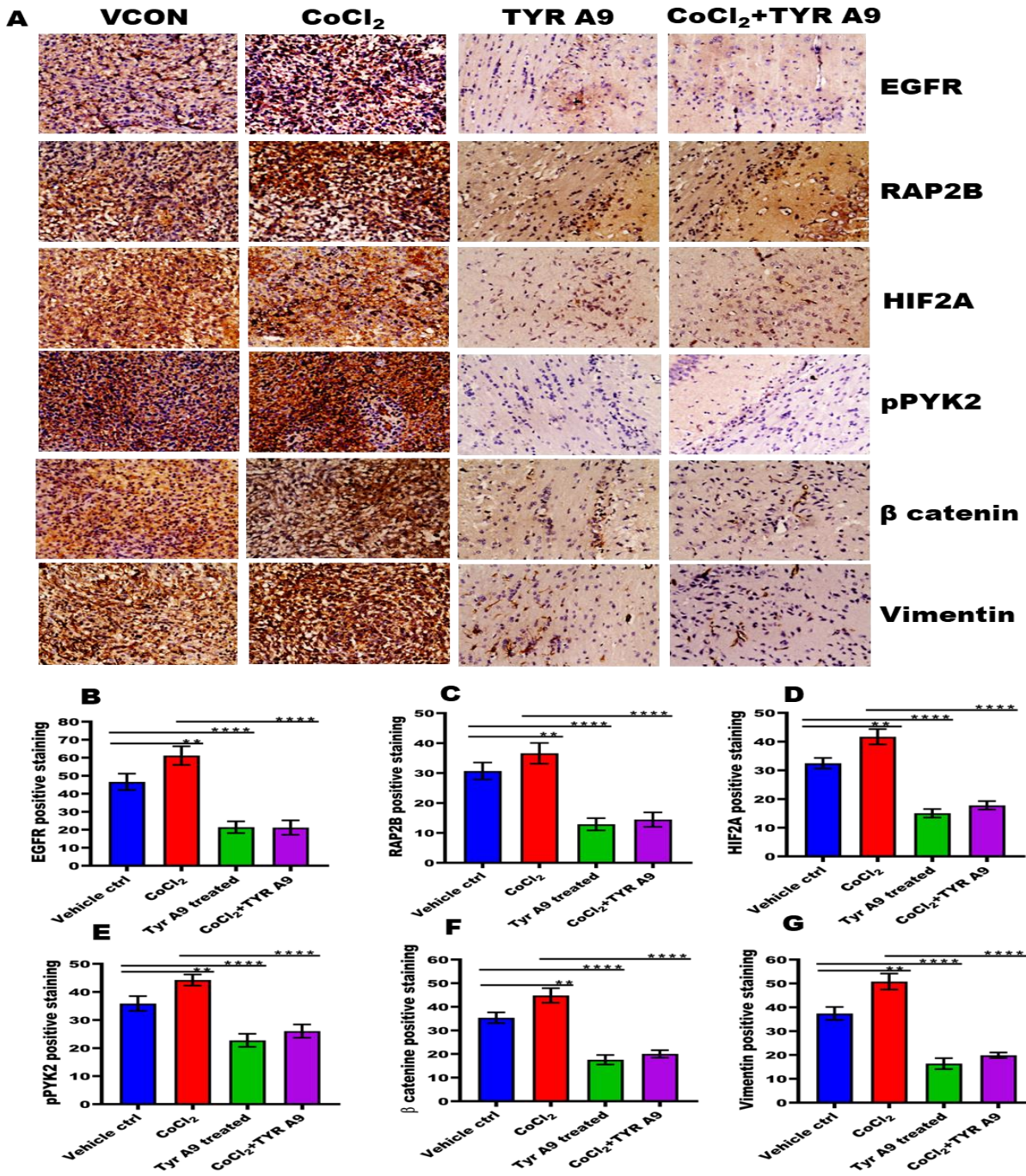

Figure 5: TYR A9 therapeutic effect on protein expressions: (A), IHC images and respective densitometry analysis graphs showing significantly reduced staining of **(B)** pEGFR, **(C)** RAP2B, **(D)** HIF2A, **(E)** pPYK2, **(F)** β catenin, and **(G)** Vimentin in TYR A9 and $CoCl_2$+TYR A9 compared to $CoCl_2$ and vehicle-treated glioma rats (****p<0.0001). Statistical significance represented as ****p<0.0.0001.

5.6.3. Tyrphostin A9 treatment maintained sensorimotor coordination, motor function, and equilibrium in glioma rat hypoxia vs normoxia.

In our study, cylinder test demonstrated the number of rearing was elevated in both TYR A9 (33.25±4.19) and $CoCl_2$+TYR A9 (31.76±4.85) as compared to $CoCl_2$ (14±1.58) and vehicle-treated glioma rat (19.75±2.78), (***p = 0.0002), (***p = 0.0004) **(Figure 6C)**. Furthermore, there was no difference in the rearing rate between TYR A9 and $CoCl_2$+TYR A9. Glioma rats showed paw slippage characteristics and coordination loss induced by C6 glioma cells implanted in the dorsal striatum. A simple beam balance test showed motor coordination in the brain. This test revealed that TYR A9 and $CoCl_2$+TYR A9 exhibited less contralateral foot slipping in the average time (4.53±0.577) and (6.66±0.88) to transverse the beam compared to $CoCl_2$ (time to transverse 18.07±0.83) and vehicle (time to transverse 13±1.15) (***p = 0.0003), (***p = 0.0005) **(Figure 6D)**. Our finding Barnes maze test showed that the primary latency within a shorter time interval (33.5±4.5) and (47.7±4.97) with less rate of primary errors in TYR A9 treated group and $CoCl_2$+TYR A9 group compared to $CoCl_2$ (92±6.61) and vehicle-treated glioma rats (75.35±6.26), (***p = 0.0007), (***p = 0.0003) **(Figure 6B)**. Glioma rats with vehicle-treated and $CoCl_2$ treated 5 rats out of 8 with mild symptoms showed more primary latency and errors. The heat map results showed that the TYR A9 and $CoCl_2$+TYR A9 spent maximum time close to the escape hole after the primary latency during probe trial on day 5 compared to $CoCl_2$ and vehicle-treated glioma rats. The majority of the rats in the $CoCl_2$ group showed freezing behavior in the centre of the maze and found the escape hole after multiple poke, and vehicle-treated rats found the escape platform after multiple primary errors **(Figure 6A, B)**. Based on Barne maze results, there was no difference in primary latency between TYR A9 and $CoCl_2$+TYR A9. Interestingly, we found that the TYR A9 and $CoCl_2$+TYR A9 groups showed that improved spatial reference memory skills with minor error rate than $CoCl_2$ and vehicle-treated glioma rats. We also performed rotarod test to evaluate the coordinated motor function in rats treated with vehicle, $CoCl_2$, TYR A9 and $CoCl_2$+TYR A9. Rats with mild symptoms were used for 5 days of rotarod training. Each group of rats were tested on day 7. Glioma rats treated with TYR A9 (spent time 145.7±1.76 sec) on rotarod and $CoCl_2$+TYR A9 (spent time 137.6±2.08 sec) on rotarod spent more time or more latency to fall from the rotating rotarod as compared to $CoCl_2$ (spent time 49.33±1.72 sec) and vehicle-treated glioma rats (spent time 61.37±1.67 sec) **(Figure 7A)**. Latency time was calculated for each rat from the all-experimental groups. Densitometry analysis results suggested that a significant difference was found in motor performance on days 7, 8, and 9 after training

at two different 10 rpm (***p = 0.0003), (***p = 0.0001) and 15 rpm (****p<0.0001) **(Figure 7B, C)**. Relative fall latency was quantified for each group by two-way ANOVA.

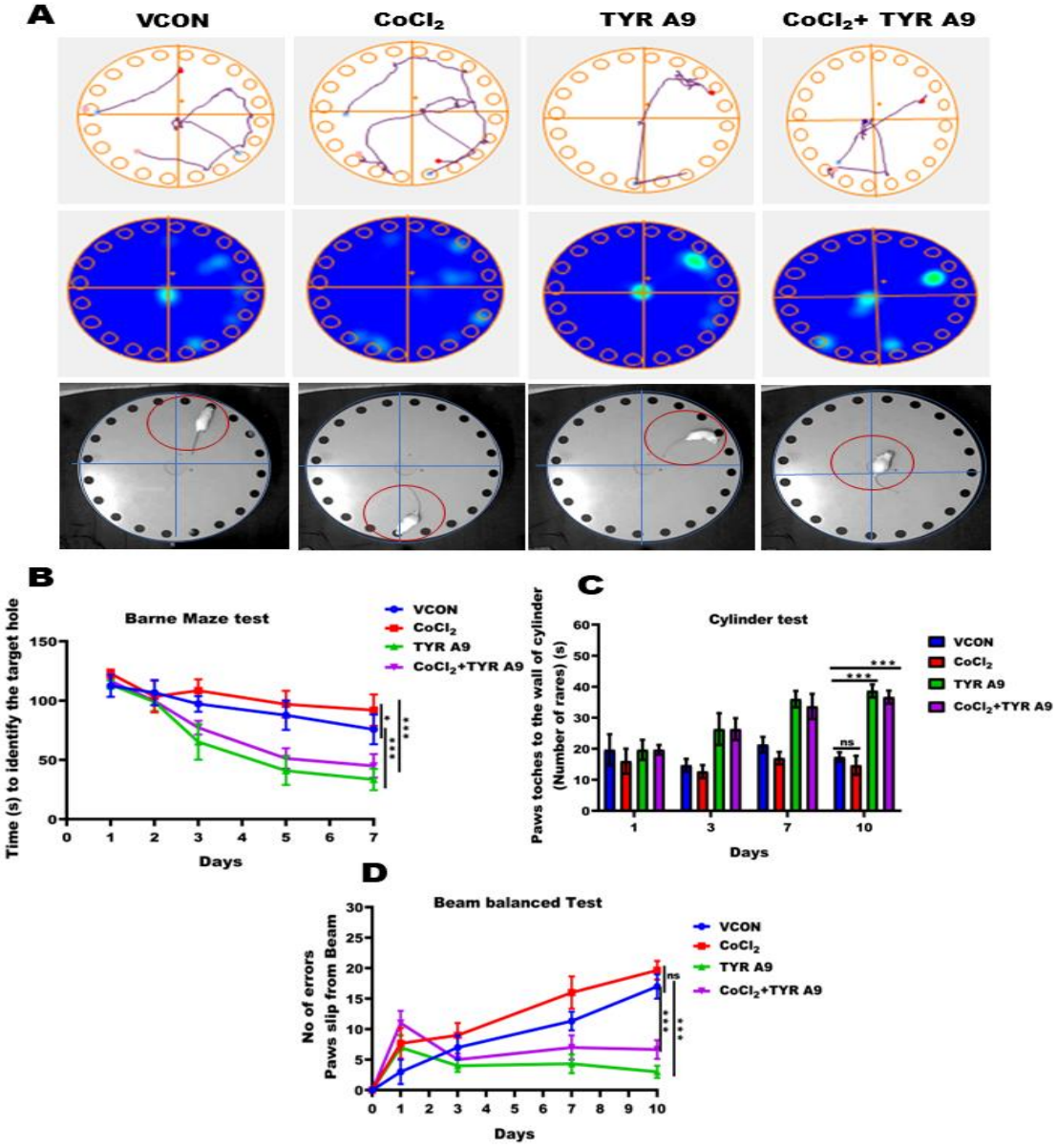

Figure 6: TYR A9 therapeutic effects on cognitive functions: (A, B) Barnes maze experiment depicting primary latency within a short time interval in TYR A9 and $CoCl_2$+TYR A9 compared to $CoCl_2$ and vehicle-treated glioma rats. **(C)**, The cylinder test exhibiting an increased number of rearing in both the TYR A9 and $CoCl_2$+TYR A9 groups compared to $CoCl_2$ and vehicle-treated glioma rats. **(D)**, The beam balance test result shows a characteristic of contralateral foot slipping. TYR A9 and $CoCl_2$+TYR A9 treated group showed less foot slippage and took the least time to transverse the beam compared to $CoCl_2$ and vehicle-treated glioma rats. Statistical significance denoted as *p<0.05, ***p<0.001.

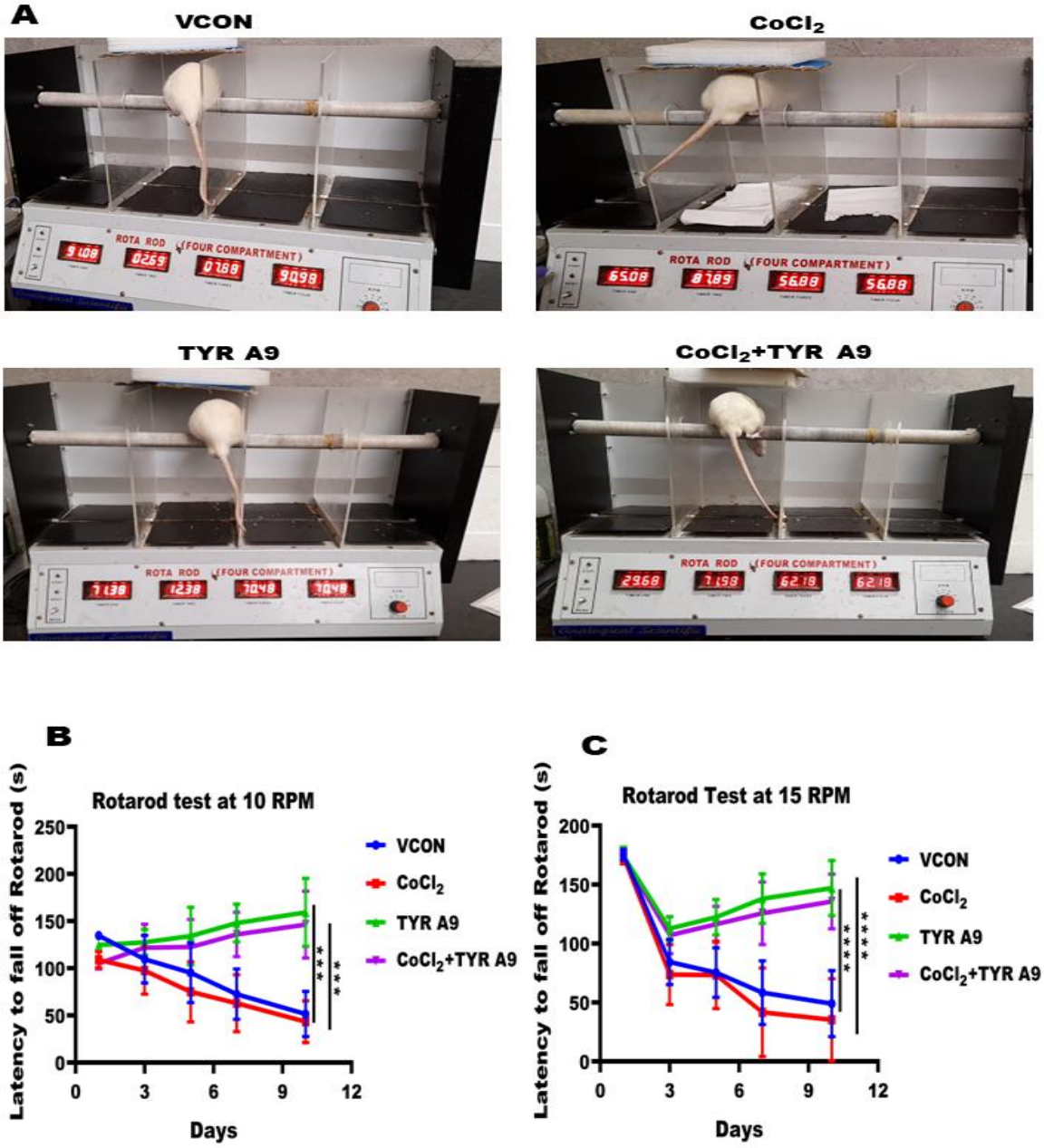

Figure 7: Effects of TYR A9 treatment on motor function of glioma rats: (A), The rotarod test shows improved motor function in glioma rats treated with TYR A9 and $CoCl_2$+TYR A9 compared to $CoCl_2$ and vehicle-treated glioma rats. **(B, C)**, Densitometry analysis results show rats tested at 10 and 15 rpm had more latency to fall from rotating rods in TYR A9 and $CoCl_2$+TYR A9 group, suggesting better motor performance than $CoCl_2$ and vehicle-treated glioma rats. Statistical significance represented as ***p<0.001, ****p<0.0.0001.

5.7. Discussion

Neurocognitive impairments are common among brain tumor patients; 80% of patients were identified through neurocognitive tests [12b]. The majority of patients with malignant brain tumors like meningiomas and malignant gliomas exhibit defects in various neurocognitive domains. In contrast, neurocognition impairments were not associated with the location of brain tumors [13]. The C6 rat glioma model is one of the crucial experimental models used in neuro-oncology to examine the development and invasion of high-grade gliomas [14]. The C6 cells are spindle-like and implanted into the adult Wistar rat brain to create a glioma model that unveils the same histological characteristics as human GBM, including foci of tumor necrosis, nuclear polymorphism, and a high mitotic index **[**15, 16]. Previous literature suggested that TYR A9 treatment is potentially used to protect and restore neuronal and axonal damage in neurodegenerative diseases [17]. In the present study, we demonstrated that implantation of C6 glioma cells, the progression of tumor glioma, behavioral assessment, and following treatment started in the given baseline time 10, 20, 25, 30, 35, 40, 45, 50, and 55days, in support of previous study [18, 19]. Here, in the current study, we investigated the anticancer efficacy of TYR A9 and its effect in the maintenance of cognitive function in glioma rat hypoxia vs normoxia. Previously reported that Tyrphostin A9 protects nerve growth in both the central and peripheral nervous systems, which encourages nerve regeneration [20]. In the present study, experimental group vehicle control and $CoCl_2$ treated glioma rat evidenced that increased tumor growth impaired brain function, but TYR A9 and $CoCl_2$+TYR A9 treatment decreased tumor growth and maintained brain function in the glioma rat hypoxia vs normoxia in support of previous report [16]. Histopathological analysis such as Hematoxylin and Eosin (H&E) staining showed increased cellularity and nuclear atypia in the vehicle, and $CoCl_2$-treated glioma rats compared to TYR A9 and $CoCl_2$+TYR A9 treated glioma rats. Ki-67- IHC staining showed decreased staining with restricted tumor growth in TYR A9 and $CoCl_2$+TYR A9 treated glioma rats. Glioma rats treated with vehicle and $CoCl_2$ drastically decreased body weight but maintained in TYR A9 and $CoCl_2$+TYRA9 treatment. High oncogenic protein expression promotes tumor growth, leading to cognitive impairments in glioma rats [16]. Immunohistochemistry (IHC) staining results demonstrated that decreased expression of RAP2B, HIF2A, EGFR, pPYK2, and vimentin in TYR A9 and $CoCl_2$+TYR A9 compared to $CoCl_2$ and vehicle-treated glioma rats.

Previously reported that vehicle-treated glioma rat-induced neuroinflammation [21] and treatment of $CoCl_2$ enhanced neuroinflammation, which strongly impacted cognitive impairment [22]. The present study demonstrated that vehicle and $CoCl_2$-treated glioma rats could potentiate cognitive impairment

after tumor formation at 15 to 20 days of implantation. We also observed that glioma rats treated with $CoCl_2$ worsened survival, greater cognitive impairment and altered behavior from days 15-20, such as loss of rearing and exploration, insensitive to touch escape. We administered TYR A9 drug treatment in glioma rats at day 10 after C6 cells implantation, and another group of $CoCl_2$+TYR A9 glioma rats pretreated with $CoCl_2$ for five days, and after one-day intervals started TYR A9 treatment for 10 days. TYR A9 and $CoCl_2$+TYR A9 group rats showed an improvement in behavioral patterns from day 25 to 30, such as exploration, i.e., exploring each and every corner, grooming, rearing, and improved in touch sensing, body balance, and locomotory behavior as compared to vehicle and $CoCl_2$ treated glioma rat. Most of the vehicle and $CoCl_2$-treated glioma rats died on days 15, 17, and 20 because of high tumor burden and hypoxic tumor microenvironment supporting of previous report [23]. In the present study, we planned to perform behavioral tests in the vehicle, and $CoCl_2$-treated glioma rats with mild symptoms survived up to 30 to 40 days. After their survival vehicle, $CoCl_2$, TYR A9, and $CoCl_2$+TYR A9 treated glioma rats were exposed to the beam balanced test on day 27-30 with 3 trials/day. Barne maze test training on days 33 to 36 with three sessions/day and days 38 to 39 as a probe trial, as a general practice. We performed a cylinder test that revealed the number of rearing was significantly improved in both the TYR A9 and $CoCl_2$+TYR A9 compared to vehicle and $CoCl_2$ glioma rats. The beam balance test results showed a characteristic of contralateral foot slipping. Glioma rats treated with TYR A9 and $CoCl_2$+TYR A9 showed less slipping and take least time to transverse the beam compared to vehicle control and $CoCl_2$-treated glioma rats. 1XPBS-treated rats were used as a reference. Our results from the Barnes maze test exposed that glioma rats treated with TYR A9 and $CoCl_2$+TYR A9 showed less primary latency with short interval than the vehicle and $CoCl_2$ group. The primary error rate increased in the vehicle and $CoCl_2$ treated compared to the TYR A9 and $CoCl_2$+TYR A9 group. 1XPBS treated rat primary latency time used as a reference. The heat maps showed that they spent maximum time into the escape hole with less primary latency in TYR A9 and $CoCl_2$+TYR A9 treated glioma rats compared to the vehicle and $CoCl_2$ treated glioma rats on day 5 in probe trial. Overall, based on the Barnes maze results, TYR A9 and $CoCl_2$+TYR A9 treated glioma rats unveiled improved spatial reference memory skills with reduced error rate as compared to vehicle and $CoCl_2$ treated glioma rats. The rotarod test showed the motor ability of glioma rats. Glioma rats treated with TYR A9 and $CoCl_2$+TYR A9 spent more time on the rotating rod or had more latency to fall from the rotarod than vehicle control and $CoCl_2$ treated. We scheduled a 3 to 4-day interval gap between each test because it is not advisable to conduct subsequent cognitive tests. Inhibition of these RAP2B/HIF2A/pPYK2-EMT signaling proteins by TYR A9 suggests that TYR

A9 could be used as a new therapeutic approach to maintain cognitive function and anticancer effect against glioma under hypoxia.

5.8. Conclusion

Overall, TYR A9 demonstrated strong anticancer effectiveness in an established experimental C6 rat glioma model and protection against the cognitive impairment induced by $CoCl_2$ and vehicle-treated glioma rats. Histopathological results revealed that decreased expression of RAP2B, HIF2A, EGFR, pPYK2, and vimentin in TYR A9 and $CoCl_2$+TYR A9 treated glioma rats, indicating that explored one of the potential mechanisms to target glioma. In conclusion, we understood that 1.5 mg/kg (body weight) of TYR A9 inhibited glioma growth and malignancy, improved the survivability and maintained cognitive function of glioma rats in hypoxia vs normoxia. Inhibition of RAP2B/HIF2A/pPYK2-EMT by TYR A9 signaling pathway in hypoxia and normoxia, suggesting that TYR A9 could be a new therapeutic approach against glioma.

5.9. Additional Information

Study approval

For the following details, refer to **objective 3**, **page no 117**.

Supporting information

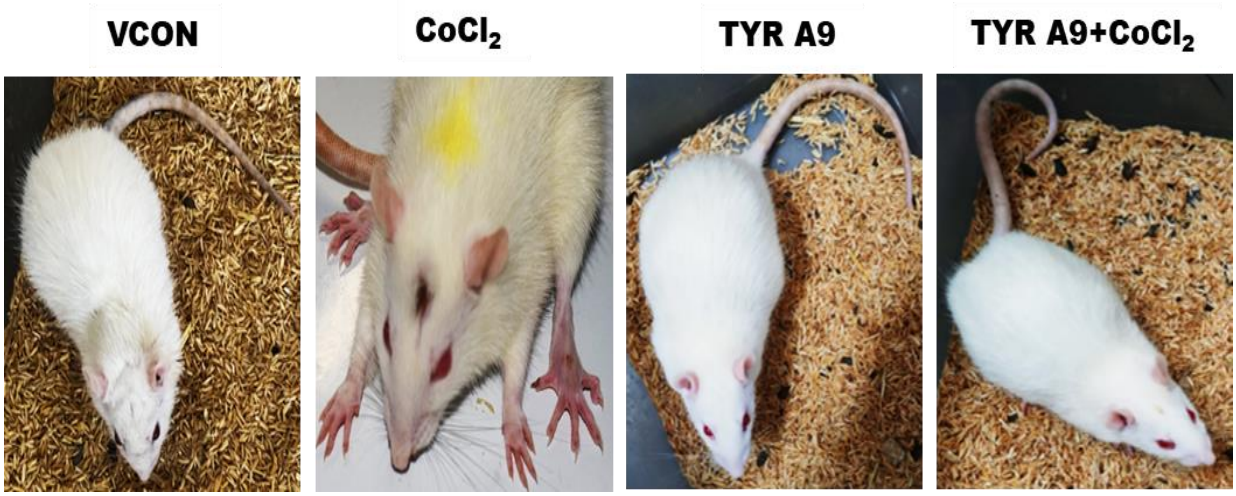

Figure 1: Rat images represented morphological changes in loss of fur density and stiff body, loss of coordination in $CoCl_2$ treated glioma rat, loss of fur density, and numbness in hind limb in vehicle-treated glioma rat. TYR A9 and $CoCl_2$+TYR A9 treated glioma rats show maintained fur density with shining and healthy compared to $CoCl_2$ and vehicle-treated glioma rats.

TYR A9 treatment induces apoptosis in glioma rats' hypoxia vs normoxia

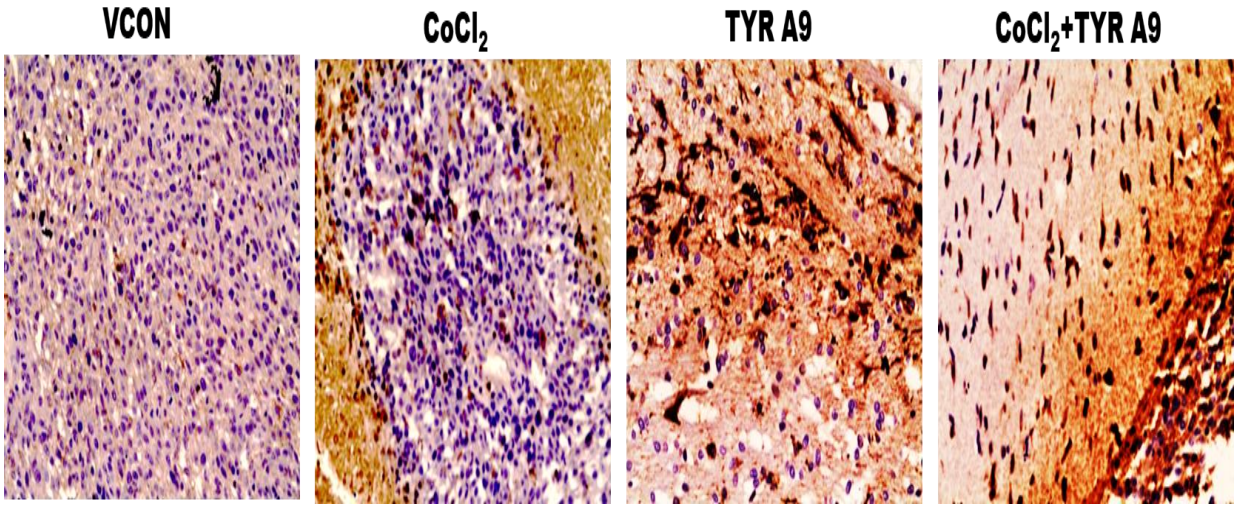

Figure 2: IHC staining shows more positive cleaved caspase 3 staining in TYR A9 and $CoCl_2$+TYR A9 compared to $CoCl_2$ and vehicle-treated glioma rats.

Cylinder test after TYR A9 treatment in rat glioma hypoxia vs normoxia

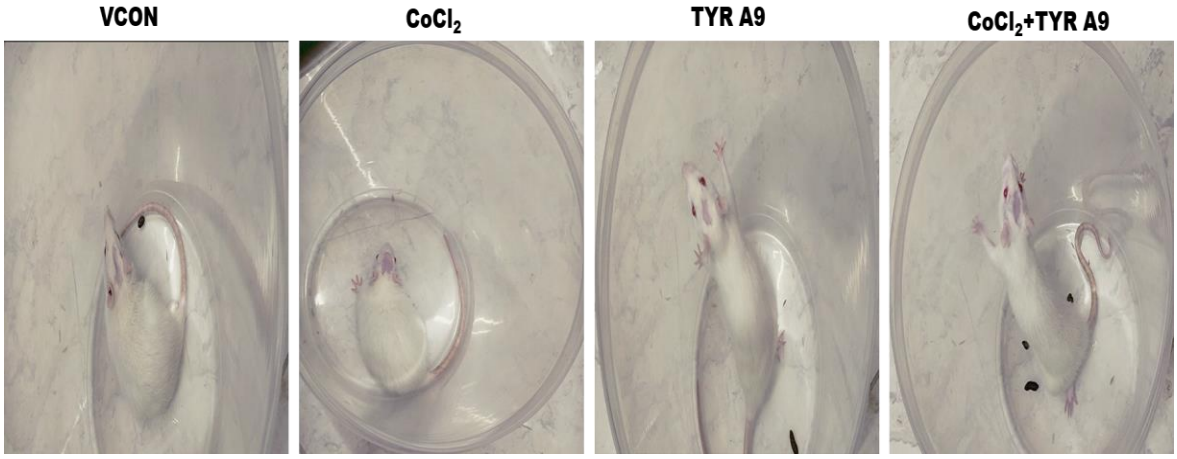

Figure 3: Cylinder test images showed more exploratory and rearing in TYR A9 and $CoCl_2$+TYR A9 treated rats compared to $CoCl_2$ and vehicle-treated glioma rats.

Beam balance test after TYR A9 treatment in glioma rat hypoxia vs. normoxia

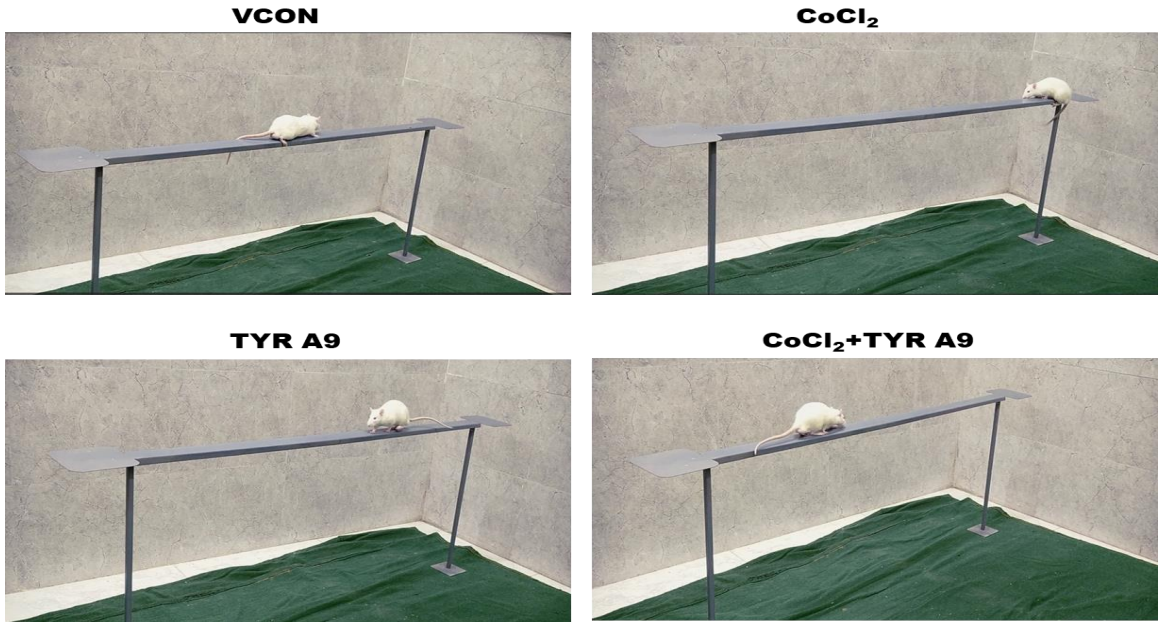

Figure 4: Illustrating beam balanced test represents improved motor coordination in TYR A9 and $CoCl_2$+TYR A9 treated glioma rats compared to $CoCl_2$ and vehicle-treated glioma rats.

5.10. References

1. Zhang, X., *et al*., Experiment and observation on invasion of brain glioma in vivo. Journal of clinical neuroscience, 2002. **9**(6): p. 668-671.
2. Group, G.M.-a.T.G., Chemotherapy in adult high-grade glioma: a systematic review and meta-analysis of individual patient data from 12 randomized trials. The Lancet, 2002. **359**(9311): p. 1011-1018.
3. Yamini, B., *et al*., Transcriptional targeting of adenovirally delivered tumor necrosis factor α by temozolomide in experimental glioblastoma. Cancer research, 2004. 64(18): p. 6381-6384.
4. Jallo, G.I., *et al*., A novel brainstem tumor model: functional and histopathological characterization. Child's Nervous System, 2006. **22**: p. 1519-1525.
5. Deutsch, M., *et al*., Intra-cerebral ventricular infusion of 5-iodo-2-deoxyuridine (IUDR) as a radiosensitizer in the treatment of a rat glioma. International Journal of Radiation Oncology* Biology* Physics, 1990. **19**(1): p. 85-87.
6. Workman, P., *et al*., Committee of the National Cancer Research, I., 2010. Guidelines for the welfare and use of animals in cancer research. Br. J. Cancer. **102**(1555): p. e1577.

7. D'Angelo, C., *et al*., State and trait anxiety and depression in patients with primary brain tumors before and after surgery: 1-year longitudinal study. Journal of neurosurgery, 2008. **108**(2): p. 281-286.
8. Bower, J.E., Behavioral symptoms in breast cancer patients and survivors: fatigue, insomnia, depression, and cognitive disturbance. Journal of clinical oncology: official journal of the American Society of Clinical Oncology, 2008. **26**(5): p. 768.
9. Gillespie, J., *et al*., Inhibition of pancreatic cancer cell growth in vitro by the tyrphostin group of tyrosine kinase inhibitors. British journal of cancer, 1993. **68**(6): p. 1122-1126.
10. Liang, B.C. and E. Ullyatt, Chemosensitization of glioblastoma cells to bis-dichloroethyl-nitrosourea with tyrphostin AG17. Clinical cancer research: an official journal of the American Association for Cancer Research, 1998. **4**(3): p. 773-781.
11. Yadav, N., *et al*., Tyrphostin A9 attenuates glioblastoma growth by suppressing PYK2/EGFR-ERK signaling pathway. Journal of Neuro-Oncology, 2023. **163**(3): p. 675-692.
12. a) Shi, G. and Z. Zhang, Rap2B promotes the proliferation and migration of human glioma cells via activation of the ERK pathway. Oncol Lett, 2021. **21**(4): p. 314. b) Day, J., *et al*., Neurocognitive deficits and neurocognitive rehabilitation in adult brain tumors. Current treatment options in neurology, 2016. **18**: p. 1-16.
13. Hoffermann, M., *et al*., Pre-and postoperative neurocognitive deficits in brain tumor patients assessed by a computer based screening test. Journal of Clinical Neuroscience, 2017. **36**: p. 31-36.
14. Barth, R.F. and B. Kaur, Rat brain tumor models in experimental neuro-oncology: the C6, 9L, T9, RG2, F98, BT4C, RT-2 and CNS-1 gliomas. Journal of neuro-oncology, 2009. **94**: p. 299-312.
15. Grobben, B., P. De Deyn, and H. Slegers, Rat C6 glioma as experimental model system for the study of glioblastoma growth and invasion. Cell and tissue research, 2002. **310**: p. 257-270.
16. Souza, T.K.F., *et al*., Image and motor behavior for monitoring tumor growth in C6 glioma model. PLoS One, 2018. **13**(7): p. e0201453.
17. Gill, R.S., *et al*., The dopamine D4 receptor activates intracellular platelet-derived growth factor receptor β to stimulate ERK1/2. Cellular signalling, 2010. **22**(2): p. 285-290.
18. Vannini, E., *et al*., Progression of motor deficits in glioma-bearing mice: Impact of CNF1 therapy at symptomatic stages. Oncotarget, 2017. **8**(14): p. 23539.
19. Hicks, W.H., *et al*., Contemporary mouse models in glioma research. Cells, 2021. **10**(3): p. 712.
20. Dai, X., *et al*., Tyrphostin A9 protects axons in experimental autoimmune encephalomyelitis through activation of ERKs. Life sciences, 2022. 294: p. 120383.
21. Giakoumettis, D., A. Kritis, and N. Foroglou, C6 cell line: The gold standard in glioma research. Hippokratia, 2018. **22**(3): p. 105.
22. Kim, S.-R., *et al*., Epigallocatechin gallate protects against hypoxia-induced inflammation in microglia via NF-κB suppression and Nrf-2/HO-1 activation. International Journal of Molecular Sciences, 2022. **23**(7): p. 4004.
23. Hao, S., *et al*., AG-1031 and AG-1503 improve cognitive deficits by promoting apoptosis and inhibiting autophagy in C6 glioma model rats. Brain Research, 2018. **1699**: p. 1-8.

Discussion and summary

Glioma is an umbrella term used to categorize primary brain tumors based on their presumed cell origin. These include astrocytic tumors (astrocytomas, anaplastic astrocytomas, and glioblastomas), oligodendrogliomas, ependymomas, and mixed gliomas [1, 2, 3]. The most common and malignant type of brain tumor is called glioblastoma multiforme. It accounts for more than 60% of adult brain tumors. It is still a deadly tumor instead of a variety of modern therapies against GBM but has a median survival of approximately 14 to 15 months [4, 5]. Hypoxia is a prominent characteristic of GBM and its microenvironment associated with tumor growth, progression, and resistance to conventional cancer therapy. The master regulators of the transcriptional response to hypoxia in tumor cells and their microenvironment are called hypoxia-inducible factors (HIFs); one family member such as HIF2A, highly expressed in various cancers, including glioma under hypoxia. According to previous reports and existing databases, overexpression of HIF2A genes in high-grade astrocytoma and its expression correlated with patients' poor survival. Several studies have evidenced that RAP2B also highly expressed in various cancers and plays a significant role in cancer development. The oncogenic role of RAP2B in different cancers progression through FAK/EMT signaling [6, 7, 8]. Based on existing literature, In the present study we investigated potential biomarkers and developed a therapeutic approach with potent anticancer drug and molecular targets against GBM in hypoxia [4]. Our research showed that overexpression of RAP2B and HIF2A associated with pathological grading of astrocytomas and patients' poor survival. Increased expression of RAP2B/HIF2A in malignant astrocytoma positively correlated with pPYK2-EMT signaling, suggesting that it may have an etiological role in the malignancy and poor prognosis of GBM. Furthermore, in the present finding, we investigated the important role of RAP2B-mediated activation of the HIF2A/FAK/PYK2-EMT signaling pathway in GBM cell progression under $CoCl_2$ induced hypoxia. Our results evidenced that overexpression of RAP2B enhanced the expression of HIF2A/PYK2/FAK-EMT signaling proteins and promoted proliferation and migration in both GBM cells under $CoCl_2$-induced hypoxia. These results verify our clinical data in GBM cell lines and suggest that understanding the clinical and functional aspects of RAP2B/HIF2A and their etiological relevance with EMT in astrocytoma is purposeful. *In vitro* results showed that $CoCl_2$-induced hypoxia increased RAP2B expression, evidencing that RAP2B is a hypoxia-responsive gene. Overexpression of RAP2B increased HIF2A expression under normoxia but enhanced under hypoxia in GBM cells. This suggests that RAP2B is essential for HIF2A stabilization under hypoxia and normoxia. Finally, we demonstrated that the RAP2B/HIF2A axis enhanced activation of pPYK2/pFAK-EMT signaling involved in GBM cell

survival and growth in hypoxia, therefore implying that the RAP2B/HIF2A axis could be a novel potential therapeutic target against GBM in hypoxia.

Several studies have evidenced that a combination of different drugs and molecularly targeted treatment, such as cytotoxic chemotherapy, compared to single-drug treatment have synergistic anti-tumor effects. Although RAP2B, HIF2A, PYK2, and EMT proteins are reported in gliomas, but RAP2B/HIF2A mediated activation of PYK2-EMT signaling in gliomas is still unknown. More research is needed to determine its translational relevance. Therefore, the present study used siRNA-mediated knockdown of RAP2B (molecular target) and anticancer drug TYR A9 (nontoxic dose) treatment against GBM cell progression in hypoxia supporting previous report [9]. Although there is currently no information regarding astrocytoma malignancy and chemoresistance, emerging reports demonstrated the therapeutic significance of RAP2B/HIF2A by molecular approach siRNA mediated knockdown of RAP2B and TYR A9. We demonstrated that combined treatment of TYR A9 (nontoxic dose) and RAP2B knockdown (siRAP2B) significantly inhibited GBM cell proliferation and migration by attenuating RAP2B/HIF2A/pPYK2-EMT signaling in hypoxia. Based on our present results, we concluded that RAP2B knockdown increased anticancer efficacy of TYR A9 even at nontoxic dose and inhibited proliferation and migration as well as sensitized GBM cells to induced apoptosis under hypoxia. Based on the MTT, clonogenic, and wound healing assay, we also showed that TYR A9 sensitizes TMZ-resistant cell lines (LN18) and inhibits proliferation and migration, showing its consistent anticancer efficacy. In this study, we found evidence that the administration of TYR A9 suppressed GBM cell proliferation and migration by blocking the pPYK2/EGFR-ERK1/2 signaling pathway. *In vitro* observations were represented by *in vivo* data. H&E staining demonstrated that restricted tumor growth and IHC-staining showed decreased Ki-67 staining in TYR A9 treated compared to vehicle-treated glioma rats.

Additionally, we showed that TYR A9 treatment improved survival and maintained body weight compared to vehicle-treated glioma rats. Furthermore, TYR A9-treated glioma rats showed decreased staining of pEGFR, pPYK2, and pERK1/2 confirmed through IHC, indicating the inhibition of the pPYK2/EGFR-ERK1/2 signaling pathway compared to vehicle-treated glioma rats. Our finding evidenced that increased cleaved caspase 3 staining proves apoptosis induction in TYR A9 treated glioma rats, suggesting that TYR A9 treated glioma rats induced apoptosis and decreased tumor growth.

We conducted an *in-vitro* RAP2B overexpression and knockdown in $CoCl_2$-induced hypoxia. The present study investigated TYR A9 anticancer efficacy in the Wistar rat glioma model treated with $CoCl_2$. *In vitro* study further validated with i*n vivo* data and established the relationship between

RAP2B/HIF2A/pPYK2-EMT signaling and $CoCl_2$-induced hypoxia. The present finding investigated the TYR A9 anticancer effect on RAP2B/HIF2A/pPYK2-EMT signaling in glioma rats without and with $CoCl_2$. Histopathological examination such as H&E staining showed that restricted tumor growth, maintained body weight, and IHC represented decreased Ki-67 staining in TYR A9 and $CoCl_2$+TYR A9 treated glioma rats compared to vehicle and $CoCl_2$ treated glioma rats. Subsequently, we also demonstrated that decreased staining of RAP2B, HIF2A, EGFR, pPYK2, β-catenin, and vimentin in TYR A9 and $CoCl_2$+TYR A9 treated compared to vehicle and $CoCl_2$ treated glioma rats. This indicating that anticancer efficacy of TYR A9 inhibited glioma growth and proliferations in hypoxia supporting previous report [10]. Additionally, the behavioral test was performed to measure how cognitive function was disturbed as the tumor progressed in the glioma model. Further, we demonstrated the effect of TYR A9 on the improvement of cognitive impairment and altered behavior of glioma rats induced by $CoCl_2$. Our finding observed cognitive impairment in the glioma rat model after tumor formation at 15 to 20 days of C6 cell implantation. $CoCl_2$-treated glioma rats showed worst survival with greater cognitive impairment because $CoCl_2$ treatment might induce neuroinflammation that strongly leads to cognitive impairment. The cylinder test exhibited that increased number of rearing in both TYR A9 and $CoCl_2$+TYR A9 compared to vehicle and $CoCl_2$-treated glioma rats. The beam balance test results showed a characteristic of contralateral foot slipping. Glioma rats treated with TYR A9 and $CoCl_2$+TYR A9 showed less foot slipping and took less time to transverse the beam than vehicle and $CoCl_2$ treated. Our Barne maze test revealed that glioma rats treated with TYR A9 and $CoCl_2$+TYR A9 showed primary latency within a short time interval compared to the vehicle and $CoCl_2$ groups. The heat maps showed that TYR A9 and $CoCl_2$+TYR A9 treated spent more time in the escape platform with fewer primary errors compared to the vehicle and $CoCl_2$-treated glioma rats during the probe trial on day 5. Based on Barne maze test results, TYR A9 and $CoCl_2$+TYR A9 treated glioma rats revealed better spatial reference memory skills with less error rate than the vehicle and $CoCl_2$ treated. The rotarod test was used to evaluate coordinated motor function. Glioma rats treated with TYR A9 and $CoCl_2$+TYR A9 spent more time and had more latency to fall from the rotating rod than vehicle and $CoCl_2$ treated. For all the cognitive tests, 1X PBS-treated rats were used as a reference. Based on the outcomes of our study, we understood that 1.5mg/kg of body weight TYR A9 inhibited glioma growth and malignancy and improved survivability of glioma rats. This evidence shows that TYR A9 also helps neuroprotection and restores cognitive function in the glioma model *in vivo*.

References

1. Umans, R.A. and H. Sontheimer, Combating malignant astrocytes: Strategies mitigating tumor invasion. Neuroscience research, 2018. **126**: p. 22-30.
2. Schwartzbaum, J.A., *et al.*, Epidemiology and molecular pathology of glioma. Nature clinical practice Neurology, 2006. **2**(9): p. 494-503.
3. Agnihotri, S., *et al*., Glioblastoma, a brief review of history, molecular genetics, animal models and novel therapeutic strategies. Arch Immunol Ther Exp (Warsz), 2013. **61**(1): p. 25-41.
4. Hanif, F., *et al*., Glioblastoma multiforme: a review of its epidemiology and pathogenesis through clinical presentation and treatment. Asian Pacific journal of cancer prevention: APJCP, 2017. **18**(1): p. 3.
5. Thakkar, J.P., *et al*., Epidemiologic and molecular prognostic review of glioblastoma. Cancer epidemiology, biomarkers & prevention, 2014. **23**(10): p. 1985-1996.
6. Di, J., *et al*., Rap2B promotes cell proliferation, migration and invasion in prostate cancer. Medical Oncology, 2016. **33**: p. 1-10.
7. McLeod, S.J., *et al*., The Rap GTPases regulate integrin-mediated adhesion, cell spreading, actin polymerization, and Pyk2 tyrosine phosphorylation in B lymphocytes. Journal of Biological Chemistry, 2004. **279**(13): p. 12009-12019.
8. Masalha, M., *et al*., MiR-199a-3p Induces Mesenchymal to Epithelial Transition of Keratinocytes by Targeting RAP2B. International Journal of Molecular Sciences, 2022. **23**(23): p. 15401.
9. Lee, Y.T., Y.J. Tan, and C.E. Oon, Molecular targeted therapy: Treating cancer with specificity. European journal of pharmacology, 2018. **834**: p. 188-196.
10. Bijli, K.M., *et al*., Proline-rich tyrosine kinase 2 downregulates peroxisome proliferator–activated receptor gamma to promote hypoxia-induced pulmonary artery smooth muscle cell proliferation. Pulmonary Circulation, 2016. **6**(2): p. 202-210.

Conference Certificates and Publication

ConferenceSeries.com

CERTIFICATE
OF RECOGNITION

Conference Series LLC Ltd. is proud to present this Certificate to

Ms. Neera Yadav

University of Hyderabad, India

For presenting an **Oral Presentation** at the Webinar of **6th International Conference on Neuro-Oncology and Brain Tumor** (**Neuro Oncology 2020**) during June 22-23, 2020.

Title: **"Downregulation of RAP2B promotes human astrocytoma inhibited by involvement of oncogenic mi-RNA"**

Catherine Maurice
University Health Network
Princess Margaret Cancer Centre, Canada

Asia Conference Series

ISNO
Indian Society of Neuro-Oncology

ISNOCON 2021

12th Annual Conference of Indian Society of Neuro-Oncology

Certificate

This is to certify that

Neera Yadav

has presented a **E Poster** titled

Downregulation of RAP2B promotes astrocytoma progression by involvement of MiRNA

ISNOCON 2021, hosted virtually from

15th - 17th April, 2021

Dr. Shaleen Kumar	Dr. Tejpal Gupta	Dr. Geeta Chacko	Dr. Ranjith Moorthy
President	General Secretary	Organizing Chairperson	Organizing Secretary
ISNO	ISNO	ISNOCON 2021	ISNOCON 2021

LADY DOAK COLLEGE

SEMPER PRO VERITATE

Lady Doak College, Madurai

(An Autonomous Institution Affiliated to Madurai Kamaraj University)
College with Potential for Excellence
Re-accredited by NAAC with Grade A (3rd cycle : 3.44 out of 4)

Certificate

This is to certify that ~~Dr~~/~~Mr~~/Ms. Neera Yadav of University of Hyderabad, Telangana. participated in the National Level Workshop on Animal Cell Culture Techniques (Sponsored by DBT, TNSCST, NCSTC & DST-GOI) from 4th - 8th September, 2017, organised by the Department of Biotechnology, Lady Doak College, Madurai.

Dr. Christianna Singh
Principal & Secretary

Dr. Priyatharsini Rajendran
Co-ordinator
Dept. of Biotechnology

Dr. P. Abirami
Ms. S. Kalaivani Priyadarshini
Organising Secretaries
Dept. of Biotechnology

AS-UoH Joint Workshop on Frontiers in Life Sciences

Septemeber 16-17, 2016

Certificate

This is to certify that Dr/Ms /Mr. Neera Yadav has participated/~~presented a poster~~ in AS-UoH Joint Workshop on Frontiers in Life Sciences organized during Septemeber 16-17, 2016 at SLS Auditorium, University of Hyderabad, Hyderabad, India.

Sue L-Chao

Dr. Sue Lin-Chao
Coordinator
Academia Sinica

JSPrakash

Dr. J.S.S. Prakash
Coordinator
University of Hyderabad

BioQUEST 2016

October 20 & 21, 2016

School of Life Sciences, University of Hyderabad, Hyderabad - 500 046, INDIA

Certificate of Participation

This is to certify that Prof./Dr./Mr./Ms. Neera Yadav

from Department of Biotechnology & Bioinformatics

has participated in the "BioQuest 2016" held on October 20th & 21st, 2016.

Dean
School of Life Sciences

JSS ACADEMY OF HIGHER EDUCATION & RESEARCH
(DEEMED TO BE UNIVERSITY) MYSURU

JSS ACADEMY OF HIGHER EDUCATION & RESEARCH

(Deemed to be University), Accredited 'A+' Grade by NAAC,
Sri Shivarathreeshwara Nagar, Mysuru – 570 015

JSS COLLEGE OF PHARMACY, MYSURU

In association with

Society for Neurochemistry, India (SNCI)

SNCI-CON 2019

International Conference on

NEUROCHEMISTRY AND NEUROPHARMACOLOGY: FROM BENCH TO BEDSIDE

&

32nd Annual Meeting of

SOCIETY FOR NEUROCHEMISTRY, INDIA (SNCI),

Certificate of Appreciation

Awarded to

Dr./Mr./Ms Neera Yadav

for ~~Oral~~ / Poster Presentation entitled

The clinical and functional importance of RAP2B gene in astrocytoma progression and screening of novel compounds to target astrocytoma.

in the International Conference on "Neurochemistry and Neuropharmacology: From Bench to Bedside" (SNCI-CON2019) during 14th to 16th, March 2019

Dr. S.N. Manjula Convener (SNCI-CON, 2019)	***Dr. C. Saravana Babu*** Organizing Secretary(SNCI-CON, 2019) JSS College of Pharmacy, Mysuru	***Prof. P. Prakash Babu*** General Secretary Society for Neurochemistry, India	***Dr. T.M. Pramod Kumar*** Principal JSS College of Pharmacy, Mysuru

We are Ranked 10th by NIRF, MHRD, Government of India

NAAC A+ 2018

2018 nirf NATIONAL INSTITUTIONAL RANKING FRAMEWORK 37th in INDIA

THE Emerging Economies

STARS RATED FOR EXCELLENCE

2019 THE 401-500 251-300

JSS ACADEMY OF HIGHER EDUCATION & RESEARCH
(DEEMED TO BE UNIVERSITY) MYSURU

JSS ACADEMY OF HIGHER EDUCATION & RESEARCH

(Deemed to be University), Accredited 'A+' Grade by NAAC,
Sri Shivarathreeshwara Nagar, Mysuru – 570 015

JSS COLLEGE OF PHARMACY, MYSURU

In association with

Society for Neurochemistry, India (SNCI)

SNCI-CON 2019

International Conference on

NEUROCHEMISTRY AND NEUROPHARMACOLOGY: FROM BENCH TO BEDSIDE

&

32nd Annual Meeting of

SOCIETY FOR NEUROCHEMISTRY, INDIA (SNCI),

Certificate of Participation

We have the pleasure to confirm the participation of

Dr./Mr./Ms Neera Yadav

in the International Conference on "Neurochemistry and Neuropharmacology: From Bench to Bedside" (SNCI-CON2019) during 14th to 16th, March 2019

Dr. K.L. Krishna	***Dr. C. Saravana Babu***	***Prof. P Prakash Babu***	***Dr. T.M. Pramod Kumar***
Convener (SNCI-CON, 2019)	Organizing Secretary(SNCI-CON, 2019) JSS College of Pharmacy, Mysuru	General Secretary Society for Neurochemistry, India	Principal JSS College of Pharmacy, Mysuru

We are Ranked 10th by NIRF, MHRD, Government of India

NAAC A+ 2018

2018 nirf NATIONAL INSTITUTIONAL RANKING FRAMEWORK 37th in INDIA

THE Emerging Economies

STARS RATED FOR EXCELLENCE

2019 THE 401-500 251-300

SNCI 2021

35th Annual Conference of Society for Neurochemistry, India
University of Hyderabad, 2nd-4th December 2021

Participation Certificate

This is to certify that

Neera Yadav

has participated in SNCI 2021 annual conference (hybrid) entitled,

"Neurodegeneration and Cognition-Recent Advances in Neurological Diseases"

hosted from 2nd-4th December 2021.

Prof. P. Prakash Babu
Convener
SNCI

Prof. Ramesh Kumar Mishra
Organising Secretary
SNCI 2021

Journal of Neuro-Oncology (2023) 163:675–692
https://doi.org/10.1007/s11060-023-04383-7

RESEARCH

Tyrphostin A9 attenuates glioblastoma growth by suppressing PYK2/EGFR-ERK signaling pathway

Neera Yadav[1] · Deepak Babu[1] · Sailaja Madigubba[4] · Manas Panigrahi[2] · Prakash Babu Phanithi[3]

Received: 20 April 2023 / Accepted: 24 June 2023 / Published online: 6 July 2023

Abstract

Purpose Glioblastoma (GBM) is a fatal primary brain tumor with extremely poor clinical outcomes. The anticancer efficiency of tyrosine kinase inhibitors (TKIs) has been shown in GBM and other cancer, with limited therapeutic outcomes. In the current study, we aimed to investigate the clinical impact of active proline-rich tyrosine kinase-2 (PYK2) and epidermal growth factor receptor (EGFR) in GBM and evaluate its druggability by a synthetic TKI-Tyrphostin A9 (TYR A9).

Methods The expression profile of PYK2 and EGFR in astrocytoma biopsies (n = 48) and GBM cell lines were evaluated through quantitative PCR, western blots, and immunohistochemistry. The clinical association of phospho-PYK2 and EGFR was analyzed with various clinicopathological features and the Kaplan–Meier survival curve. The phospho-PYK2 and EGFR druggability and subsequent anticancer efficacy of TYR A9 was evaluated in GBM cell lines and intracranial C6 glioma model.

Results Our expression data revealed an increased phospho-PYK2, and EGFR expression aggravates astrocytoma malignancy and is associated with patients' poor survival. The mRNA and protein correlation analysis showed a positive association between phospho-PYK2 and EGFR in GBM tissues. The in-vitro studies demonstrated that TYR A9 reduced GBM cell growth, cell migration, and induced apoptosis by attenuating PYK2/EGFR-ERK signaling. The in-vivo data showed TYR A9 treatment dramatically reduced glioma growth with augmented animal survival by repressing PYK2/EGFR-ERK signaling.

Conclusion Altogether, this study report that increased phospho-PYK2 and EGFR expression in astrocytoma was associated with poor prognosis. The in-vitro and in-vivo evidence underlined translational implication of TYR A9 by suppressing PYK2/EGFR-ERK modulated signaling pathway.

Extended author information available on the last page of the article

CD&T/6110 Biotechnology
01/02/2024

हैदराबाद विश्वविद्यालय || UNIVERSITY OF HYDERABAD

परीक्षा नियंत्रक का कार्यालय/Office of the Controller of Examinations

शैक्षणिक अनुभाग/Academic Section

UH/AR/A/2024/541

Date:31.01.2024

OFFICE ORDER

Sub: Re-Registration request of Ph.D. Scholars – Reg.
Ref: Vice Chancellor's orders dated: 29.01.2024.

###

The following Ph.D. students are hereby informed that their request for Re-registration of Ph.D. programme has been approved by the Competent Authority. Accordingly their names have been Re-Registered in the rolls of the University.

S.No.	Regn. No.	Name of the Research Scholar	Subject	Duration for submission of thesis (last date)
01.	13LPPH08	Ms. Doris Abhirupa Pradhan	Plant Sciences	23.07.2024
02.	15MCPC15	Mr. Akshay Badola	Computer Science	22.07.2024
03.	16LTPH10	Ms. Neera Yadav	Biotechnology	21.07.2024

The above Scholars have to submit their Ph.D. thesis as mentioned in the last column of the table against their names i.e., six months from the date of application of the scholar, by paying applicable thesis submission fee. No further time beyond the date mentioned in the last column against their names will be given.

31/1/24
Asst.Registrar
(Academic)

To
Individual concerned
Through the supervisor

Copy to

1. The Dean,School of Life Sciences
2. The Dean, SCIS
3. The Head, Dept. of Plant Sciences
4. The Head, Dept.of Biotechnology & Bioinformatics
5. The Supervisor of the students
6. Chief Warden
7. Dean, Students' Welfare
8. Librarian
9. A.R. (F&S) Section
10. DSW Fellowships
11. A.A.O.
12. E-Governance cell
13. Personal File

UNIVERSITY OF HYDERABAD
NOTIFICATION OF RESULTS

Exams/908
21/3/17

Course: Ph.D.
Subject: Biotechnology

Month & Year: November, 2016
Semester: I

Sl.. No	Regn.No.	Name of the Student	Course No. Credits-4	Course No. Credits-3	Course No. Credits-5
			BT 801	BT-802	BT-803
1	15LTPH11	M.Kishore	Pass	Pass	Pass
2	15LTPH06	Pratibha Khuhwaha	Pass	Pass	Pass
3	16LTPH01	B Narsimulu	Fail	Pass	Pass
4	16LTPH02	Bhawangirkar Shubhangi Govindprasad	Fail	Pass	AB
5	16LTPH03	Chukhu Muj	Pass	Pass	Pass
6	16LTPH05	Dipesh Kumar Nayak	Pass	Pass	Pass
7	16LTPH06	Gandhari Shankar	Pass	Pass	Pass
8	16LTPH07	K.Manati	Pass	Pass	Pass
9	16LTPH08	Lekha Gandhi	Pass	Pass	Pass
10	16LTPH09	Molgara Krishnaiah Goud	AB	AB	AB
11	16LTPH10	Neera Yadav	Fail	Pass	Pass
12	16LTPH11	Nupurfangaria	Pass	Pass	Pass
13	16LTPH12	Y Priya	Pass	Pass	Pass
14	16LTPH13	Yogesh Patidar	Pass	Fail	Pass

Tourse No. **Title of the Course**

BT- Analytical Techniques
BT- Research Ethics, Data Analysis and Biostatistics
BT- Lab Work & Seminar

28-2-17
Controller of Examination

Copy to
Head Deaprtment of Animal Sciences

1 — Exams/1427
28/6/17

UNIVERSITY OF HYDERABAD
NOTIFICATION OF RESULTS

Course: Ph.D.
Subject: Plant Sciences

Month & Year: April, 2017
Semester: I Supplementary

Sl. No	Regn.No.	Name of the Student	Course No. Credits-3	Course No. Credits-3
			AB-801	AB-802
1	15LAPH18	SUKALPA MONDAL	PASS	-
2	16LTPH01	B.NARSIMULU	PASS	-
3	16LTPH02	BHAWANGIRKAR SHUBHANGI GOVINDPRASAD	PASS	-
4	16LTPH10	NEERA YADAV	PASS	-
5	16LPPH06	JYOTHI PALLEBOINA	PASS	PASS
6	16LPPH17	SIRIPURAM SRINIVAS	PASS	PASS
7	15LPPH12	KUNAL BABARAO	PASS	-
8	16MDPH01	R.V.L.NARAYANA	PASS	-
9	16LAPH02	M.MOTILAL	-	PASS

Course No. Title of the Course

AB-801 Analytical Techniques
AB-802 Research Ethics, Data Analysis and Biostatistics

22.6.17
Controllor of Examination
O/C Anjali

Dated: 22.06.2017

Copy to

1. Head Department of Animal Biology

Edumi 22/6/17

DR All 29/6/17

CE 559 23/6/17

Mechanism of Astrocytoma Progression: Role of RAP2B and HIF2A in Hypoxia

by Neera Yadav

Submission date: 13-Mar-2024 02:56PM (UTC+0530)
Submission ID: 2319317885
File name: Neera_final_thesis_2024_for_Plag_Check_11_march_2024.docx (405.42K)
Word count: 26086
Character count: 148469

Mechanism of Astrocytoma Progression: Role of RAP2B and HIF2A in Hypoxia

ORIGINALITY REPORT

25%	8%	25%	2%
SIMILARITY INDEX	INTERNET SOURCES	PUBLICATIONS	STUDENT PAPERS

PRIMARY SOURCES

1	Neera Yadav, Deepak Babu, Sailaja Madigubba, Manas Panigrahi, Prakash Babu Phanithi. "Tyrphostin A9 attenuates glioblastoma growth by suppressing PYK2/EGFR-ERK signaling pathway", Journal of Neuro-Oncology, 2023 Publication	18%
2	dspace.uohyd.ac.in Internet Source	1%
3	www.ncbi.nlm.nih.gov Internet Source	<1%
4	www.dovepress.com Internet Source	<1%
5	link.springer.com Internet Source	<1%
6	Deepak Babu, Ramulu Chintal, Manas Panigrahi, Prakash Babu Phanithi. "Distinct expression and function of breast cancer	<1%

25/5/2024
Prof. P. Prakash Babu
Department of Biotechnology & Bioinformatic
School of Life Sciences
University of Hyderabad
Hyderabad-500 046. (T.S.)

metastasis suppressor 1 in mutant P53 glioblastoma", Cellular Oncology, 2022
Publication

7	worldwidescience.org Internet Source	<1 %
8	journals.sagepub.com Internet Source	<1 %
9	thno.org Internet Source	<1 %
10	Yi-Gen Peng, Zheng-Qun Zhang, Yan-bin Chen, Jian-An Huang. "Rap2b promotes proliferation, migration, and invasion of lung cancer cells", Journal of Receptors and Signal Transduction, 2015 Publication	<1 %
11	effiloop.com Internet Source	<1 %
12	www.mdpi.com Internet Source	<1 %
13	Vera L. Silva, Wafa' T. Al-Jamal. "Exploiting the cancer niche: Tumor-associated macrophages and hypoxia as promising synergistic targets for nano-based therapy", Journal of Controlled Release, 2017 Publication	<1 %
14	Submitted to Cranfield University Student Paper	

		<1%
15	www.frontiersin.org Internet Source	<1%
16	Submitted to University of Hyderabad, Hyderabad Student Paper	<1%
17	portlandpress.com Internet Source	<1%
18	P Santos, D Murtinho, AS Pires Lourenço, J Araújo, R Martins, AM Abrantes, MF Botelho, MES Serra. "PO-416 Cytotoxicity of Ru (II) and Ru (III) salen complexes against breast and colorectal cancer cell lines", Poster Presentation: Experimental/Molecular Therapeutics, Pharmacogenomics, 2018 Publication	<1%
19	Submitted to Karunya University Student Paper	<1%
20	Soumya Alige Mahabala Rao, Arivazhagan Arimappamagan, Paritosh Pandey, Vani Santosh et al. "miR-219-5p Inhibits Receptor Tyrosine Kinase Pathway by Targeting EGFR in Glioblastoma", PLoS ONE, 2013 Publication	<1%
21	www.nature.com Internet Source	<1%

22	Kaiser M. Bijli, Bum-Yong Kang, Roy L. Sutliff, C. Michael Hart. "Proline-Rich Tyrosine Kinase 2 Downregulates Peroxisome Proliferator–Activated Receptor Gamma to Promote Hypoxia-Induced Pulmonary Artery Smooth Muscle Cell Proliferation", Pulmonary Circulation, 2016 Publication	<1 %
23	Zhongxu Hu, Xiaolei Hu, Haiyan Xiao, Youjie Zeng, Minghao Jiang, Dai Li, Tao Song. "SYN1 is associated with immune infiltrates and might be a prognostic biomarker for glioma", Research Square Platform LLC, 2023 Publication	<1 %
24	www.ijdb.ehu.es Internet Source	<1 %
25	Roberta Rudà, Francesco Bruno, Tamara Ius, Antonio Silvani et al. "IDH wild-type grade 2 diffuse astrocytomas: prognostic factors and impact of treatments within molecular subgroups", Neuro-Oncology, 2022 Publication	<1 %
26	www.tandfonline.com Internet Source	<1 %
27	www.thno.org Internet Source	<1 %

28	s3-ap-southeast-1.amazonaws.com Internet Source	<1 %
29	Li Ding, Ruonan Sun, Xinyue Zhang. "Rap2b siRNA significantly enhances the anticancer therapeutic efficacy of Adriamycin in a gold nanoshell-based drug/gene co-delivery system", Oncotarget, 2017 Publication	<1 %
30	M. S. Nandhu, Jes Paul, Korah P. Kuruvila, Pretty M. Abraham, Sherin Antony, C. S. Paulose. "Glutamate and NMDA receptors activation leads to cerebellar dysfunction and impaired motor coordination in unilateral 6-hydroxydopamine lesioned Parkinson's rat: functional recovery with bone marrow cells, serotonin and GABA", Molecular and Cellular Biochemistry, 2011 Publication	<1 %
31	Jan Panada, Valeriya Klopava, Tatsiana Kulahava, Nina Frolova, Yaroslav Faletrov, Vladimir Shkumatov. "New 3β-hydroxysteroid-indolamine conjugates: design, synthesis and inhibition of C6 glioma cell proliferation", Steroids, 2020 Publication	<1 %
32	Submitted to Mahidol University Student Paper	<1 %

33	Quinn T Ostrom, Gino Cioffi, Kristin Waite, Carol Kruchko, Jill S Barnholtz-Sloan. "CBTRUS Statistical Report: Primary Brain and Other Central Nervous System Tumors Diagnosed in the United States in 2014–2018", Neuro-Oncology, 2021 Publication	<1 %
34	ebin.pub Internet Source	<1 %
35	journals.plos.org Internet Source	<1 %
36	mdpi-res.com Internet Source	<1 %
37	Adamu Imam Isa. "Exploring signaling pathway crosstalk in glioma by mapping miRNA and WNT pathways: A review", International Journal of Biological Macromolecules, 2023 Publication	<1 %
38	Zi-Hui Wang, Jin Li, Qian Liu, Jian-Chang Qian et al. "A modified nucleoside O6-methyl-2′-deoxyguanosine-5′-triphosphate exhibits anti-glioblastoma activity in a caspase-independent manner", Pharmacological Research, 2024 Publication	<1 %
	academic.oup.com	

39	Internet Source	<1%
40	coek.info Internet Source	<1%
41	prism.ucalgary.ca Internet Source	<1%
42	pure.manchester.ac.uk Internet Source	<1%
43	Submitted to IIT Delhi Student Paper	<1%
44	bmccomplementalternmed.biomedcentral.com Internet Source	<1%
45	jcs.biologists.org Internet Source	<1%
46	topsecretapiaccess.dovepress.com Internet Source	<1%
47	"Tumors of the Central Nervous System, Volume 1", Springer Science and Business Media LLC, 2011 Publication	<1%
48	Lai, Lin, Liu, Yang, Lu. "Monocarboxylate Transporter 4 Regulates Glioblastoma Motility and Monocyte Binding Ability", Cancers, 2020 Publication	<1%

49	Internet Source	<1%
50	"Abstracts", Brain Pathology, 9/2006 Publication	<1%
51	docksci.com Internet Source	<1%
52	elischolar.library.yale.edu Internet Source	<1%
53	escholarship.org Internet Source	<1%
54	ijbc.ir Internet Source	<1%
55	synapse.koreamed.org Internet Source	<1%
56	www.spandidos-publications.com Internet Source	<1%

Exclude quotes	On	Exclude matches	< 14 words
Exclude bibliography	On		